

GEOCHRONOLOGICAL ANALYSIS AS A TEST OF THE PRESENCE OF THE SONORA  
ALLOCHTHON IN THE SIERRA LAS PINTAS, BAJA CALIFORNIA, MEXICO

By Claire K. Pringle

A Thesis

Submitted in Partial Fulfillment  
of the Requirements for the Degree of  
Master of Science  
in Geology

Northern Arizona University

December 2021

Approved:

Nancy R. Riggs, Ph.D., Chair

Pilar Navas-Parejo, Ph.D.

Michelangelo Martini, Ph.D.

Michael H. Ort, Ph.D.

## ABSTRACT

### GEOCHRONOLOGICAL ANALYSIS AS A TEST OF THE PRESENCE OF THE SONORA ALLOCHTHON IN THE SIERRA LAS PINTAS, BAJA CALIFORNIA, MEXICO

CLAIRE K. PRINGLE

Formation of the final supercontinent, Pangea, culminated in late Paleozoic time with closing of the Rheic ocean and collision of Gondwana and Laurentia. This resulted in the hypothesized 3,000-km-long Ouachita-Marathon-Sonora orogenic belt (OMS) along the southern margin of Laurentia. The Sonora allochthon, the westernmost segment of the OMS, is dominantly located in Chihuahua and Sonora, Mexico, but recent studies have suggested that the orogen continues into northern Baja California, where sedimentary rocks in the Sierra Las Pintas have been correlated to allochthon stratigraphy in Sonora. This study provides the first detrital zircon geochronological analysis of the Sierra Las Pintas to test the hypothesis that Sonora allochthon strata are present and further correlation can be made to the Sonora allochthon documented in central Sonora.

Detrital zircon geochronology of the Sierra Las Pintas strata indicates major sources from the Peninsular Ranges batholith and the Permo-Triassic arc, as well as minor sources from Gondwana, the Grenville orogen, Granite-Rhyolite provinces, Yavapai-Mazatzal provinces and the Archean craton. Provenance analysis suggests that most of the detritus was derived from the Peninsular Ranges batholith to the west, the Cordilleran Permo-Triassic arc to the northeast, crustal provinces of the Laurentian craton to the north, and Gondwana to the south. A Late Cretaceous maximum depositional age is determined for Sierra Las Pintas strata and stratigraphic analysis indicates deposition in the Peninsular Ranges batholith forearc along the continental slope and

ocean basin. Geochronologic analyses suggest that the Sonora allochthon is not present in the Sierra Las Pintas and the succession cannot be correlated to the Sonora allochthon in central Sonora. Provenance interpretation of strata in the Sonora allochthon of central Sonora agrees with previous literature and provides strong detrital zircon evidence of Gondwanan source, which has rarely been identified in previous studies. Although the results of this study do not support the hypothesis that the Sonora allochthon is present in the Sierra Las Pintas, the strata record a mixed provenance of Gondwanan and Laurentian source regions, as well as Cretaceous Cordilleran arc activity.

© Claire Kathleen Pringle 2020

## ACKNOWLEDGEMENTS

This research was supported by the Geological Society of America via the Graduate Student Research Grant, the Ronald C. Blakey scholarship, the Bedwell Award, the Walter and Rosemarie Hochstrasser scholarship, and by Pioneer Natural Resources. Additional grants from Dirección General de Asuntos del Personal Académico of the Universidad Nacional Autónoma de México UNAM-DGAPA-PAPIIT IN106920 and Consejo Nacional de Ciencia y Tecnología CONACyT Ciencia de Frontera Project 7351 paid for field work expenses and helped to cover the cost of geochronologic analyses.

First and foremost, I would like to thank my family. To my husband Rhett, thank you for your immense sacrifice, incredible patience, and unconditional love and support throughout this journey. Thank you to my kids for being the cutest lab assistants, always keeping things exciting at home, and giving me laughter every day. You all have encouraged me and brought me joy on the hardest of days, sacrificed as I was pursuing my dreams as a geologist, and inspired me to accomplish my goals. I am forever grateful to be yours.

Second, I would like to thank Nancy Riggs, for being my thesis advisor, friend, and mentor these past few years. I have had the great pleasure of working with you during some of my most formative years yet, including the birth of my children, moving to 3 different states, a global pandemic, countless hours spent in the field, and hours of discussion on zoom... it has been an honor to work with you and learn from your vast knowledge of geology. Thank you to my wonderful research committee Pilar Navas-Parejo, Michelangelo Martini, and Michael Ort. To Pilar and Miche, it has been a great joy to explore the mountains of Baja California, enjoy ceviche and huevos rancheros in the field, discuss the great complexities of the Sierra Las Pintas,

and learn from your great geologic expertise. Thanks to Michael for being a part of this committee, many great volcanology discussions, and supporting me in this degree. A great thanks to Andrew Kylander-Clark for analyzing and reducing all detrital zircon data for this study when the labs were closed due to a global pandemic. Additional thanks to Luigi Solari for analyzing detrital zircon samples collected from Sonora and Gareth Seward for assistance with cathodoluminescence.

Finally, thank you to my friends and family who have supported me throughout this process. It truly takes a village, and I would not be here today without all the love and support from the wonderful people in my life. Thank you to my parents, Scott and Cindy Andrews, and sisters, Hilary Andrews and Sarah Brown. You have encouraged me to follow my dreams as a geologist from the very beginning and been a constant lifeline and source of joy. I am so grateful for you all. Thank you to my in-laws for housing us and providing us childcare and loving support when we needed it the most. Thank you to all my friends and to my fellow graduate students for being great companions through it all!

## TABLE OF CONTENTS

<b>ABSTRACT</b> .....	<b>ii</b>
<b>COPYRIGHT PAGE</b> .....	<b>iv</b>
<b>ACKNOWLEDGEMENTS</b> .....	<b>v</b>
<b>TABLE OF CONTENTS</b> .....	<b>vii</b>
<b>LIST OF TABLES</b> .....	<b>ix</b>
<b>LIST OF FIGURES</b> .....	<b>x</b>
<b>DEDICATION</b> .....	<b>xiii</b>
<b>1.0 INTRODUCTION</b> .....	<b>1</b>
1.1 PALEOTECTONIC AND PALEOGEOGRAPHIC SETTING .....	3
1.2 GEOLOGIC BACKGROUND OF THE SONORA ALLOCHTHON.....	12
<b>2.0 METHODS</b> .....	<b>20</b>
2.1 FIELD METHODS .....	20
2.2 LABORATORY METHODS .....	23
<b>3.0 RESULTS</b> .....	<b>29</b>
3.1 LITHOLOGY, STRATIGRAPHY, AND PETROGRAPHY.....	29
3.1.1 Arroyo Grande Group.....	32
3.1.2 Sierra Las Pintas Group.....	55
3.1.3 Minas de Barita Area.....	62
3.2 DETRITAL ZIRCON U-PB GEOCHRONOLOGY AND TRACE ELEMENT GEOCHEMISTRY.....	65
3.2.1 Arroyo Grande Group Detrital Ages .....	65
3.2.2 Sierra Las Pintas Group Detrital Ages .....	79
3.2.3 Minas de Barita Area Detrital Ages .....	87
3.2.4 Sierra Las Pintas Area Trace Element Geochemistry .....	93
<b>4.0 DISCUSSION</b> .....	<b>99</b>

4.1 DETRITAL ZIRCON AGES AND PROVENANCE ANALYSIS.....	99
4.1.1 Provenance Interpretation of the Arroyo Grande Group .....	104
4.1.2 Provenance Interpretation of the Sierra Las Pintas Group .....	112
4.1.3 Provenance Interpretation of the Minas de Barita Area .....	117
4.1.4 Comparison of Field Areas.....	120
4.2 LITHOLOGIES AND DEPOSITIONAL HISTORY.....	126
4.2.1 Depositional History of the Arroyo Grande Group.....	126
4.2.2 Depositional History of the Sierra Las Pintas Group.....	133
4.2.3 Depositional History of the Minas de Barita Area .....	135
4.3 TECTONIC EVOLUTION.....	136
4.3.1 Origin of Cretaceous Zircon.....	137
4.3.2 Cretaceous Sierra Las Pintas Area .....	139
4.3.3 Outstanding Research Problems and Recommended Future Studies.....	141
<b>CONCLUSIONS .....</b>	<b>145</b>
<b>REFERENCES.....</b>	<b>151</b>
<b>APPENDICES .....</b>	<b>152</b>
APPENDIX Ia.....	152
APPENDIX Ib.....	162
APPENDIX Ic.....	168
APPENDIX IIa.....	172
APPENDIX IIb .....	183
APPENDIX IIIa .....	195
APPENDIX IIIb.....	200
APPENDIX IV.....	205
APPENDIX V .....	209



## LIST OF TABLES

<b>TABLE 1:</b> List of samples .....	22
<b>TABLE 2:</b> Redefined Arroyo Grande Group units .....	23
<b>TABLE 3:</b> Summary of field observations .....	30
<b>TABLE 4:</b> Summary of petrographic analysis.....	31
<b>TABLE 5:</b> Reanalysis of Cretaceous zircon .....	101

## LIST OF FIGURES

<b>FIGURE 1:</b> Regional index map .....	2
<b>FIGURE 2:</b> Index map of the Sierra Las Pintas Area.....	3
<b>FIGURE 3:</b> Generalized correlative stratigraphic chart of Sonora allochthon strata .....	5
<b>FIGURE 4:</b> Map of major age provinces and terranes .....	6
<b>FIGURE 5:</b> Geologic map of the Minas de Barita Area.....	15
<b>FIGURE 6:</b> Geologic map of the Sierra Las Pintas Group.....	16
<b>FIGURE 7:</b> Geologic map of the Arroyo Grande Group .....	17
<b>FIGURE 8:</b> Updated geologic map of the Arroyo Grande Group.....	32
<b>FIGURE 9:</b> Generalized stratigraphic column of the Arroyo Grande Group.....	33
<b>FIGURE 10:</b> Arroyo Grande Group Unit 1 measured section .....	35
<b>FIGURE 11:</b> Arroyo Grande Group outcrop photographs of Unit 1.....	36
<b>FIGURE 12:</b> Arroyo Grande Group Unit 2 measured section .....	38
<b>FIGURE 13:</b> Arroyo Grande Group outcrop photographs of Unit 2.....	39
<b>FIGURE 14:</b> Arroyo Grande Group Lower Unit 3 measured section.....	42
<b>FIGURE 15:</b> Arroyo Grande Group Upper Unit 3 measured section .....	43
<b>FIGURE 16:</b> Arroyo Grande Group outcrop photographs of Unit 3.....	44
<b>FIGURE 17:</b> Arroyo Grande Group photomicrographs of Unit3.....	47
<b>FIGURE 18:</b> Arroyo Grande Group Unit 4 measured section .....	50
<b>FIGURE 19:</b> Arroyo Grande Group outcrop photographs of Unit 4.....	51
<b>FIGURE 20:</b> Arroyo Grande Group photomicrographs of Unit 4.....	53
<b>FIGURE 21:</b> Arroyo Grande Group outcrop and photomicrographs of Unit 5.....	55
<b>FIGURE 22:</b> Sierra Las Pintas Group outcrop photographs of Unit SP1 .....	56

<b>FIGURE 23:</b> Sierra Las Pintas Group photomicrographs of Unit SP1 .....	57
<b>FIGURE 24:</b> Sierra Las Pintas Group Unit SP2 measured section .....	59
<b>FIGURE 25:</b> Sierra Las Pintas Group outcrop photographs of Unit SP2 .....	60
<b>FIGURE 26:</b> Sierra Las Pintas Group photomicrographs of Unit SP2 .....	61
<b>FIGURE 27:</b> Sierra Las Pintas Group outcrop photograph of Unit SP4 .....	62
<b>FIGURE 28:</b> Facies profile of the Mina México Formation .....	64
<b>FIGURE 29:</b> Detrital zircon age data for sample LP070120-1 .....	66
<b>FIGURE 30:</b> KDE plot for sample LP070120-2 .....	68
<b>FIGURE 31:</b> Detrital zircon age data for sample LP080120-1 .....	70
<b>FIGURE 32:</b> Detrital zircon age data for sample LP080120-8 .....	72
<b>FIGURE 33:</b> Detrital zircon age data for sample LP080120-9 .....	74
<b>FIGURE 34:</b> Detrital zircon age data for sample LP090120-2 .....	76
<b>FIGURE 35:</b> Detrital zircon age data for sample LP090120-3 .....	78
<b>FIGURE 36:</b> Detrital zircon age data for sample LP100120-1 .....	80
<b>FIGURE 37:</b> Detrital zircon age data for sample LP110120-1 .....	82
<b>FIGURE 38:</b> Detrital zircon age data for sample 18-LP-10 .....	84
<b>FIGURE 39:</b> Detrital zircon age data for sample X181218 .....	86
<b>FIGURE 40:</b> Detrital zircon age data for sample 13-11-SR2 .....	88
<b>FIGURE 41:</b> Detrital zircon age data for sample 13-11-SR3 .....	90
<b>FIGURE 42:</b> Detrital zircon age data for sample 12-11-SR2 .....	92
<b>FIGURE 43:</b> Geochemical bivariate plots for Permo-Triassic zircon of the Arroyo Grande Group .....	94
<b>FIGURE 44:</b> Geochemical bivariate plots for Permo-Triassic zircon of the Sierra Las Pintas Group .....	95

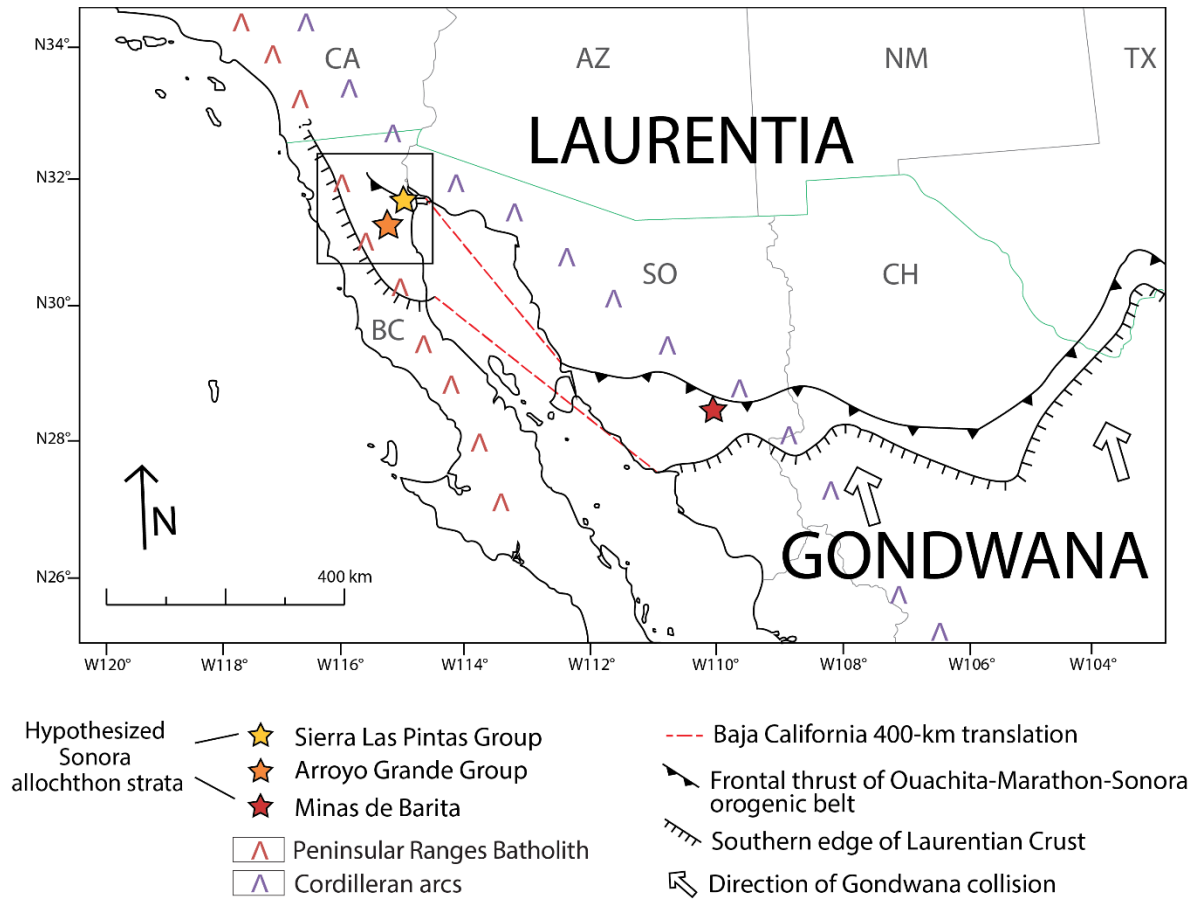
<b>FIGURE 45:</b> Geochemical bivariate plots for Permo-Triassic zircon of the Sierra Las Pintas Area.....	96
<b>FIGURE 46:</b> Geochemical bivariate plots for Cretaceous zircon of the Arroyo Grande Group .....	97
<b>FIGURE 47:</b> Geochemical bivariate plots for Cretaceous zircon of the Sierra Las Pintas Group .....	98
<b>FIGURE 48:</b> Geochemical bivariate plots for Cretaceous zircon of the Sierra Las Pintas Area .....	99
<b>FIGURE 49:</b> Cathodoluminescence image of sample LP080120-9.....	103
<b>FIGURE 50:</b> Provenance pie chart map of the Arroyo Grande Group .....	104
<b>FIGURE 51:</b> Normalized stacked PDPs of Permo-Triassic Arroyo Grande Group samples.....	108
<b>FIGURE 52:</b> Normalized stacked PDPs of Cretaceous Arroyo Grande Group samples .....	111
<b>FIGURE 53:</b> Provenance pie chart map of the Sierra Las Pintas Group.....	113
<b>FIGURE 54:</b> Normalized stacked PDPs of the Sierra Las Pintas Group samples .....	116
<b>FIGURE 55:</b> Provenance pie chart map of the Minas de Barita Area.....	117
<b>FIGURE 56:</b> Normalized stacked PDPs of the Minas de Barita Area samples .....	119
<b>FIGURE 57:</b> Provenance pie chart map of all field areas .....	121
<b>FIGURE 58:</b> Normalized stacked PDPs of all field areas .....	124
<b>FIGURE 59:</b> Normalized stacked PDPs of all field areas compared to previous literature.....	125
<b>FIGURE 60:</b> Depositional History of the Arroyo Grande Group .....	127
<b>FIGURE 61:</b> Chronostratigraphic column of the Arroyo Grande Group .....	128
<b>FIGURE 62:</b> Comparison of photomicrographs of Unit 3 and Unit 5 .....	138

## **DEDICATION**

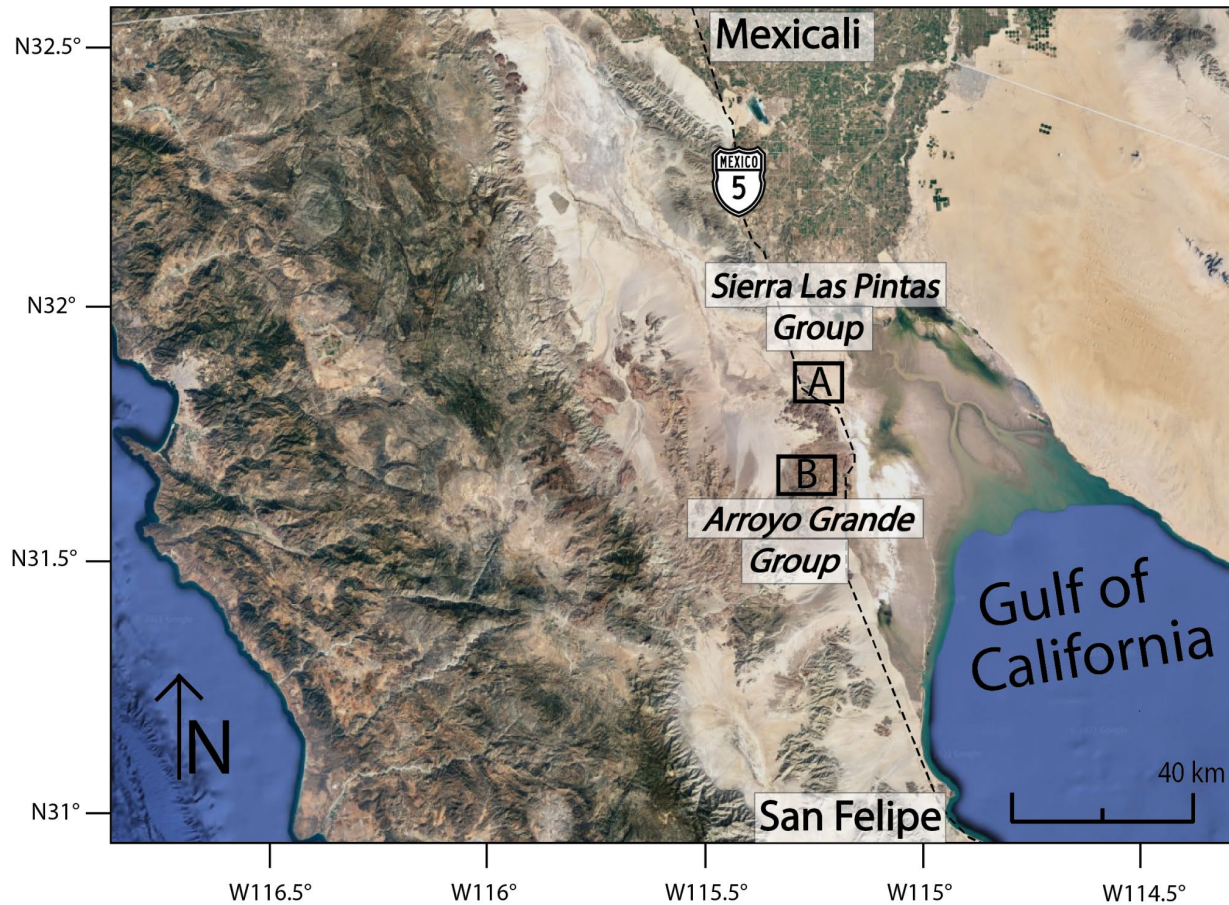
This thesis is dedicated to my husband Rhett and my children Judah, Levi, and Eliza. Life is so much richer and full of joy thanks to you.

## 1.0 INTRODUCTION

The Sonora allochthon, hypothesized to be the westernmost segment of the Ouachita-Marathon-Sonora (OMS) orogen, was formed due to the collision of Gondwana and Laurentia when continental-slope and -rise deposits of Gondwana were thrust northward onto the southern continental carbonate shelf of Laurentia late in Permian time (Poole and Perry, 1997; Poole et al., 2000; 2005; Figure 1). Leier-Engelhardt (1993) hypothesized that Sonora allochthon strata documented in Sonora, Mexico, can be correlated to similar strata of the Sierra Las Pintas Group and the Arroyo Grande Group of the Sierra Las Pintas in northeastern Baja California, Mexico (Figures 1-2). The Sierra Las Pintas is divided into a northern and southern area that are composed of deep-water metasedimentary and metavolcanic rocks that exhibit similar stratigraphy to Lower Ordovician to Upper Pennsylvanian deep-water strata documented in the Minas de Barita area of Sonora, Mexico (Figure 1; Gastil et al., 1991; Stewart and Poole, 2002; Poole et al., 2005). While the metasedimentary facies and biostratigraphy of the proposed Sonora allochthon of Baja California correlate to strata found in central Sonora (Leier-Engelhardt, 1993; Poole et al., 2008; Navas-Parejo et al., 2018), previously no geochronological analysis of the Sierra Las Pintas has been completed. This study is the first to conduct dating by detrital zircon U-Pb methods to test the hypothesis that Sonora allochthon strata are present in the Sierra Las Pintas. This study utilizes geologic mapping, geochronological analysis, petrographic analysis, and zircon trace element geochemistry to determine the provenance, depositional setting, and tectonic evolution of the Sierra Las Pintas strata. Furthermore, a comparison of the geochronological data of the Sierra Las Pintas to similar strata found in the Minas de Barita area of Sonora, Mexico, is utilized to determine whether a correlation can be made between these two regions.



**Figure 1.** Regional map showing present-day positions of Laurentia, Gondwana, the Peninsular Ranges batholith, the Cordilleran arcs and the Ouachita-Marathon-Sonora orogenic belt. Red lines show the 400-km translation of Baja California and indicate the proposed displacement of the frontal thrust of Ouachita-Marathon-Sonora orogenic belt and the southern edge of Laurentian crust due to Cenozoic opening of the Gulf of California. Proposed locations of the western Sonora allochthon include the Sierra Las Pintas Group (yellow star) and the Arroyo Grande Group (orange star). The central Sonora allochthon is shown located in the Minas de Barita area (red star) of Sonora, Mexico. The black box indicates the location of the index map of Figure 2. Modified from Kimbrough et al., (2001), Poole et al. (2005), and Whitmeyer and Karlstrom (2007).



**Figure 2.** Index map showing the locations of the Sierra Las Pintas Group and the Arroyo Grande Group of the Sierra Las Pintas. See Figure 6 (A) and Figure 7 (B) for more detailed geologic maps of each field area.

## 1.1 PALEOTECTONIC AND PALEOGEOGRAPHIC SETTING

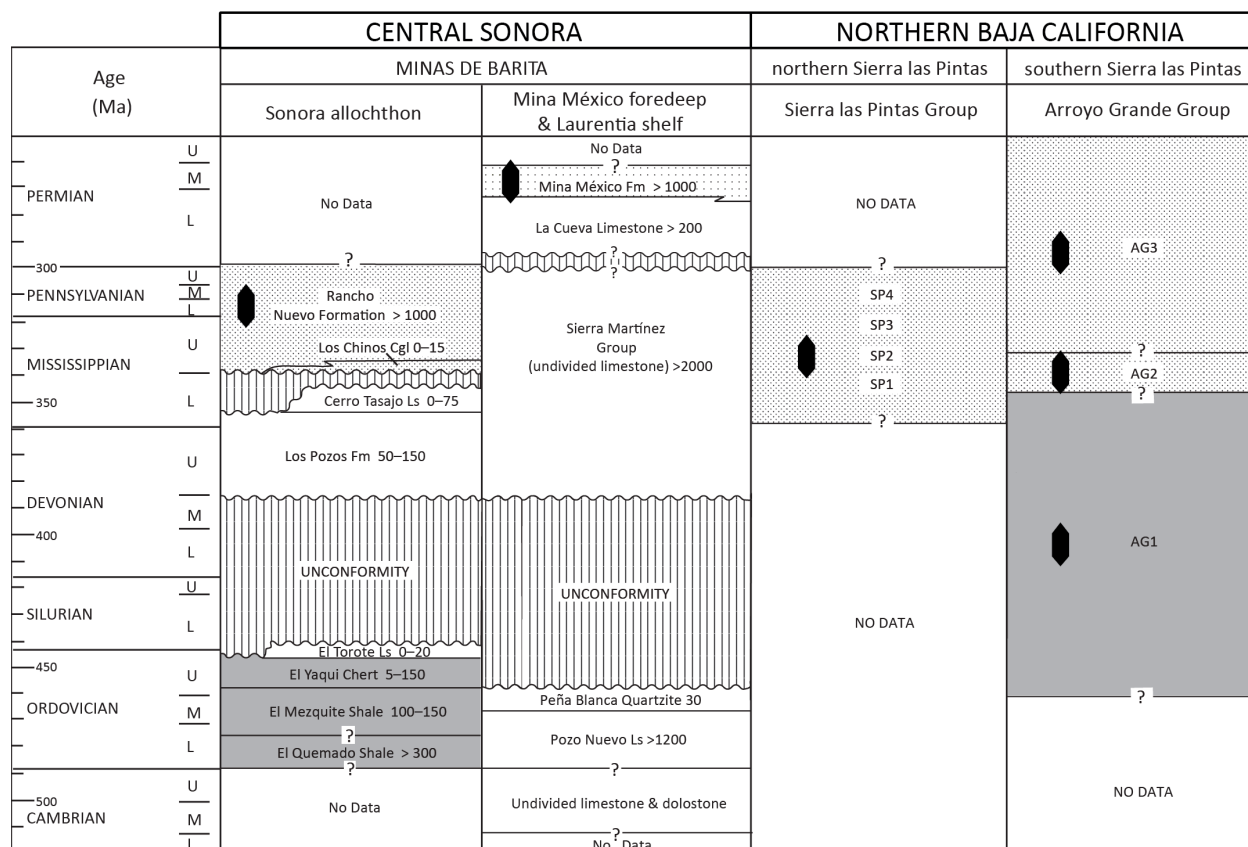
### *Previous Work*

Initial studies by McEldowney (1970) interpreted the northern Sierra Las Pintas metasedimentary rocks as Paleozoic due to the presence of fossils such as Paleozoic lophophyllid corals and brachiopods. Further stratigraphic studies and geologic mapping established a correlation between rocks of the northern and southern Sierra Las Pintas (James, 1973; La Borde, 1967). Leier-Engelhardt (1993) completed geologic maps of the northern and southern areas of the Sierra Las Pintas and suggested correlation of the metasedimentary lithology of the western



Sonora allochthon in Baja California to similar stratigraphy found in central Sonora, Mexico, (Figure 3). Extensive biostratigraphic work by Navas-Parejo et al. (2018) further correlated metasedimentary rocks of the northern Sierra Las Pintas to formations found in central Sonora allochthon based on similar biostratigraphic and petrographic data.

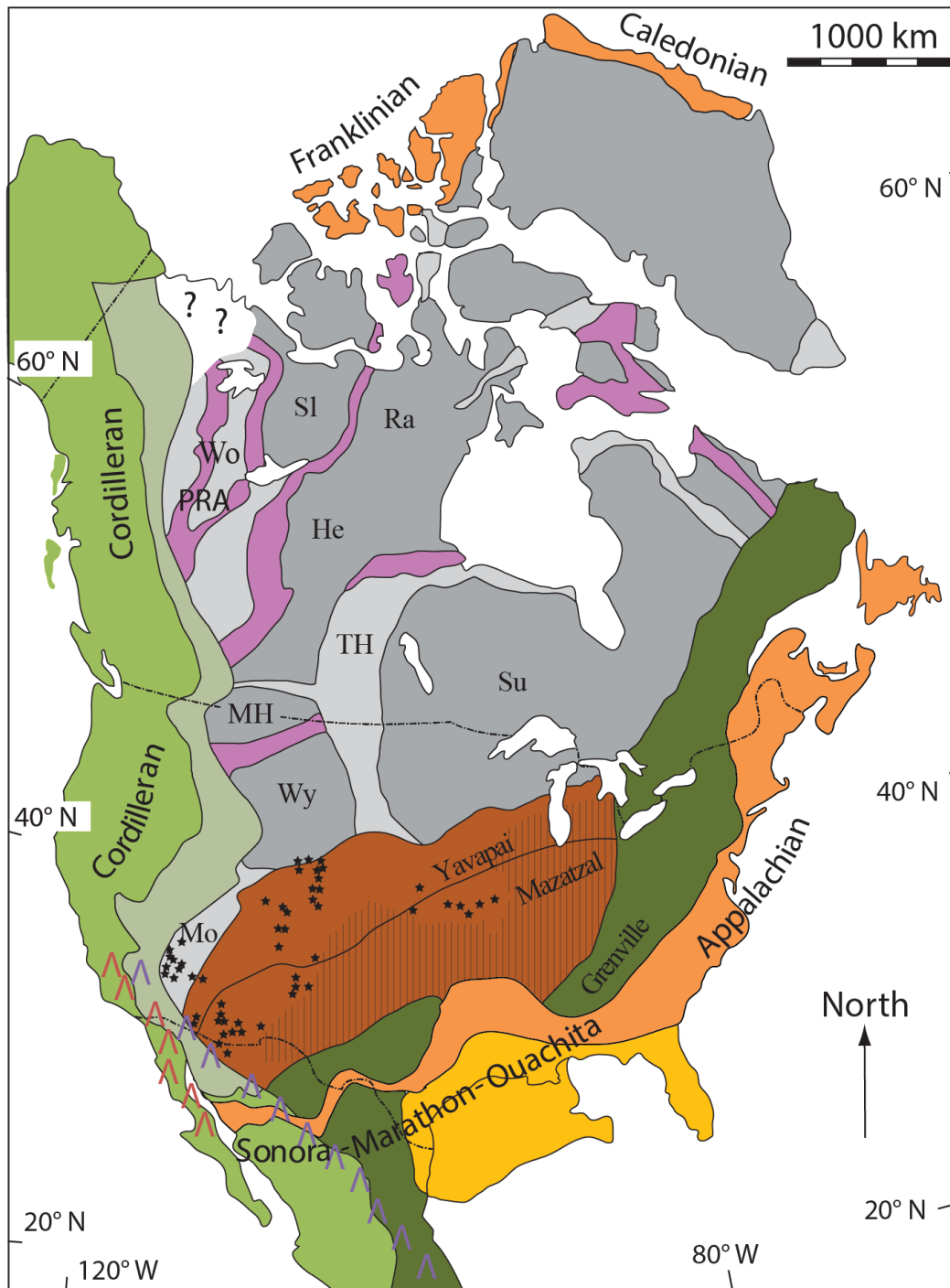
An initial detrital zircon study by Gehrels and Stewart (1998) was conducted on Cambrian to Triassic strata of Sonora, Mexico. Poole et al. (2008) analyzed detrital zircon grains from deep-water strata of the Los Pozos Formation and Mina México Formation exposed in the Minas de Barita area of central Sonora. The study was continued with further U-Pb geochronology and Hf isotope analysis by Gehrels and Pecha (2014). The analysis included samples from Sonora shelf-facies strata and re-analyzed samples from the Los Pozos Formation and Mina México Formation by Poole et al. (2008) (Figure 3). No geochronologic analysis has been previously completed of the proposed Sonora allochthon of the Sierra Las Pintas.



**Figure 3.** Generalized stratigraphic chart of Paleozoic strata showing previous correlations of the Sonora allochthon from central Sonora and from northern Baja California. The stratigraphic level of detrital zircon samples is indicated by the zircon cartoon. Similar patterns represent correlative strata. Stipple indicates flysch facies. Approximate unit thicknesses in meters. Modified time scale and correlative strata determined based on Leier-Engelhardt (1993), Poole et al., (2005; 2008), Stevens et al., (2014), Navas-Parejo et al., (2018), and Lara-Peña et al., (2020).

### *Paleotectonic Setting*

Provenance groupings for this study are largely determined based on extensive provenance analysis done by Hoffman (1989), Saleeby et al. (1992), Gehrels et al. (1995), Dickinson and Lawton (2001), Blakey (2007), Whitmeyer and Karlstrom (2007), Poole et al., (2008), Gehrels and Pecha (2014), Saleeby and Dunne (2015), and numerous others. The main source regions that are identified in this study are summarized here. Figure 4 provides the locations of major age provinces and terranes of central North America that are utilized for these provenance determinations.



- |   |   |
|---|---|
| Peninsular Ranges Batholith (ca. 140–90 Ma) | Grenville orogen (1.2–1.0 Ga)             |
| Cordilleran arcs (ca. 280–220 Ma)           | 1.48–1.34 Ga Magmatic Prov                |
| Cordilleran margin                          | Yavapai-Mazatzal (1.8–1.7 Ga; 1.7–1.6 Ga) |
| Cordilleran passive margin                  | Juvenile arcs (2.0–1.8 Ga)                |
| Peri-Laurentia terranes (500–300 Ma)        | Archean & 2.3–1.8 Ga Prov                 |
| Peri-Gondwana Prov (720–500 Ma)             | Archean (>2.5 Ga)                         |

**Figure 4.** Locations of major age provinces and terranes of central North America utilized for provenance determinations used in this study. PRA – Peace River Arch region; Mo – Mojave province; Wy – Wyoming province; MH – Medicine Hat province; Su – Superior province; TH – Trans-Hudson province; Ra – Rae province; He – Hearne province; Sl – Slave province; Wo – Wopmay province. Adapted from Saleeby et al (1992), Gehrels et al. (1995), Dickinson and Lawton (2001), Kimbrough et al., (2001), Poole et al., (2005), Whitmeyer and Karlstrom (2007), and Gehrels and Pecha (2014).

### **Building the Laurentian and Gondwanan Continents**

The core of Laurentia was assembled during the Paleoproterozoic from 2000-1800 Ma. Much of the continental shield was formed from Archean continents (3000-2500 Ma) that collided together, such as the Slave (2700-2500 Ma) and Rae-Hearne continent-continent collisional event (1960-1830 Ma), and the Slave-Rae-Hearne assembly collision of the Superior craton (1830-1800 Ma). The Archean continents that collided with smaller continental fragments such as Wyoming, Medicine Hat, Sask Marshfield, and Nain terranes primarily compose the core of the North American continent and resulted in the Trans-Hudson orogen (Dickinson, 1983; Hoffman, 1989; Dickinson and Gehrels, 2003; Whitmeyer & Karlstrom, 2007).

Arc-continent accretion of juvenile volcanic arcs and oceanic terranes added to the North American craton. Major accretionary provinces include the Yavapai (1800-1700 Ma) and Mazatzal (1700-1650 Ma) that were added to Laurentia during the Yavapai-Mazatzal orogeny (1700-1600 Ma). The Granite-Rhyolite province (1500-1300 Ma) was another major tectonic event associated with A-type intracratonic magmatism. The Llano-Grenville province (1300-1000 Ma) was added to the continent during the Grenville orogeny (1250-950 Ma) (Dickinson and Gehrels, 2003; Whitmeyer & Karlstrom, 2007).

Formation of Gondwana as summarized by Meert and Van Der Voo (1997) began around 800-650 Ma with the East African orogeny as present-day India, Madagascar, and Sri Lanka collided with East Africa. This event was followed by the Brasiliano orogeny (600-530 Ma) as South America and Africa collided. Final Gondwana assembly occurred with the Kuunga orogeny (~550 Ma) with amalgamation of Australia and Antarctica (Hoffman, 1989; Wortman et al., 2000). Peri-Gondwanan terranes that are thought to have accreted during the Appalachian orogenies include the Avalon terrane, Carolina terrane, and Suwannee terrane (635-535 Ma) (Blakey, 2007; Dickinson and Gehrels, 2003).

### **Pangea Formation**

The collision of Laurentia and Gondwana and subsequent formation of Pangea had a major effect on global tectonism, eustasy, global climate patterns and sediment supply with evidence seen spanning the globe throughout North America, central Eurasia, and northwestern Europe (Murphy and Nance, 1991; Blakey, 2007). The tectonic history of Pangea can be summarized as break-up of the previous supercontinent, Rodinia, in Late Proterozoic time, assembly of Laurussia and Laurasia throughout Paleozoic time, assembly of western Pangea and closing of the Paleotethys Ocean beginning in Mississippian time, followed by the final assembly of eastern Pangea with coeval initial break-up of western Pangea (Murphy and Nance, 1991; Ziegler, 1992; Dickinson and Lawton, 2001; Hatcher, 2002; Stampfli et al., 2002; Blakey, 2007). The collision and accretion of Gondwana, Laurentia/Baltica, and Siberia-Kazakhstan-Asia continental masses during the final assembly of western Pangea in Carboniferous time resulted in an accretionary orogenic system (Stampfli et al., 2002; Cawood and Buchan, 2007). The final oblique collision closed the Rheic Ocean and distributed collisional forces differently along the orogenic front in a zipper fashion from eastern to western Pangea (Dickinson and Lawton, 2001;

Hatcher, 2002; Blakey, 2007). These tectonic events resulted in the formation of the Appalachian orogen (500-280 Ma) and the Ouachita-Marathon-Sonora orogen (300-250 Ma) (Dickinson, 1983; Becker et al., 2006; Blakey, 2007; Kröner et al., 2016). Reorganization of the plates due to transpressional and transtensional tectonics followed collision until rifting began in Triassic time (Blakey, 2007).

### **Ouachita-Marathon-Sonora Orogen**

The Ouachita-Marathon-Sonora orogen (OMS) is a 3,000-km deformation belt of three segments that collectively span the southern margin of North America from Mississippi to Oklahoma (Ouachita), southwest through Texas (Marathon) and westward through Chihuahua and Sonora, ending in Baja California, Sonora (Figure 1; Poole et al., 2005). Many authors (e.g., Ross (1986), Handschy et al. (1987), Dickinson and Lawton (2001)) and others subscribe to the view that the farthest extent of the Ouachita-Marathon belt terminates in eastern Mexico and does not include the Sonora segment. Stratigraphic and structural data support the continuation of the orogen to the west into Central Sonora and Baja California as the Sonora allochthon (Gastil et al., 1991; Poole et al., 2005). Inferred remnants of the Gondwanan volcanic arc with associated fore-arc and back-arc assemblages that amalgamated from the collision are exposed in southern Sonora and Sinaloa as the El Fuerte Block along the northern margin of Gondwana (Poole et al., 2005). Crustal blocks of eastern Mexico including the Coahuila block, the Tampico and Del Sur blocks, and the Yucatan-Chiapas block are interpreted as fragments of the Gondwanan continent and were also sutured to Laurentia during the collision (Dickinson and Lawton, 2001). Despite various crustal elements and volcanic arcs of Gondwana identified in Mexico, zircon that ranges in age from 750-500 Ma and is considered characteristic of Gondwanan provenance are rare in southwestern North America. Westward termination of

Ouachita-Marathon-Sonora orogenesis occurred along the orogenic belt with deformation ending in Late Pennsylvanian time in the Ouachita Mountains, early Permian time in the Marathon region, and middle Permian (Guadalupian) time in the Sonora region (Poole et al., 2005; Stevens et al., 2014; Lara-Peña et al., 2020).

While cross-cutting younger features such as plutonic and volcanic rocks of the Sierra Madre Occidental, as well as fold-and-thrust belts of the Sierra Madre Oriental, interrupt the continuous orogenic belt of the OMS, each segment is linked through stratigraphic similarities, persistent biostratigraphy, deformation features and detrital zircon ages (Hatcher et al., 1989; Poole et al., 2005). Stratigraphic correlations of characteristic sections of the Sonora, Marathon, and Ouachita segments indicate similar successions of strata and erosional hiatuses (Poole et al., 2005). Paleozoic rocks of each segment of the OMS are primarily deep-water deposits with fossils such as radiolarians, graptolites, conodonts, sponge spicules, fusulinids, and brachiopods (Poole et al., 2005). Foreland basins formed adjacent to basement uplifts that developed in the continental crust during orogenesis, including foredeeps that formed subparallel to the orogenic front due to crustal flexure and isostatic loading during collision (Hatcher et al., 1989; Poole et al., 2005).

### **Related Subsequent Orogenesis**

Concurrent with final Pangea amalgamation in late Paleozoic time (Poole et al., 2005; 2008), continuing transtensional and transform tectonics led to rifting within the supercontinent, which would eventually break apart into the present-day continents (Blakey, 2007). Subduction of the Farallon plate beneath southwestern North America was initiated in late Permian time and began to build the Cordilleran system, shaping much of the western coast of the Americas

(Dickinson, 2004; Cecil et al., 2018). Permian plutons (270-260 Ma) in Sonora, Mexico, and Permian-Middle Triassic plutons (275-235 Ma) in the Mojave Desert have been interpreted as the root of the continental arc that developed along the southwestern Laurentian margin (Riggs et al., 2010; Cecil et al., 2018). Cecil et al. (2018) identified more evolved Hf and Nd isotopic signatures of the Sonoran Permo-Triassic magmatism than isotopic signatures of Permo-Triassic magmatism in northern Mojave region, suggesting the regions contain two distinct magmatic systems. Subduction complexes and intra-oceanic island arcs, such as the Guerrero superterrane, were accreted to southwest North American during mid-Mesozoic time that led to growth of the Cordilleran continental margin through arc-continent collision-accretion (Dickinson and Lawton, 2001; Dickinson, 2004). Continued subduction beneath Laurentia and accretion of terranes during Mesozoic time led to the formation of the Cretaceous Sierra Nevada and the Peninsular Ranges batholiths (Dickinson, 2004; Cecil et al., 2018). The Peninsular Ranges batholith spans southern California to southern Baja California (Figure 4) and was emplaced between 140-80 Ma with an eastward younging across Alta and Baja California, likely due to changes of dip and velocity of the subducting slab (Ortega-Rivera, 2003; Sedlock, 2003). The Peninsular Ranges batholith is divided into a western (140-105 Ma) and eastern belt (105-80 Ma) (Silver and Chappell, 2011; Busby, 2004). The western Peninsular Ranges batholith contains 140-105 Ma plutons and 125-118 Ma volcanic rocks. The eastern Peninsular Ranges batholith contains 105-80 Ma plutons that invade Phanerozoic metasedimentary, metavolcanic and metaplutonic rocks (Ortega-Rivera, 2003). The western Cordillera experienced crustal shortening due to the Sevier and Laramide orogenies, subsequent stretching and large-scale transform tectonics from Late Cretaceous to Cenozoic time (Ortega-Rivera, 2003). By Miocene time, transform faulting led to



opening of the Gulf of California and consequent 300-500 km northward translation of the Baja peninsula to its current location (Ortega-Rivera, 2003; Sedlock, 2003).

### ***Paleogeography of Cretaceous Baja California***

Paleogeographic reconstruction of Late Cretaceous northern Baja California by Bottjer (1984) suggests a west-facing forearc basin made up of the Peninsular Ranges batholith and portions of the western Transverse Ranges. Upper Cretaceous strata were deposited in nonmarine, shallow-marine, shelf, slope, and deep-sea fan environments with west-directed transport patterns. Paleocurrent directions in Baja California during this time are consistently toward the west (Busby-Spera and Boles, 1986).

## **1.2 GEOLOGIC BACKGROUND OF THE SONORA ALLOCHTHON**

The Sonora allochthon was emplaced during latest early-middle Permian time and major thrusting associated with emplacement of the allochthon likely ended before Triassic time, followed by formation of rift basins from transtensional and extensional faulting in the Early and Middle Triassic epochs (Poole et al., 2005). The Sonora allochthon consists of deep-water continental-rise and ocean-basin rocks that were emplaced onto continental-shelf and deep-water foredeep rocks of southern Laurentia (Poole et al., 2005; 2008; Stevens et al., 2014).

### ***Stratigraphy of central Sonora, Mexico***

Poole and Amaya-Martínez (2000) described the Sonora allochthon of central Sonora as composed of continental-slope and -rise deposits; a foreland basin north and subparallel to the orogenic belt were filled with sediment eroding from the advancing orogeny. The Sonora allochthon can be divided into pre-Upper Mississippian pre-orogenic continental-rise deposits

that are approximately 600-800 m thick and post-Lower Mississippian synorogenic turbidite deposits approximately 1,000 m thick. Pre-orogenic deposits were folded and faulted in the Mississippian Los Chinos deformational event. Those deposits underlie synorogenic siliceous turbiditic sediments that were emplaced during the Sonora orogeny in Carboniferous-Permian time that also folded and thrust the entirety of the Paleozoic oceanic-rock sequence.

The best exposure of Paleozoic outcrops in central Sonora are found in the Minas de Barita area, which contains the Sonora allochthon, the Mina México foredeep and Laurentian shelf deposits (Figure 5). Sonora allochthon strata of the Minas de Barita are generally composed of Ordovician, Devonian, and Mississippian to Pennsylvanian formations, including the Rancho Nuevo Formation (Figure 2) that are primarily made up of deep-water successions including radiolarian chert, shale, mudstone, siltstone, stratiform barite, sandstone, quartzite, limestone and conglomerate lithologies (Poole and Amaya-Martínez, 2000; Poole et al., 2008; Stevens et al., 2014; Navas-Parejo et al., 2018). The Rancho Nuevo Formation was described by Poole et al. (2005; 2008) as synorogenic strata of the Sonora allochthon estimated to be thicker than 1000 m. The formation is composed of Upper Mississippian mudstone, siltstone, chert, barite, and Lower to Upper Pennsylvanian interbedded turbiditic mudstone, siltstone, sandstone, conglomerate, chert, barite, limestone, and minor dolostone. Radiolarians, conodonts, and fusulinids are identified within the formation.

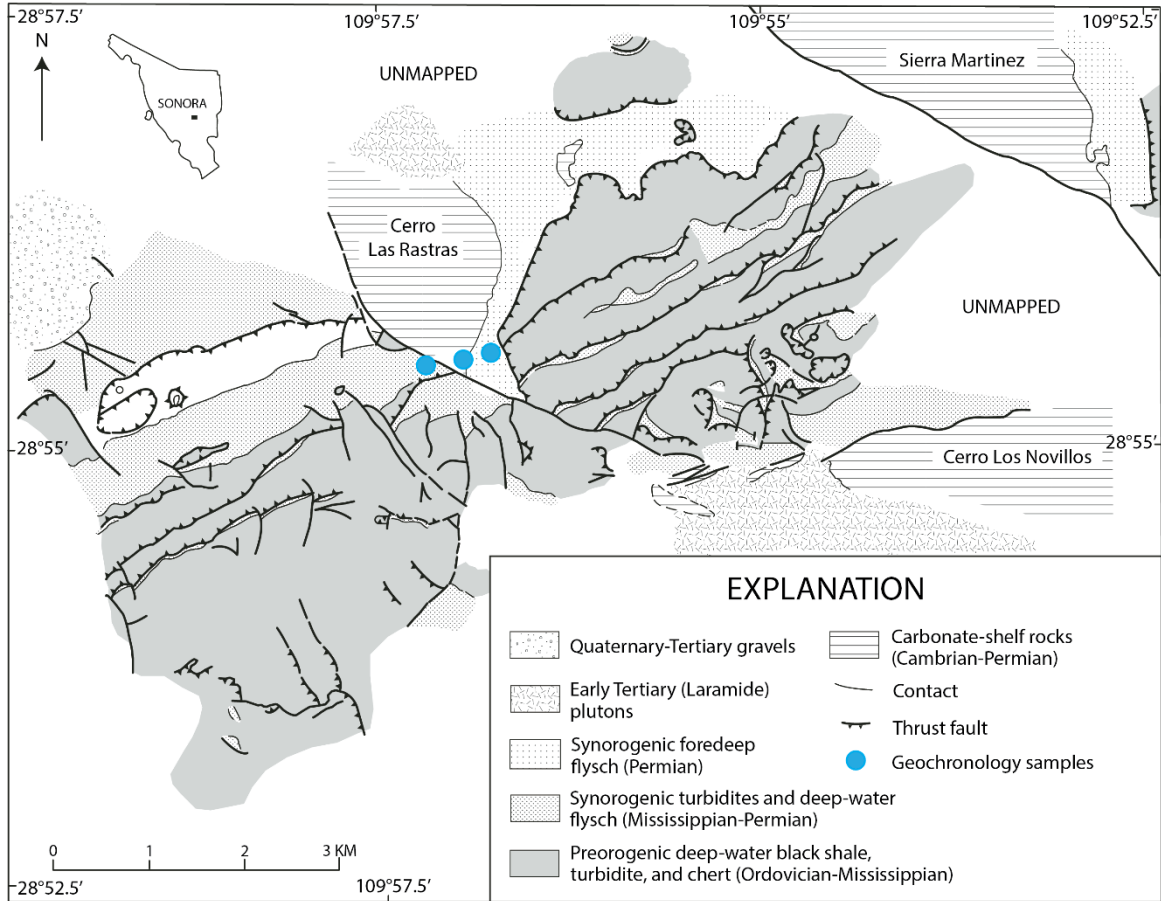
The Mina México Formation was described by Poole et al. (2005, 2008) as approximately 1000 m of turbiditic siltstones, fine sandstones, and sparse turbiditic lime grainstones that represent the lower to middle Permian Mina México foredeep that accumulated in front of the evolving Sonora allochthon on the outer part of the Laurentian continental shelf. The Mina México Formation is a synorogenic turbidite sequence that tectonically underlies part

of the Sonora allochthon strata. The foredeep was formed along the leading edge of the Sonora allochthon and on the outer exposure of the Laurentian continental shelf in response to crustal flexing and isostatic loading.

Initial detrital zircon studies by Gehrels and Stewart (1998) determined provenance of Cambrian to Triassic strata throughout Sonora, Mexico. In central Sonora, they determined that the source of the middle Permian Mina México Formation of the Santa Teresa foredeep was likely recycled Precambrian rocks of the southwestern North America and northernmost Sonora. Poole et al. (2008) presented U-Pb isotopic ages of detrital zircon from Upper Devonian Los Pozos Formation of the Sonora allochthon and middle Permian carbonate sandstone of the Mina México foredeep that established similar ages to the middle Permian Mina México Formation of the Santa Teresa foredeep from Gehrels and Stewart (1998) (Figure 3). Gehrels and Pecha (2014) continued the detrital zircon study of Sonoran strata by Gehrels and Stewart (1998) and Poole et al. (2008) with further U-Pb geochronology and Hf isotope geochemistry. U-Pb ages and  $\epsilon_{\text{Hf}}$  signatures showed that Devonian strata were locally derived from basement provinces that are likely made up of detritus from recycled underlying Cambrian and Neoproterozoic strata. The Permian strata yielded zircon grains with U-Pb ages and  $\epsilon_{\text{Hf}}$  signatures similar to the Mojave-Yavapai-Mazatzal provinces, 1.48-1.34 Ga local basement rocks, the Grenville orogen, or local recycled Devonian strata (Gehrels and Stewart, 1998; Poole et al., 2008; Gehrels and Pecha, 2014).

Stevens et al. (2014) reported fusulinid faunas in Sonora that indicated three depositional settings: off-shelf continental-rise and ocean basin (Sonora allochthon), shallow continental shelf (Laurentian carbonate shelf) and foredeep basin on the continental shelf (Mina México Basin). The Sonora allochthon overlies the middle Permian foredeep deposits of the Mina México basin

and underlies Triassic deposits unaffected by thrusting; allochthon emplacement must have ceased by late Permian time.

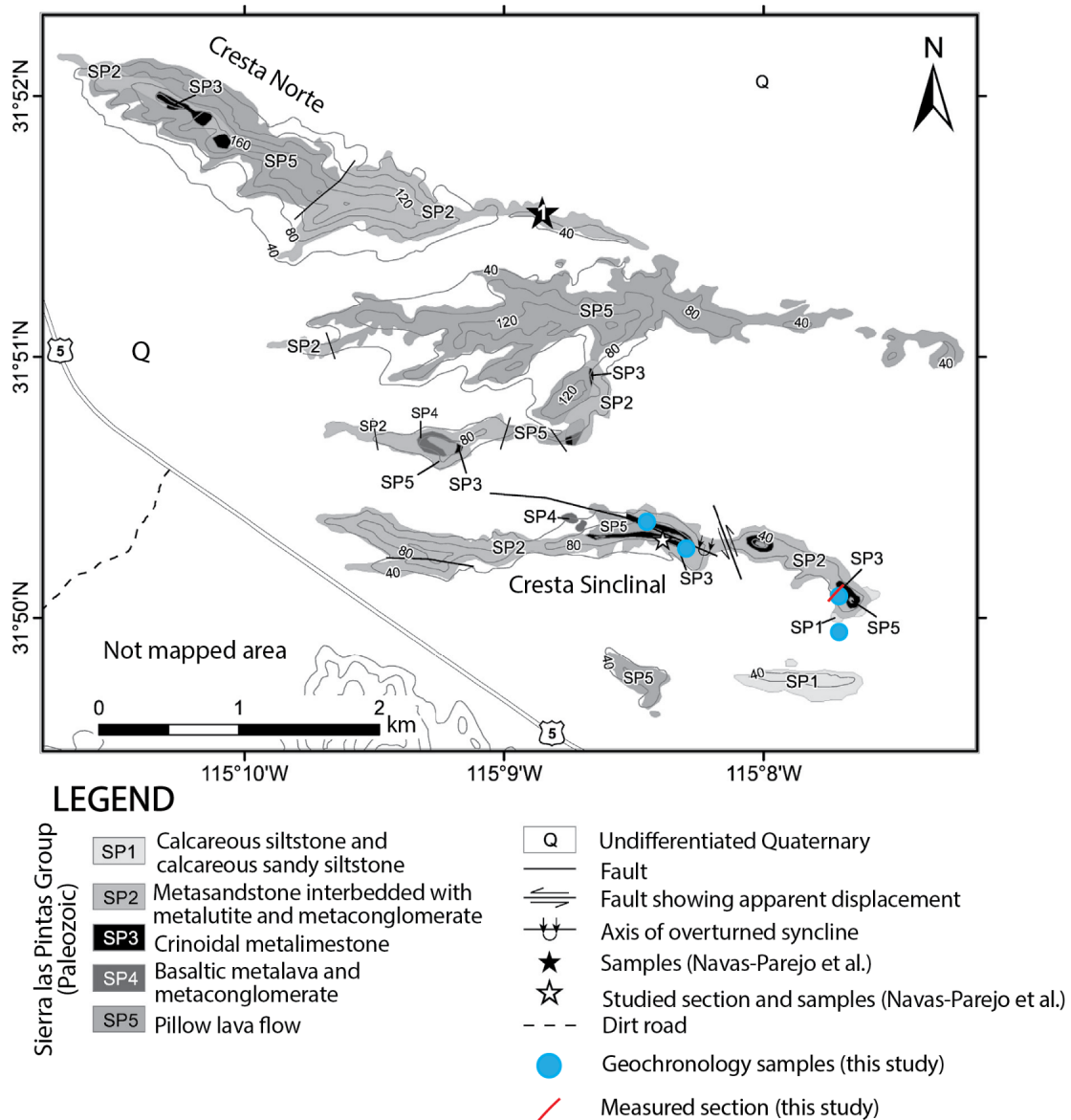


**Figure 5.** Simplified geologic map of the Minas de Barita area (modified from Poole et al., 2008). Location of detrital zircon samples collected for this study are indicated by the circles.

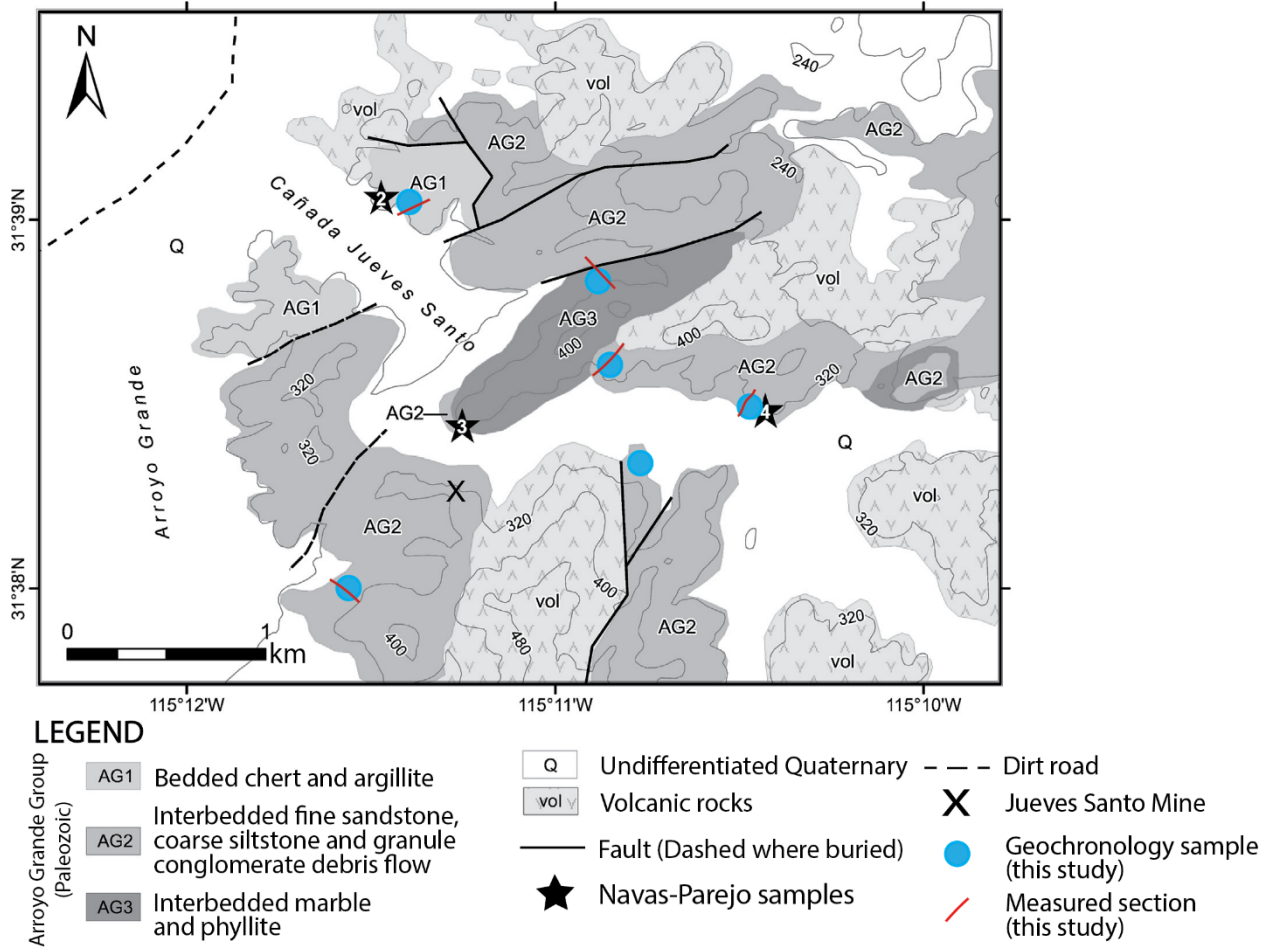
### *Stratigraphy of the Sierra Las Pintas, Baja California*

The Sierra Las Pintas is located within the floodplain of the Colorado River delta in northern Baja California, approximately 110 km south of Mexicali and 60 km north of San Felipe (Figure 2). Leier-Engelhardt (1993) inferred that the strata of the Sierra Las Pintas have undergone varying degrees of metamorphism due to late Paleozoic collision of Gondwana and

Laurentia. The Sierra Las Pintas strata are predominantly low- to high- greenschist-facies metasedimentary rocks that are separated into a northern area defined as the Sierra Las Pintas Group and a southern area referred to as the Arroyo Grande Group (Figure 2, 6-7). Leier-Engelhardt (1986, 1993) presented geologic maps of the northern and southern Sierra Las Pintas that subdivided the rocks into six units of the Sierra Las Pintas Group and four units of the Arroyo Grande Group.



**Figure 6.** Geologic map of the northern Sierra Las Pintas area by Navas-Parejo et al. (2018) including location of measured section and detrital zircon samples from this study.



**Figure 7.** Geologic map of the Arroyo Grande field area by Navas-Parejo et al. (2018) showing detrital zircon sample locations and measured section lines from this study.

### ***Sierra Las Pintas Group***

Leier-Engelhardt (1993) initially mapped and interpreted the strata of the Sierra Las Pintas Group. The Sierra Las Pintas contains four east-west-trending ridges that exhibit increasing metamorphic grade northward. Leier-Engelhardt (1993) inferred that the strata of the

Sierra Las Pintas Group are Carboniferous metasedimentary rocks due to the presence of Carboniferous fossils such as crinoids, solitary corals, and brachiopods (McEldowney, 1970; Leier-Engelhardt, 1986, 1993; Navas-Parejo, 2018). The metasedimentary rocks are overlain by basaltic flows and pillow basalts. Leier-Engelhardt (1993) divided the Sierra Las Pintas Group into six geologic units, SP1-SP6, that were later modified by Navas-Parejo et al. (2018; Figure 6). SP1 is described as bedded finely-laminated siltstone, calcareous siltstone, and calcareous sandstone classified as calcitic and immature lithic arkose. Original textures have been obliterated due to metamorphism that sheared the grains along the long axis, parallel to the east-west-trending ridge. SP2 is a dark-gray subarkosic siltstone, shale, and mudstone interbedded with pale-brown calcareous siltstone. SP2 also contains lenses of crinoidal packstone and granule conglomerate. SP3 is a dark yellowish-orange sandy crinoidal packstone that is considered a marker bed due to the presence of Paleozoic lophophyllid corals, brachiopods, and crinoid ossicles. The packstone is composed of fine sand and crinoid debris within a sparry calcite cement. SP4 is composed of coarsening-upward beds of massive granule, pebble, and cobble conglomerate that contain clasts of siltstone, sandstone, carbonate, and volcanic rock fragments. SP5 is composed of dark-gray pillow breccia at the base, overlying massive basalt flows, minor hyalotuff, and rare pillow basalt. Most of the basalt flow has been metamorphosed to chlorite. An irregular contact, possibly an unconformity, is interpreted between SP4 and SP5. SP6 is composed of bedded chert that has been thoroughly recrystallized and is interbedded with shaly limestone beds with sharp contacts. No known stratigraphic relation is identified between SP6 and other units. Initial geochemical results led to an interpretation that the volcanic rocks were formed in a transitional tectonic setting in regions of extreme continental lithospheric attenuation (Leier-Engelhardt, 1993). Navas-Parejo et al. (2018) suggested that the presence of crinoid fauna

indicates Middle Pennsylvanian to early Permian-age strata in the northern Sierra Las Pintas, which correlate with Paleozoic strata in Sonora, Mexico. Leier-Engelhardt (1993) inferred that Units SP1-SP4 of the northern Sierra Las Pintas were deposited onto a continental slope or at the base of the slope. Navas-Parejo et al. (2018) later interpreted the slope deposits to have been derived from high-grade metamorphic rocks and from a shallow-water platform due to the presence of crinoidal fauna, indicating a crinoid meadow.

### ***Arroyo Grande Group***

Leier-Engelhardt (1993) also completed the initial mapping of the Arroyo Grande Group of the southern Sierra Las Pintas, which was later modified by Navas-Parejo et al. (2018; Figure 6). Leier-Engelhardt (1993) interpreted the strata of the Arroyo Grande Group as Lower Devonian to Lower Mississippian siliciclastic rocks that have undergone greenschist-grade metamorphism, later overprinted by Tertiary hydrothermal alteration. These units contain sedimentary structures that indicate deposition by turbidity currents and the metasedimentary units are overlain by basaltic flows and pillow basalts. Leier-Engelhardt (1993) initially described and divided the strata of the Arroyo Grande Group into subunits AG1-AG4. AG1 is described as gray, rhythmically bedded chert and argillite. Platform-type conodonts identified as *Polygnathus* sp. in the upper part of the sequence led Leier-Engelhardt (1993) to infer a late Early Devonian to Early Mississippian age for the succession. The unexposed base of AG2 is interpreted as a fault between AG1 and AG2. AG2, the thickest and most varied unit, is described as a sequence of coarsening-upward, finely laminated, fine-grained sandstone and mudstone. The entire unit has undergone metamorphism, but some original sedimentary features are preserved. AG3 is highly deformed and mineralized and described as predominantly interbedded marble and phyllite, originally limestone and calcareous shale. Leier-Engelhardt



(1993) inferred that the folding and mineralization noted in unit AG3 was due to post-Miocene faulting. AG3 is interbedded with the calcareous upper part of AG2 and is inferred to have a gradational contact. The contact between AG3 and AG4 is not exposed. AG4 is described as composed of dark-greenish gray pillow basalts and massive basalt flows. This unit shows the greatest hydrothermal alteration of the Arroyo Grande Group. AG4 is described as locally interbedded with AG2. The general stratigraphy of the Arroyo Grande Group shows similarities to strata found in the Sierra Las Pintas Group and has been loosely correlated (Leier-Engelhardt et al., 1993; Poole et al., 2005; 2008; Navas-Parejo et al., 2018; Figure 2).

## **2.0 METHODS**

### **2.1 FIELD METHODS**

This study tests the hypothesis that correlation can be made between inferred strata of the Sonora allochthon of central Sonora and Baja California, as well as provide evidence of Gondwanan provenance through extensive geochronologic analysis. Samples were collected from the proposed Sonora allochthon strata of the Minas de Barita area in Sonora, Mexico, the Sierra Las Pintas Group and the Arroyo Grande Group of Baja California, Mexico (Figure 1). Field characteristics were noted and samples were collected for detrital zircon geochronology and petrographic analysis from each of these areas. A total of 14 samples were collected for detrital zircon U-Pb dating and trace element analysis (Table 1). Each sample weighed approximately 10 kg and was collected from the coarsest grain bed within the unit. A total of 18 hand samples were also collected for petrographic analysis throughout each of the field areas (Table 1).

In Baja California, field work was conducted in the Arroyo Grande Group and Sierra Las Pintas Group in January 2020. Significant differences were noted in the geology of the Arroyo Grande Group from previous work and five new units were defined. Table 2 lists updated unit names with corresponding original unit names as described by Leier-Engelhardt (1993). Samples were collected from each unit, eight for detrital zircon geochronology and 16 for petrographic analysis (Figure 6; Table 1). Due to the pervasive folding and metamorphism of the strata, sedimentary structures are not well preserved in the area and stratigraphic sections do not depict lateral continuity. Stratigraphic sections were measured using a meter stick, Brunton compass, and a handheld GPS device along locations where detrital zircon samples were collected.

In the Sierra Las Pintas Group, two samples were collected for geochronologic analysis as well as hand samples for petrographic analysis (Figure 7). A stratigraphic section was measured at the collection of sample LP110120-1. A previous reconnaissance study in 2019 included collection of two other samples by committee members Dr. Nancy Riggs and Dr. Pilar Navas-Parejo for detrital zircon geochronology that were analyzed for this study (Table 1).

In Sonora, Mexico, eight samples were collected for detrital zircon geochronology by committee members Dr. Pilar Navas-Parejo and Dr. Michelangelo Martini from the Sonora allochthon of the Minas de Barita area. Samples were taken from the Mina México and Rancho Nuevo Formations. Unfortunately, only three of the samples contained sufficient zircon for analysis (Table 1).

Field Area	Sample Name	Unit	GPS Location	Purpose	# of Zircon
Arroyo Grande Group	LP070120-1	1	31°38'55.85" N, 115°11'21.21" W	DZ	180
	LP070120-2	2	31°38'45.89" N, 115°11'01.51" W	DZ	180
	LP080120-1	3	31°38'34.05" N, 115°10'53.20" W	DZ + TS	50
	LP080120-2	3	31°38'32.62" N, 115°10'53.04" W	TS	
	LP080120-3	3	31°38'32.62" N, 115°10'53.04" W	TS	
	LP080120-4	3	31°38'30.95" N, 115°10'52.01" W	TS	
	LP080120-5	3	31°38'30.95" N, 115°10'52.01" W	TS	
	LP080120-6	3	31°38'30.95" N, 115°10'52.01" W	TS	
	LP080120-8	3	31°38'27.53" N, 115°10'28.99" W	DZ + TS	180
	LP080120-9	3	31°38'27.53" N, 115°10'28.99" W	DZ + TS	180
	LP090120-1	3	31°38'17.76" N, 115°11' 34.12" W	TS	
	LP090120-2	4	31°38'09.22" N, 115°11,16.61" W	DZ + TS	180
	LP090120-3	4	31°38'09.22" N, 115°11,16.61" W	DZ + TS	180
	LP120120-1	3	31°38'22.64" N, 115°11'24.43" W	TS	
	LP120120-2	3	31°38'12.18" N, 115°11'47.82" W	TS	
	LP130120-1	3	31°38'23.7"N, 115°10'47.04" W	DZ	15
	LP130120-2	5	31°38' 23.31" N 115°10' 44.40" W	TS	
	LP140120-1	3	31°38'20.64" N, 115°10'30.06" W	TS	
	LP140120-2	3	31°38'20.4" N, 115°10'25.98" W	TS	
	Sierra Las Pintas Group	LP100120-1	SP1	31°49'56.77" N, 115°07'44.35" W	DZ + TS
LP110120-1		SP2	31° 50'2.71" N, 115°07'43.73" W	DZ	180
LP110120-2		SP2	31° 50'2.71" N, 115°07'43.73" W	TS	
18-LP-10		SP2	31°50'09.66" N, 115°08'16.57" W	DZ	155
X181218		SP4	31° 50' 18.25", 115° 8' 22.33" W	DZ	19
Minas de Barita Area	13-11-SR2	Rancho Nuevo Fm	28°55'27.26" N, 109°57'02.97" W	DZ	74
	12-11-SR2	Mina México Fm	28°55'39.22" N, 109°56'55.17" W	DZ	90
	13-11-SR3 A+B	Mina México Fm	28°55'57.15" N, 109°56'37.19" W	DZ	72

**Table 1.** Sample names, formations, units, GPS locations, purpose of collection and amount of zircon processed. TS = thin section; DZ = detrital zircon; Fm = formation.

Arroyo Grande Group Unit Names		
This Study	Leier-Engelhardt (1993)	
Unit 5	vol	
Unit 4	AG2	
Unit 3		AG3
Unit 2		
Unit 1	AG1	

**Table 2.** Updated unit names for Arroyo Grande Group and corresponding original unit names by Leier-Engelhardt (1993).

## 2.2 LABORATORY METHODS

### *Petrography*

A total of 17 thin sections were created for petrographic analysis from the Arroyo Grande Group and two from the Sierra Las Pintas Group of Baja California (Table 1). The large quantity of samples collected from Unit 3 of the Arroyo Grande Group was intended to track any changes moving upsection. Thin sections were analyzed using an Olympus petrographic microscope. Due to the pervasive metamorphism of the rocks, original individual minerals could not be identified

and point counting was not possible. Petrographic analysis was used to aid in determining the primary composition of the samples and support provenance analyses.

### ***Zircon U-Pb Geochronology***

Zircon is a common accessory mineral found in igneous, metamorphic, and sedimentary rocks. Zircon forms by crystallization in a magmatic or metamorphic setting and can retain its crystallization age, regardless of weathering or erosion (Cawood et al., 2012). Zircon grains are highly resistant to physical abrasion and chemical breakdown and are preserved as detrital zircon in sedimentary deposits. The crystals have a high closure temperature of  $>900$  °C (Davis et al., 2003). The resistant nature of zircon allows for preservation of original U and accumulated radiogenic Pb contents in the zircon grain, even through reheating events (Barth et al., 2013). Zircon is typically dated using the U-Pb decay scheme in which  $^{238}\text{U}$  decays to  $^{206}\text{Pb}$  with a half-life of 4.47 Ga, and  $^{235}\text{U}$  decays to  $^{207}\text{Pb}$  with a half-life of 710 Ma. The uranium-lead ratios from both decay systems can be used to determine the age of the zircon grain.

Analysis of detrital zircon that have accumulated in sedimentary rocks provides a range of ages and populations that reflects various suites of recycled magmatic material that have been incorporated into the sedimentary package (Gehrels, 2012). The youngest suite of statistically valid zircon ages found within a sedimentary package provides an estimate of maximum depositional age (MDA). The various populations of zircon ages within a sedimentary deposit can provide insight to the provenance of a rock and can be utilized along with maximum depositional ages to reconstruct the tectonic setting of a sedimentary unit on a regional scale.

All zircon samples collected for this study were processed in the mineral separation lab at Northern Arizona University, following standard zircon extraction procedures (Gehrels, 2000). Each sample was passed through the jaw crusher and roller mill, then filtered through a 500- $\mu\text{m}$

sieve. Grains less than 500  $\mu\text{m}$  were run across a Gemeni water table, which separates the sample into light, medium, and heavy fractions based on the density of the grains. Zircon grains would be expected in the heavy fraction based on its higher density. The heavy fraction was passed through a Frantz magnetic separator, which divides the sample at increasing intervals up to 1 ampere to extract all magnetic minerals. The remaining non-magnetic sample was passed through methylene iodide ( $\rho = 3.32 \text{ g/cm}^3$ ) and stirred to allow the denser minerals, such as zircon, to sink to the bottom of the liquid. The minerals were then rinsed in acetone and dried under a heat lamp. Finally, the remainder of the processed sample was examined under a light microscope to separate out individual zircon crystals.

When selecting detrital zircon grains for analysis, 150-200 grains were selected randomly per sample and no preference was given shape or size of zircon, to adhere to standard zircon provenance study practices (Gehrels, 2012). For samples that did not contain 150-200 zircon grains, all zircon grains were selected for analysis. Selected grains were secured on double sided tape, fixed within a 1-inch diameter puck, epoxied and polished to expose the interior of the grains. Once mounted, zircon grains from the Sierra Las Pintas Group and Arroyo Grande Group samples were then analyzed for U-Th-Pb and trace element concentrations at the University of California Santa Barbara (UCSB) laser-ablation split-stream petrochronology lab by Dr. Andrew Kylander-Clark. Mounted zircon grains from the Minas de Barita samples were analyzed by Dr. Luigi Solari at Laboratorio de Estudios Isotópicos del Centro de Geociencias of the Universidad Nacional Autónoma de México (LEI).

Analysis was done using a Photon Machines 193 nm excimer laser with a HeLex sample cell at a 25- $\mu\text{m}$  beam coupled to a Nu Instruments Plasma high-resolution multi-collector inductively-coupled plasma mass spectrometer (HR-MC-ICP-MS) for U and Pb isotope analysis

and an Agilent 7700x quadrupole inductively coupled plasma mass spectrometer (ICP-MS) for measurement of trace element concentrations. U-Pb and trace element analyses in August 2021 were calibrated using the primary standard Plesovice ( $337.71 \pm 0.37$  Ma; Sláma et al., 2008) every 10 grains, and alternating secondary standards 91500 ( $1062.4 \pm 0.4$  Ma; Wiedenbeck et al., 1995) GJ-1 ( $601.9 \pm 0.7$  Ma; Horstwood et al., 2016), and Piexé (564 Ma; Dickinson and Gehrels, 2003). Each run began with four to six measurements of Mali and four of the glass standard NIST-612; most runs ended with one-two NIST grains. The values of the standard were within 1-2% of the published values and error assessment of the data follows Kylander-Clark et al. (2013). U-Pb and trace element analyses were obtained simultaneously to ensure that the same growth zones were sampled within each zircon crystal. The data were reduced using the software package Iolite 2.5 in WaveMetrics IgorPro 6.37. Grains older than 90 Ma that were calculated to be discordant by >15% or reversely discordant by >5% were discarded. Grains with an uncertainty > 10% of the age are also not reported in the discussion. Reported ages for grains younger than approximately 1.0 Ga are  $^{206}\text{Pb}/^{238}\text{U}$  ages. Grains older than approximately 1.0 Ga (or after a significant age gap in the data) report  $^{207}\text{Pb}/^{206}\text{U}$  ages for the zircon grains. All analytical data can be found in Supplemental Table 1.

### ***Graphical Displays***

The populations of zircon ages for each sample are displayed using a traditional histogram with age in Ma along the x-axis and the numbers of grains for each bin, or age grouping, along the y-axis using Kernel Density Estimation (KDE) plots and Probability Density Plots (PDPs). KDE plots group the ages of all zircon grains in a sample into bins and show the dominant age populations for the sample (Vermeesch, 2018). Probability density functions are a statistical measure that suggests the likely outcome of a value, or in terms of geochronology

analysis, the age of the zircon. Probability density plots provide a visualization of the probability density of zircon ages for a sample, but there is criticism that PDPs lack theoretical basis as a probability density estimator (Vermeesch, 2012). The PDP can be overlain on a KDE plot to provide the probability density of grains. The major age peaks determined from the analysis can be compared to known source areas to determine the provenance of the sample. Plots for this study were created using IsoplotR (Vermeesch, 2018). Kernel and histogram bandwidths of 40 were used for the plots.

Other plots used for analysis include concordia diagrams and weighted mean plots. By plotting the two decay systems of a zircon against one another, a 'concordia' curve is created. Grains that plot off the concordia curve are considered discordant and could have been affected by hydrothermal alteration or metamorphism that causes lead loss or inheritance of uranium. Weighted mean plots are used to highlight a set of ages for a sample by calculating the weighted mean age. This plot weights each measurement by its uncertainty and can be utilized to represent a relevant population of ages, such as the youngest spectrum of zircon for a sample. The mean square of weighted deviates (MSWD) is also calculated to evaluate the likelihood that a set of zircon are related and reflect the same source. MSWD is determined by comparing the scatter of ages against their uncertainty. A MSWD value of one or less can be considered a sufficient fit to explain the scatter of ages compared to uncertainty and it is reasonable to assume the grains are related. A MSWD value of greater than one means that the uncertainty is not sufficient to explain the scatter of ages and the grains are likely not related.

By utilizing each of these plots, a maximum depositional age (MDA) for a sample can be determined. PDPs are the simplest method used to estimate MDA as the largest population of youngest ages for a sample, or peak in age probability, is a reasonable estimation for the MDA.



When the largest population of youngest grains from a PDP plot is coupled with the weighted mean plot and associated MSWD containing a value close to 1, the likelihood that the set of ages are coeval can be evaluated and a reliable MDA for the sample can be determined (Dickinson et al., 2009; Dobbs, 2017; Lodes, 2019).

### ***Zircon Trace Element Geochemistry***

Trace element geochemistry in conjunction with geochronologic analysis provides information about the host magma environment, variations in melt compositions, and can be used to further understand the evolution of an arc (Hoskin and Schaltegger, 2003; Grimes et al., 2007; Barth et al., 2013; Van Lankvelt, 2016). Although concentrations of trace elements such as U, Th, Y, and REEs can vary significantly within zircon suites, trace element ratios can show systematic variation and can be used to interpret source rock provenance (Grimes et al., 2007; Barth et al., 2013). For this study, four geochemical plots U vs Yb, Hf vs U/Yb, Th/U vs age, and Yd/Gd vs age were used to further understand source rock provenance. Th/U and Yb/Gd ratios can provide insight to the composition of the host. Th/U ratios can also help discriminate between metamorphic and magmatic zircon as ratios for magmatic zircon (0.2-4) are typically much higher than metamorphic zircon (<0.07) (Rubatto, 2002; Grimes et al., 2015; Kirkland et al., 2015; Van Lankvelt et al., 2016). U vs Yb and Hf vs U/Yb ratios are used to discriminate zircon that crystallized in oceanic or continental crustal settings (Grimes et al., 2007, 2011; Barth et al., 2013; Kirkland et al., 2015). U vs Yb and Hf vs U/Yb geochemical diagrams created for this study use continental vs oceanic signature discrimination based on established fields from Grimes et al., (2007).

## **3.0 RESULTS**

### **3.1 LITHOLOGY, STRATIGRAPHY, AND PETROGRAPHY**

The field areas investigated for this study are the Arroyo Grande Group, the Sierra Las Pintas Group, and Minas de Barita area. Field observations for each unit from the three field areas are summarized in Table 3 and results of petrographic analysis are summarized in Table 4. Detailed descriptions of each unit are presented here, along with stratigraphic columns for each unit, outcrop photographs and photomicrographs (Figures 10-27). An updated detailed geologic map was created for the Arroyo Grande Group, including redefined units from previous literature (Figure 8; Table 2).

Field Area	Unit	Lithology	Color	Grain size	Sorting	Sedimentary structures	Clasts
AGG	1	Radiolarian chert; metashale; metasiltstone	Dark gray - brown; light gray; gray	vf - f	Well sorted	Slumping, parallel laminations, pinching out of layers, convolute bedding	Siltstone intraclast, mud rip-up clasts
AGG	2	Met limestone; metashale; metasiltstone; diagenetic chert	Light gray - tan; tan to gray; light gray; black	vf - f	Well sorted	Slumping, flame structure, convolute bedding, parallel laminations	N/A
AGG	3	Siliciclastic metasandstone; volcaniclastic metasandstone; metasiltstone	Tan - dark brown; light green; light gray	vf - c	Moderate to well sorted	Cross-bedding, parallel laminations, coarsening upward, boudinage	N/A
AGG	4	Metaconglomerate; metashale; metasiltstone; metasandstone;	Dark brown - purple; light gray - light brown; light gray - brown; light brown - dark brown	vf - c	Poor to moderate	Slumping, parallel laminations, sheared clasts	Chert, shale, sandstone, siltstone, limestone
AGG	5	Felsic dikes; Miocene volcanics	Light orange, light tan, pink	N/A	N/A	N/A	N/A
SLP	SP1	Metasandstone; calcareous metashale; metasiltstone	Tan - light orange; light to dark brown; light brown	vf - f	Well sorted	Parallel laminations	N/A
SLP	SP2	Metasandstone; metashale; metaconglomerate	Light brown - orange; dark brown; tan	f - c	Moderate to well sorted	Parallel laminations, ripple-cross laminations	Crinoids, quartz, plagioclase
SLP	SP4	Basaltic metalava; metaconglomerate	Black, light brown	N/A	N/A	N/A	N/A
MB	Rancho Nuevo Fm	Calcareous sandstone; shale; chert	N/A	N/A	Moderate to poorly sorted	Fining upward sequences, cross laminations, parallel laminations, massive to inverse grading	Skeletal and mudstone intraclasts, extraclasts of chert, calcareous and non-calcareous shale
MB	Mina México Fm	Siliciclastic sandstone; siltstone; conglomerate	Tan - light brown; light gray - blue; light brown	N/A	Moderate to poorly sorted	Parallel laminations, ripple-cross laminations, inverse grading, soft-sediment deformation, syn-sedimentary faults	Skeletal intraclasts, ichnofossils

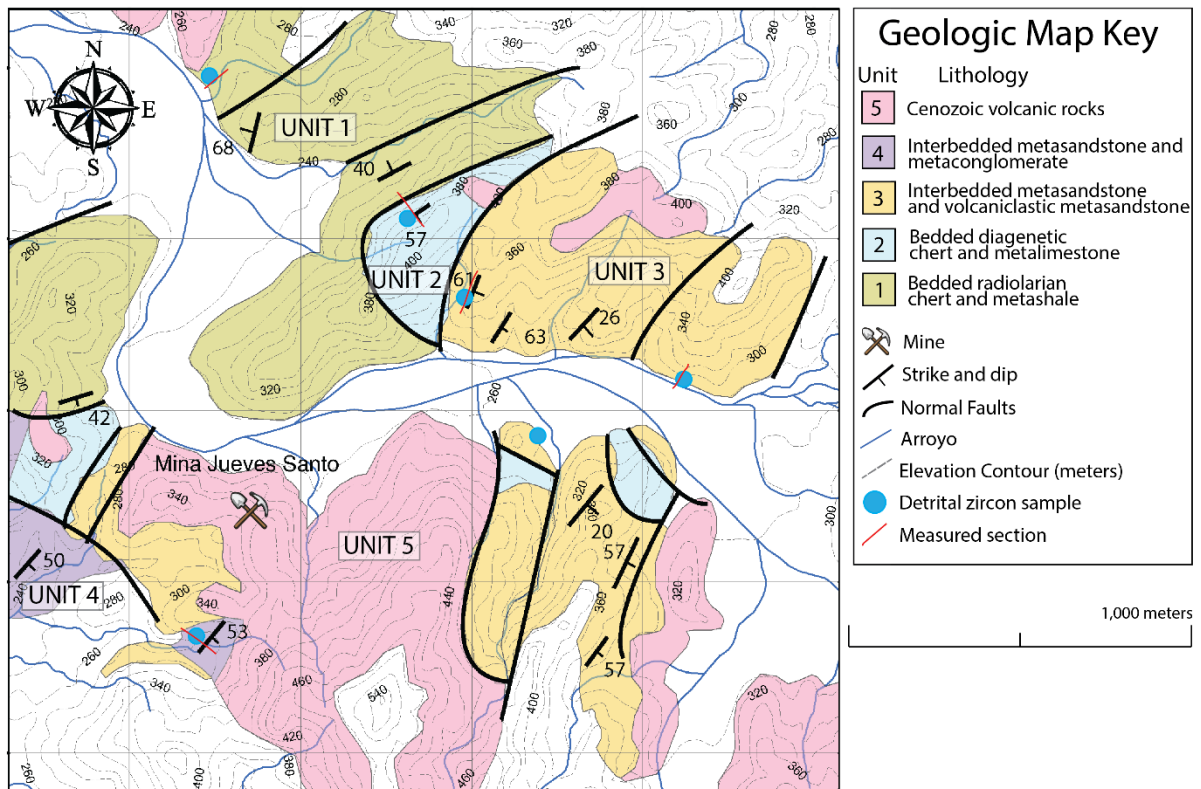
**Table 3.** Summary of units and descriptions from field observations in the Arroyo Grande Group (AGG), Sierra Las Pintas Group (SLP), and Minas de Barita (MB) area. Grain size abbreviations: vf = very fine, f = fine, c = coarse.

Sample name	Lithology	Formation	Unit	Composition
LP080120-1	Volcaniclastic siltstone	AGG	3	50% fine-grained plagioclase feldspar, carlsbad twinning; 35% amphibole, locally replaced; 10% other; 5% oxides
LP080120-2	Very fine-grained volcaniclastic sandstone	AGG	3	50% very fine-grained plagioclase feldspar, carlsbad and albite twinning, sericitization; 35% amphibole, locally replaced; 10% other; 5% calcite veins
LP080120-3	Fine-grained volcaniclastic sandstone	AGG	3	15% plagioclase feldspar phenocryst, carlsbad and albite twinning, sericitization; 35% fine-grained plagioclase feldspar; 45% actinolite, locally replaced; 5% oxide
LP080120-4	Very-fine to fine-grained siliciclastic siltstone	AGG	3	80% well-sorted, fine- to very fine-grained quartz; 15% amphibole, locally replaced; 3% calcite veins; 2% oxides
LP080120-5	Fine-grained volcaniclastic sandstone	AGG	3	40% fine-grained plagioclase feldspar, carlsbad twinning; 35% tremolite, locally replaced; 15% oxides
LP080120-6	Fine-grained volcaniclastic siltstone	AGG	3	65% poorly-sorted, fine-grained plagioclase feldspar; 30% plagioclase feldspar phenocrysts, sericitization; 5% calcite veins
LP080120-8	Coarse-grained siliciclastic sandstone	AGG	3	67% very well-sorted, coarse-grained quartz, undulatory extinction; 25% fine-grained plagioclase feldspar, albite twinning; 5% tremolite; 3% calcite veins
LP080120-9	Coarse-grained volcaniclastic sandstone	AGG	3	45% coarse-grained, relict plagioclase feldspar, sericitization; 50% tremolite, locally replaced; 5% oxides
LP090120-1	Coarse-grained volcaniclastic sandstone	AGG	3	50% poorly-sorted, coarse-grained plagioclase feldspar, albite and carlsbad twinning; 20% tremolite, locally replaced; 3% oxide; volcanic lithic matrix, sericitization
LP120120-1	Coarse-grained volcaniclastic sandstone	AGG	3	40% coarse-grained plagioclase feldspar, albite and carlsbad twinning; 20% volcanic lithic fragments, 15% tremolite, locally replaced; 10% hematite cement, 5% oxides
LP120120-2	Fine-grained volcaniclastic sandstone	AGG	3	45% well-sorted, fine-grained feldspathic matrix; 30% tremolite, locally replaced; 20% fine-grained quartz, undulatory extinction; 5% volcanic lithic fragments
LP130120-1	Coarse-grained volcaniclastic sandstone	AGG	3	50% coarse-grained plagioclase feldspar, albite twinning; 25% tremolite, locally replaced; 18% volcanic lithic fragments; 5% calcite; 2% oxides
LP140120-1	Coarse-grained volcaniclastic sandstone	AGG	3	55% coarse-grained plagioclase feldspar, albite twinning, sericitization; 30% tremolite, locally replaced; 12% volcanic lithic fragments; 3% oxides
LP140120-2	Coarse-grained siliciclastic sandstone	AGG	3	85% very well-sorted quartz (60% coarse-grained, 40% very fine-grained), undulatory extinction; 10% volcanic lithic fragments; 5% muscovite mica
LP090120-2	Sandstone lens in conglomerate	AGG	4	70% very well-sorted quartz (30% coarse-grained, 70% very fine-grained), undulatory extinction; 20% micaceous matrix, 5% tremolite, 5% oxides
LP090120-3	Conglomerate with shale, siltstone, and chert clasts	AGG	4	50% poorly-sorted, fine-grained quartz, undulatory extinction; 25% micaceous and very fine-grained quartz matrix; 15% chert clasts, sheared; 5% sedimentary lithic fragments, sheared; 5% volcanoclastic lithic fragments
LP130120-2	Volcanic dike	AGG	5	60% coarse-grained plagioclase feldspar, albite twinning, sericitization; 20% tremolite, locally replaced; 10% volcanic lithic fragments; 5% oxides; 5% hematite cement
LP100120-1	Very fine-grained sandstone	SLP	SP1	60% well-sorted quartz (20% coarse-grained, 80% very fine-grained), undulatory extinction; 32% micaceous matrix; 5% tremolite, locally replaced; 2% oxides, 1% very fine-grained plagioclase feldspar, albite twinning
LP110120-2	Very coarse-grained sandstone	SLP	SP2	45% well-sorted quartz (80% very coarse-grained, 20% fine-grained), undulatory extinction, rare myrmekitic intergrowth; 30% calcite; 14% micaceous matrix; 10% tremolite, locally replaced; 1% very fine-grained plagioclase feldspar, carlsbad twinning

**Table 4.** Summary of petrographic analysis for all thin sections collected from Arroyo Grande Group (AGG) and Sierra Las Pintas Group (SLP). Composition estimations determined based on Journal of Sedimentary Petrography estimation comparison chart (Folk, 1951).

### 3.1.1 ARROYO GRANDE GROUP

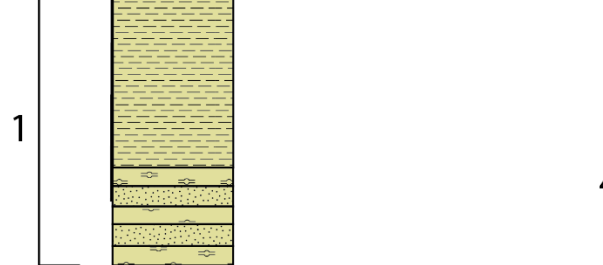
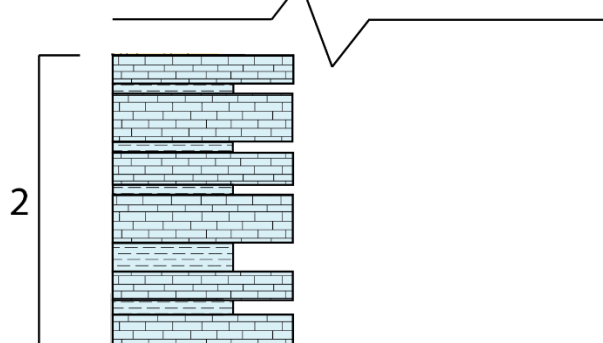
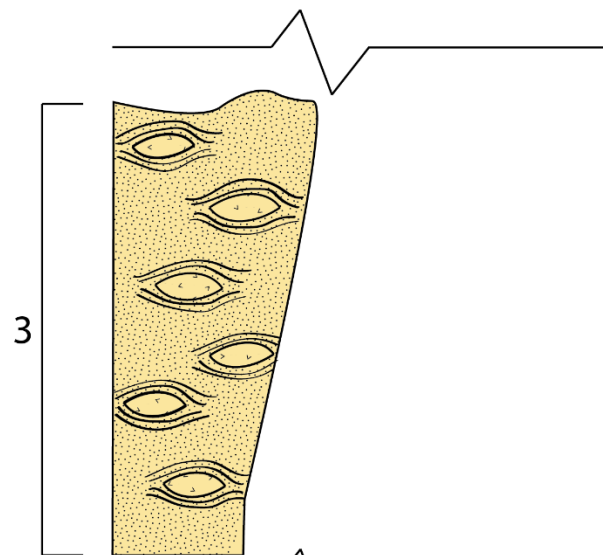
The units of the Arroyo Grande Group are (1) bedded radiolarian chert and metashale, (2) bedded diagenetic chert and metalimestone, (3) interbedded siliciclastic metasandstone, volcaniclastic metasandstone, and metashale (4) interbedded metasandstone, metaconglomerate and metashale, and (5) volcanic rocks (Figures 8-9). The total thickness of the Arroyo Grande Group and its individual units is unknown due to structural complications and prevalent folding.



**Figure 8.** Geologic map of the Arroyo Grande Group showing detrital zircon sample locations and measured section lines. Geologic map (H. Morales, in prep.) created with M. Martini, H. Morales, and P. Navas-Parejo.


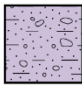
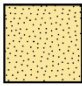
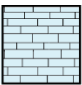
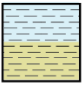
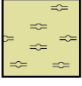


# Generalized Stratigraphic Section

Units



Sh | vf | f | m | c | g | p | c

### Key

-  Miocene Volcanic rocks
-  Metaconglomerate
-  Siliciclastic Metasandstone
-  Metalimestone
-  Cherty Metashale
-  Radiolarian Chert
-  Volcaniclastic Metasandstone
-  Metashale laminations

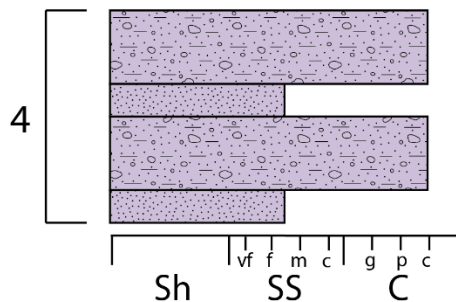
Sh: Metashale

SS: Metasandstone

vf: very fine  
f: fine  
m: medium  
c: coarse

C: Metaconglomerate

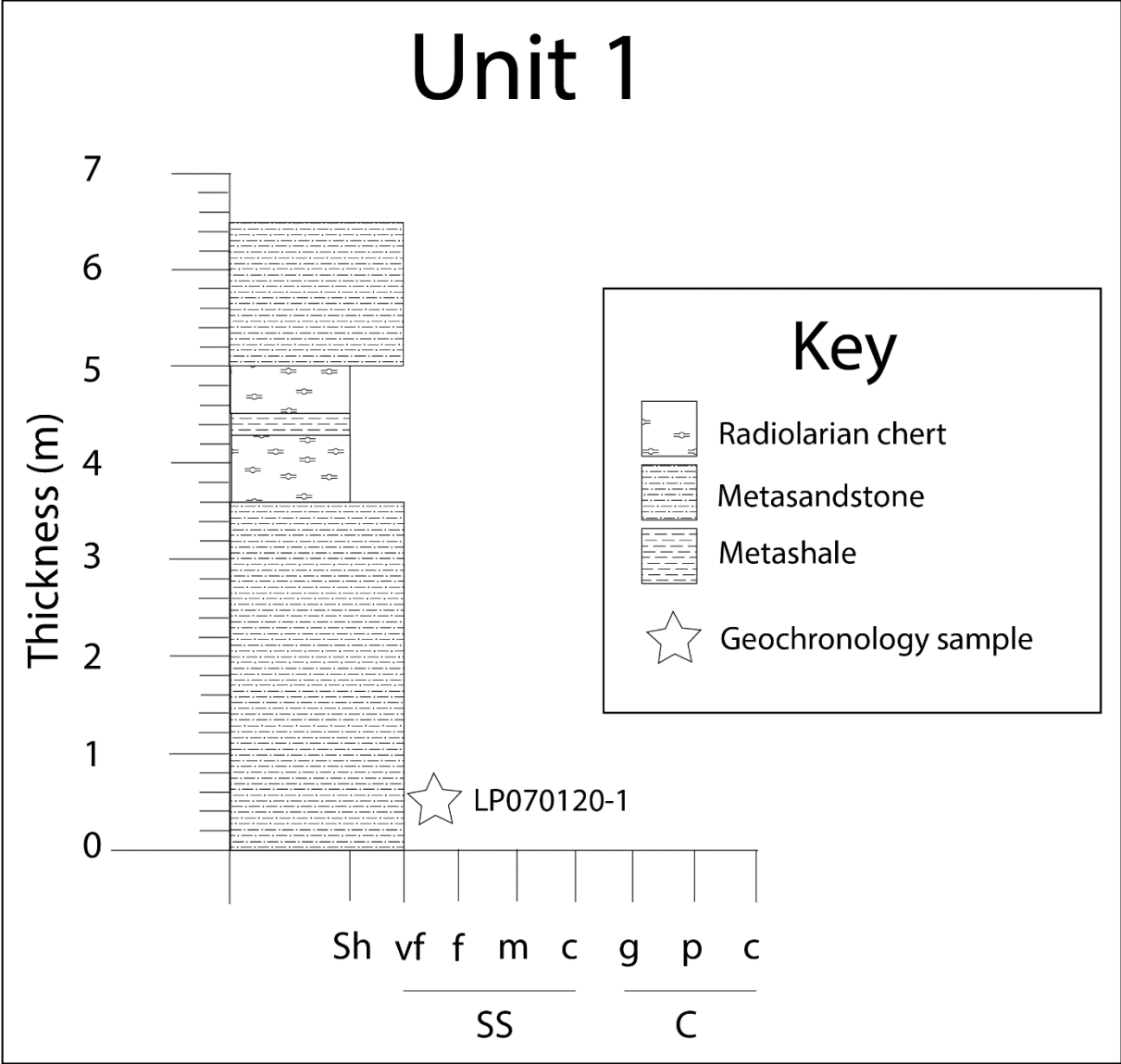
g: granule  
p: pebble  
c: cobble



**Figure 9.** Generalized stratigraphic section for all the units of the Arroyo Grande Group assuming strata are upright and young to the east. There is a fault contact between Units 2 and 3 and the stratigraphic relation between Unit 4 and other units is unknown. Grain-size subdivisions indicated along the x-axis (Sh - metashale, SS - metasandstone, vf – very fine, f - fine, m - medium, c - coarse, C - metaconglomerate, g - granular, p - pebble, c - cobble).

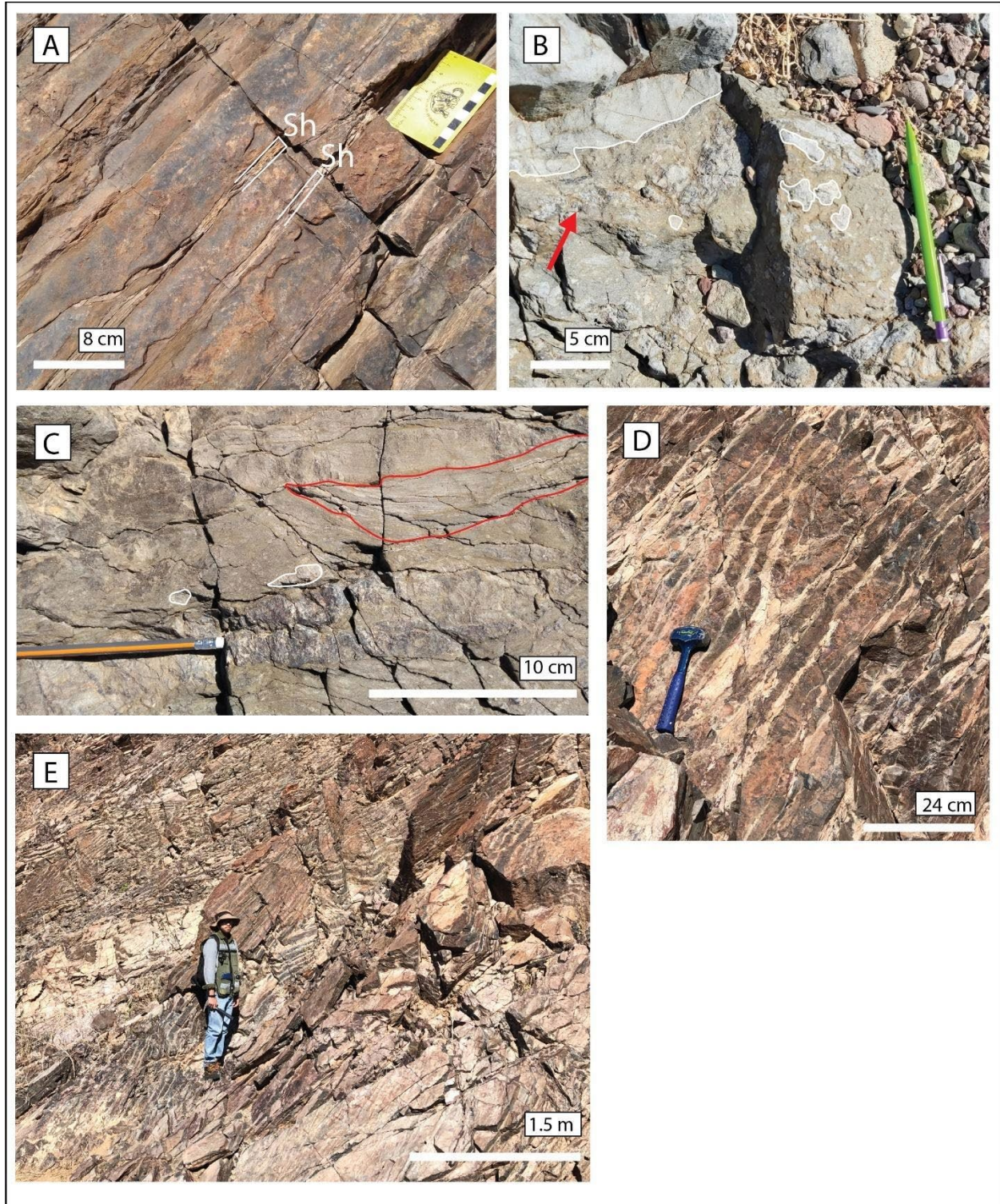
### ***Unit 1 outcrop observations***

Unit 1 is dark-brown to dark-gray radiolarian chert interbedded with light-gray to tan, fine-grained, siliciclastic metashale and metasandstone packages (Figure 10). The base of Unit 1 contains pervasive isoclinal folds (Figure 11D-E). The base of this unit is faulted against younger volcanic rocks. Radiolarian chert layers are typically 5-10 cm in thickness and alternate with 1-3-cm metashale beds (Figure 11A). Soft-sediment-deformation structures, slumping, sediment shearing, parallel laminations, syn-sedimentary faults and folds, and pinching out of very fine-grained metasandstone layers are common in the metashale layers (Figure 11B-C). Fine-grained metashale layers contain intraclasts of very fine-grained metasandstone (Figure 11B-C). The contact with Unit 2 is gradational as Unit 1 transitions into interbedded cherty metashale and metalimestone of Unit 2. Detrital zircon sample LP070120-1 was collected from the base of this unit; no thin sections were created (Figure 8).



**Figure 10.** Measured stratigraphic section of Unit 1. Grain-size subdivisions indicated along the x-axis (Sh - metashale, SS - metasandstone, vf – very fine, f - fine, m - medium, c - coarse, C - metaconglomerate, g - granular, p - pebble, c - cobble).



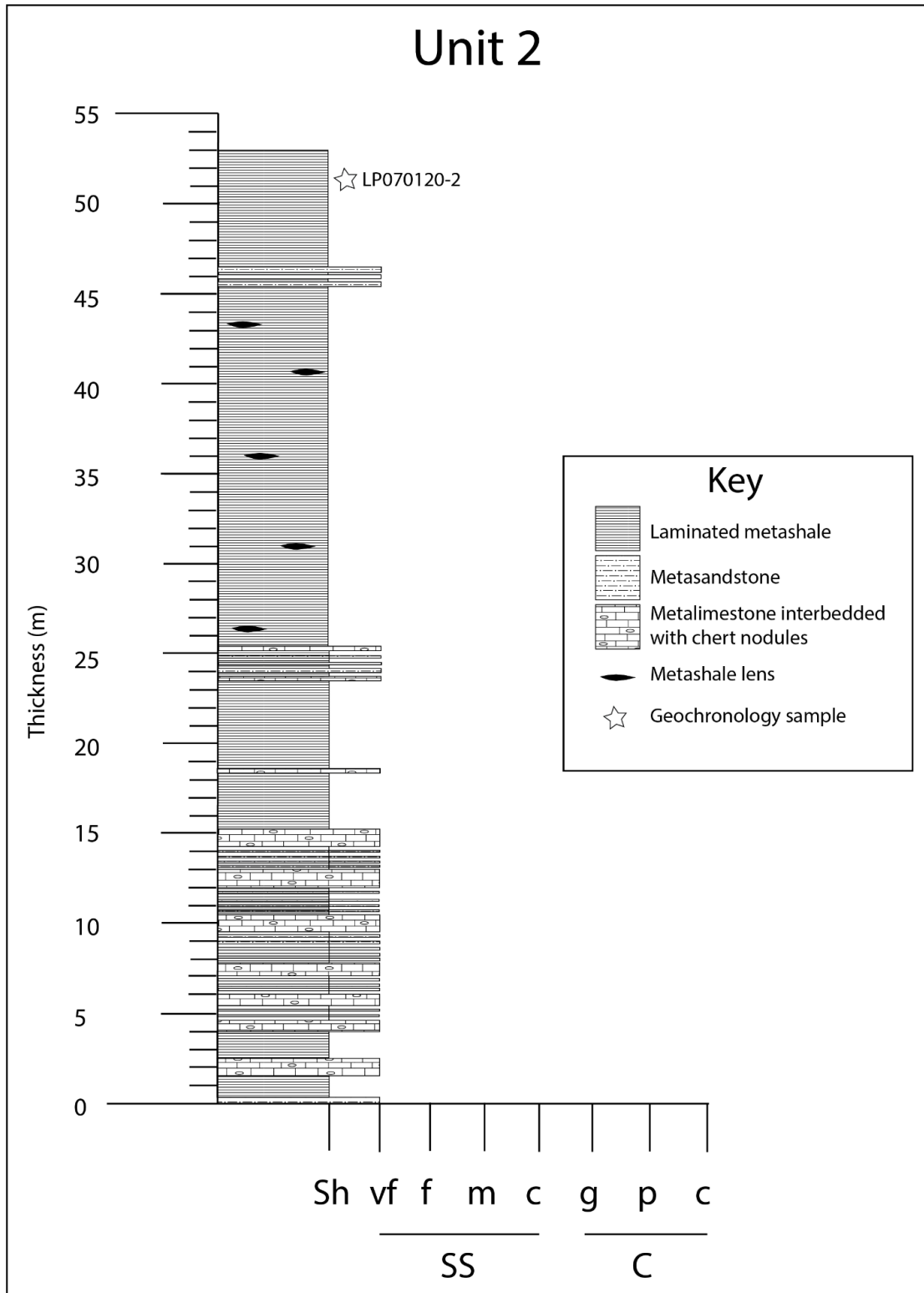


**Figure 11.** Outcrop photographs of Unit 1: **(A)** Alternating dark brown radiolarian chert (8-10 cm) and thin, parallel-laminated, gray metashale (Sh) layers (1-3 cm). Photo by P. Navas-Parejo. **(B)** Soft-sediment-deformation structures (red arrow) with rip-up clasts of metashale (outlined in white). Pencil approximately 14.5 cm. Photo by M. Martini. **(C)** Radiolarian chert with rip-up clasts (outlined in white) and beds of metashale containing parallel laminations that pinch out

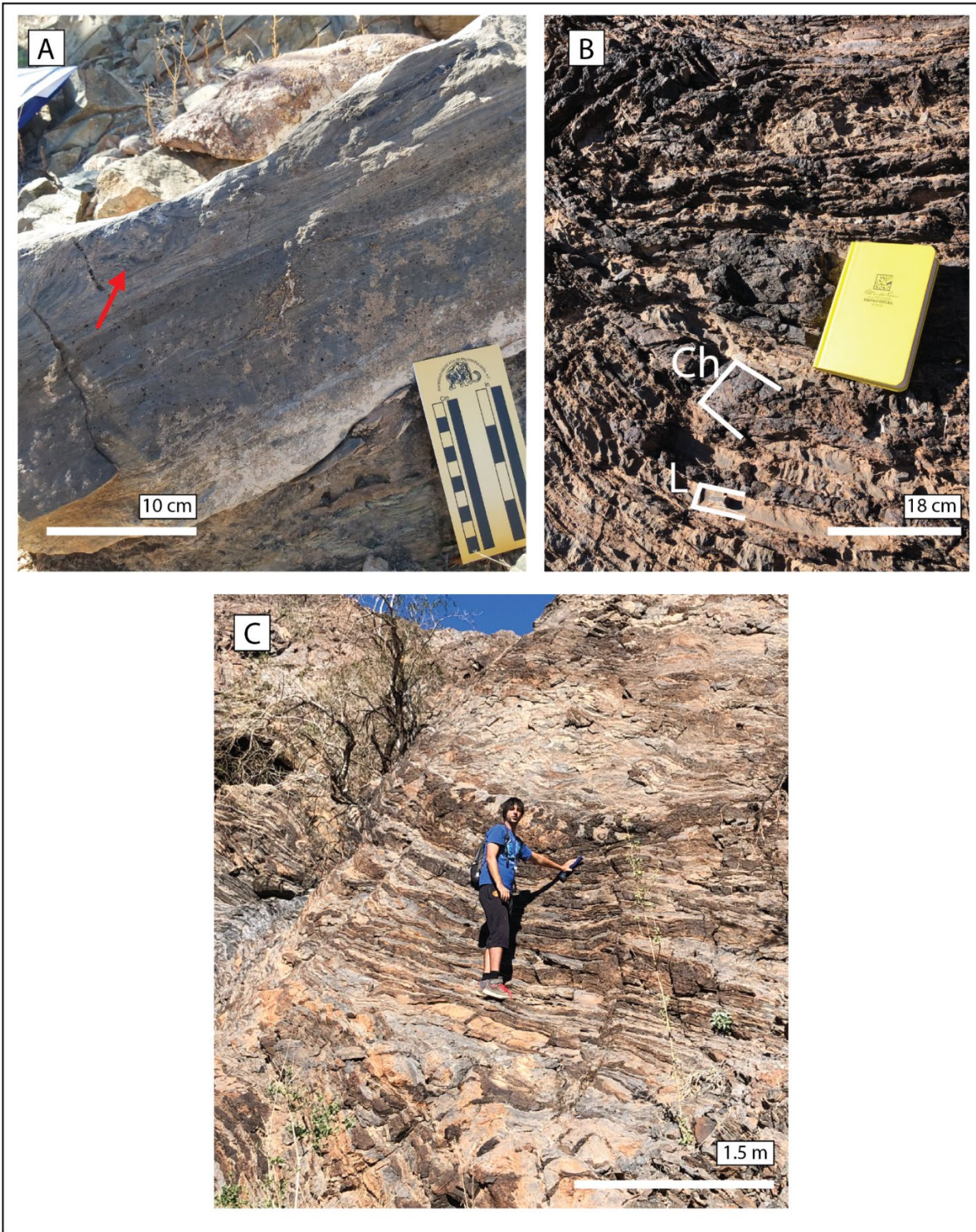
(outlined in red). Photo by P. Navas-Parejo. **(D)** Isoclinal folds with competent chert layers interbedded with light-gray metashale layers. Hammer approximately 24 cm. Photo by M. Martini. **(E)** Large-scale isoclinal folds throughout the entire unit.

### ***Unit 2 outcrop observations***

Unit 2 contains recrystallized, light-gray to tan (orange weathered) metalimestone moderately to pervasively replaced by dark-gray diagenetic chert and interbedded with tan to gray cherty metashale and very fine-grained metasandstone (Figure 12). The base of Unit 2 is predominantly cherty metashale with a few large metalimestone packages interbedded with thin beds of metashale. Cherty metashale layers contain very-fine parallel laminations and soft-sediment-deformation structures (Figure 13A). Higher upsection, metalimestone packages increase and are pervasively replaced by diagenetic chert (5-20 cm in thickness) with metalimestone layers ranging from 5-10 cm in thickness (Figure 13B). Many faults and isoclinal folds are present throughout Unit 2 (Figure 13C). Detrital zircon sample LP070120-2 was collected from the base of this unit; no thin sections were made (Figure 8). Unit 2 is in fault contact with Unit 3.



**Figure 12.** Measured stratigraphic section of Unit 2. Grain-size subdivisions indicated along the x-axis (Sh - metashale, SS - metasandstone, vf – very fine, f - fine, m - medium, c - coarse, C - metaconglomerate, g - granular, p - pebble, c - cobble).



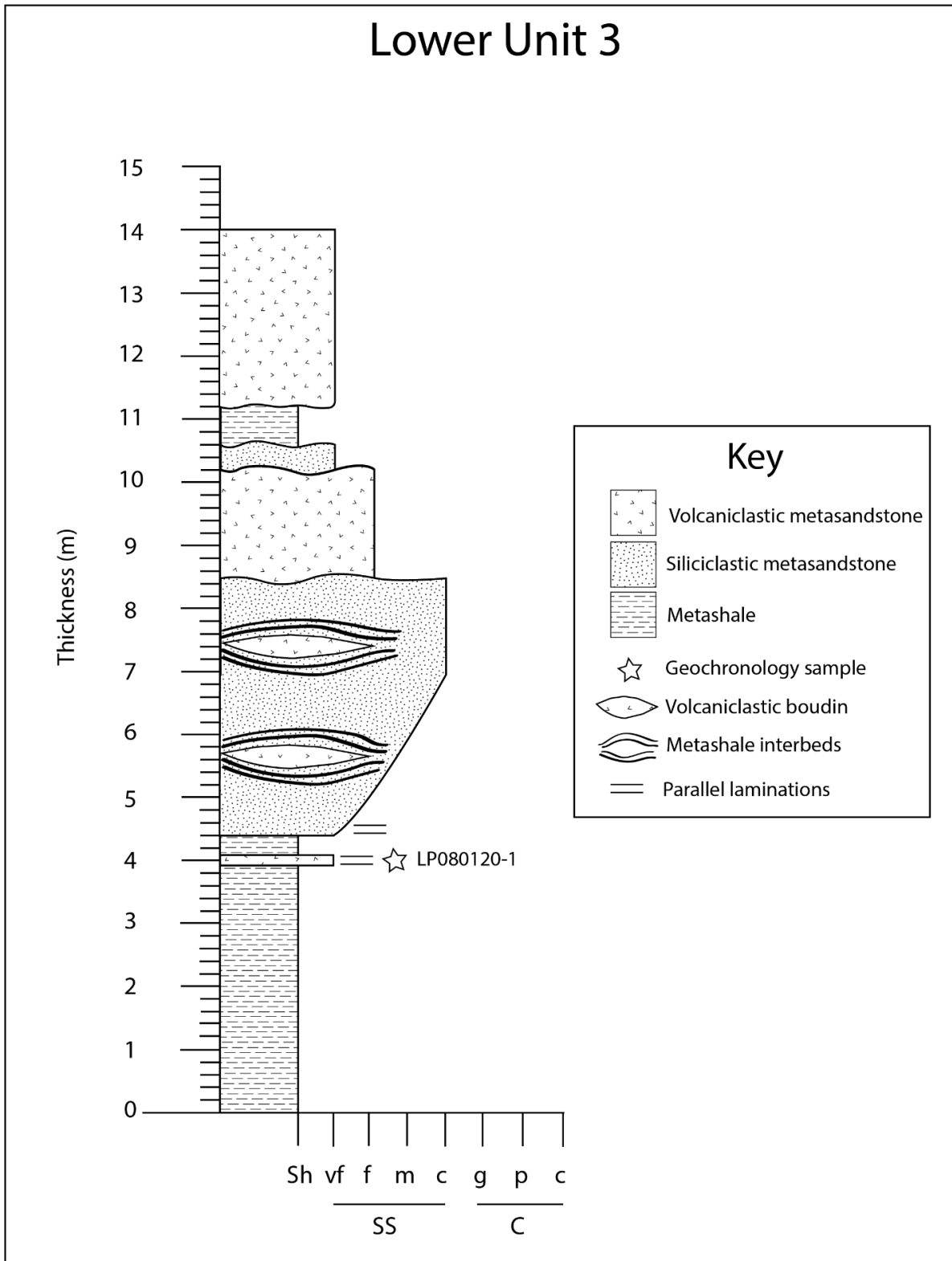
**Figure 13.** Outcrop photographs of Unit 2: **(A)** Cherty metashale containing soft-sediment-deformation structures (red arrow) and parallel laminations. Photo by M. Martini. **(B)** Metalimestone pervasively replaced by dark-gray, diagenetic chert. Notebook is 18- cm long. **(C)** Interbedded layers of cherty metashale (gray to tan), metalimestone (tan to light orange) and diagenetic chert (dark brown).

### *Unit 3 outcrop observations*

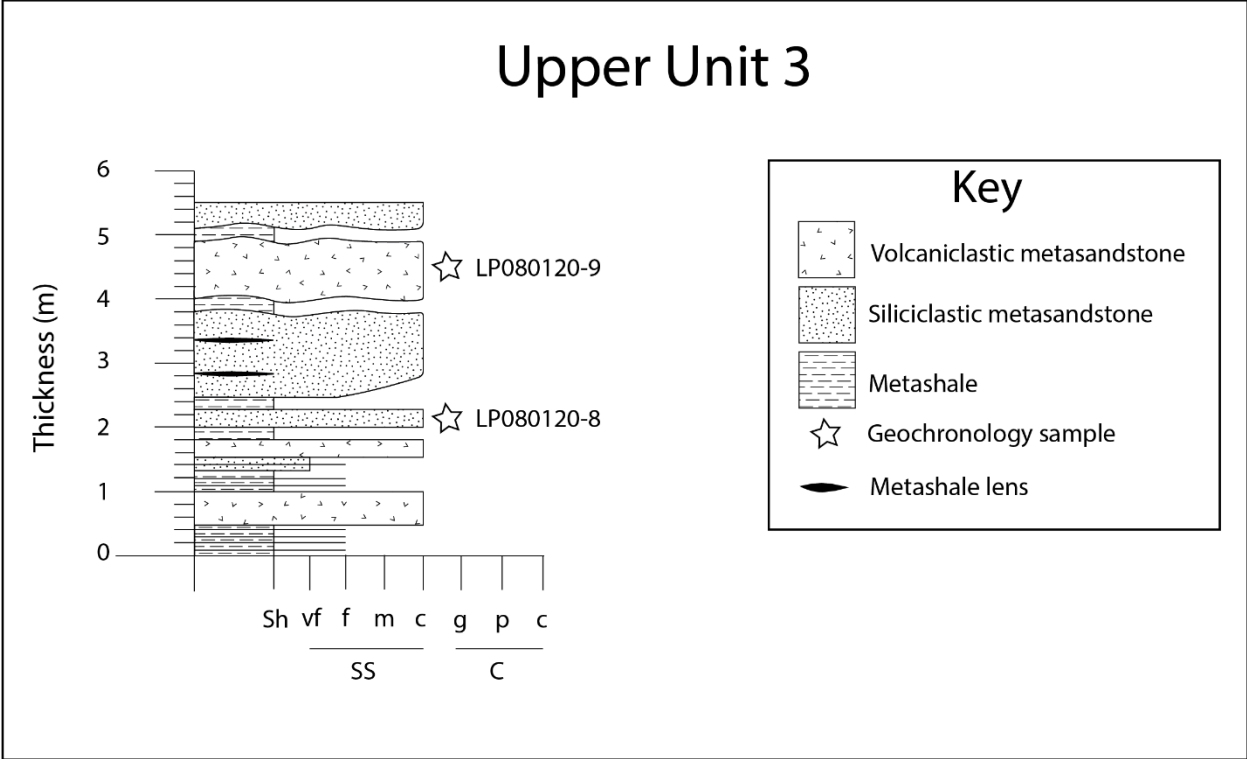
Unit 3 is a metavolcaniclastic-siliciclastic sedimentary succession with alternating recrystallized and boudinaged volcaniclastic metasandstone lenses and recrystallized siliciclastic metasandstone packages, interbedded with metashale throughout. The siliciclastic metasedimentary packages range from metashale to coarse-grained metasandstone. The base of the unit is predominantly tan to dark-brown, siliciclastic metashale that contains light-green (tan to orange weathered) boudinaged very fine- to fine-grained volcaniclastic metasandstone interbedded with thin beds of very fine-grained siliciclastic metasandstone layers (5-20 cm in thickness) containing parallel laminations (Figure 14). Boudinaged volcaniclastic metasandstone lenses typically range from 20 cm to 1 m in thickness (Figure 16A). Often the boudins are encased in finely laminated metashale beds (Figure 16B). Sample LP080120-1 was collected from a volcaniclastic metasandstone lens near the base of the unit (Figure 8).

The base of the unit contains primarily very fine-grained volcaniclastic metasandstone lenses that progressively become more abundant, coarser-grained, and thicker packages upsection (Figure 15). Sedimentary structures such as parallel laminations and ripples are more common within siliciclastic metasandstones upsection. Partial turbidite sequences showing complete to incomplete Bouma sequences are observed within siliciclastic metasedimentary units (Figure 16C-D). Bouma sequence layers include massive, graded metasandstone (Ta), plane

parallel laminae (Tb), low-angle cross-beds (Tc) and parallel laminations (Td) within fine-grained metasandstone layers. Upsection, the volcanoclastic boudins (VC) are coarser-grained, more fractured, and typically weather dark brown to reddish orange while the bedded siliciclastic metasandstone (SS) is more compact, finer grained, weathers tan to light orange, and contains complete to incomplete Bouma sequences (16E). Samples LP080120-8 and LP080120-9 were collected from the siliciclastic metasandstone and the volcanoclastic boudinage lenses (respectively) toward the top of the unit. Sample LP130120-1 was also collected from a volcanoclastic boudinage lens on the southern side of the arroyo (Figure 8). Unit 3 is in fault contact with volcanic rocks of Unit 5 and the relation with Unit 4 could not be determined.



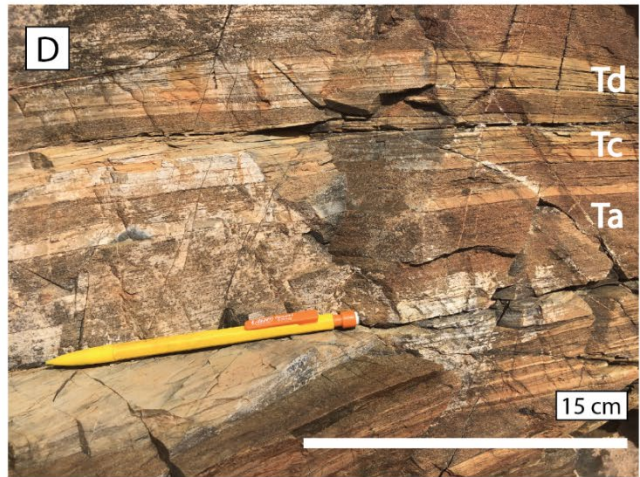
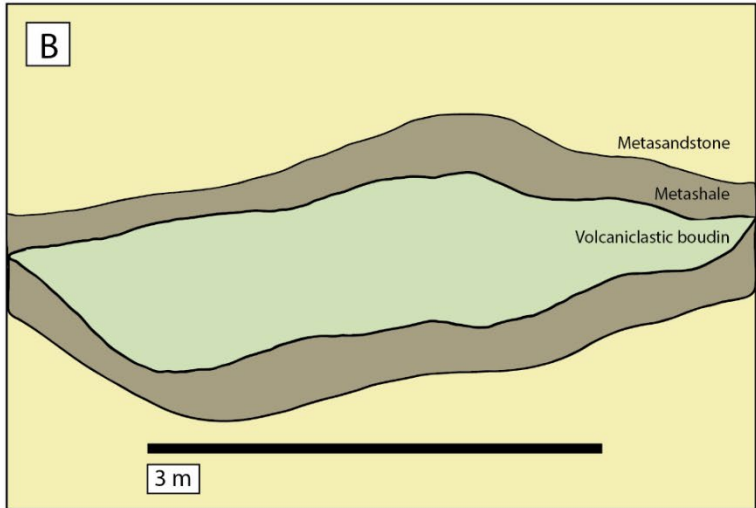
**Figure 14.** Measured stratigraphic section of the base of Unit 3 containing sample LP080120-1. Grain-size subdivisions indicated along the x-axis (Sh - metashale, SS - metasandstone, vf – very fine, f - fine, m - medium, c - coarse, C - metaconglomerate, g - granular, p - pebble, c - cobble).



**Figure 15.** Measured stratigraphic section of the top of Unit 3. Grain-size subdivisions indicated along the x-axis (Sh - metashale, SS - metasandstone, vf – very fine, f - fine, m - medium, c - coarse, C - metaconglomerate, g - granular, p - pebble, c - cobble).







**Figure 16.** Outcrop photographs of Unit 3: **(A)** Type section of Unit 3 showing alternating tan to light-brown, fine- to coarse-grained siliciclastic metasandstone, laminated metashale layers (drawn in white) and volcanoclastic metasandstone boudins (outlined in red). Photo by M. Martini. **(B)** Cross-section sketch of volcanoclastic boudins surrounded by metashale layers within fine- to coarse-grained metasandstone packages. **(C-D)** Partial Bouma sequence within siliciclastic metasandstone packages including Bouma layers Ta, Tb, Tc and Td. Photo C by M. Martini. **(E)** Alternating layers of siliciclastic metasandstone (SS) and volcanoclastic metasandstone boudin lens (VC). A small volcanoclastic boudin (outlined in red) is present within the siliciclastic metasandstone.

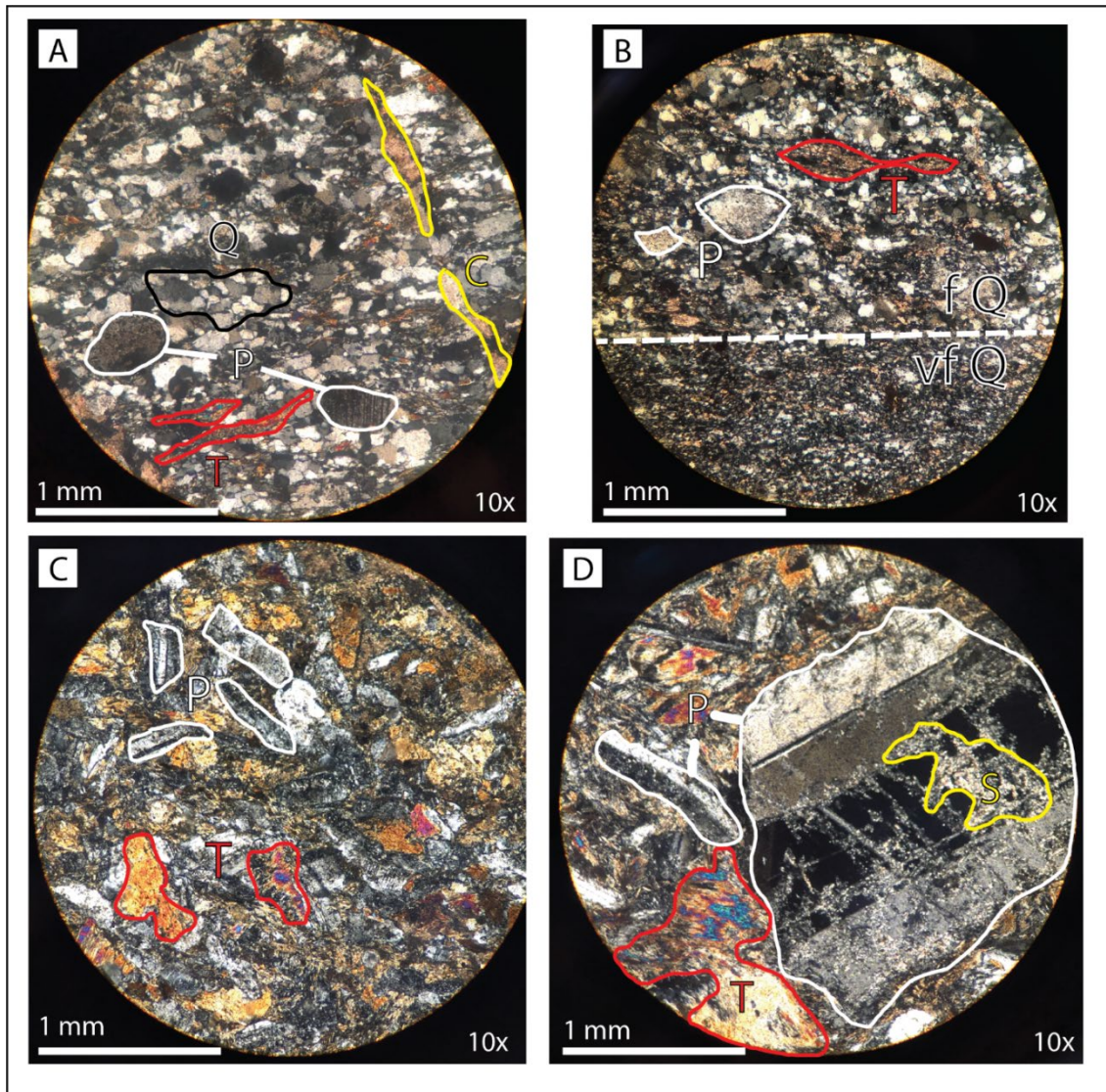
### *Unit 3 petrographic observations*

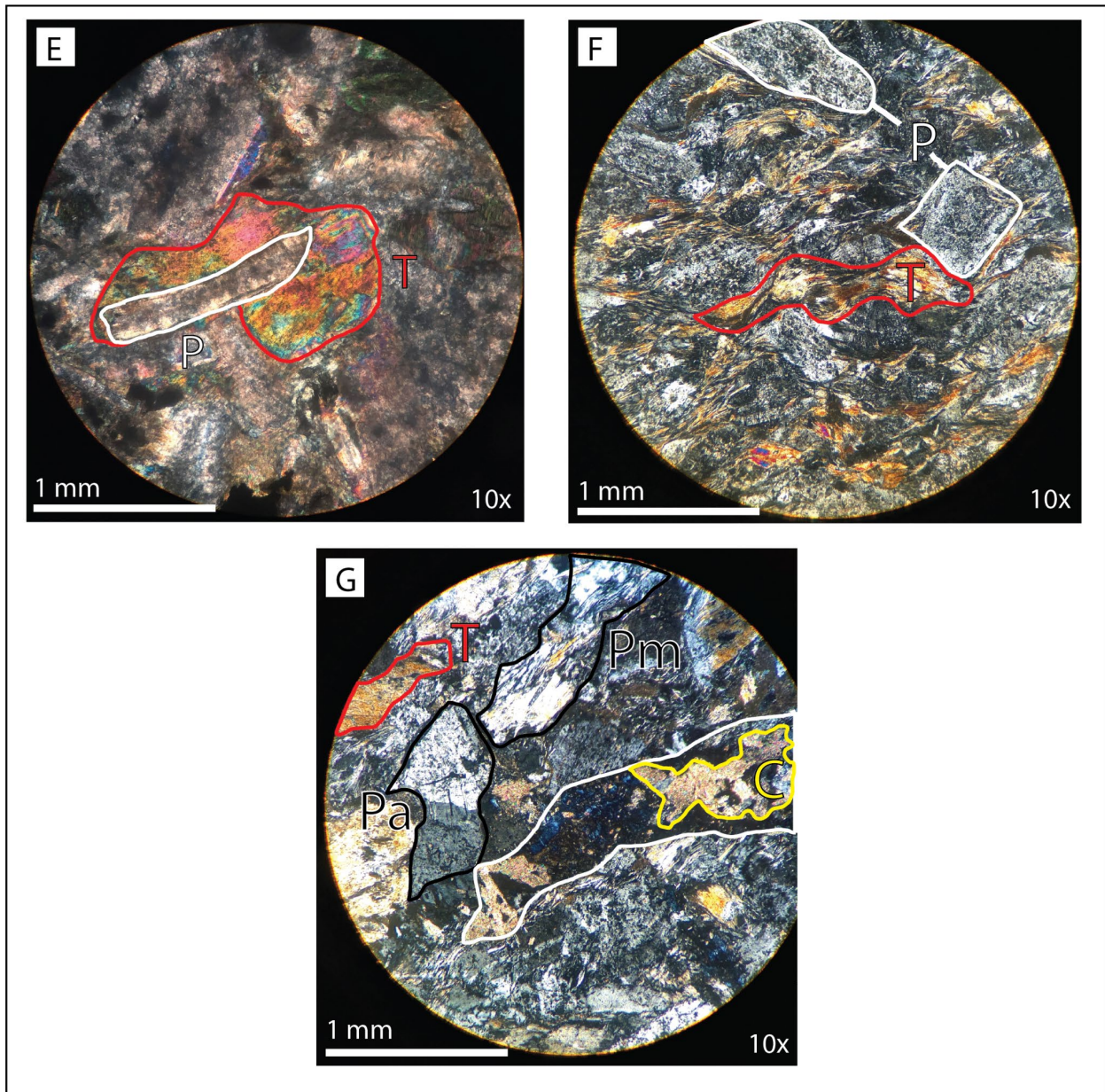
Samples were collected for petrographic analysis of siliciclastic and volcanoclastic metasandstones throughout the entirety of the unit (Table 1). Samples collected from very fine- to coarse-grained siliciclastic metasandstones of Unit 3 are primarily composed of quartz-feldspars, amphibole, calcite, and muscovite. Common accessory minerals include oxides and lithic fragments. The metasandstones have undergone extensive metamorphism and are primarily composed of sub-rounded, fine- to coarse-grained quartz with sutured boundaries (Figure 17A). Quartz grains typically show undulatory extinction. The quartz grains are well sorted and the matrix contains bands of tremolite and muscovite. Some samples contain alternating beds of fine-grained and coarse-grained quartz (Figure 17B). Secondary calcite veins, oxides and rare, well-rounded plagioclase feldspars with albite twinning are present throughout the sample as well.

Samples collected from volcanoclastic metasandstones of Unit 3 (Table 1) are primarily composed of plagioclase feldspar, tremolite, actinolite, epidote, quartz, and volcanic lithic fragments. Most samples are predominantly feldspathic with extensive sericitization and epidote replacement. Replacement of feldspar and pyroxene minerals by tremolite, actinolite and epidote is prevalent throughout the samples as bands or intergrown with feldspar (Figure 17C-D). Within

some of the samples, the feldspar minerals have been altered to clay. Secondary calcite veins, volcanic lithic fragments, oxides, and hematite cement are also seen within the samples. Samples are typically very poorly sorted and plagioclase feldspar grains have often been sheared and stretched (Figure 17E-F). The matrix often contains bands of secondary tremolite (Figure 17F).

Extensive metamorphism throughout all of Unit 3 is evidenced by sericitized feldspars, amphibole replacement, calcite veins, and feldspar alteration to clay. Rare myrmekitic intergrowth is identified within plagioclase feldspars (Figure 17G).



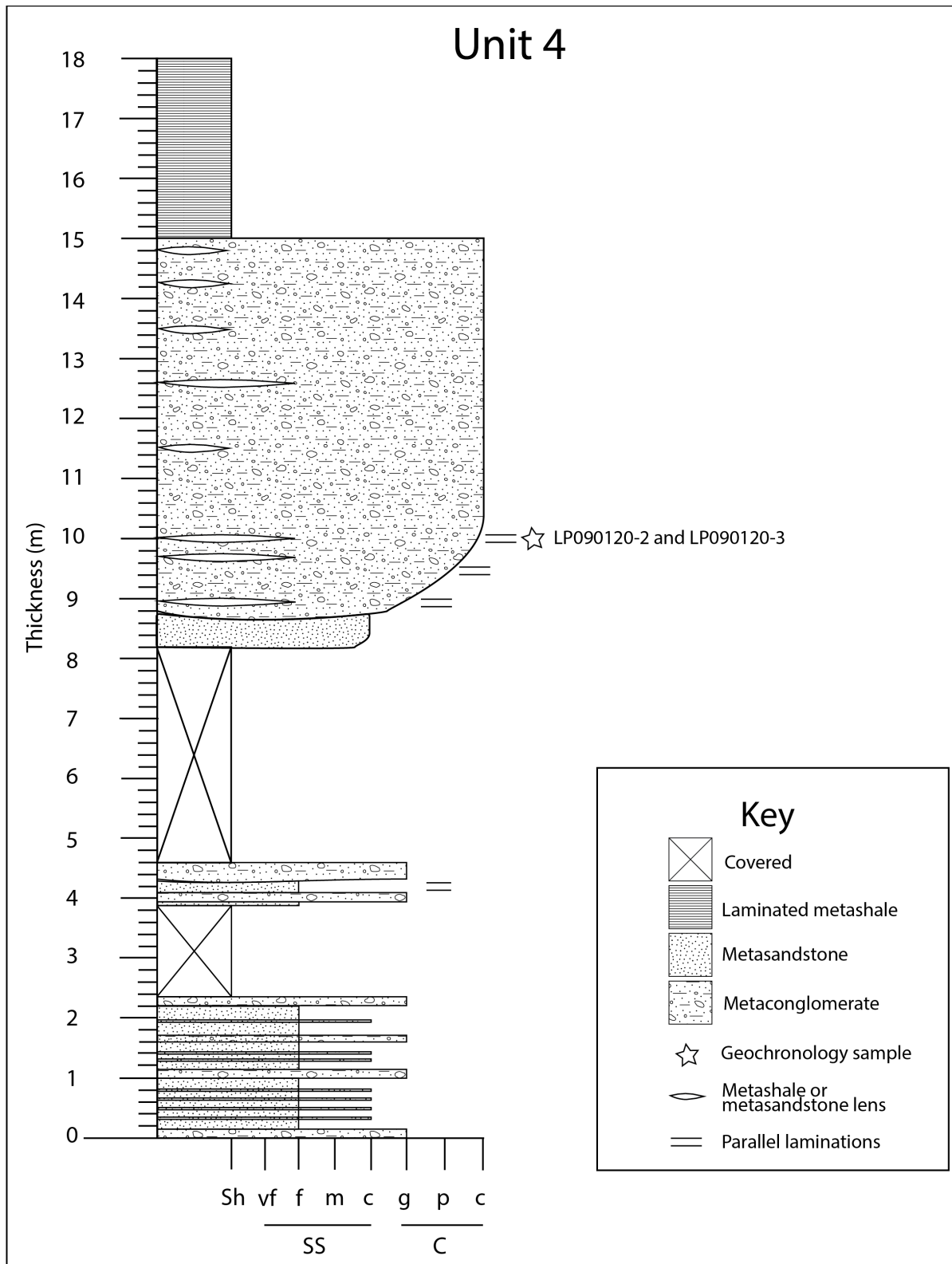


**Figure 17.** Photomicrographs of Unit 3 in cross-polarized light: **(A)** Metasandstone sample LP080120-8 composed primarily of coarse-grained quartz exhibiting undulatory extinction (Q), plagioclase feldspars (P) with twinning, tremolite bands (T), and secondary calcite veins (C). **(B)** Siliciclastic meatsandstone sample LP080120-4 showing alternating fine-grained (f Q) and very fine-grained (vf Q) quartz beds. Primarily composed of fine-grained quartz with scarce phenocrysts of plagioclase feldspar (P) and bands of secondary tremolite (T). **(C)** Sample LP080120-1 of a volcanoclastic boudin showing primarily plagioclase feldspar (P) with carlsbad twinning and pervasive tremolite (T) replacement. **(D)** Sample LP080120-3 containing large plagioclase feldspar phenocryst (P) with carlsbad-albite twinning, sericitization (S) within the feldspar and pervasive tremolite replacement (T). **(E)** Sample LP080120-9 containing highly

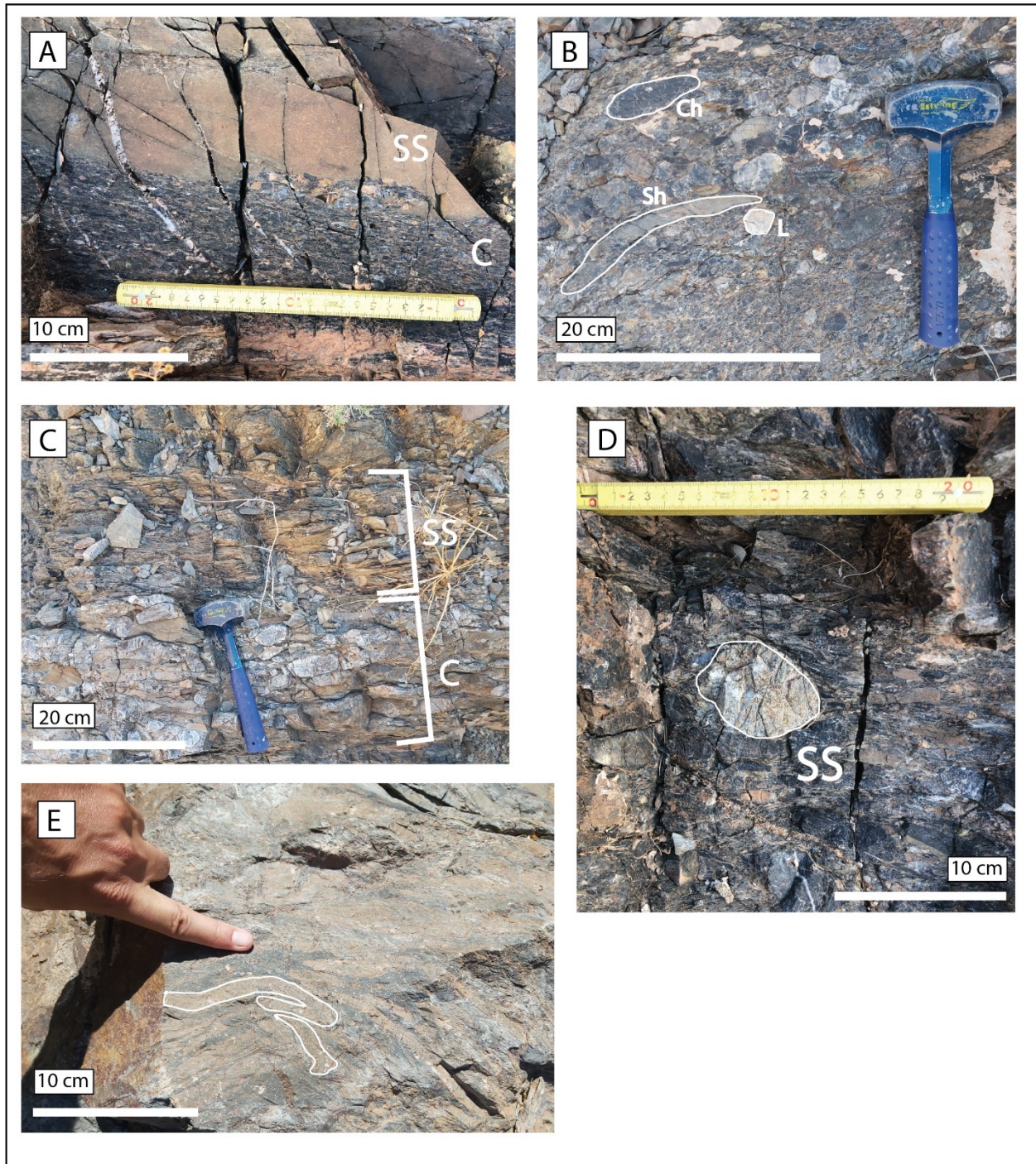
metamorphosed volcanoclastic boudin showing rare plagioclase feldspar phenocryst (P) that is being actively replaced by tremolite (T). (F) Sample LP140120-1 showing plagioclase feldspar phenocrysts (P) that have been stretched and sheared. The matrix contains bands of secondary tremolite (T). (G) Sample LP130120-1 is primarily composed of plagioclase feldspar and tremolite replacement (T), as well as calcite (C) precipitation outlined in yellow. Note the plagioclase feldspars display myrmekitic intergrowth of quartz (Pm) and albite twinning (Pa).

#### ***Unit 4 outcrop observations***

Unit 4 is a coarse-grained metaconglomerate interbedded with metashale and very fine- to coarse-grained metasandstone (Figure 18). Within the eastern exposure of the metaconglomerate, the base of the unit contains light-brown, very fine-grained metasandstone layers with thin interbeds (5-10 cm) of metaconglomerate containing granular chert, limestone, and shale clasts (1-5 cm) as well as sedimentary and volcanic lithic fragments within a dark gray to purple matrix (Figure 19A). The metaconglomerate also contains sheared and stretched clasts of black chert (1-3 cm in thickness), white limestone (3-8 cm in thickness), and light-gray shale lenses (1-3 cm in thickness) (Figure 19B). The unit coarsens upward into fine- to medium-grained metasandstone with parallel laminations interbedded with much thicker metaconglomerate beds (10-40 cm) that contain cobble-size (6-40 cm) clasts (Figure 19C-D). The metaconglomerate contains soft-sediment-deformation structures and evidence of slumping (Figure 19E). The western exposure of the metaconglomerate is highly faulted, contains granular clasts of chert, limestone, and shale and is typically light gray to brown in color. Detrital zircon samples LP090120-2 and LP090120-3 were collected from the metasandstone and metaconglomerate (respectively) of the eastern exposure of this unit (Figure 8). Unfortunately, due to pervasive faulting throughout the area, the stratigraphic relation with Units 1-3 could not be established.



**Figure 18.** Measured stratigraphic section of Unit 4. Grain-size subdivisions indicated along the x-axis (Sh - metashale, SS - metasandstone, vf – very fine, f - fine, m - medium, c - coarse, C - metaconglomerate, g - granular, p - pebble, c - cobble).



**Figure 19.** Outcrop photographs of Unit 4: **(A)** Base of Unit 4 is composed of interbedded metasandstone (SS) and metaconglomerate (C) packages with granule-size clasts. **(B)** Metaconglomerate containing sandstone, chert (Ch), and limestone (L) cobbles with deformed shale (Sh) lenses throughout. Hammer is approximately 24 cm in length. Photo by M. Martini. **(C)** Alternating highly fractured, medium-grained metasandstone beds (SS) with parallel laminations and metaconglomerate beds (C) with cobble-size clasts. Photo by M. Martini. **(D)**

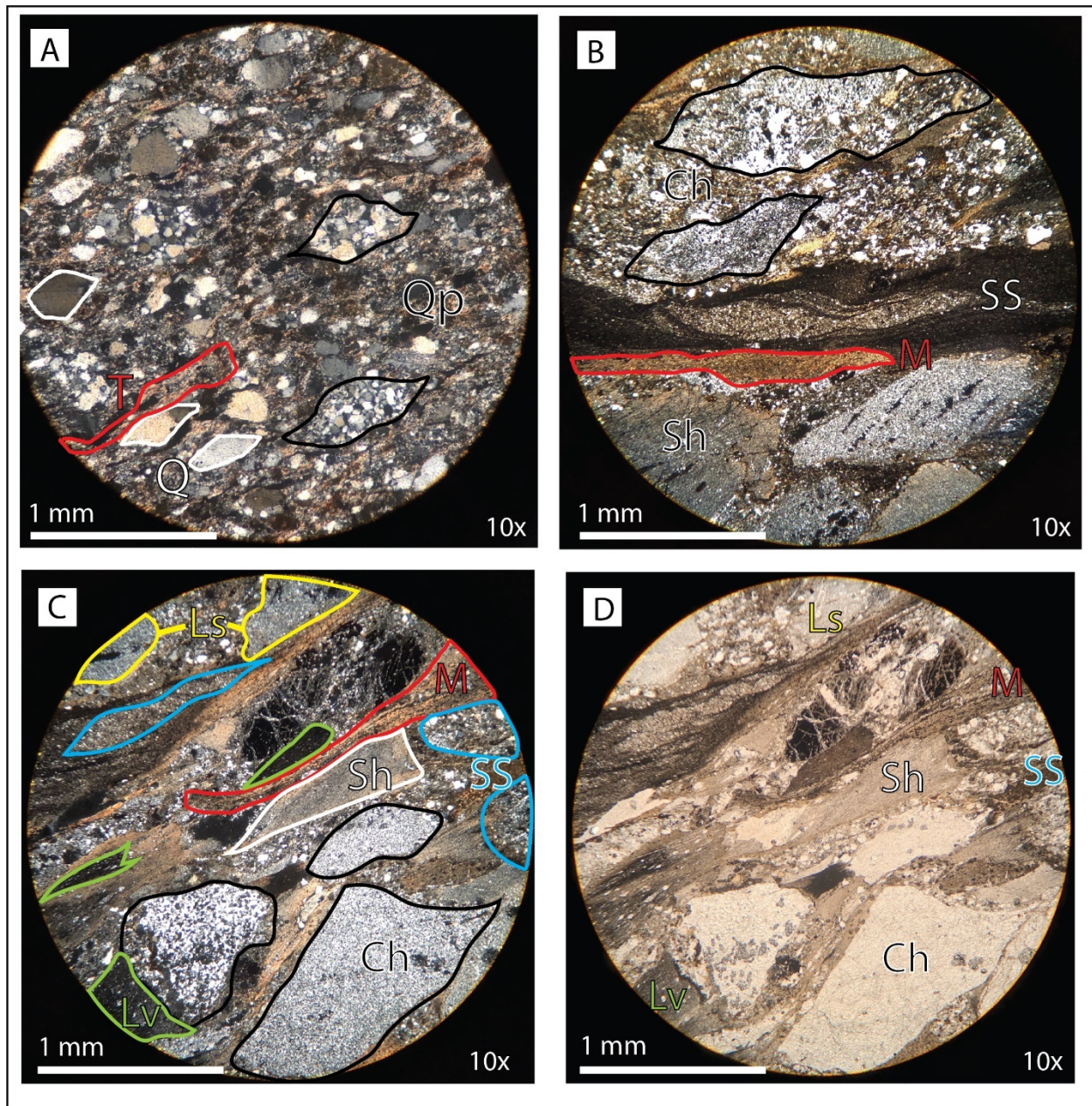


Unit 4 composed of poorly-sorted metaconglomerate with 7.5-cm wide sandstone cobble (SS). **(E)** Metaconglomerate with soft-sediment-deformation structures and slumped shale lens (outlined in white). Photo by M. Martini.

#### ***Unit 4 petrographic observations***

Thin sections were created from metasandstone and metaconglomerate samples for petrographic analysis (Table 1). Sample LP090120-2 was collected from a fine-grained metasandstone lens within a metaconglomerate package. The main mineral assemblage for the sample consists of monocrystalline quartz clasts, clasts of polycrystalline quartz, tremolite, and muscovite with secondary oxide minerals. The metasandstone has undergone extensive metamorphism and quartz grains are sub-rounded and stretched (Figure 20A). Quartz exhibits undulatory extinction. The metasandstone is well sorted and the matrix contains bands of tremolite and muscovite.

Sample LP090120-3 is a granular metaconglomerate that contains clasts of chert and shale, bands of muscovite, siltstone and sandstone lens within a polycrystalline quartz and micaceous matrix (Figure 20B). The metaconglomerate has undergone extensive metamorphism and the clasts are often stretched and sheared. Sedimentary and volcanic lithic fragments are present as well (Figure 20C-D). The metaconglomerate is poorly sorted and clasts are typically sub-rounded to angular.



**Figure 20.** Photomicrographs of interbedded metasandstone and metaconglomerate packages of Unit 4: **(A)** Metasandstone sample LP090120-2 in cross-polarized light containing primarily monocrystalline quartz clasts (Q) outlined in white, clasts of polycrystalline quartz (Qp) outlined in black and secondary tremolite mineralization (T) outlined in red within a micaceous matrix. **(B)** Metaconglomerate sample LP090120-3 in cross-polarized light showing large chert nodules (Ch) outlined in black, sandstone lens (SS) in the center, clasts of shale (Sh) and micaceous bands (M) outlined in red. **(C)** Metaconglomerate sample LP090120-3 in cross-polarized light showing large clasts of chert (Ch) outlined in black, rounded and stretched clasts of sandstone (SS) outlined in blue, shale lenses (Sh) outlined in white, volcaniclastic lithic fragments (Lv) outlined in green and sedimentary lithics (Ls) outlined in yellow. Micaceous bands (M) outlined

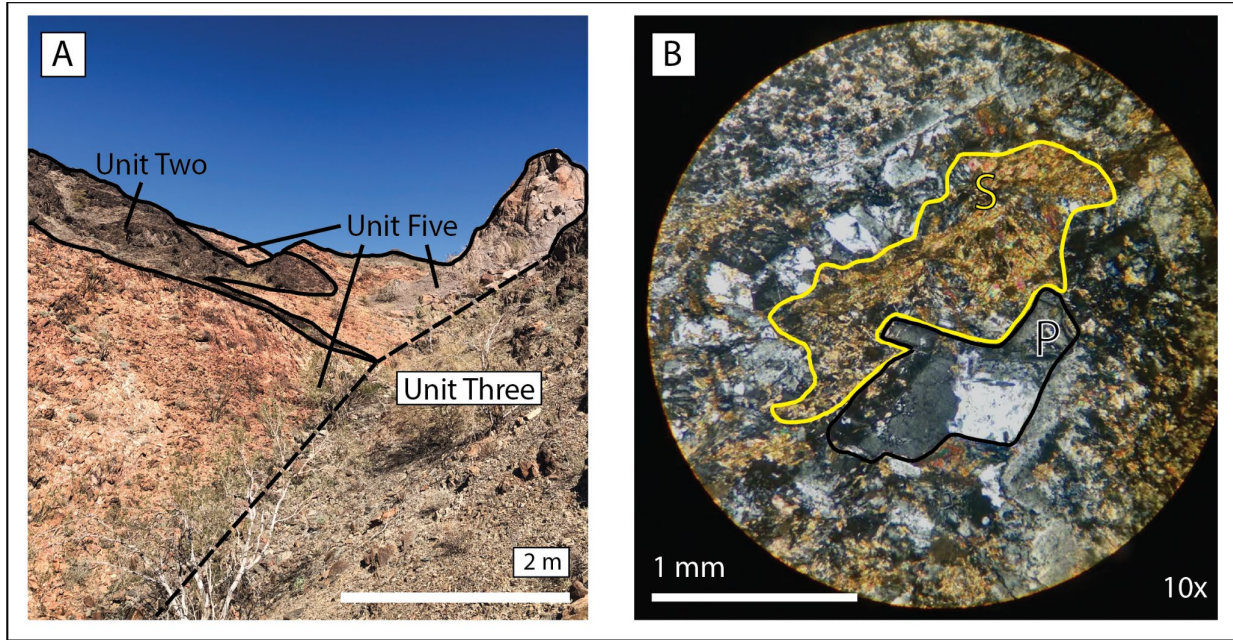
in red are present throughout the sample within a polycrystalline quartz and micaceous matrix. **(D)** Same photomicrograph as C but in plain-polarized light as a reference to note the various components of this sample.

### ***Unit 5 outcrop observations***

Unit 5 consists of volcanic rocks and felsic dikes that are interpreted to be Miocene in age (Leier-Engelhardt, 1993) (Figure 21A). The volcanic rocks are typically light pink to orange and present throughout the entirety of the Arroyo Grande Group (Figure 8). The felsic dikes intrude many of the units, creating stratigraphic contacts and baking the surrounding rocks in some places. No detrital zircon samples were collected from this unit for analysis.

### ***Unit 5 petrographic observations***

Sample LP130120-2 was collected from Unit 5 for petrographic analysis. The sample is primarily composed of interlocking plagioclase feldspar with albite twinning (Figure 21B). Large plagioclase grains have been altered by pervasive sericite mineralization and rare original feldspar shapes remain.

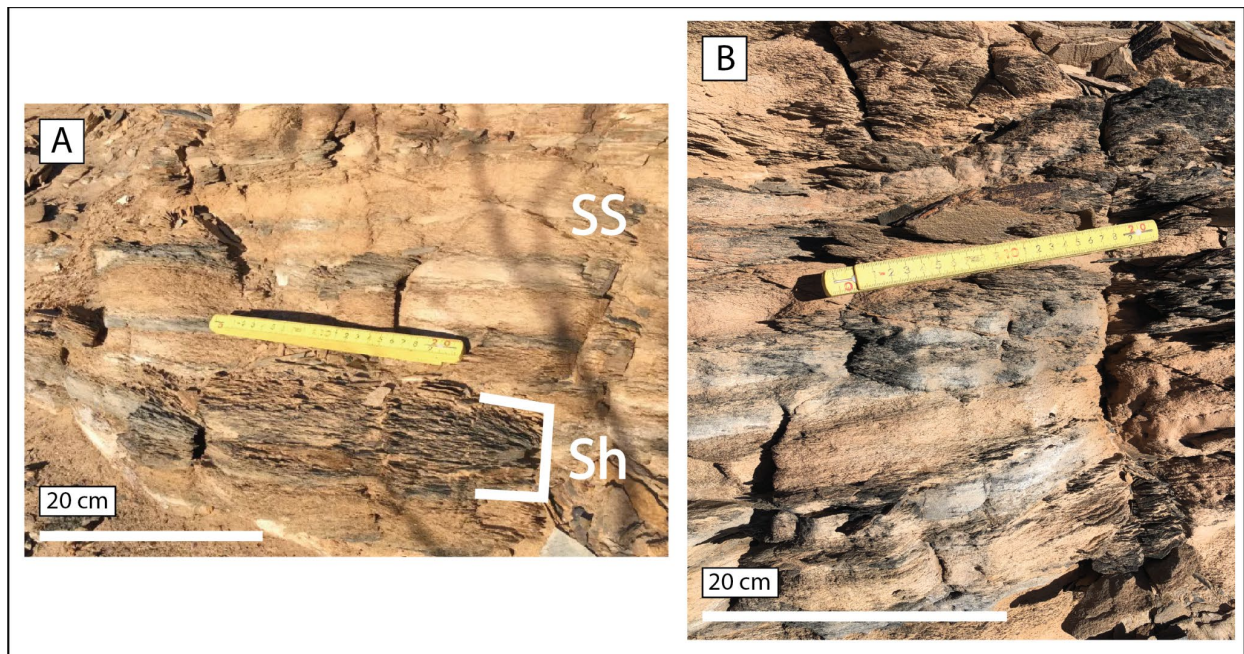


### 3.1.2 SIERRA LAS PINTAS GROUP

The lithologies originally described by Leier-Engelhardt (1993) for the Sierra Las Pintas Group and later updated by Navas-Parejo et al. (2018) are adopted for this study. The predominant lithologies for the area are (SP1) calcareous metasandstone and calcareous sandy metasandstone, (SP2) metasandstone interbedded with metashale and metaconglomerate, (SP3) crinoidal metalimestone, (SP4) basaltic metalava and metaconglomerate, (SP5) pillow lava flow, and (Q) undifferentiated Quaternary. From the Sierra Las Pintas Group, samples were collected from SP1, SP2, and SP4 for detrital zircon and petrographic analysis (Figure 5). The minimum thickness of the Sierra las Pintas Group is estimated to be approximately 520 m (Leier-Engelhardt, 1986).

### *SP1 outcrop observations*

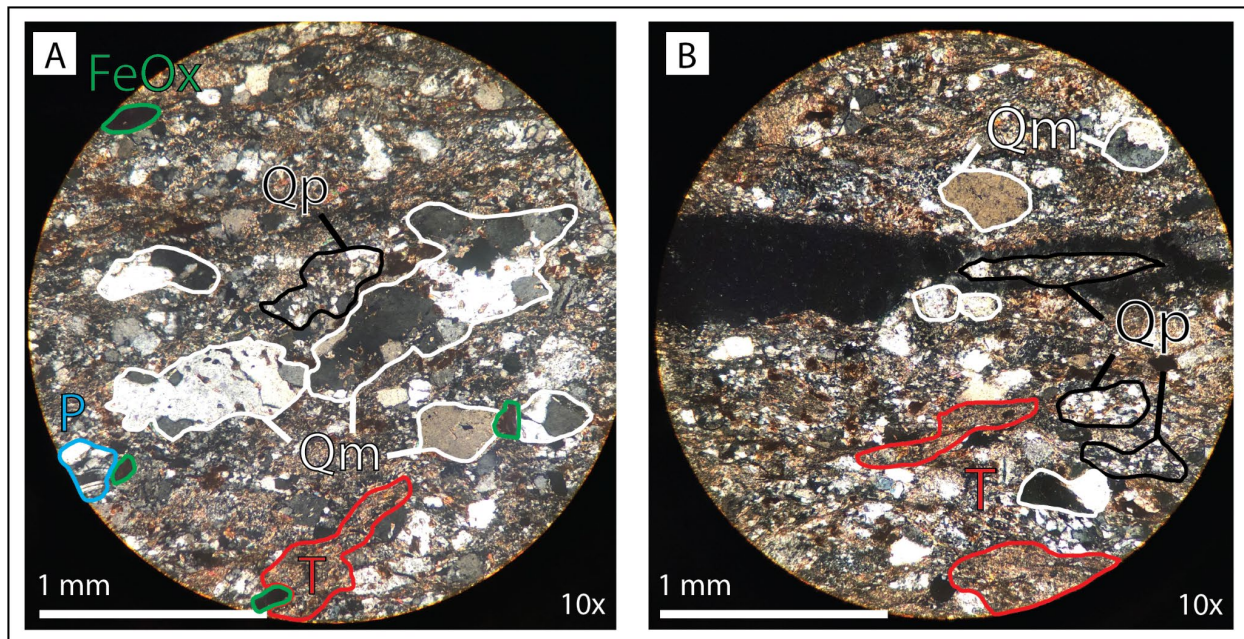
SP1 is primarily composed of packages of very fine- to medium-grained metasandstone interbedded with calcareous metashale. The metasandstone ranges from tan to light orange and is highly fractured and completely recrystallized. Sedimentary structures are not preserved except for parallel laminations in the metasandstone. At the base of the unit, alternating beds of very fine-grained metasandstone (10-40 cm in thickness) are interbedded with finely-laminated, thin metashale beds (5-10 cm) and range in color from light to dark brown (Figure 22A). The unit coarsens upsection into a fine-grained metasandstone and is interbedded with metashale (Figure 22B). Unit SP1 continues to coarsen into Unit SP2, forming a gradational contact. Detrital zircon sample LP100120-1 was collected from a very fine-grained metasandstone of Unit SP1.



**Figure 22.** Outcrop photographs of the metasandstone of Unit SP1. **(A)** Very fine-grained metasandstone (SS) of SP1 interbedded with highly foliated, dark-brown beds of metashale (Sh) ranging from 5-10 cm in thickness. **(B)** Fine- to medium-grained metasandstone ranging from white to tan to light orange and showing foliation. Metasandstone is interbedded with thin metashale layers (dark brown).

### *SP1 petrographic observations*

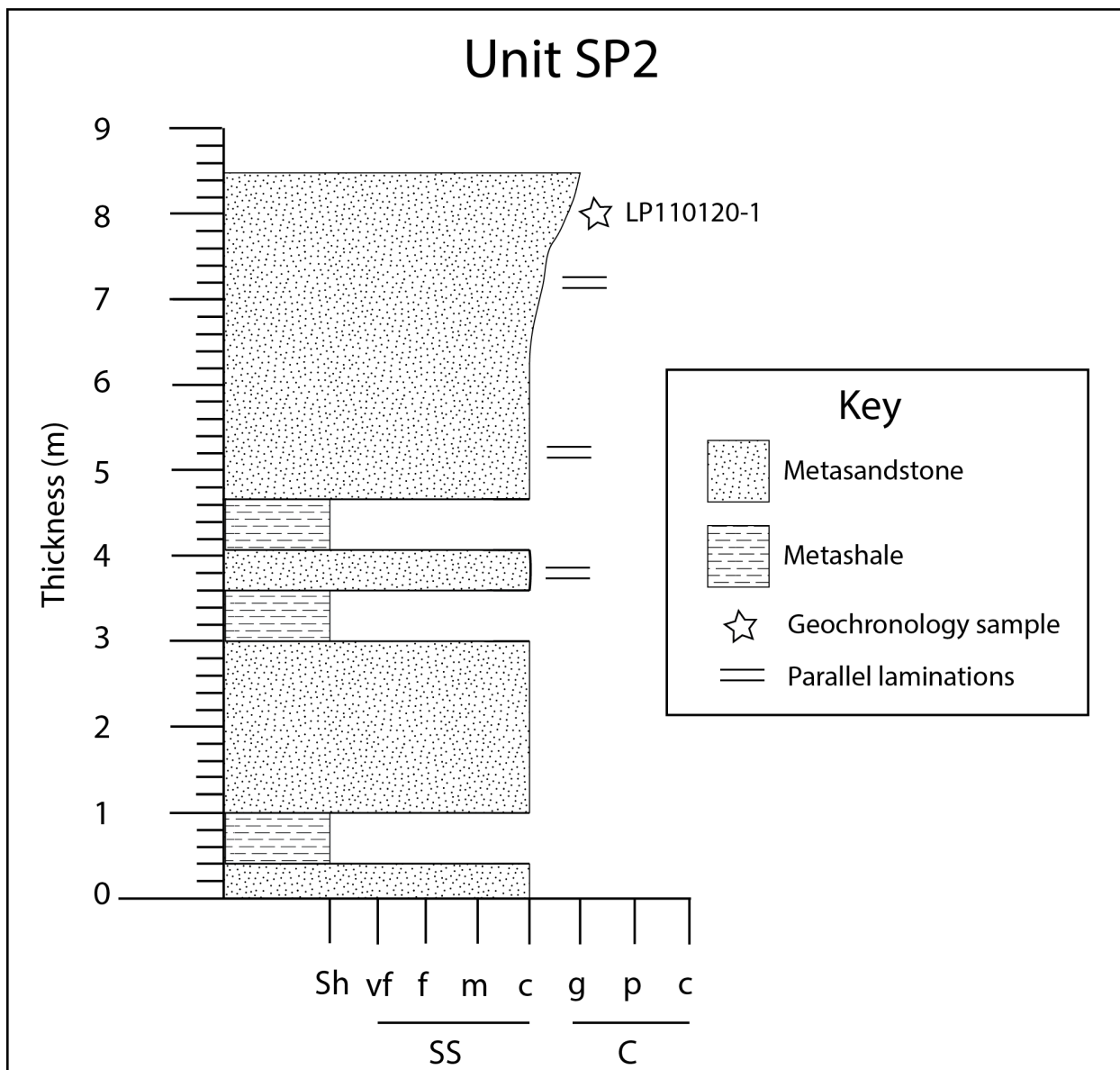
A thin section was made from the metasandstone of Unit SP1 (sample LP100120-1) that was utilized for petrographic analysis. The sample is composed of monocrystalline quartz, tremolite replacement, minor plagioclase feldspar with albite twinning and oxide minerals. The monocrystalline quartz grains have been stretched and sheared significantly and contain sutured boundaries due to pressure solution during compaction (Figure 23A). Quartz grains exhibit undulatory extinction. Pervasive sericite mineralization and tremolite banding are present throughout the matrix. The matrix is primarily micaceous and polycrystalline quartz (Figure 23B).



polycrystalline quartz. Thin bands of secondary tremolite (T) replacement (outlined in red) present throughout the matrix.

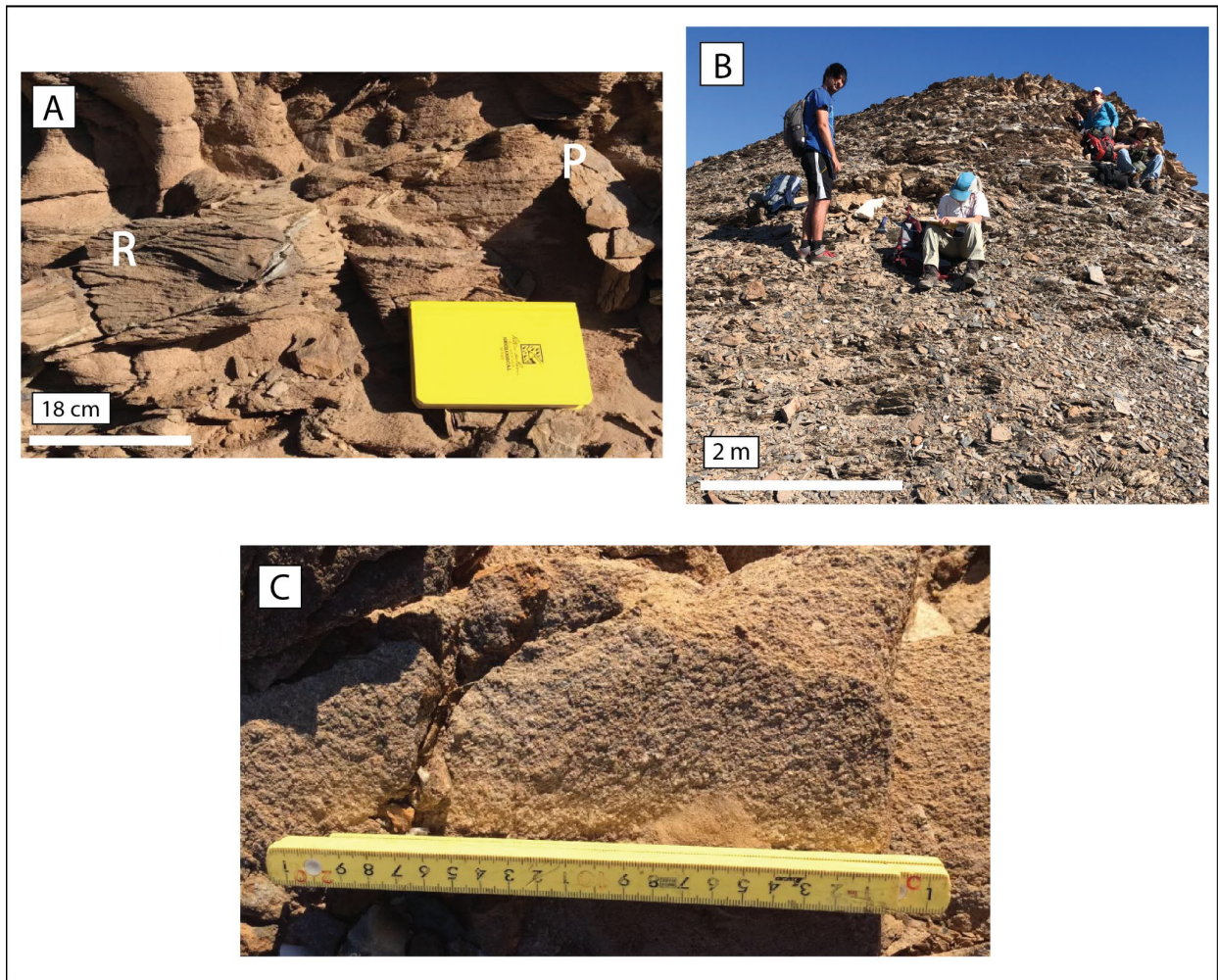
### ***SP2 outcrop observations***

SP2 is a calcareous very fine- to coarse-grained metasandstone interbedded with metashale and metaconglomerate beds. The entirety of the unit has undergone greenschist metamorphism and consequently, most of the sedimentary features have been obscured except for faint ripple bedding and fine parallel laminations within the metasandstone (Figure 25A). The entire unit is recrystallized and fractured (Figure 25B). The base of the unit is fine-grained, light-brown to orange metasandstone beds (5-10 cm thickness) interbedded with dark-brown, thin beds of metashale (1-3 cm thickness). The unit coarsens upsection to coarse-grained metasandstone where sample LP110120-1 was collected (Figure 24). Sample 18-LP-10 was also collected for detrital zircon geochronology by committee member Dr. Pilar Navas-Parejo from a very coarse-grained metasandstone. At the top of the unit, the section continues to coarsen into a tan, granular metaconglomerate containing gray crinoids, white quartz, and plagioclase feldspar (Figure 25C). Frequency of metashale beds decreases while moving upsection.



**Figure 24.** Measured section of Unit SP2 of the Sierra Las Pintas Group. Grain-size subdivisions indicated along the x-axis (Sh - metashale, SS - metasandstone, vf – very fine, f - fine, m - medium, c - coarse, C - metaconglomerate, g - granular, p - pebble, c - cobble).



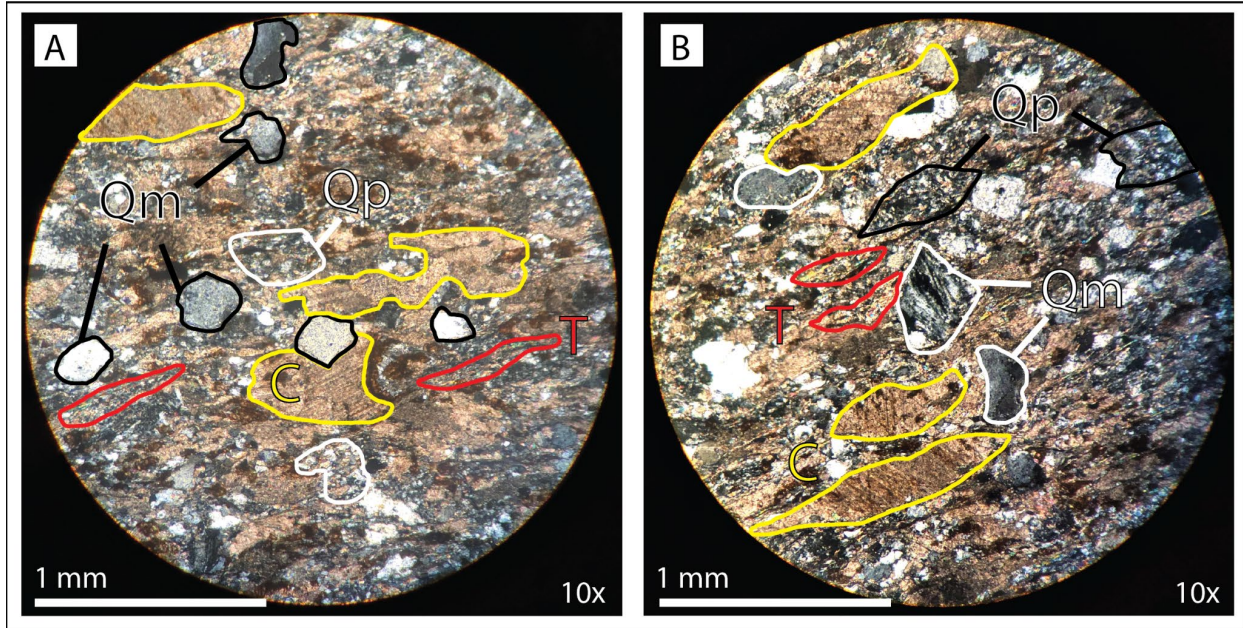


**Figure 25.** Outcrop photographs of metasandstone of Unit SP2. **(A)** Rare ripples (R) and parallel laminations (P) within the metasandstone. **(B)** Highly fractured and recrystallized metasandstone outcrop of SP2. **(C)** Granular metaconglomerate of upper SP2.

### ***SP2 petrographic observations***

Sample LP110120-1 was collected from a very coarse-grained metasandstone of unit SP2. The main mineral assemblages of the sample include monocrystalline quartz, clasts of polycrystalline quartz, calcite plates, and tremolite banding within a micaceous matrix (Figure 26A). The quartz grains are well sorted and exhibit undulatory extinction. Rare plagioclase feldspars with carlsbad twinning are present throughout. Grains are sub-rounded, have been

stretched and flattened, and contain rare myrmekitic intergrowth and pervasive sericitization due to metamorphism (Figure 26B). Large bands of calcite are present throughout the sample and the metasandstone of SP2 contains a higher percentage of calcite than the metasandstone of SP1.



#### ***Unit SP4***

One sample, X181218, was collected for detrital zircon geochronology from Unit SP4 by committee member, Dr. Nancy Riggs, as part of a reconnaissance study for the area. The sampled interval is described as metasandstone, metaconglomerate, and basaltic metalava that displays globular structures, resembling a pillow-lava flow (Figure 27).



**Figure 27.** Outcrop photograph of black basaltic metalava and metasandstone. Yellow measure stick is approximately 23- cm long. Photo by N. Riggs.

### **3.1.3 MINAS DE BARITA AREA**

Central Sonora sample collection and field observations were documented by committee members Dr. Pilar Navas-Parejo and Dr. Michelangelo Martini in the Minas de Barita area (Figure 3). Stratigraphic columns were not created during sample collection as exposures from this area are described as very poor and discontinuous. However, a generalized stratigraphic section was created from the field descriptions (Figure 28).

Primary deposits for the Minas de Barita area include (1) carbonate-shelf rocks (Permian-Cambrian), (2) pre-orogenic deep-water black shale, turbidite deposits, and chert (Mississippian-Ordovician; Sonora allochthon), (3) syn-orogenic deep-water turbidite deposits (Upper Mississippian-Pennsylvanian; Rancho Nuevo Formation), (4) syn-orogenic foredeep turbidite deposits (Permian; Mina México Formation), (5) early Cenozoic (Laramide) plutons, and (6)

Quaternary gravels (Poole et al., 2008; Figure 5). Samples were collected for geochronology analysis from the Rancho Nuevo Formation and Mina México Formation.

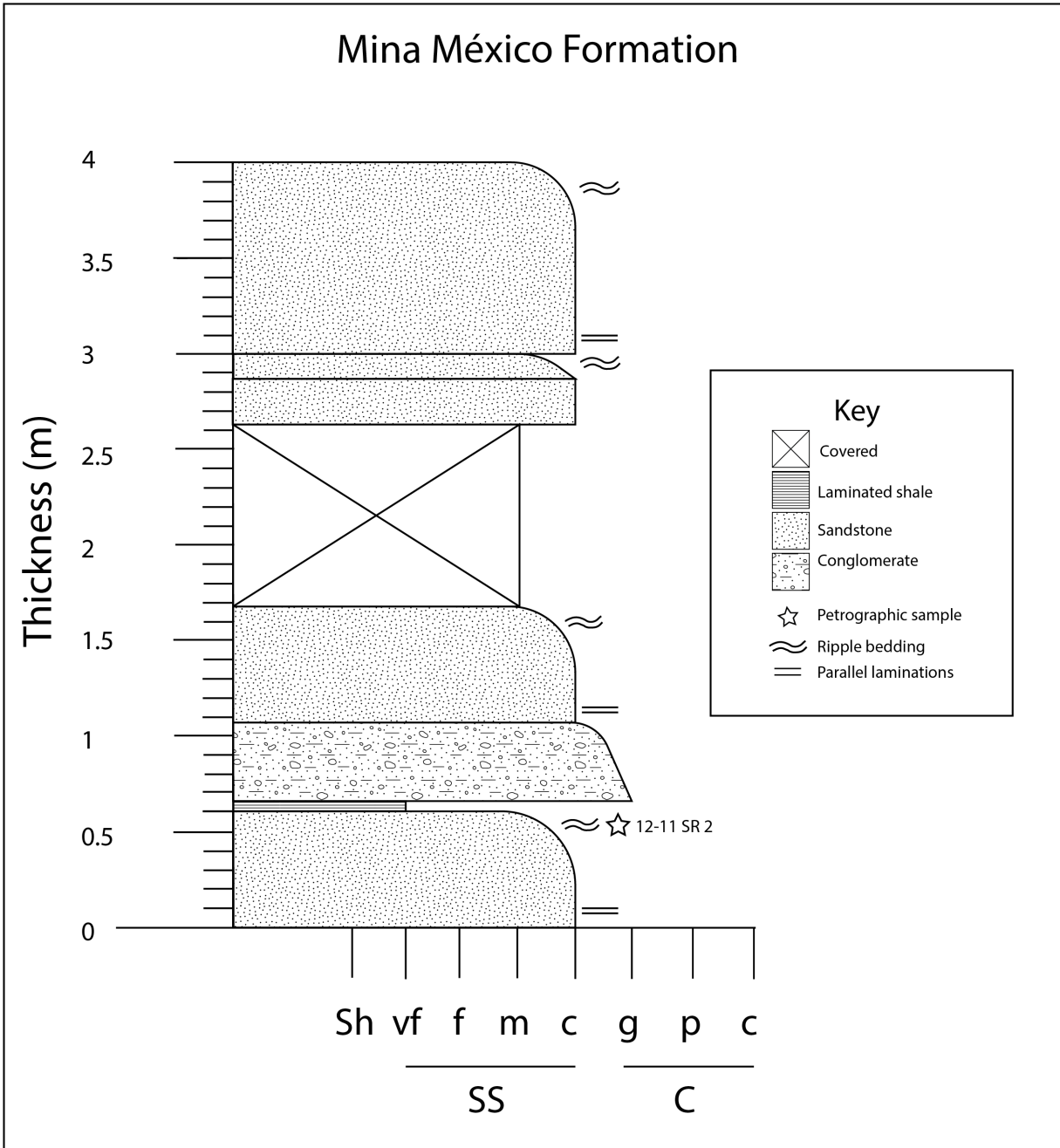
### ***Rancho Nuevo Formation***

M. Martini described the sampled outcrop as a 10-m-thick exposure of stacked calcareous debris-flow deposits approximately 1 m or less in thickness. The debris-flow deposits show inverse grading, most of the framework grains are skeletal and mudstone intraclasts of fusulinids, and the base of these deposits are non-erosive. Upsection, the deposits are overlain by a granule- to pebble-debris-flow conglomerates dominated by extraclasts of chert, calcareous, and non-calcareous shale. Sample 13-11-SR2 was collected from poorly sorted sedimentary packages containing chert and shale. Another sample was collected from a 6-m-thick exposure of siltstone and claystone of a turbidite deposit from the lower Rancho Nuevo Formation but did not yield enough zircon for analysis.

### ***Mina México Formation***

The exposure is described as an interbedding of two different kinds of deposits: 1) quartz-rich, very fine- to fine-grained sandstone and shale that display typical structures of turbiditic deposits and 2) calcareous, sandy debris-flow deposits dominated by skeletal intraclasts mostly of fusulinids. Sample 12-11SR2 was collected from a quartz-rich sandstone of this sequence containing ripple marks, normal grading, and parallel laminations (Figure 28). Sample 13-11-SR3 was collected from a quartz-rich sandstone that was highly fractured and oxidized. Primary sedimentary structures preserved from this sequence include ripple marks and parallel laminations. A sample was also collected from fine- and very-fine-grained sandstone of the Mina

México Formation that contained some ichnofossils, fluidification structures and numerous cm-scale, normal, syn-sedimentary faults but did not yield enough zircon for analysis.



**Figure 28.** Generalized stratigraphic section of the Mina México Formation. Grain-size subdivisions indicated along the x-axis (Sh - shale, SS - sandstone, vf – very fine, f - fine, m - medium, c - coarse, C - conglomerate, g - granular, p - pebble, c - cobble).

## 3.2 DETRITAL ZIRCON U-PB GEOCHRONOLOGY AND TRACE ELEMENT GEOCHEMISTRY

### *Results Summary*

A total of 15 samples were collected for geochronological analysis from this study; eight samples collected from the Arroyo Grande Group, four samples from the Sierra Las Pintas Group, and three from the Minas de Barita area (Table 1). A total of 1,968 zircon grains were processed and analyzed and 1,763 of those grains were concordant and are portrayed in the KDE plots (Figures 29-42). The zircons for this study range from sharp euhedral, well-rounded, to subhedral in shape and varied from yellow, pink, white, to clear. Trace-element concentrations were also plotted for each sample that contained two distinct age groups: Permo-Triassic grains with ages 275-240 Ma and Cretaceous grains with ages 140-90 Ma (Figures 43-48).

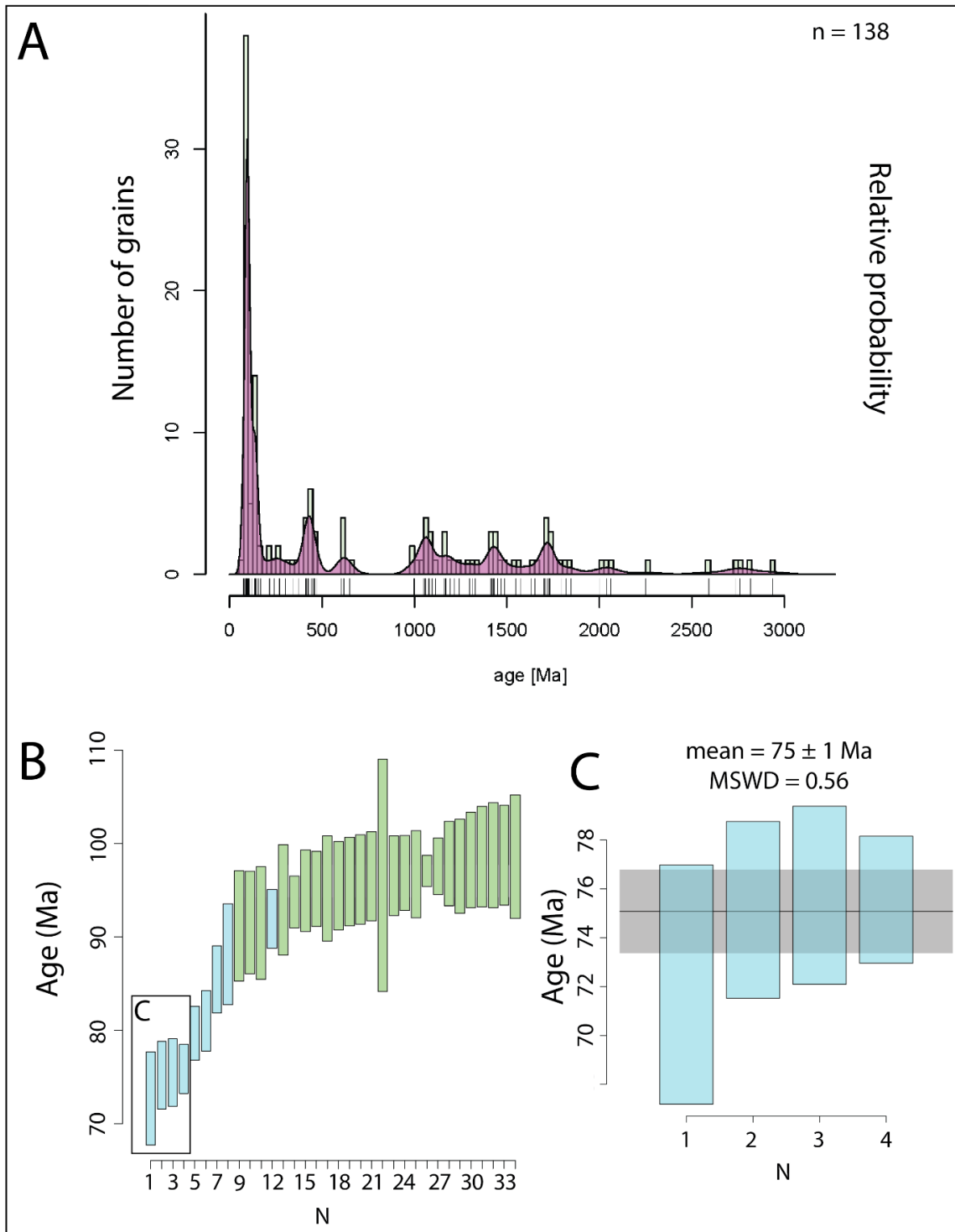
### 3.2.1 Arroyo Grande Group Detrital Ages

In total, 900 grains were concordant from the eight samples collected from the Arroyo Grande Group (Figure 8). In general, samples contained either a Cretaceous or Permian age MDA. Samples yielded age spectra with major age peaks at ca. 90-140 Ma, ca. 280-250 Ma, ca. 750-430 Ma, ca. 1750-1550 Ma, and ca. 2800-2600 Ma.

### *Unit 1*

Sample LP070120-1 was collected from a 3-m interval of dark-gray, very fine-grained cherty siltstone of Unit 1 (Figure 10). The sample contained 138 concordant zircon grains with major age peaks at ca. 70-150 Ma ( $n = 57$ ), ca. 650-430 Ma ( $n = 11$ ), and ca. 1300-950 Ma ( $n = 18$ ) (Figure 29A). The largest population of youngest zircon grains ( $n = 34$ ) from the sample ranges from 104 to 73 Ma (Figure 29B). Within that population, a younger subset of zircon

grains (blue rectangles) has an average age of  $75 \pm 1$  Ma and a calculated MSWD of 0.56, which is interpreted as the maximum depositional age for the sample (Figure 29C).

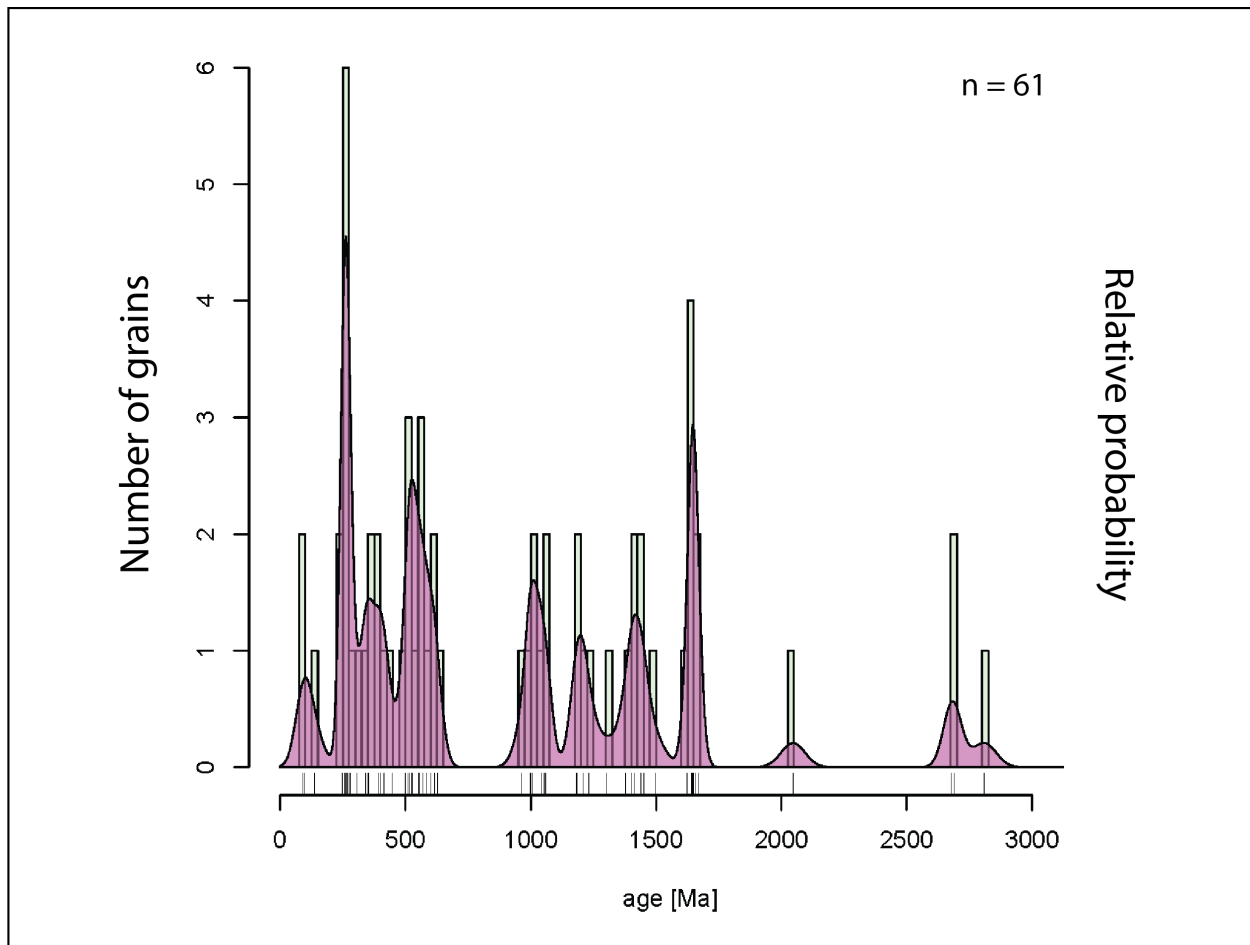


**Figure 29.** Detrital zircon age data for sample LP070120-1: **(A)** KDE plot shows major peaks at ca. 150-70 Ma, ca. 650-430 Ma, and ca. 1300-950 Ma. **(B)** Weighted mean plot showing the largest population of youngest zircon grains ( $n = 34$ ). Blue rectangles indicate youngest zircon grains that do not fall within two-sigma uncertainty of the rest of the population. **(C)** Youngest subset of zircon from the sample ( $n = 4$ ) with a mean age of  $75 \pm 1$  Ma and MSWD = 0.56.

## *Unit 2*

Sample LP070120-2 was collected from a 3-m interval of dark-brown to dark-gray, very fine-grained, cherty shale of Unit 2 (Figure 12). The sample yielded 61 concordant zircon grains with major age peaks at ca. 280-250 Ma ( $n = 9$ ), ca. 650-450 Ma ( $n = 13$ ), ca. 1300-1000 Ma ( $n = 12$ ), and ca. 1700-1600 Ma ( $n = 7$ ) (Figure 30). A trip occurred during isotopic analysis and 76 grains were not analyzed. Though the sample contains three Cretaceous grains at 91 Ma, 97 Ma, and 137 Ma, the grains do not fall within two-sigma uncertainty of each other and therefore are not considered related. The population of Permo-Triassic grains ( $n = 9$ ) in the sample ranges from 279 to 249 Ma, but the grains also did not fall within error of each other and could not be considered when determining maximum depositional age for the sample; weighted mean plots were not created.





**Figure 30.** KDE plot for sample LP070120-2 shows major peaks at ca. 280-250 Ma, ca. 650-450 Ma, and ca. 1700-1600 Ma.

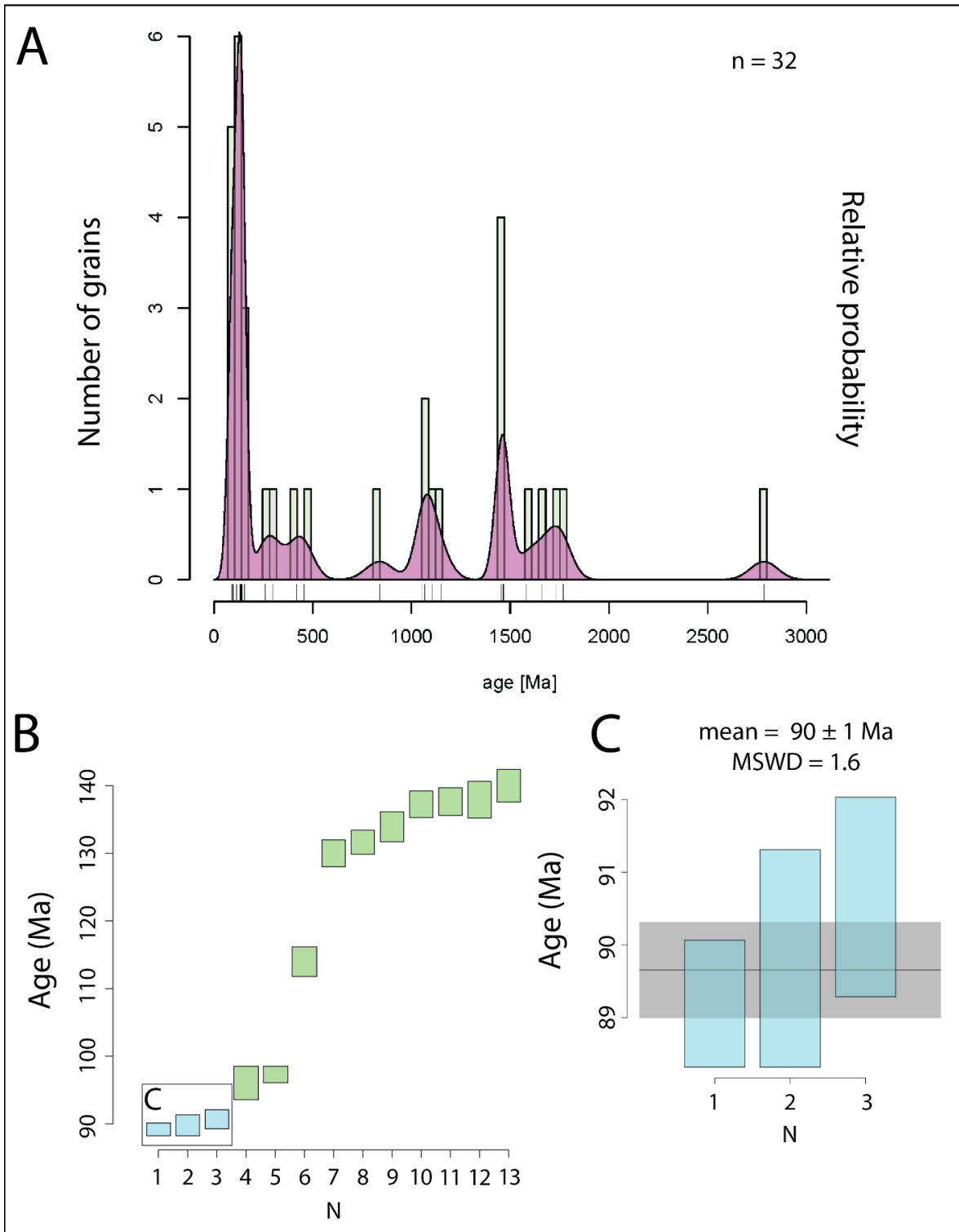
### *Unit 3*

Four samples were collected from Unit 3, LP080120-1, LP080120-8, LP080120-9, and LP130120-1 (Figure 8). The samples were collected from siliciclastic metasediment (LP080120-8) and volcaniclastic metasediment boudins (LP080120-1, LP080120-9, LP130120-1). The siliciclastic metasediment sample has a Permian MDA, while the volcaniclastic metasediment boudin samples contain Cretaceous MDAs. The prominent age peaks for the

samples range from ca. 150-90 Ma, ca. 280-240 Ma, ca. 750-450 Ma, ca. 1300-750 Ma, and ca. 2800-2600 Ma.

***Sample LP080120-1***

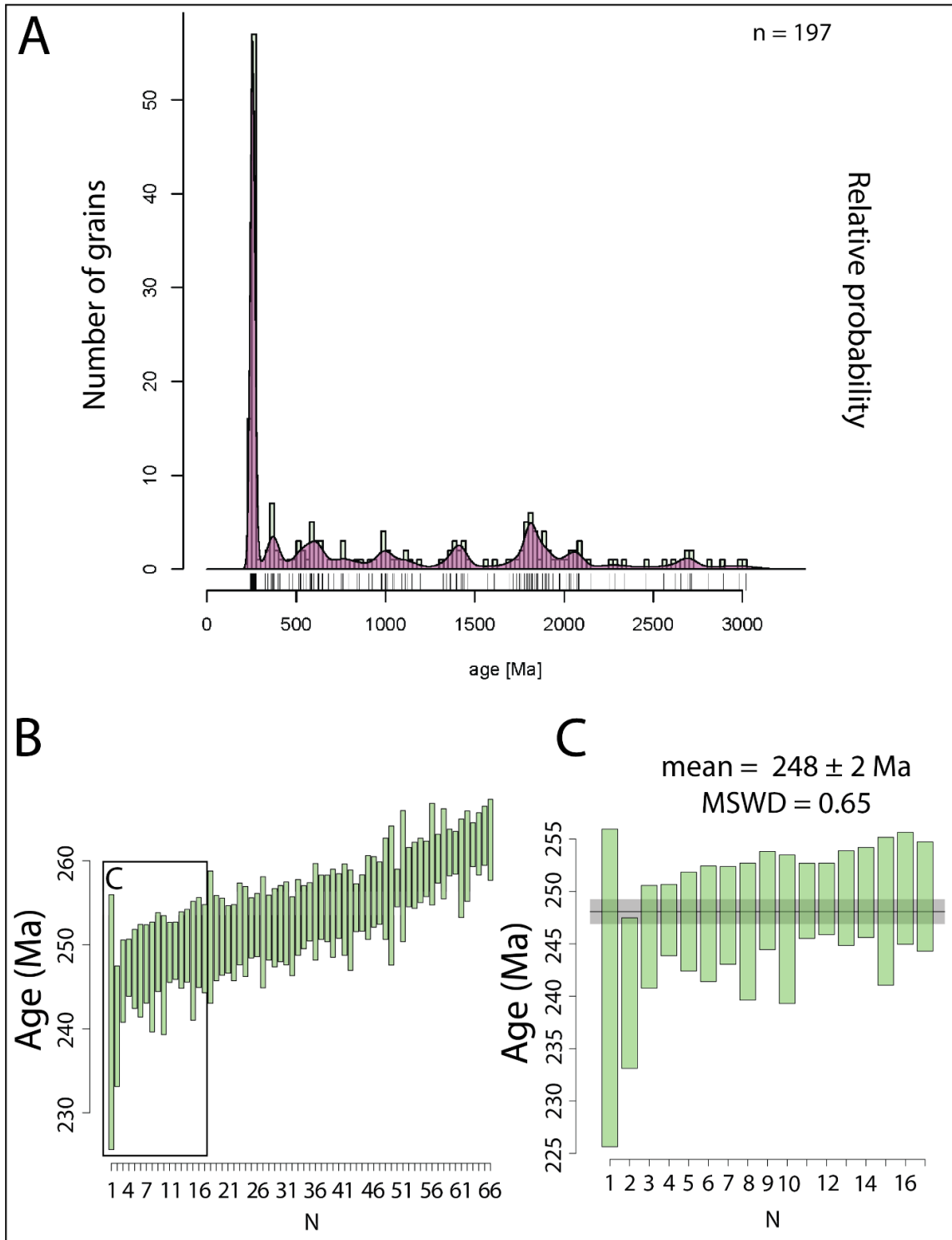
Sample LP080120-1 was collected from a 60-cm interval of tan to orange (weathered) and light-green (fresh), very fine-grained volcanoclastic metasandstone boudin near the base of Unit 3 (Figure 8, 14). The sample yielded 32 concordant zircon grains with major age peaks at ca. 140-90 Ma ( $n = 14$ ), ca. 1250-800 Ma ( $n = 5$ ), and ca. 1550-1450 Ma ( $n = 4$ ) (Figure 31A). The largest population of youngest zircon grains ( $n = 13$ ) for the sample ranges from 140 to 89 Ma (Figure 31B). Within that population, a younger subset of zircon grains (blue rectangles) has an average age of  $90 \pm 1$  Ma with a MSWD of 1.6, which is interpreted as the maximum depositional age (Figure 31C).



**Figure 31.** Detrital zircon age data for sample LP080120-1: **(A)** KDE plot shows major peaks at ca. 140-90 Ma, ca. 1250-800 Ma, and ca. 1550-1450 Ma. **(B)** Weighted mean plot showing the largest population of youngest zircon grains ( $n = 13$ ). Blue rectangles indicate youngest zircon grains that do not fall within two-sigma uncertainty of the rest of the population. **(C)** Youngest subset of zircon from the sample ( $n = 3$ ) with a mean age of  $90 \pm 1$  Ma and MSWD = 1.6.

### ***Sample LP080120-8***

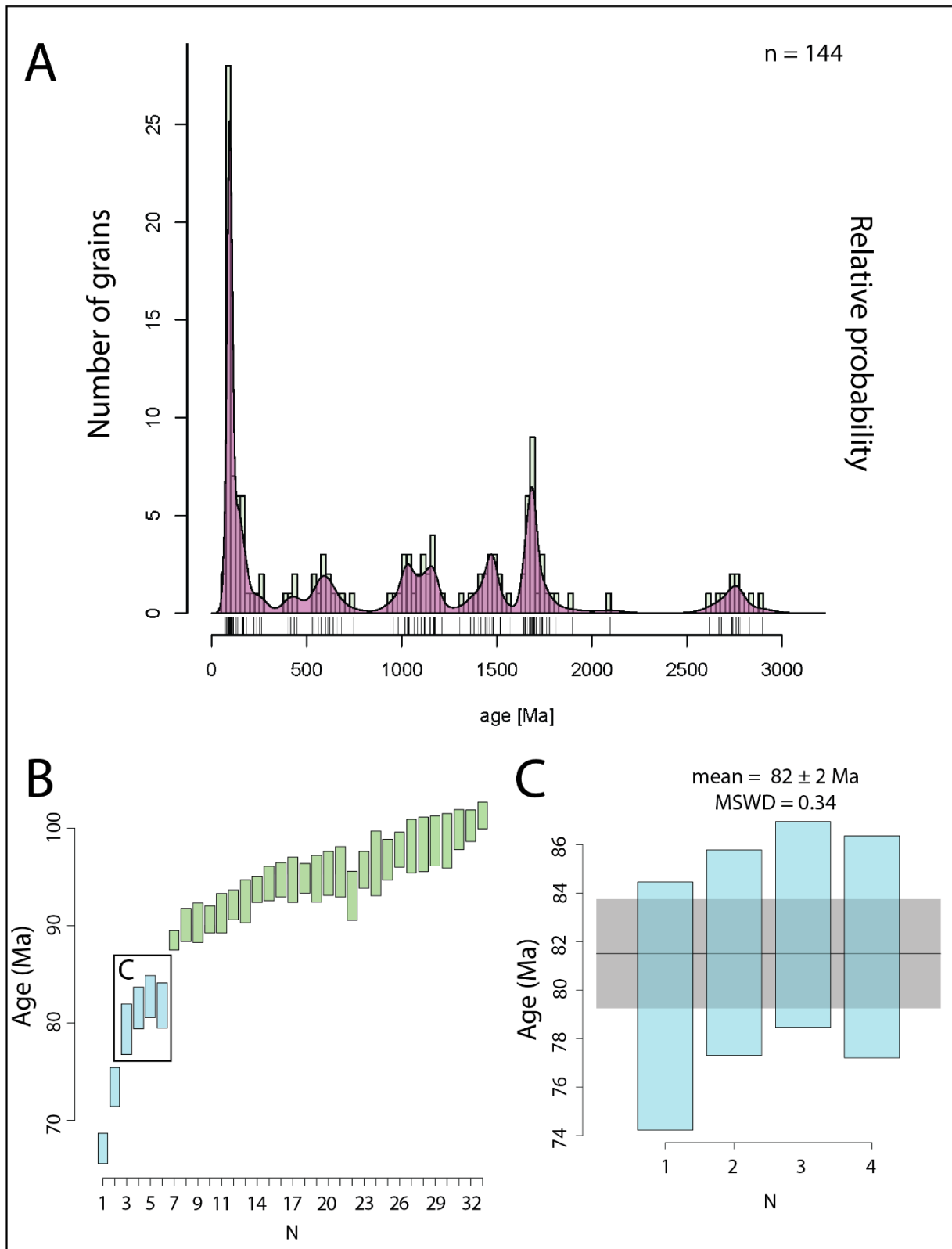
Sample LP080120-8 was collected from a 2-m interval of reddish-brown (weathered) and tan to orange (fresh), coarse-grained siliciclastic metasandstone (Figure 15). The sample yielded 197 concordant zircon grains with major age peaks at ca. 280-240 Ma ( $n = 74$ ), ca. 800-450 Ma ( $n = 24$ ), and ca. 1500-1300 Ma ( $n = 13$ ), and Archean grains ( $n = 51$ ) (Figure 32A). The youngest and most prominent zircon population ( $n = 66$ ) for the sample ranges from 263 to 234 Ma (Figure 32B). Within that population, the youngest subset of zircon grains ( $n = 17$ ) has an average age of  $248 \pm 2$  Ma and MSWD of 0.65, which is interpreted as the maximum depositional age of the sample (Figure 32C).



**Figure 32.** Detrital zircon age data for sample LP080120-8: **(A)** KDE plot shows major peaks at ca. 280-240 Ma, ca. 800-450 Ma, ca. 1500-1300 Ma, and Archean grains. **(B)** Weighted mean plot showing the youngest population of zircon grains ( $n = 66$ ) ranging from 263 to 234 Ma. **(C)** Weighted mean plot showing the youngest subset of zircon grains ( $n = 17$ ) with an average age of  $248 \pm 2$  Ma and MSWD = 0.65.

### ***Sample LP080120-9***

Sample LP080120-9 was collected from a 3-m interval of reddish-brown to black (weathered) and dark gray to green (fresh), coarse-grained volcanoclastic metasediment boudin (Figure 8, 15). The sample yielded 144 concordant zircon grains with major age peaks at ca. 140-70 Ma ( $n = 43$ ), ca. 750-500 Ma ( $n = 12$ ), ca. 1200-900 Ma ( $n = 22$ ), and ca. 1750-1600 Ma ( $n = 16$ ) (Figure 33A). The youngest population of zircon for the sample ( $n = 33$ ) ranges from 95 to 67 Ma (Figure 33B). Within that population, a younger subset of zircon grains (blue rectangles) has an average age of  $82 \pm 2$  Ma and MSWD of 0.34, which is interpreted as the maximum depositional age for the sample (Figure 33C).



**Figure 33.** Detrital zircon age data for sample LP080120-9: **(A)** KDE plot shows major peaks at ca. 140-70 Ma, ca. 750-500 Ma, ca. 1200-900 Ma, and ca. 1750-1600 Ma. **(B)** Weighted mean

plot showing the youngest population of zircon grains ( $n = 33$ ). Blue rectangles indicate youngest zircon grains that do not fall within two-sigma uncertainty of the rest of the population. **(C)** Youngest subset of zircon from the sample ( $n = 4$ ) with an average age of  $82 \pm 2$  Ma and  $MSWD = 0.34$ .

### ***Sample LP130120-1***

Sample LP130120-1 was collected from a 2.5-m interval of light-brown to orange (weathered) and light-green (fresh), very coarse-grained volcanoclastic metasandstone boudin. Only 10 zircon grains could be extracted and analyzed from this sample. Age peaks include ca. 100-90 Ma ( $n = 2$ ), ca. 650-550 Ma ( $n = 2$ ), ca. 1300-950 Ma ( $n = 3$ ), and ca. 1500-1400 Ma ( $n = 3$ ). LP130120-1 does not have enough data to create a KDE plot, determine the youngest population, or maximum depositional age of the sample.

## **Unit 4**

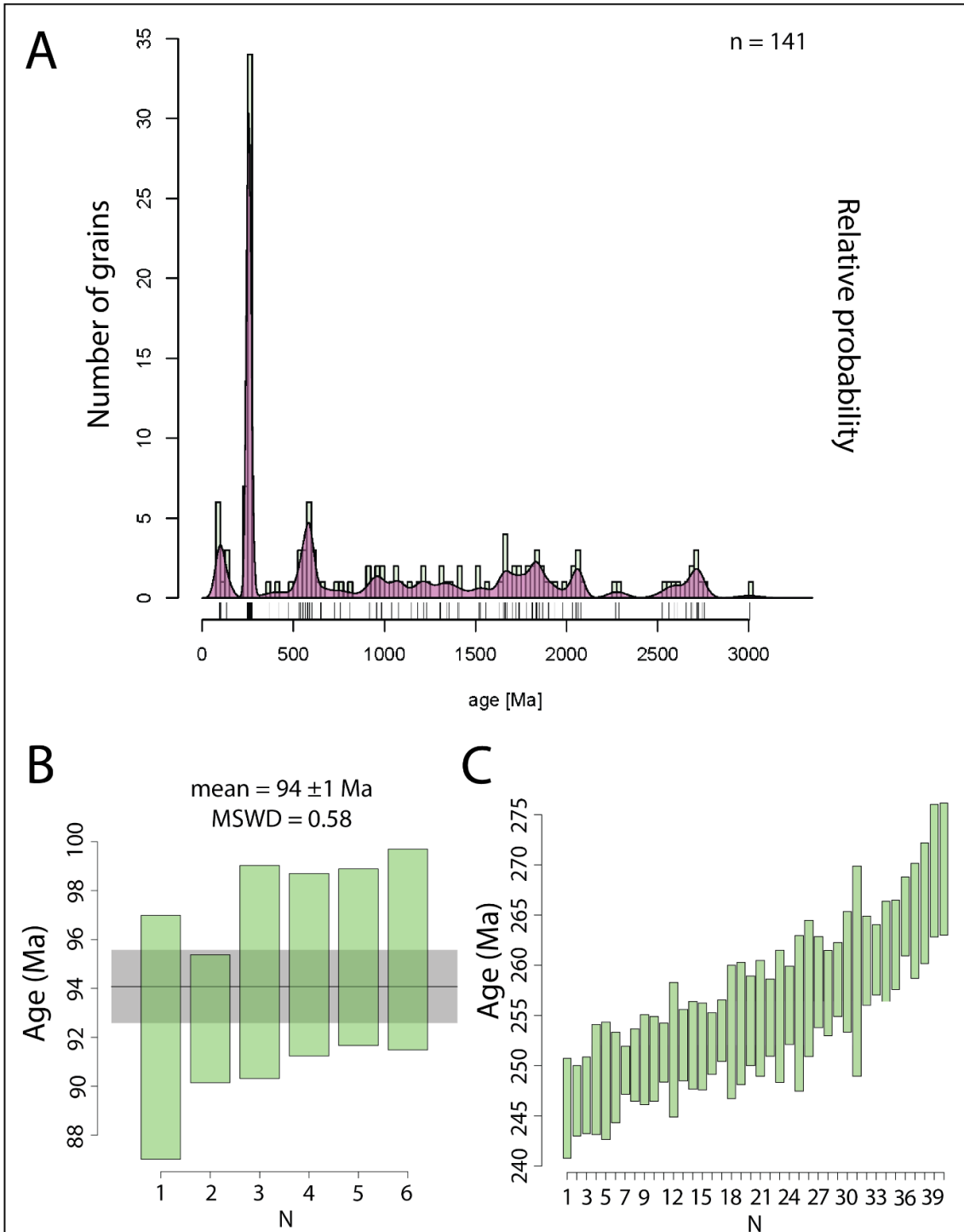
Two samples were collected from Unit 4, LP090120-2 and LP090120-3 (Figure 8). The samples were collected from interbedded metasandstone (LP090120-2) and metaconglomerate layers (LP090120-3). The major age groups for the samples are ca. 280-250 Ma, ca. 750-450 Ma, ca. 1300-750 Ma, and ca. 2800-2600 Ma. Both samples had a youngest population of zircon ranging from 140-90 Ma with an average age of about ca. 95 Ma that could be used for MDA.

### ***Sample LP090120-2***

Sample LP090120-2 was collected from a 40-cm interval of dark-green metasandstone (Figure 8, 18). The sample yielded 141 concordant zircon grains with major age peaks at ca. 275-245 Ma ( $n = 41$ ), ca. 750-450 Ma ( $n = 21$ ), ca. 1300-900 Ma ( $n = 17$ ), and Archean grains ( $n = 34$ ) (Figure 34A). The sample contains a small population of Cretaceous grains ( $n = 6$ ) with an



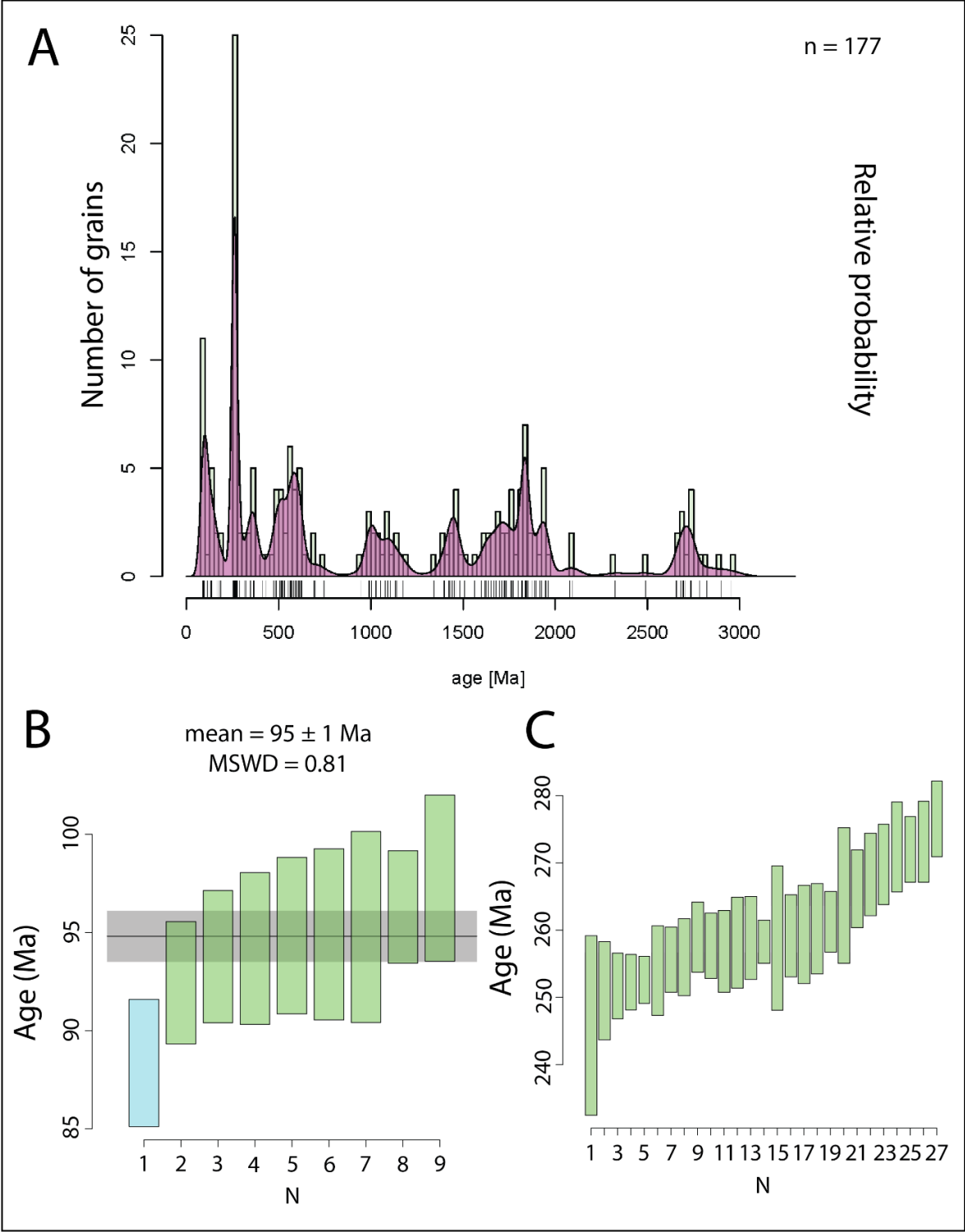
average age of  $94 \pm 1$  Ma and a MSWD of 0.58 that is interpreted as the maximum depositional age (Figure 34B). The sample also contains a large population of Permo-Triassic grains ( $n = 40$ ) that range from 274 to 246 Ma (Figure 34C).



**Figure 34.** Detrital zircon age data for sample LP090120-2: **(A)** KDE plot shows major peaks at ca. 275-245 Ma, ca. 750-450 Ma, ca. 1300-900 Ma, and ca. 2800-2600 Ma. **(B)** Weighted mean plot showing the youngest population of zircon grains ( $n = 6$ ) with an average age of  $94 \pm 1$  Ma and MSWD = 0.58. **(C)** Weighted mean plots showing large Permian population of zircon grains ( $n = 40$ ) ranging from 274-246 Ma.

### ***Sample LP090120-3***

Sample LP090120-3 was collected from a 3-m interval of dark-gray to purple metaconglomerate (Figure 8, 18). The sample yielded 177 concordant zircon grains with major age peaks at ca. 140-90 Ma ( $n = 17$ ), ca. 280-250 Ma ( $n = 27$ ), ca. 700-450 Ma ( $n = 30$ ), ca. 1750-1550 Ma ( $n = 12$ ), and Archean grains ( $n = 46$ ) (Figure 35A). The youngest population of grains ( $n = 9$ ) for the sample has an average age of  $95 \pm 1$  Ma and a MSWD of 0.81, which is interpreted as the maximum depositional age (Figure 35B). The sample also contains a large population of Permo-Triassic grains ( $n = 27$ ) ranging from 277 to 248 Ma (Figure 35C).



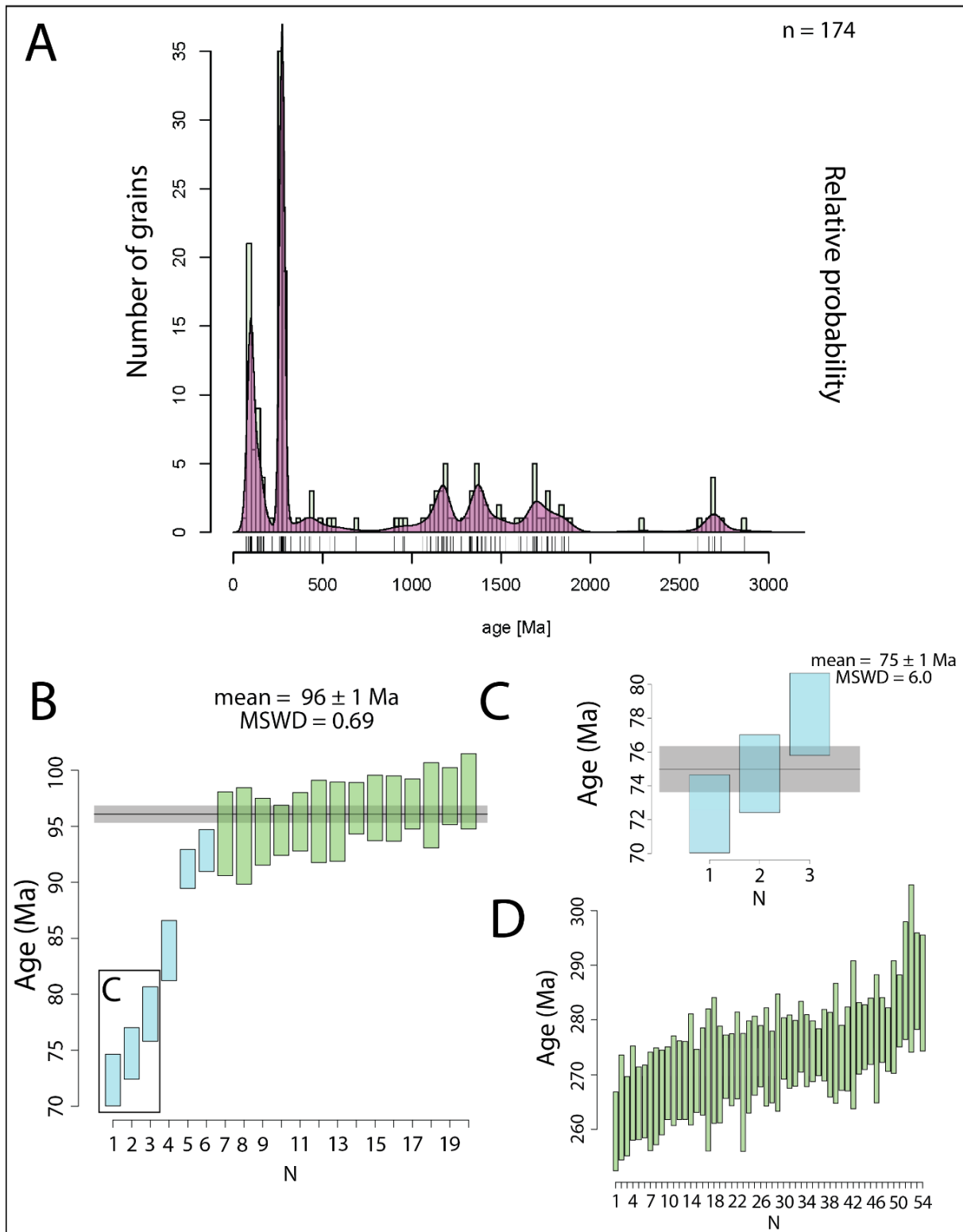
### 3.2.2 Sierra Las Pintas Group Detrital Ages

A total of 515 grains were concordant from the four samples collected from the Sierra Las Pintas Group (Figure 6). In general, the samples contain a youngest population of Cretaceous zircon as well as a larger population of Permian grains (except for one sample that has a Permian MDA). Prominent peaks from all the samples include ca. 150-70 Ma, ca. 280-240 Ma, ca. 750-430 Ma, and ca. 1750-1550 Ma.

#### Unit SP1

##### *Sample LP100120-1*

Sample LP100120-1 was collected from unit SP1 (Figure 6) from a 40-cm interval of light-brown to orange, very fine-grained metasandstone that is interbedded with thin beds of dark-gray to black metashale beds. The sample yielded 174 concordant zircon grains with major age peaks at ca. 150-70 Ma ( $n = 38$ ), ca. 280-240 Ma ( $n = 55$ ), ca. 1250-850 Ma ( $n = 21$ ), and ca. 1550-1300 Ma ( $n = 19$ ) (Figure 36A). The youngest population of zircon ( $n = 20$ ) from the sample has an average age of  $96 \pm 1$  Ma with a MSWD of 0.46 that is interpreted as the maximum depositional age (Figure 36B). Blue rectangles indicate youngest zircon grains that do not fall within two-sigma uncertainty of each other and cannot reasonably be considered as the maximum depositional age with a MSWD of 6 (Figure 36C). The sample also contains a large population of Permian grains ( $n = 54$ ) that range from 279 to 260 Ma (Figure 36D).



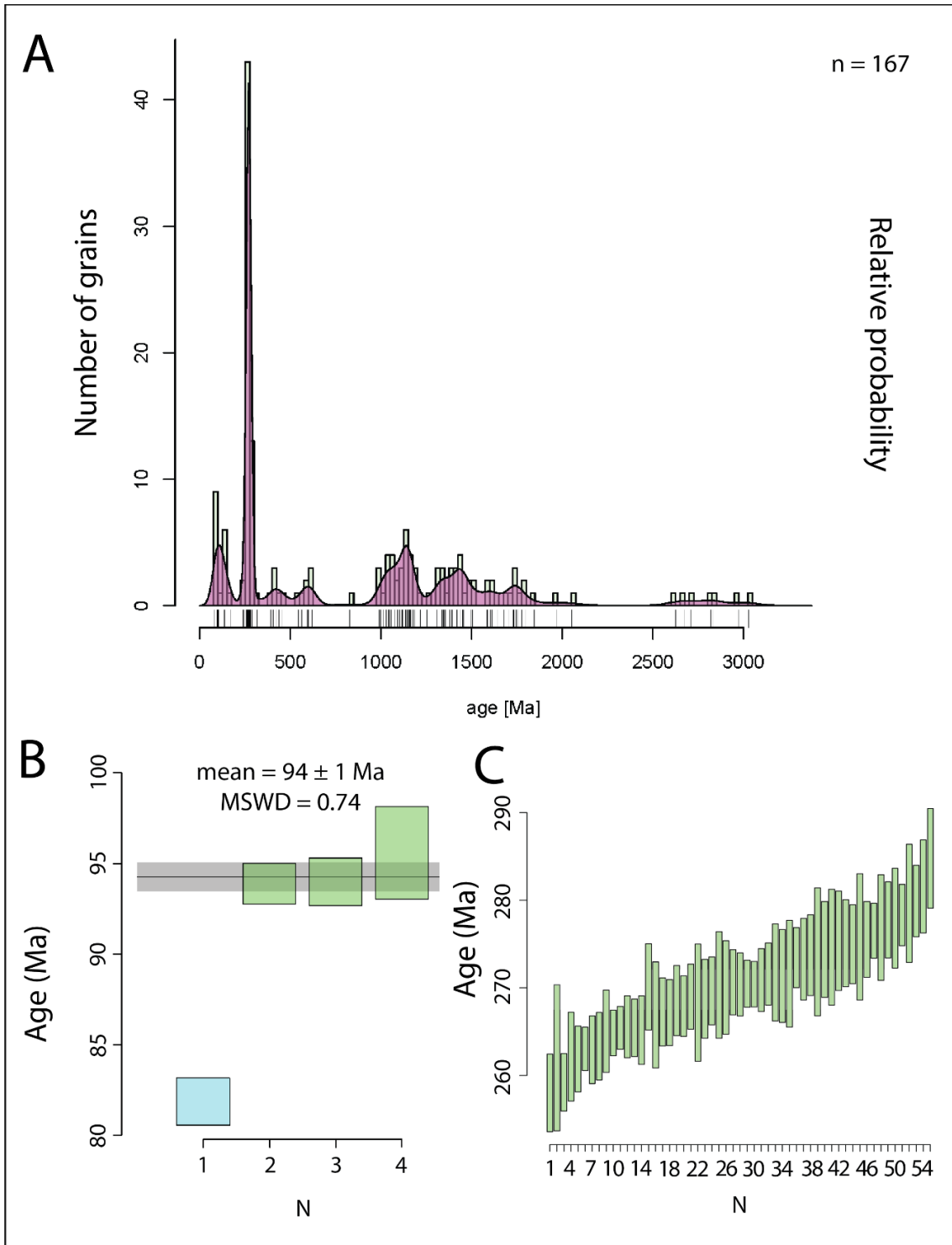
**Figure 36.** Detrital zircon age data for sample LP100120-1: **(A)** KDE plot shows major peaks at ca. 140-70 Ma and 280-240 Ma with minor age peaks at ca. 1250-850 Ma, ca. 1550-1300 Ma, and 1700-1600 Ma. **(B)** Weighted mean plot shows the youngest population of zircon grains ( $n =$

20) with an average age of approximately  $96 \pm 1$  Ma and MSWD = 0.69. Blue rectangles indicate the youngest zircon that are considered outliers for the sample. **(C)** Three youngest zircon grains from the sample that do not fall within two-sigma uncertainty of each other and have a MSWD of 6. **(D)** Weighted mean plot of a large Permian population of ages ( $n = 54$ ) ranging from 279 to 260 Ma.

## Unit SP2

### *Sample LP110120-1*

Sample LP110120-1 was collected from a 3-m interval of tan to light-orange, very coarse-grained metasandstone of Unit SP2 (Figure 8, 24). The sample yielded 167 concordant zircon grains with major age peaks at ca. 140-90 Ma ( $n = 16$ ), ca. 280-240 Ma ( $n = 58$ ), ca. 1300-950 Ma ( $n = 34$ ), and ca. 1550-1350 Ma ( $n = 20$ ) (Figure 37A). The youngest population of zircon grains from the sample has an average age of  $94 \pm 1$  Ma and a MSWD of 0.74 that is interpreted as the maximum depositional age (Figure 37B). Blue rectangle indicates an outlier in the population that is not included when calculating the maximum depositional age. The sample also contains a large Permian population of grains ( $n = 55$ ) that ranges from 284 to 258 Ma (Figure 37C).

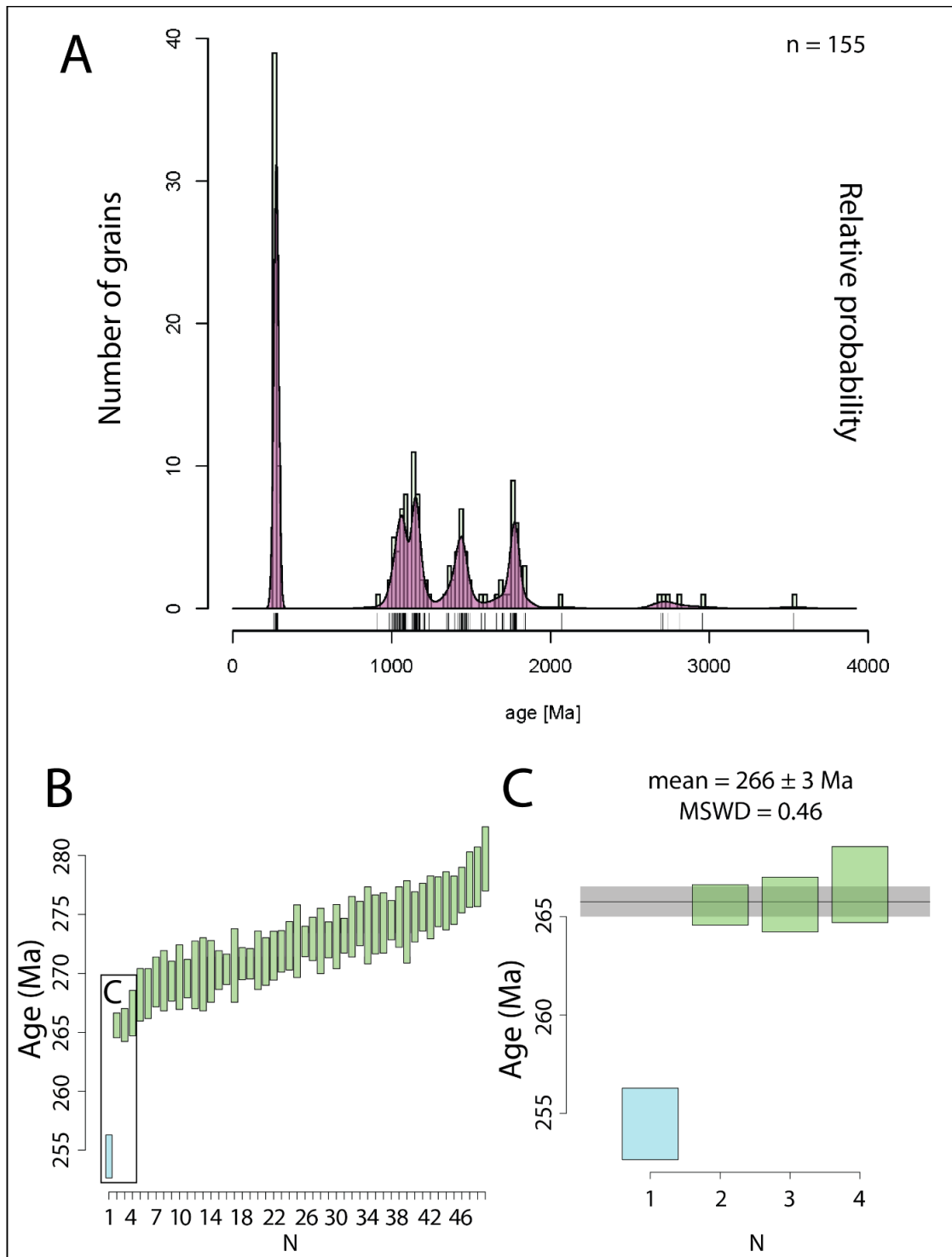


**Figure 37.** Detrital zircon age data for sample LP110120-1: **(A)** KDE plot shows major peaks at ca. 140-90 Ma, ca. 280-240 Ma, ca. 1300-950 Ma, and ca. 1550-1350 Ma. **(B)** Weighted mean plot of the youngest population of zircon grains ( $n = 7$ ) with an average age of  $94 \pm 1$  Ma and MSWD = 0.74. Blue rectangle indicates an outlier in the population. **(C)** Weighted mean plot of a large Permian population of zircon ( $n = 55$ ) that ranges from 284 to 258 Ma.

### ***Sample 18-LP-10***

Sample 18-LP-10 was collected from a very coarse-grained metasandstone of Unit SP2 (Figure 6). The sample yielded 155 concordant zircon grains with major age peaks at ca. 280-250 Ma ( $n = 49$ ), ca. 1250-1000 Ma ( $n = 50$ ), ca. 1500-1300 Ma ( $n = 23$ ), and ca. 1750-1600 Ma ( $n = 7$ ) (Figure 38A). The youngest population of zircon grains ( $n = 49$ ) ranges from 280 to 254 Ma (Figure 38B). Within that population, a younger subset of zircon grains has an average age of  $266 \pm 3$  Ma and MSWD of 0.46, which is interpreted as the maximum depositional age for the sample (Figure 38C). Blue rectangle indicates an outlier in the population and is not included when calculating the maximum depositional age.



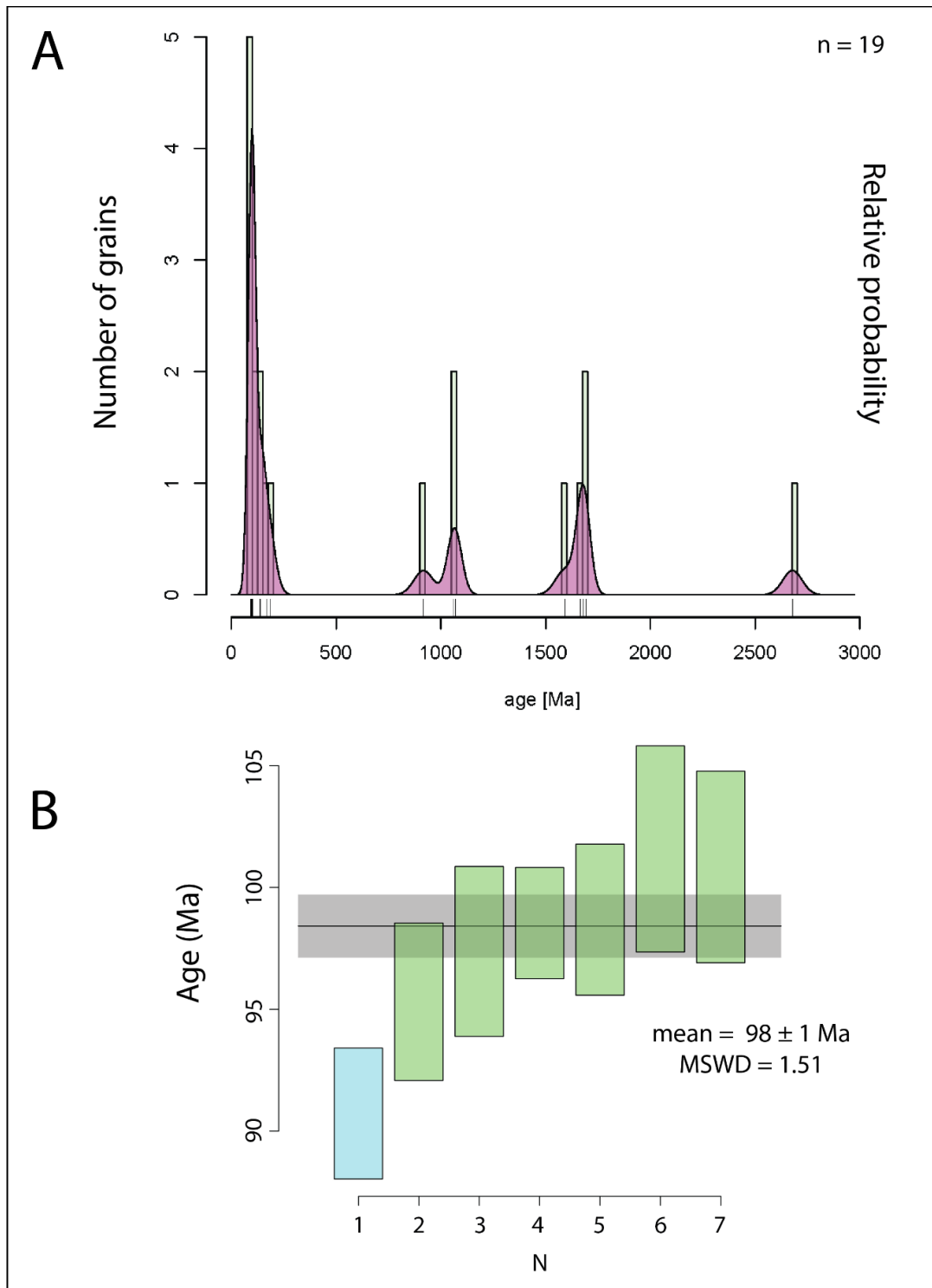


**Figure 38.** Detrital zircon age data for sample 18-LP-10: **(A)** KDE plot shows major peaks at ca. 280-250 Ma and minor age peaks at ca. 1250-1000 Ma, ca. 1500-1300 Ma, and ca. 1750-1600 Ma. **(B)** Weighted mean plot shows the youngest population of zircon grains ( $n = 49$ ) ranges from 280 to 254 Ma. Blue rectangle indicates an outlier in the population. **(C)** Youngest subset of zircon from the sample ( $n = 4$ ) with an average age of  $266 \pm 3$  Ma and  $MSWD = 0.46$ .

## Unit SP4

### *Sample X181218*

Sample X181218 was collected from basaltic metalava of Unit SP4. The sample yielded 19 concordant zircon grains with major age peaks at ca. 140-90 Ma ( $n = 9$ ), ca. 1100-850 Ma ( $n = 3$ ), and ca. 1700-1600 Ma ( $n = 4$ ) (Figure 39A). The youngest population of zircon grains has an average age of  $98 \pm 1$  Ma and MSWD of 1.51 based on the weighted mean plot (Figure 39B). The blue rectangle indicates an outlier in the population that is not included when calculating the maximum depositional age. Although the MSWD is  $>1$  and it is likely that the population contains multiple zircon sources, it is the most coherent population of youngest zircon from the sample and therefore is interpreted as the maximum depositional age.



**Figure 39.** Detrital zircon age data for sample X181218: **(A)** KDE plot shows major peaks at ca. 140-90 Ma, ca. 1100-850 Ma, and ca. 1700-1600 Ma. **(B)** Weighted mean plot shows the youngest population of zircon grains ( $n = 7$ ) with an average age of approximately  $98 \pm 1$  Ma and MSWD = 1.51. Blue rectangle indicates an outlier in the spectra.

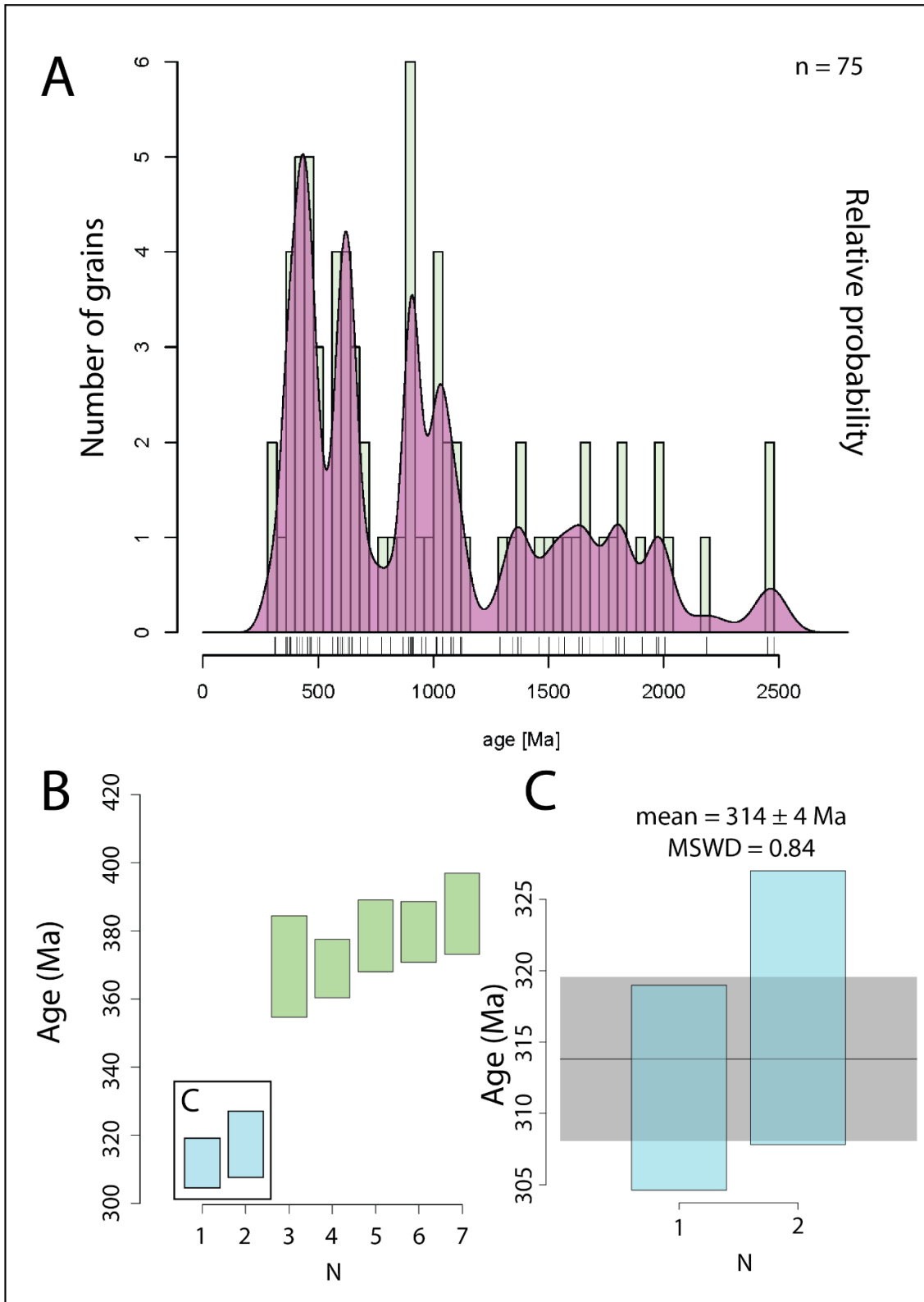
### **3.2.3 Minas de Barita Area Detrital Ages**

A total of 256 grains were concordant from the three samples collected from the Mina México Formation and Rancho Nuevo Formation of the Minas de Barita area. Major age peaks are similar for each of the samples at ca. 400-250 Ma, ca. 720-500 Ma, and ca. 1750-900 Ma.

#### **Rancho Nuevo Formation**

##### ***13-11-SR2***

Sample 13-11-SR2 was collected from the Rancho Nuevo Formation from a calcareous sandstone interbedded with chert and shale (Figure 5). The sample yielded 74 concordant zircon grains with major age peaks at ca. 430-300 Ma ( $n = 12$ ), ca. 700-450 Ma ( $n = 22$ ), ca. 1300-750 Ma ( $n = 20$ ), and Archean grains ( $n = 12$ ) (Figure 40A). The youngest population of zircon for the sample ( $n = 7$ ) ranges from 381 to 310 Ma (Figure 40B). A younger subset of zircon grains (blue rectangles) has an average age of  $314 \pm 4$  Ma with a MSWD of 0.84 and is interpreted as the maximum depositional age for the sample (Figure 40C).



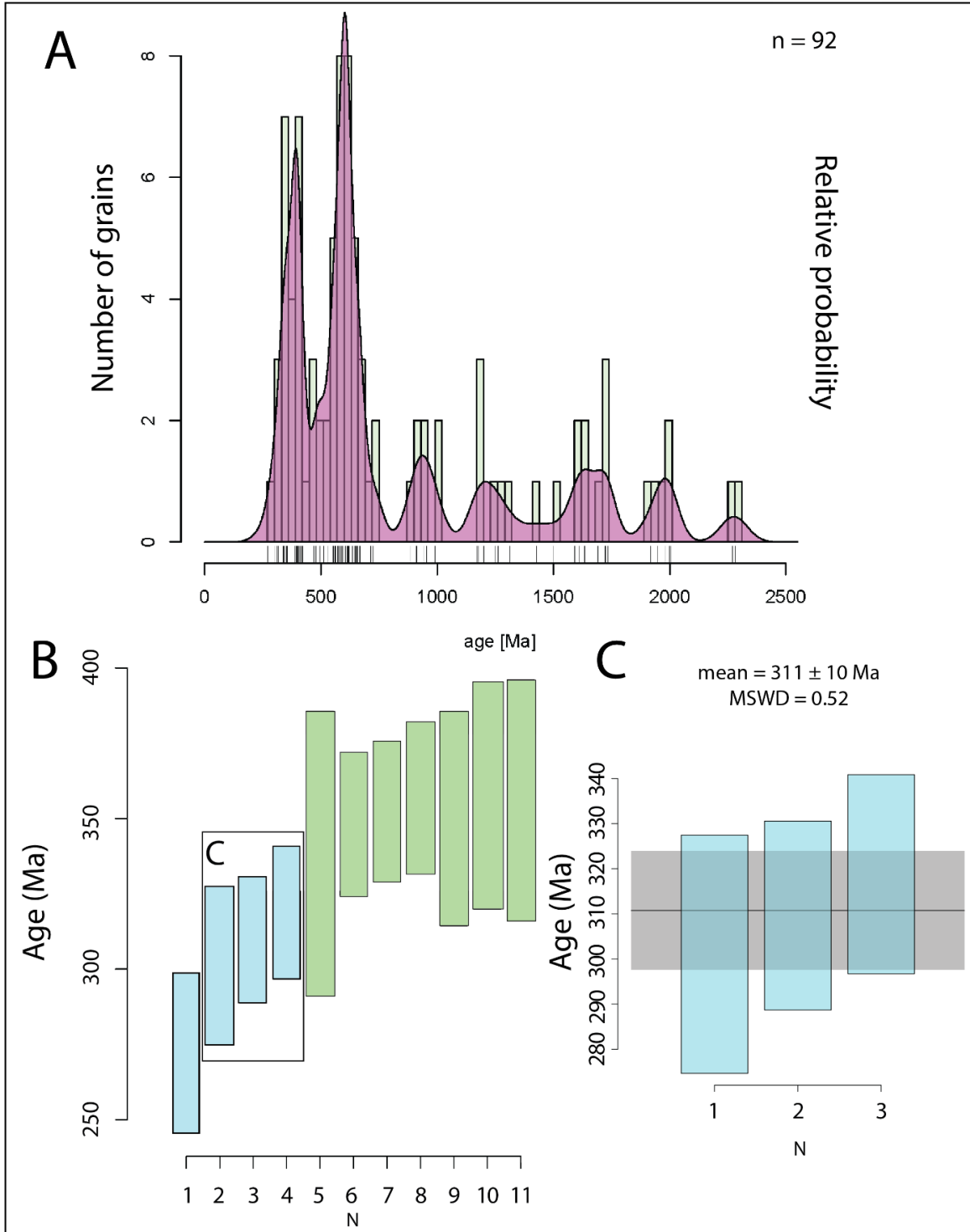
**Figure 40.** Detrital zircon age data for sample 13-11-SR2: **(A)** KDE plot shows major peaks at ca. 430-300 Ma, ca. 700-450 Ma, ca. 1300-750 Ma, and Archean grains. **(B)** Weighted mean

plot shows youngest population of zircon grains ( $n = 7$ ) ranges from 381 to 310 Ma. Blue rectangles indicate outliers for the population. (C) Youngest subset of zircon from the sample ( $n = 2$ ) with an average age of  $314 \pm 4$  Ma and MSWD of 0.84.

## **Mina México Formation**

### ***13-11-SR3***

Sample 13-11-SR3 was collected from a very fine- to fine-grained sandstone of the Mina México Formation (Figure 5). The sample yielded 92 concordant zircon grains with major age peaks at ca. 420-270 Ma ( $n = 23$ ), ca. 750-500 Ma ( $n = 39$ ), ca. 1300-900 Ma ( $n = 13$ ), and Archean grains ( $n = 9$ ) (Figure 41A). The youngest population of zircon grains ( $n = 11$ ) ranges from 355 to 300 Ma (Figure 41B). A younger subset of zircon grains (blue rectangles) does not overlap with the majority of the population and are considered statistically distinct from the youngest set of grains. The younger subset of zircon grains has an average age of  $311 \pm 10$  Ma with a MSWD of 0.52 and is interpreted as the maximum depositional age for the sample (Figure 41C).

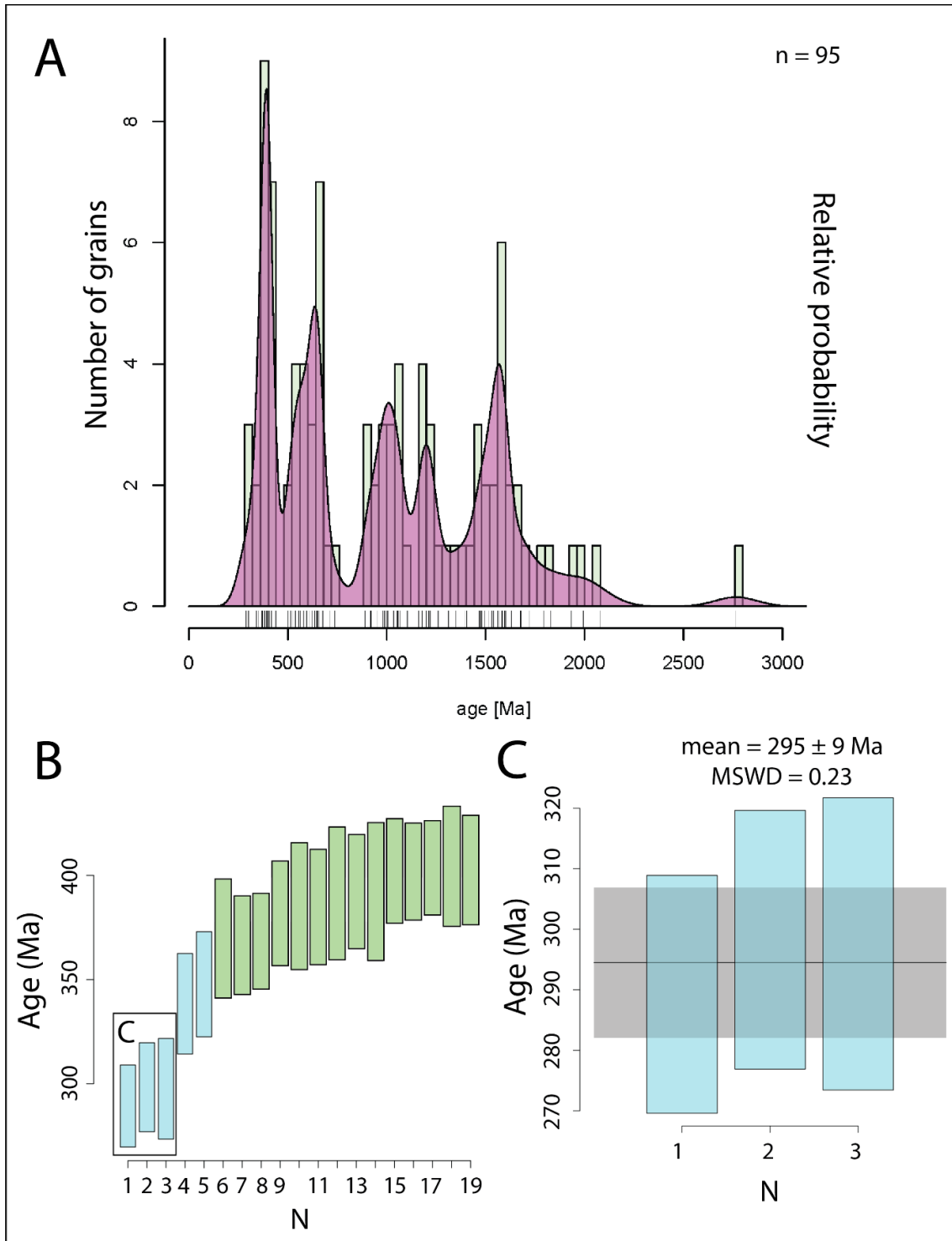


**Figure 41.** Detrital zircon age data for sample 13-11-SR3: **(A)** KDE plot shows major peaks at ca. 420-270 Ma, ca. 750-500 Ma, ca. 1300-900 Ma, and Archean grains. **(B)** Weighted mean plot shows youngest population of zircon grains ( $n = 11$ ) ranging from 355 to 300 Ma. Blue rectangles indicate outliers for the population. **(C)** Youngest subset of zircon from the sample ( $n = 3$ ) with an average age of  $311 \pm 10$  Ma and MSWD of 0.52.

### ***12-11-SR2***

Sample 12-11-SR2 was collected from a quartz-rich, fine-grained sandstone of the Mina México Formation (Figure 5). The sample yielded 95 concordant zircon grains with major age peaks at ca. 430-280 Ma ( $n = 21$ ), ca. 720-500 Ma ( $n = 22$ ), ca. 1200-900 Ma ( $n = 24$ ), and ca. 1750-1550 Ma ( $n = 12$ ) (Figure 42A). The youngest population of zircon grains ( $n = 19$ ) ranges from 402 to 289 Ma (Figure 42B). Within that population, a younger subset of zircon grains (blue rectangles) does not overlap with the majority of the population and are considered statistically distinct from the youngest set of grains. The younger subset of zircon grains has an average age of  $295 \pm 9$  Ma with a MSWD of 0.23 and is interpreted as the maximum depositional age for the sample (Figure 42C).





**Figure 42.** Detrital zircon age data for sample 12-11-SR2: **(A)** KDE plot shows major peaks at ca. 430-280 Ma, ca. 720-500 Ma, ca. 1200-900 Ma, and ca. 1750-1550 Ma. **(B)** Weighted mean plot shows youngest population of zircon grains ( $n = 19$ ) ranging from 402 to 289 Ma. **(C)** Youngest subset of zircon from the sample ( $n = 3$ ) with an average age of  $295 \pm 9$  Ma and MSWD of 0.23.

### 3.2.4 Sierra Las Pintas Area Trace Element Geochemistry

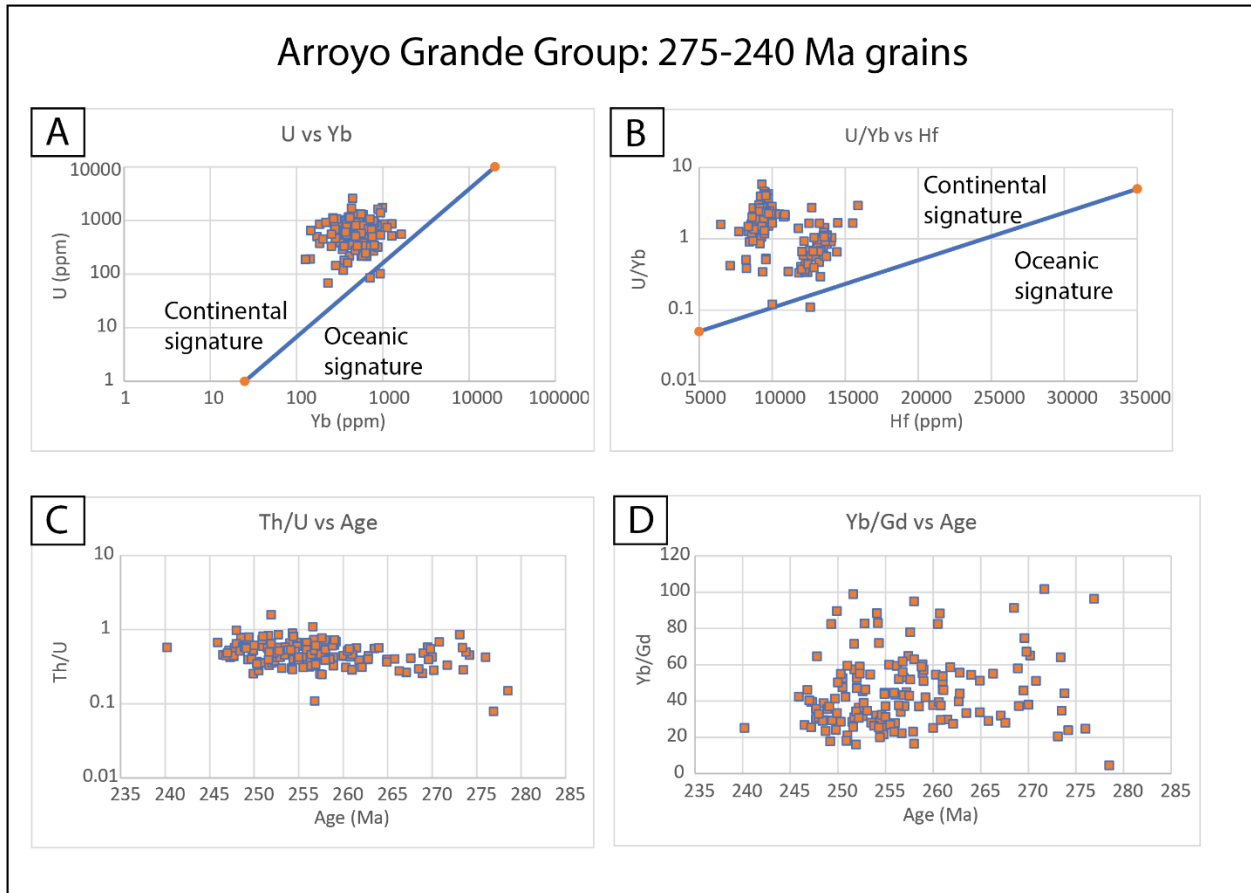
Bivariate geochemical plots were created for Cretaceous and Permo-Triassic grains from the Arroyo Grande Group and Sierra Las Pintas Group of the Sierra Las Pintas (Figures 43-48). Four geochemical bivariate plots, U vs Yb, Hf vs U/Yb, Th/U vs age, and Yd/Gd vs age were created to further understand the source rock composition and aid in interpreting the provenance of zircon grains from this study.

#### *Permo-Triassic Bivariate Plots*

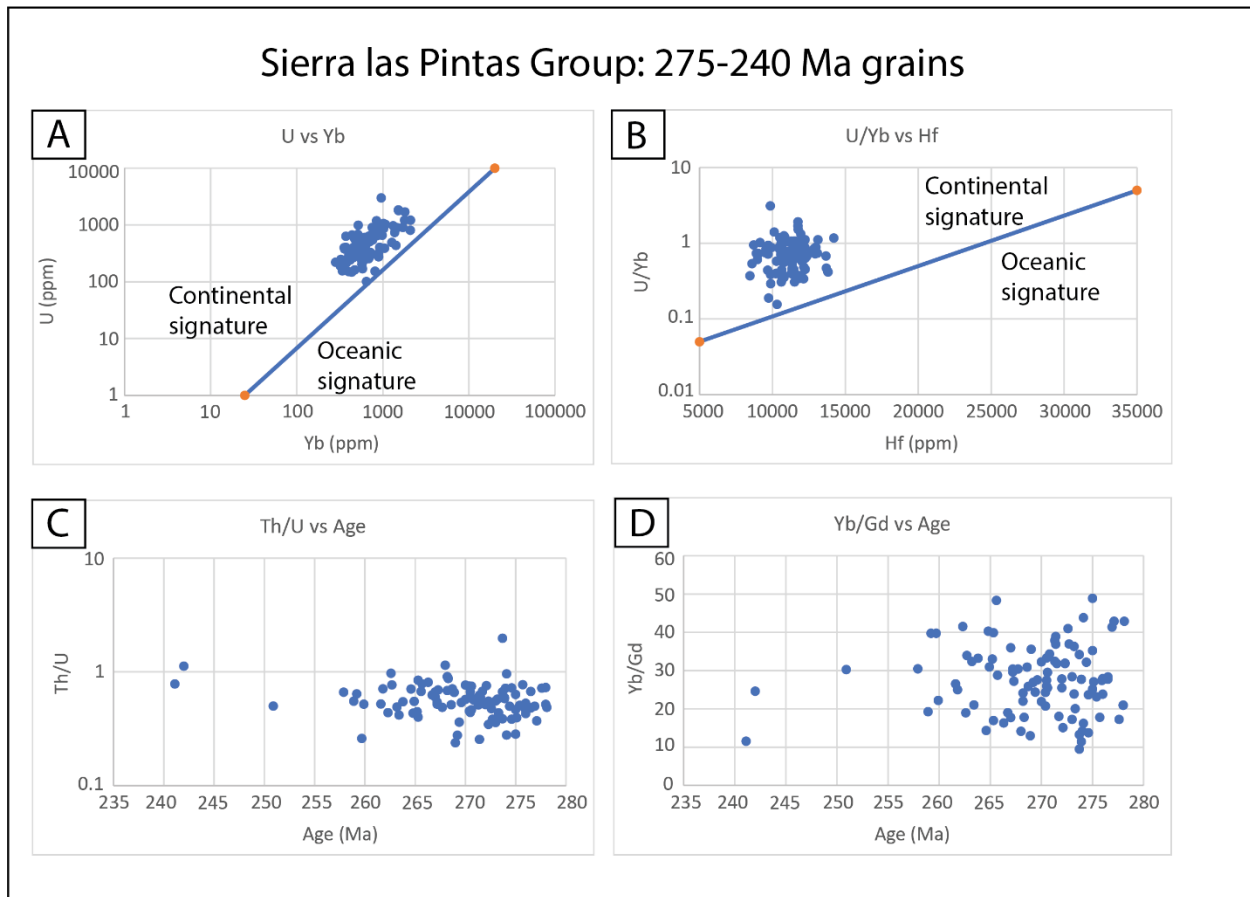
Permo-Triassic grains from the Arroyo Grande Group and the Sierra Las Pintas Group were plotted on geochemical bivariate diagrams and combined to determine if the geochemical characteristics were similar from each field area. Permo-Triassic grains from the Arroyo Grande Group all plot within the continental-arc array of Grimes et al. (2007; 2015). Th/U ratios range from approximately 0.25 to 1. Yb/Gd ratios vary dramatically and are widespread, ranging from approximately 20 to 100, with 83% of the grains greater than 30. (Figure 43). Permo-Triassic grains from the Sierra Las Pintas Group also plot within the continental-arc array of Grimes et al. (2007; 2015). Th/U ratios of zircon from the Sierra Las Pintas Group range from 0.25 to 1.2, with most of the zircon grains plotting around 0.4. Yb/Gd ratios for Sierra Las Pintas Group zircon range from 10 to 50 (Figure 44).

Bivariate trace element diagrams for 275-240 Ma grains of the Sierra Las Pintas Group and Arroyo Grande Group show many similarities (Figure 45). U vs Yb and U/Yb vs Hf plots of Permo-Triassic grains from both areas plot within the continental field. Th/U ratios for both field areas range from 0.2 to 1. The Yb/Gd ratios for the two fields generally range from 10-90, with

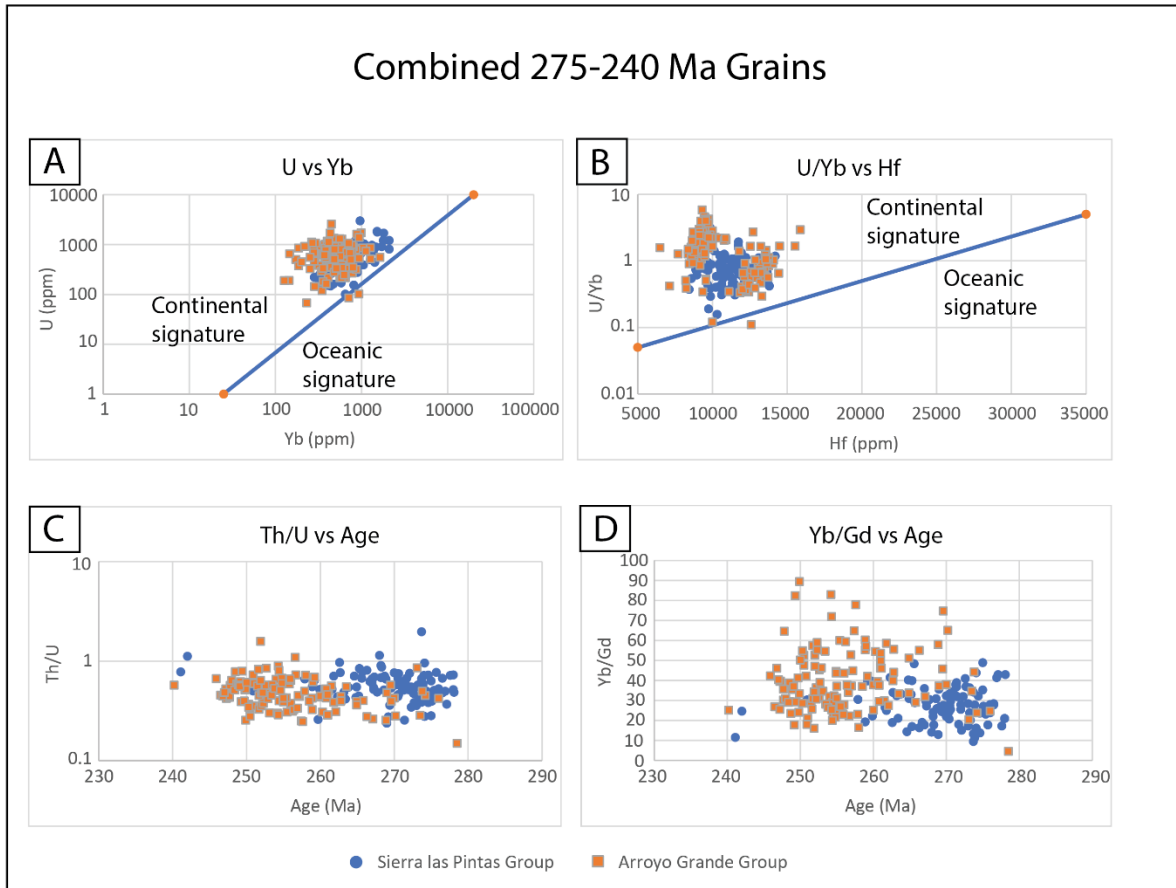
the Arroyo Grande Group zircon showing a slightly higher and more widespread range. The Arroyo Grande Group zircon suite is slightly older than Sierra Las Pintas Group zircon suite, but trace element ratios are consistent.



**Figure 43.** Geochemical bivariate plots of all 275-240 Ma age zircon grains from the Arroyo Grande Group. **A-B)** U vs Yb and Y/Yb vs Hf diagrams with grains plotting within the continental field. **C)** Th/ U vs Age plot showing Th/U ratios ranging from 0.25 to 1. **D)** Yb/Gd vs Age plot with Yb/Gd ratios between 20 and 100.



**Figure 44.** Geochemical bivariate plots for 275-240 Ma age zircon from all samples of the Sierra Las Pintas Group. **A-B)** U vs Yb and Y/Yb vs Hf diagrams with grains plotting within the continental field. **C)** Th/ U vs Age plot showing Th/U ratios ranging from 0.25-1.2. **D)** Yb/Gd vs Age plot with Yb/Gd ratios ranging from 10-50.



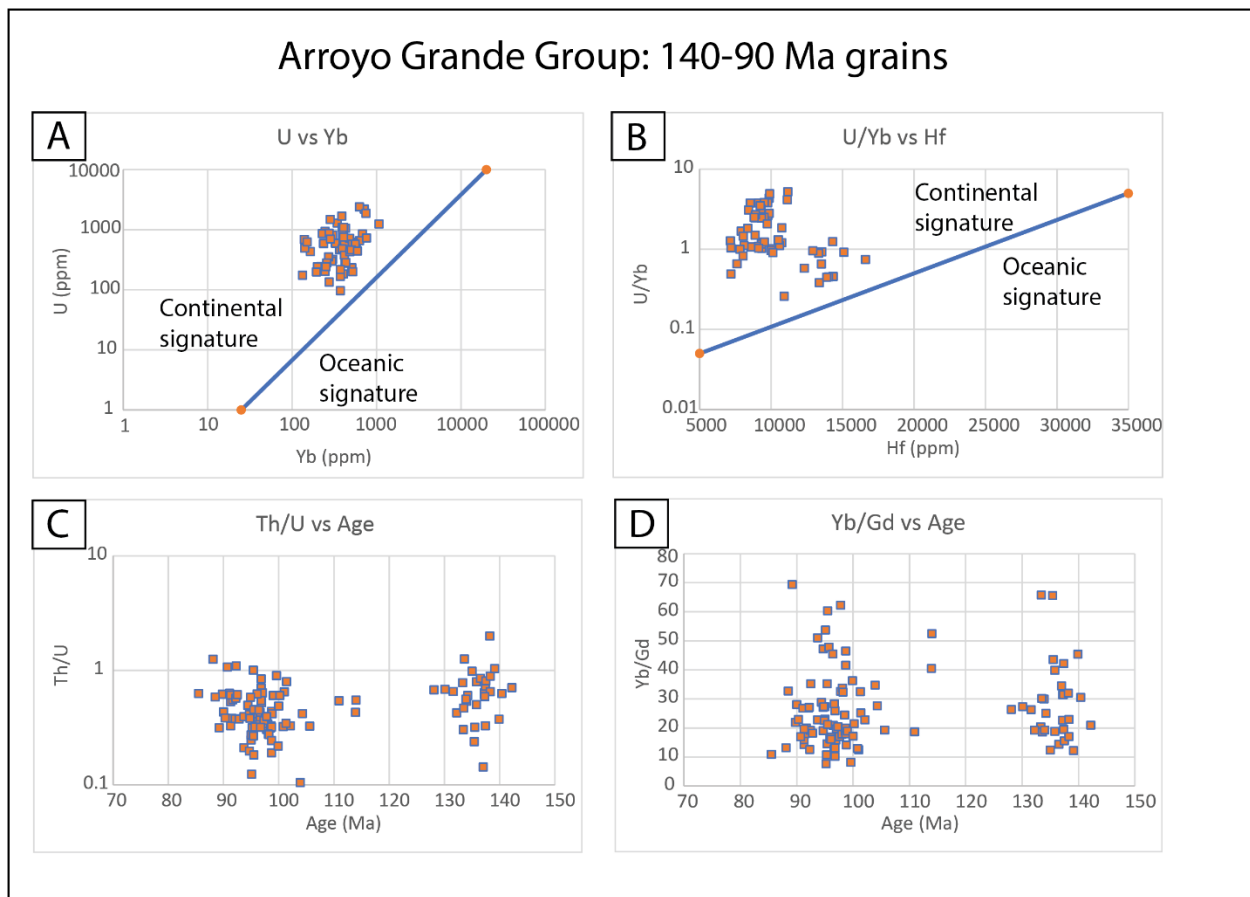
**Figure 45.** Geochemical bivariate plots for 275-240 Ma age zircon from samples collected from the Sierra Las Pintas Group and the Arroyo Grande Group. **A-B)** U vs Yb and Y/Yb vs Hf diagrams with grains plotting within the continental field. **C)** Th/ U vs Age plot showing Th/U ratios of 0.2-1. **D)** Yb/Gd vs Age plot showing Yb/Gd ratios of approximately 10-90.

### ***Cretaceous Bivariate Plots***

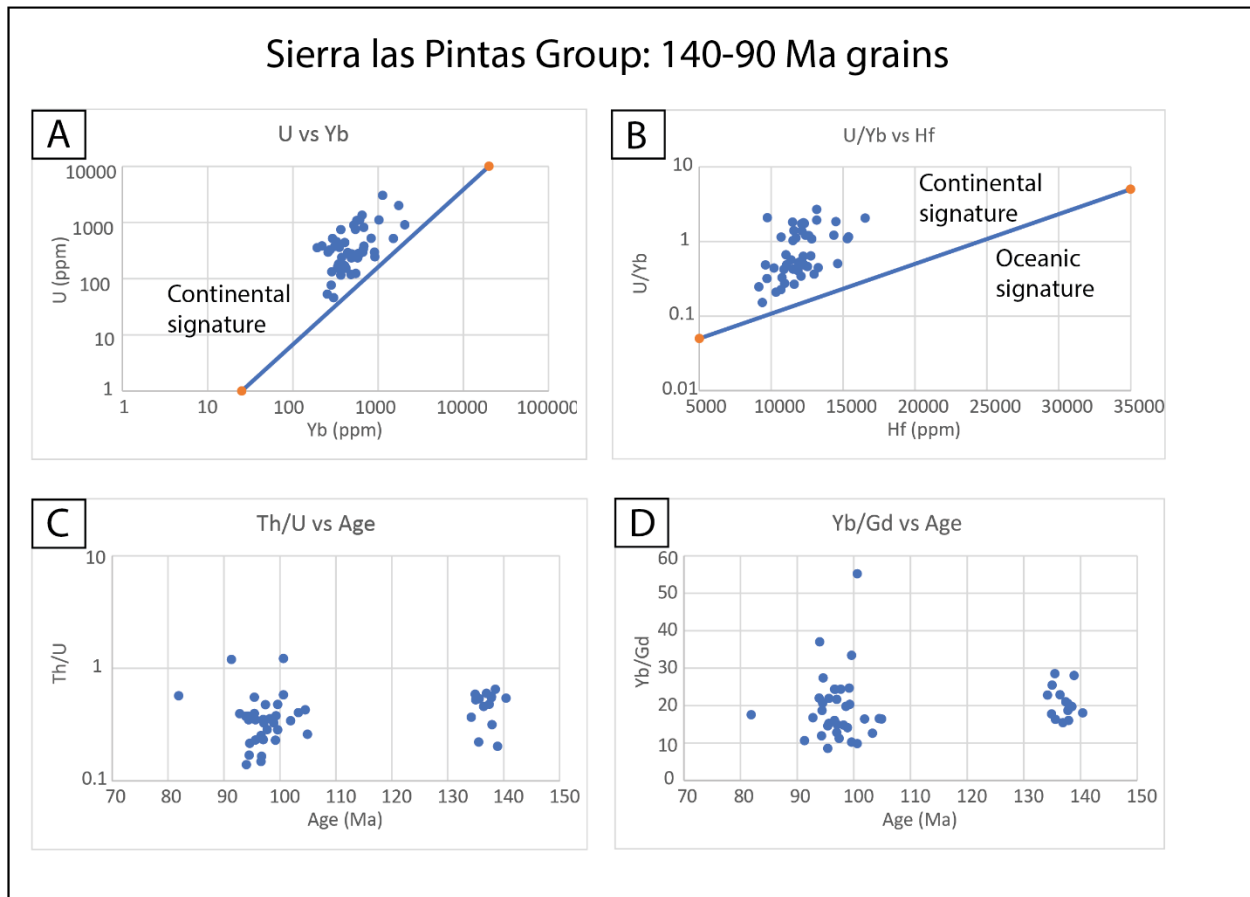
Cretaceous grains were plotted on geochemical bivariate diagrams from the Arroyo Grande Group, the Sierra Las Pintas Group and combined. The Cretaceous grains of the Arroyo Grande Group all plot within the continental arc arrays of Grimes et al. (2007; 2015) on U vs Yb and U/Yb diagrams. Th/U ratios of zircon from the Arroyo Grande Group range from 0.25 to 1. Yb/Gd ratios of the Cretaceous zircon range from 10 to 70, with 72% of the grains plotting below 30 (Figure 46). The Cretaceous grains of the Sierra Las Pintas Group also plot within the continental arc arrays of Grimes et al. (2007; 2015) on U vs Yb and U/Yb diagrams. Th/U ratios

of the Sierra Las Pintas Cretaceous zircon range from 0.15 to 1.2 and Yb/Gd ratios range from 10 to 30 (Figure 47).

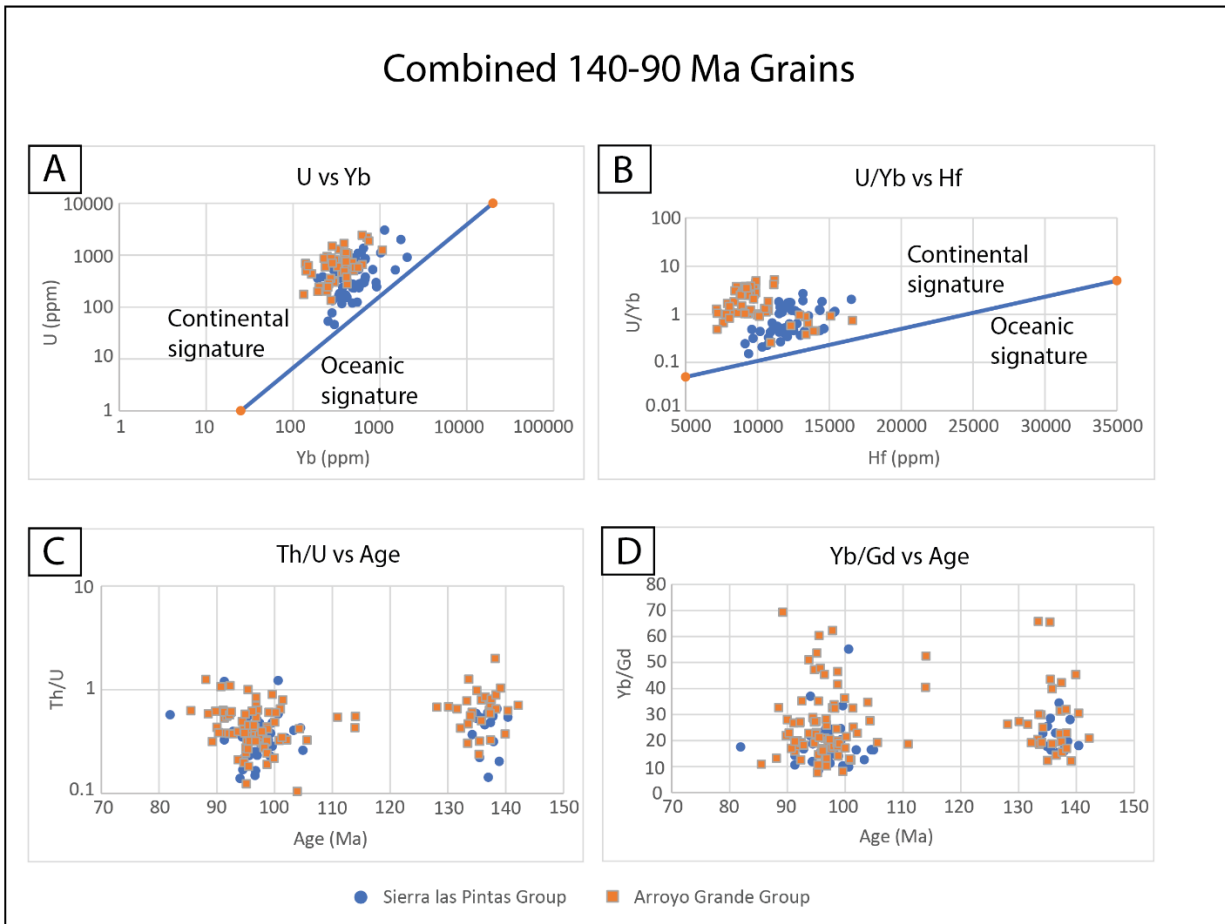
Bivariate trace element diagrams for 140-90 Ma zircon grains of the Sierra Las Pintas Group and Arroyo Grande Group show similar characteristics (Figure 48). U vs Yb and U/Yb vs Hf plots of Cretaceous grains from both areas plot within the continental field, with the Arroyo Grande Group have a slightly higher U content. Th/U and Yb/Gd ratios for both field areas plot almost exactly the same, with Th/U ratios of 0.15 to 2 and Yb/Gd ratios of 10 to 70.



**Figure 46.** Geochemical bivariate plots of all 140-90 Ma zircon grains from the Arroyo Grande Group. **A-B)** U vs Yb and U/Yb vs Hf diagrams with grains plotting within the continental field. **C)** Th/ U vs Age plot showing Th/U ratios ranging from 0.1-2. **D)** Yb/Gd vs Age plot with Yb/Gd ratios ranging from 10-70.



**Figure 47.** Geochemical bivariate plots for 140-90 Ma zircon from all samples of the Sierra Las Pintas Group. **A-B)** U vs Yb and Y/Yb vs Hf diagrams with grains plotting within the continental field. **C)** Th/ U vs Age plot showing Th/U ratios ranging from 0.15-1.2. **D)** Yb/Gd vs Age plot with Yb/Gd ratios ranging from 10-30.



**Figure 48.** Geochemical bivariate plots for 140-90 Ma age zircon from samples collected from the Sierra Las Pintas Group and the Arroyo Grande Group. **A-B)** U vs Yb and Y/Yb vs Hf diagrams with grains plotting within the continental field. **C)** Th/ U vs Age plot showing similar Th/U ratios. **D)** Yb/Gd vs Age plot with both field areas indicating similar Yb/Gd ratios.

## 4.0 DISCUSSION

### 4.1 DETRITAL ZIRCON AGES AND PROVENANCE ANALYSIS

This study provides the first geochronological analysis of the proposed Sonora allochthon strata of the Sierra Las Pintas. While previous studies (Leier-Engelhardt, 1993; Poole et al., 2005; Poole et al., 2008; Navas-Parejo et al., 2018) hypothesized that similar stratigraphy and



biostratigraphic ages allow a correlation of the strata of the Sierra Las Pintas to Sonora allochthon stratigraphy of central Sonora, the results of this study suggest an alternative story.

### ***Geochronology Re-analysis***

Detrital zircon geochronological analysis of the Sierra Las Pintas Area yielded an unexpected Cretaceous MDA for various units of the Sierra Las Pintas Group and the Arroyo Grande Group. This depositional age is much younger than the hypothesized emplacement age for the Sonora allochthon strata and measures were taken to verify that the Cretaceous zircon did not undergo hydrothermal alteration or intense metamorphism from subsequent tectonic evolution of the area. Zircon is highly resistant to metamorphism, weathering, and partial melting and can preserve original crystallization ages and geochemical composition, but specific conditions could potentially affect the isotopic age of the grain. Zircon grains can be susceptible to elemental change under aqueous conditions at a range of temperatures. Van Lankvelt (2016) determined that the rims of zircon interacting with hydrothermal fluid can re-equilibrate, experience Pb- loss, and effectively reset the isotopic clock. Partial dissolution or recrystallization of zircon can result in geochronological ages that do not reflect the original crystallization age of the zircon. Partial dissolution typically results in recrystallized zircon rims that contain a younger age than the original detrital core of a zircon. In order to account for that possibility, a random selection of Cretaceous grains underwent U-Pb isotope re-analysis, taking care to analyze the cores of the zircon (Table 5). Every zircon that was re-analyzed yielded the same isotopic age, within error, as was originally determined with the exception of one grain, LP080120-9\_144. Zircon LP080120-9\_144 appears to have an altered metamorphic rim as the detrital core age of the zircon is 800 Ma upon re-analysis, as opposed to the rim age of 172 Ma from the original analysis. Discordant zircon grains are highlighted in red (Table 5).

Field Area	Unit	Sample	Spot #	Age (Ma)		Run 2 Concordance			
				Run 1	Run 2				
Arroyo Grande Group	1	LP070120-1	LP070120_1s_70	71	72	0.8			
			LP070120_1s_96	91	97	0.93			
			LP070120_1s_108	95	96	1			
			LP070120_1L_17	96	94	0.97			
			LP070120_1s_118	97	99	0.99			
			LP070120_1s_74	99	101	0.98			
			LP070120_1s_33	100	96	1			
			LP070120_1s_36	113	102	0.94			
			LP070120_1L_21	140	135	0.99			
			LP070120_1L_15	165	164	0.99			
			LP070120_1L_37	80	67	0.28			
			LP070120_1s_67	86	71	0.2			
				3	LP080120-9	LP080120_9s_137	81	81	0.99
						LP080120_9s_40	92	93	0.95
LP080120_9L_8	95	96				0.99			
LP080120_9s_167	95	101				1.03			
LP080120_9s_2	96	98				0.99			
LP080120_9s_68	99	99				1.02			
LP080120_9s_38	104	118				0.99			
LP080120_9s_30	136	139				1.01			
LP080120_9s_156	141	142				1			
LP080120_9s_144	172	800				0.88			
LP080120_9s_51	90	93				0.76			
LP080120_9s_74	97	94	0.59						
	4	LP090120-3	LP090120_3s_111	88	97	0.98			
			LP090120_3L_36	94	96	1.01			
			LP090120_3L_50	95	96	1			
			LP090120_3s_10	115	117	1			
			LP090120_3L_26	136	134	0.97			
			LP090120_3L_48	164	167	1.02			
Sierra Las Pintas Group	SP 1	LP100120-1	LP100120_1L_40	73	77	1			
			LP100120_1s_44	76	77	0.89			
			LP100120_1s_36	95	98	0.96			
			LP100120_1s_70	97	95	0.91			
			LP100120_1s_56	98	102	0.93			
			LP100120_1L_73	100	101	1.02			
			LP100120_1s_46	102	103	1.02			
			LP100120_1L_21	135	136	0.99			
			LP100120_1L_34	138	138	1			
			LP100120_1L_89	140	117	0.98			
			LP100120_1s_54	160	168	1.02			
			LP100120_1L_62	115	94	0.22			
				SP 2	LP110120-1	LP110120_1L_4	83	83	0.96
						LP110120_1s_10	97	99	1
LP110120_1L_73	99	97				0.98			
LP110120_1s_13	138	135				1.01			
LP110120_1L_61	140	137				0.99			

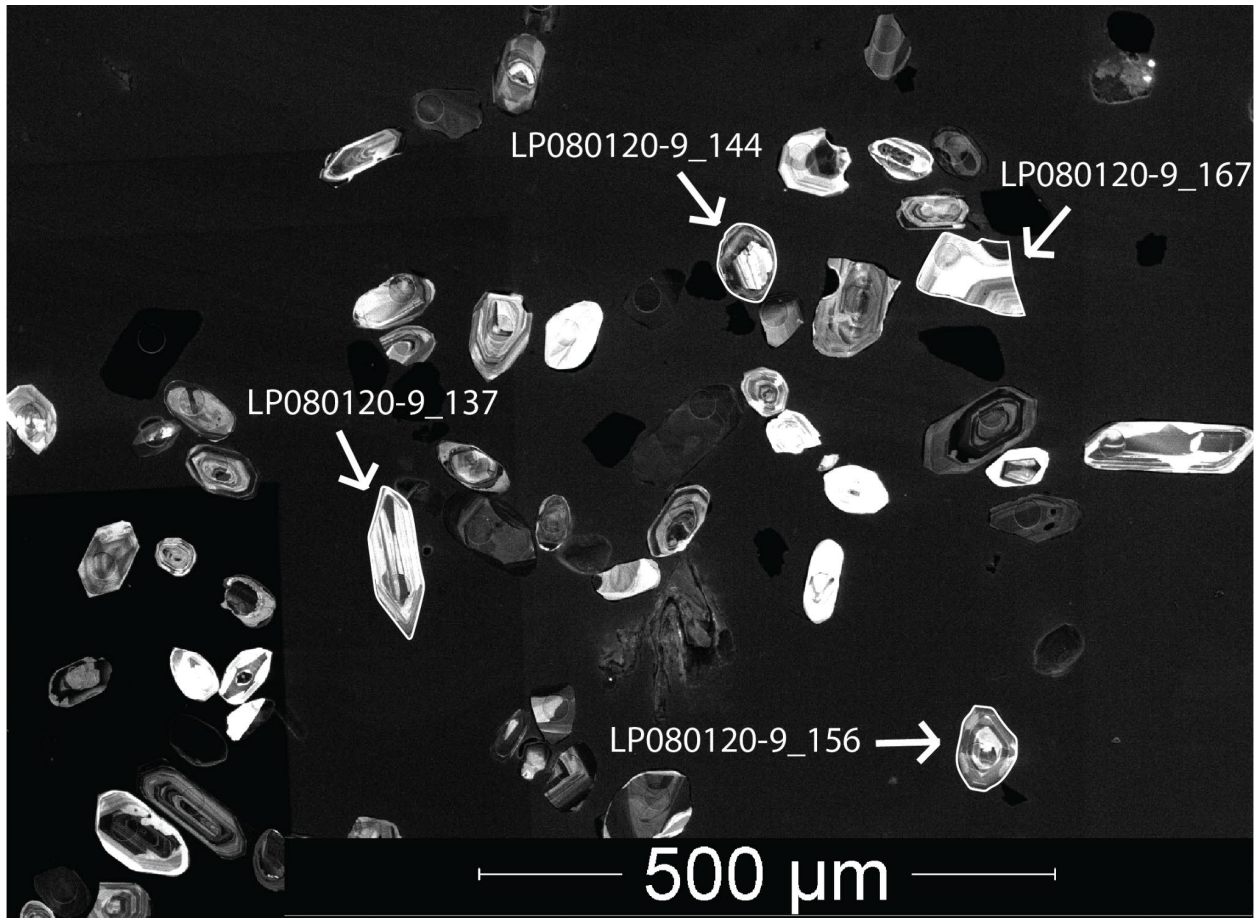
**Table 5.** Summary of the re-analysis of grains selected from samples that contained a large population of Cretaceous zircon. Discordant zircon grains are highlighted in red and the zircon grain highlighted in green contains an older core.

### *Cathodoluminescence*

Cathodoluminescence images were also taken of samples containing large suites of Cretaceous zircon to identify any characteristics indicative of metamorphic textures, hydrothermal alteration, or any identifiable patterns in zircon morphology (Figure 49). Igneous zircon will display typical oscillatory zoning that is parallel to the crystal face. Zircon that has experienced hydrothermal alteration may show complex internal textures where secondary domains cut across primary growth zones (Hoskin and Schaltegger, 2003). Zircon crystals that have been affected by hydrothermal alteration have also shown bright resorption shadows in cathodoluminescence, indicating a distinct chemical change such as elevated U and LREE concentrations (Van Lankvelt, 2016). All re-analyzed Cretaceous grains from samples LP070120-1, LP080120-9, LP100120-1, and LP110120-1 were identified from analysis maps and labelled in the cathodoluminescence images. The Cretaceous zircon grains range in size from approximately 50  $\mu\text{m}$  to 160  $\mu\text{m}$  in length and in shape from well-rounded (LP080120-9\_156) to euhedral (LP080120-9\_137) to fractured (LP080120-9\_167) (Figure 49). The majority of the grains contain oscillatory-zoned or sector-zoned (LP080120-9\_156) growth with a few exhibiting overprint by replacement zones due to metamorphism. For the rest of the re-analyzed grains, no strong indication of altered metamorphic rims or hydrothermal alteration was apparent. All cathodoluminescence images of the re-analyzed grains are in Appendix V.

No convincing data show that Cretaceous grains within a Paleozoic succession of the Arroyo Grande Group and the Sierra Las Pintas Group have been altered due to intense

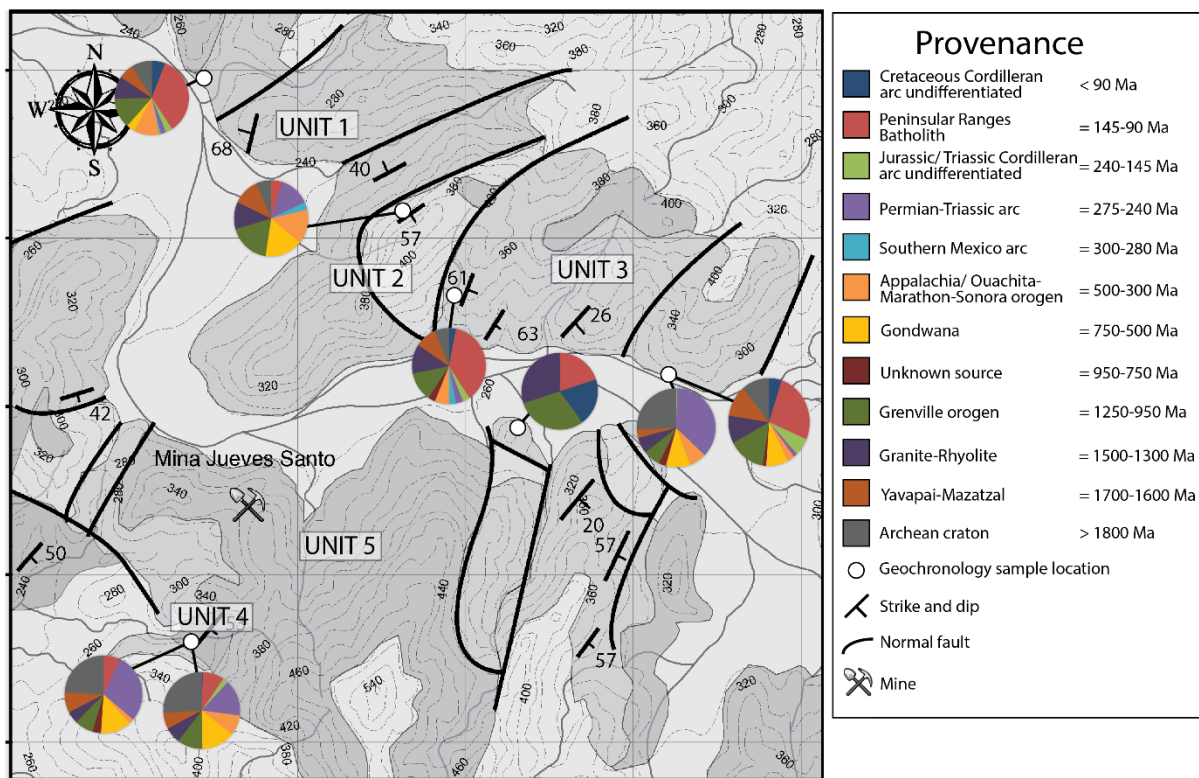
metamorphism or hydrothermal alteration. Alternative explanations for the presence of the Cretaceous grains were investigated in order to determine the provenance of the Sierra Las Pintas strata.



**Figure 49.** Cathodoluminescence image of sample LP080120-9 with one grain (LP080120-9\_144) containing an older detrital core and metamorphic rim. Other zircon grains exhibit oscillatory rings and range from euhedral to anhedral. The length of the zircon grains ranges from approximately 50 microns to 160 microns.

### 4.1.1 Provenance Interpretations of the Arroyo Grande Group

Detrital zircon geochronological analysis from the Arroyo Grande Group indicates two distinct source areas for the samples. From the eight samples collected, four samples contain a dominant Permo-Triassic population of zircon (ca. 275-240 Ma), while the other four samples contain a dominant Cretaceous population of zircon (ca. 140-90 Ma) with rare Permo-Triassic zircon (Figure 50). The following discussion of detrital zircon ages and associated provenance for the Arroyo Grande Group is split into the samples that contain a dominant Permo-Triassic zircon population and the samples that contain a dominant Cretaceous zircon population.



**Figure 50.** Geologic map of the Arroyo Grande Group with location of geochronological samples. Pie charts indicate provenance percentages of each sample.

### *Permo-Triassic Samples*

Samples containing a dominant Permo-Triassic population of zircon include LP070120-2 of Unit 2, sample LP080120-8 of Unit 3, and samples LP090120-2 and LP090120-3 of Unit 4 (Table 1; Figure 50-51). Grains ranging from 275-240 Ma make up the largest population of zircon from each sample and are most likely derived from the Cordilleran Permo-Triassic arc (Figures 30, 32, 34-35). The samples also include major age peaks at ca. 750-500 Ma, that could indicate grains derived from a Gondwanan source such as the Pan-African/Brasiliano region. Several other potential sources that could provide Gondwanan-age zircon including Avalon, Carolina, and Suwannee terranes that accreted to North America during the Appalachian orogeny and contain magmatism ranging from 550-650 Ma (Heatherington et al., 1996; Soto-Kerans et al., 2020). Sediment could have been recycled from Peri-Gondwanan terranes such as the Yucatan, Coahuila, and Oaxauia terranes that accreted to the continent during the Ouachita-Marathon-Sonora orogeny (Dickinson and Lawton, 2001; Poole et al., 2005). Rodinian syn-rift volcanic rocks are another potential source of sediment with volcanic pulses between 780 and 540 Ma (Dickinson and Gehrels, 2009; Soto-Kerans et al., 2020).

Except for LP080120-8, the samples contain a small population of 140-90 Ma zircon, suggesting derivation from the Peninsular Ranges batholith. Other minor age peaks include ca. 1250-1000 Ma, indicating derivation from the Grenville orogen, ca. 1500-1300 Ma grains are likely from the Granite-Rhyolite province, and ca. 1700-1600 Ma grains are likely derived from the Yavapai-Mazatzal province. Archean zircon grains are also present in the samples, with a peak at 3000-2500 Ma, indicating possible sediment recycling from the Archean craton and Wyoming-Slave source region. It is also possible that Archean and Paleoproterozoic grains could have been recycled from Archean crust identified in northeastern Brazil including the Amazonia

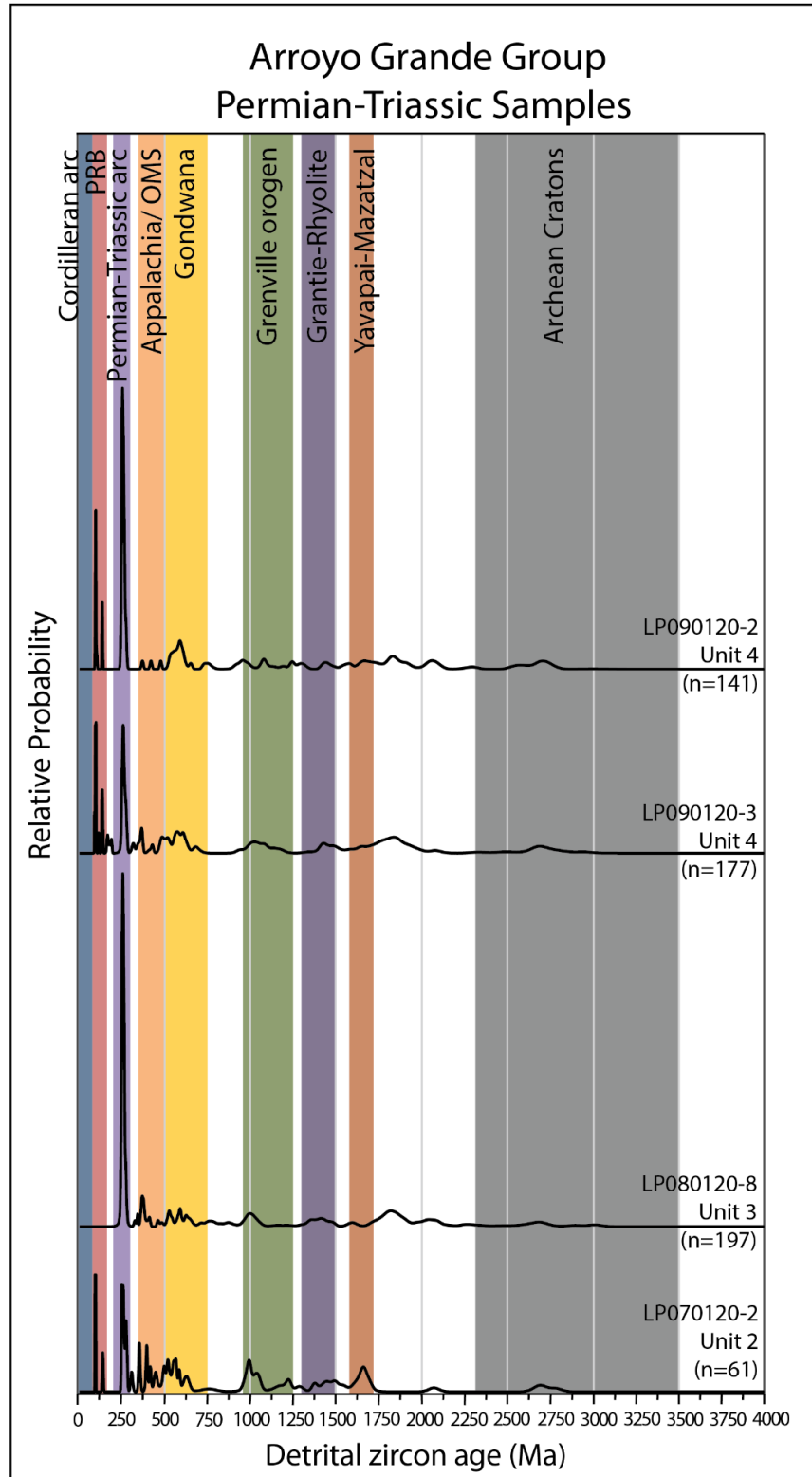
Craton (greater than 2.6 Ga), the Maroni-Itacaiunas region (2.25-1.95 Ga), or the Ventuari-Tapajós region (1.98-1.81 Ga), suggesting derivation from Gondwana (Cordani et al., 2009; Soto-Kerans et al., 2020).

Provenance analysis by Poole et al. (2008) of Sonora allochthon strata and the Mina Mexico foredeep of central Sonora indicates primary derivation from the Grenville, Granite-Rhyolite, Yavapai-Mazatzal, and Archean Wyoming provinces. The Sonora allochthon was formed due to the collision of Gondwana and Laurentia and, although a Gondwana source was not present in previous analysis, it is expected for the provenance of the Sonora allochthon. Analyses of samples from this study provide similar potential source regions identified for Sonora allochthon strata, as well as the presence of Gondwanan-age zircon. It is possible that the samples contain reworked detritus that is eroded from Sonora allochthon strata, including evidence of Gondwana. The samples also indicate a major source area from the Permo-Triassic arc. The major source areas for the samples suggest that most of the detritus was eroded from southwestern United States and northwestern Mexico (Figure 1). Small populations of zircon suggesting derivation from the Peninsular Ranges batholith establishes a Cretaceous maximum depositional age and minor sediment input from the Cretaceous Cordilleran arc to the west.

Bivariate trace element plots were created of 275-240 Ma zircon from the Arroyo Grande Group to aid in interpreting the provenance of the Permo-Triassic population (Figure 43). Permo-Triassic grains fall within the continental-arc arrays of Grimes et al. (2007; 2015) on U vs Yb and U/Yb plots. This supports the hypothesis that 275-240 Ma grains were crystallized in a continental-arc setting, likely the Cordilleran Permo-Triassic magmatic arc that developed along the Laurentian continental margin. Barth et al. (2013) observed that zircon with relatively high Th/U ratios suggest incorporation of fertile crustal sources to the host magma or an episode of

crustal thickening beneath an arc. Th/U ratios from Cordilleran arc zircon increased over time as crustal thickening occurred beneath the Cordilleran arc. Permo-Triassic grains from the Arroyo Grande Group all have Th/U ratios ranging from 0.25 to 1. Th/U ratios are all  $>0.07$  indicating primary petrogenetic origin for the zircon was magmatic. Barth et al. (2013) observed Yb/Gd ratios from Triassic and Jurassic Cordilleran arc magmas range from 30 to 60. Yb/Gd ratios from this study range from 20 to 100 and are consistent with values for arc magmas (Barth et al., 2013).





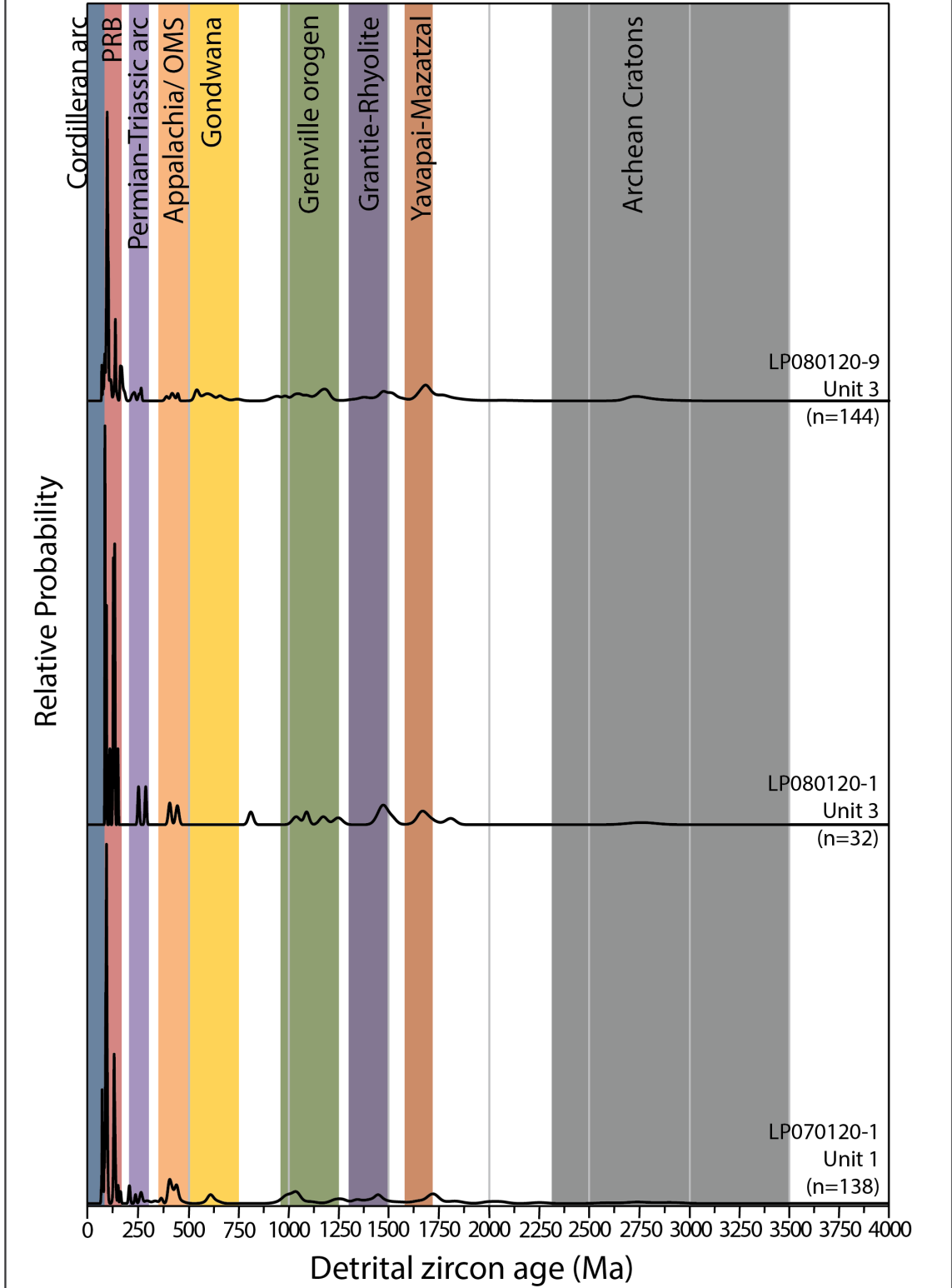
**Figure 51.** Normalized probability density plots of samples collected from the Arroyo Grande Group that contain a dominant Permo-Triassic zircon population.

### *Cretaceous Samples*

Samples containing a dominant Cretaceous population include LP070120-1 of Unit 1, and samples LP080120-1, LP080120-9, and LP130120-1 of Unit 3 (Table 1; Figures 50, 52). It should be noted that LP080120-1 and LP130120-1 were sampled from volcanoclastic material and only yielded 32 and 10 zircon grains, respectively. The youngest and the most robust suite of zircon for each sample is overwhelmingly Cretaceous grains ranging from 90-105 and 130-140 Ma, indicating a Peninsular Ranges batholith origin (Figures 29, 31, 33). Samples LP070120-1 and LP080120-9 also contain a small suite of 90-70 Ma zircon that are most likely sourced from elsewhere in the Cretaceous Cordilleran arc. The samples contain small populations of ca. 1250-950 Ma zircon grains that were probably derived from the Grenville orogeny, ca. 1500-1300 Ma zircon likely sourced from the Granite-Rhyolite province, and a suite of ca. 1700-1600 Ma zircon likely sourced from the Yavapai-Mazatzal provinces. Archean zircon grains are also present in the samples with a minor age peak from ca. 3000-2600 Ma, suggesting potential recycling from the Laurentian Archean craton or from the Amazonian craton of Gondwana. It is likely that the sediment was locally derived from foreland deposits of the Ouachita-Marathon-Sonora segments containing cratonal source areas that have been accreted to the orogen. Detrital zircon geochronology samples are enriched in quartz and durable minerals such as zircon, suggesting multiple-cycle sediment. It is interesting to note that Permo-Triassic zircon grains are rare in the samples. Zircon grains ranging from ca. 750-500 Ma, suggesting derivation from a Gondwanan source, are rare or absent in the samples as well. Provenance analysis of the Cretaceous samples indicates a primary detritus source area from the Peninsular Ranges batholith to the west, with minor input from crustal provinces and granitoid bodies of the Laurentian craton to the north.

Bivariate trace element plots were created for the 90-140 Ma zircon of the Arroyo Grande Group (Figure 46). The Cretaceous grains fall within the continental-arc arrays of Grimes et al. (2007; 2015) on U vs Yb and U/Yb plots. This indicates that Cretaceous grains of the Arroyo Grande Group crystallized in a continental-arc setting, reinforcing the Cretaceous source is likely the Peninsular Ranges batholith. Bell and Kirkpatrick (2021) determined characteristic trace element ratios of the western and eastern Peninsular Ranges batholith. The western zone is characterized by Th/U ratios from 0.27-0.62, Yb/Gd from 11-34, and U/Yb from 0.4-2.1, with most values <1. The eastern zone is characterized by Th/U ratios from 0.05-0.64, Yb/Gd ratios from 10-45, and U/Yb ratios from 0.4-8 with most values >1. In this study, Th/U ratios of Cretaceous grains range from 0.1-2 and Yb/Gd ratios range from 10-70, with 72% of the grains plotting below 30. These ratios are consistent with values observed in the western Peninsular Ranges batholith.

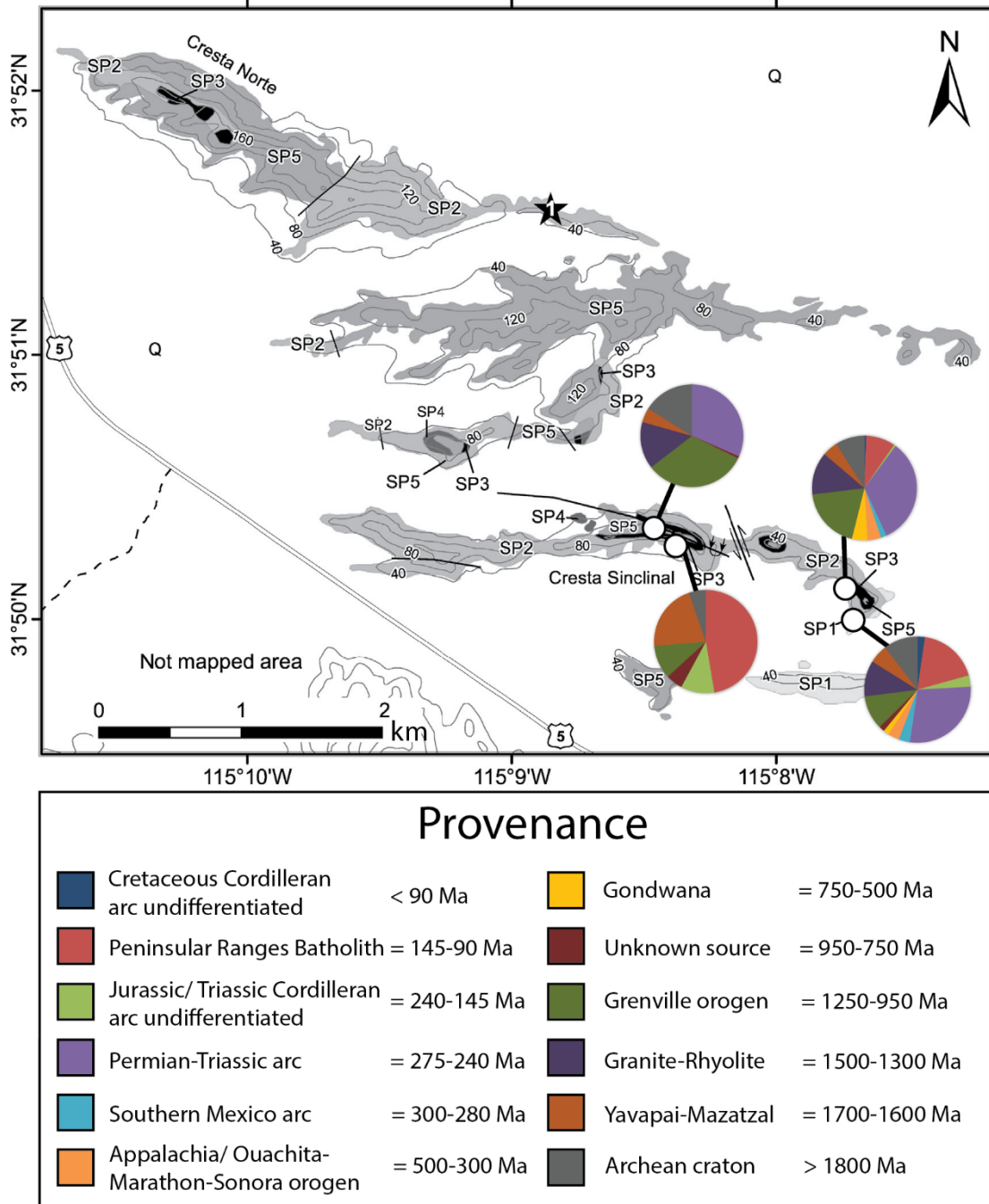
# Arroyo Grande Group Cretaceous Samples



**Figure 52.** Normalized probability density plots of samples collected from the Arroyo Grande Group that contain a dominant Cretaceous zircon population. LP130120-1 was not included as only 10 zircon grains were analyzed; however, the sample also indicated a strong Cretaceous signature.

#### **4.1.2 Provenance Interpretation of the Sierra Las Pintas Group**

Geochronological analysis of the Sierra Las Pintas Group indicates two distinct maximum depositional ages and a range of source regions for the samples (Figure 53). Three of the four samples contain a Cretaceous maximum depositional age and one sample contains a Permian maximum depositional age.



**Figure 53.** Simplified geologic map of the Sierra Las Pintas Group with location of geochronological samples. Pie charts indicate provenance percentages of each sample.

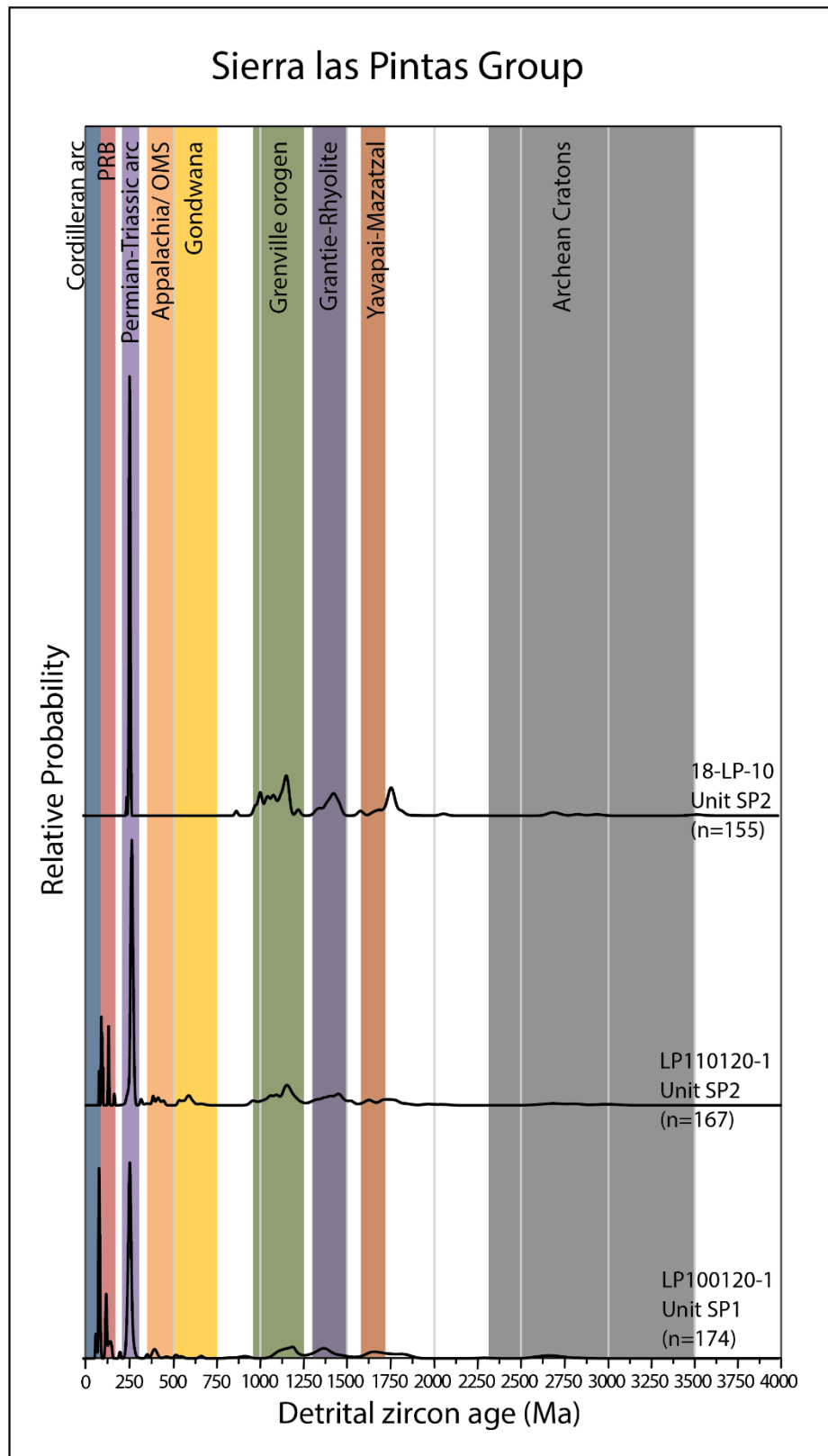
Samples LP100120-1 of Unit SP1, LP110120-1 of Unit SP2 and X181218 of Unit SP4 contain suites of zircon grains ranging from ca. 105-90 Ma and ca. 140-135 Ma (Figure 53-54). X181218 was sampled from a basalt and only yielded 19 zircon grains. Major age peaks from the

samples are synonymous with the eastern and western Peninsular Ranges batholith magmatism. The averaged maximum depositional age for the samples is approximately 96 Ma (Figures 36, 37, 39). The youngest grains from sample 18-LP-10 from SP2 range from 280-255 Ma and are likely derived from the Permo-Triassic arc (Figure 38). Samples LP100120-1 and LP110120-1 also contain a large suite of 280-240 Ma indicating a source region from the Permo-Triassic arc. All samples include minor age peaks at ca. 1250-1000 Ma indicating sediment derived from the Grenville orogen. The 1500-1300 Ma grains are probably recycled from the Granite-Rhyolite province and a suite of ca. 1700-1600 Ma grains probably originated from the Yavapai-Mazatzal province (Figure 54). Reworking of sediment from a locally derived source, such as the Ouachita-Marathon-Sonora segments, rather than derivation directly from cratonal basement complexes is also a possibility for Paleozoic zircon grains. Gondwanan-age zircon grains are rare or completely absent in samples from the Sierra Las Pintas Group. Provenance analysis of the Sierra Las Pintas Group suggests detritus was primarily eroded from the Peninsular Ranges batholith to the west, from the Permo-Triassic arc to the northeast and from Laurentia to the north.

Bivariate plots were created for both the ca. 90-140 Ma suite of zircon, as well as the ca. 275-240 Ma suite of zircon for all samples of the Sierra Las Pintas Group (Figures 44, 47). Cretaceous and Permo-Triassic grains from the Sierra Las Pintas group all plot within the continental-arc array of Grimes et al. (2007; 2015) on U vs Yb and U/Yb plots. The Th/U ratios of the Cretaceous grains range from 0.15-1.2 and the Permo-Triassic spectrum plot slightly higher at 0.25-1.2, with the majority of the zircon grains plotting around 0.4. Both zircon populations contain Th/U ratios above 0.07, indicating that the primary petrogenetic origin of the zircon grains was magmatic. While trace element ratios are overall similar from the Cretaceous

and Permo-Triassic populations of the samples, Yb/Gd ratios vary slightly and can be used when determining provenance. The Yb/Gd ratios for Cretaceous zircon are primarily 10-30, while the Permo-Triassic grains show a greater range of 10-50. Barth et al. (2013) observed Yb/Gd ratios from Triassic and Jurassic Cordilleran arc magmas range from 30 to 60 while Bell and Kirkland (2021) identified Yb/Gd ratios from the western Peninsular Ranges batholith 11-34 and the eastern zone 10-45. These Yb/Gd ratios support the hypothesis that Cretaceous zircon of the Sierra Las Pintas group are derived from the Peninsular Ranges batholith while Permo-Triassic zircon are derived from the Cordilleran Permo-Triassic arc.

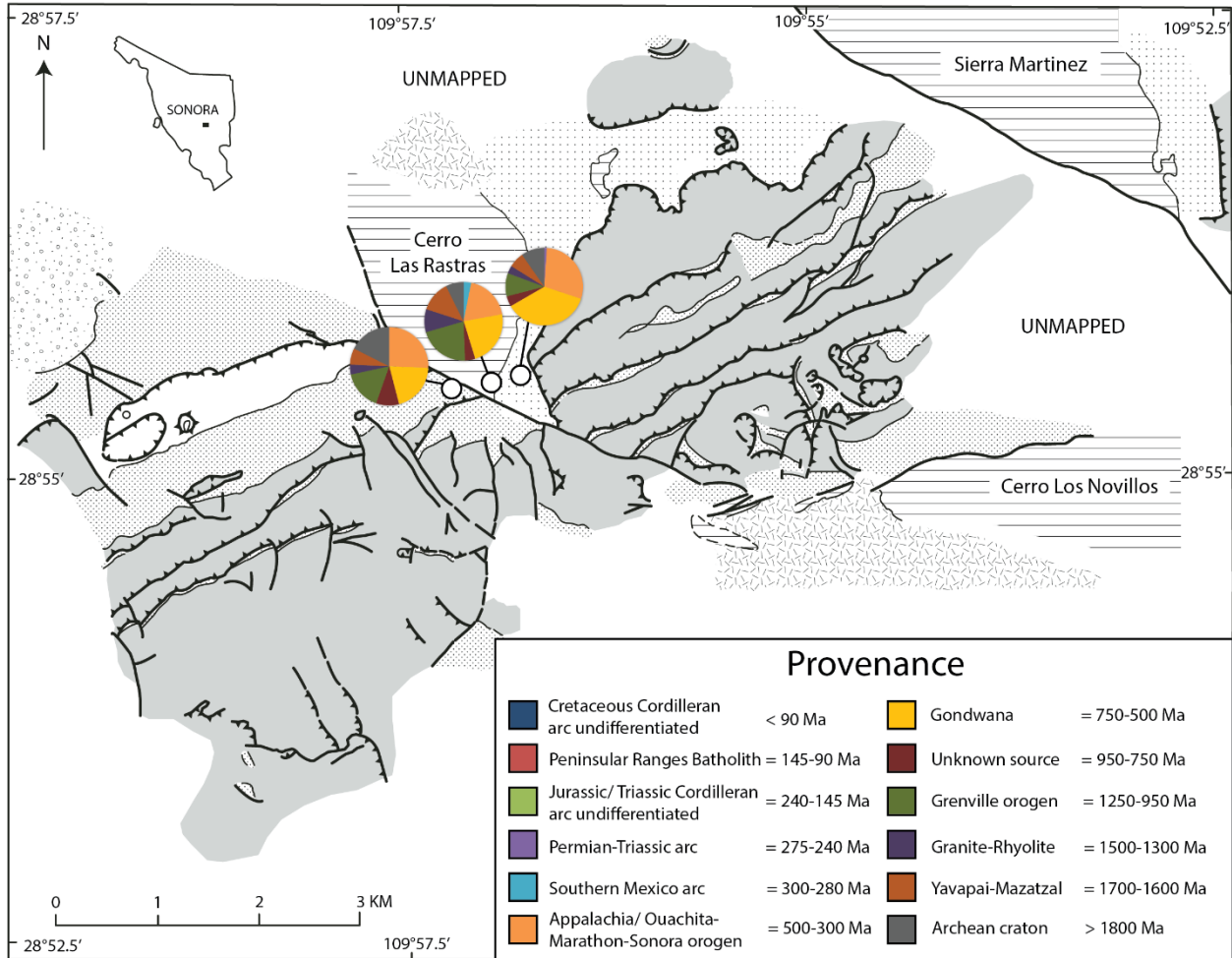




**Figure 54.** Normalized probability density plots of samples collected from the Sierra Las Pintas Group. Sample X181218 was not included as only 19 zircon grains were analyzed.

### 4.1.3. Provenance Interpretation of the Minas de Barita Area

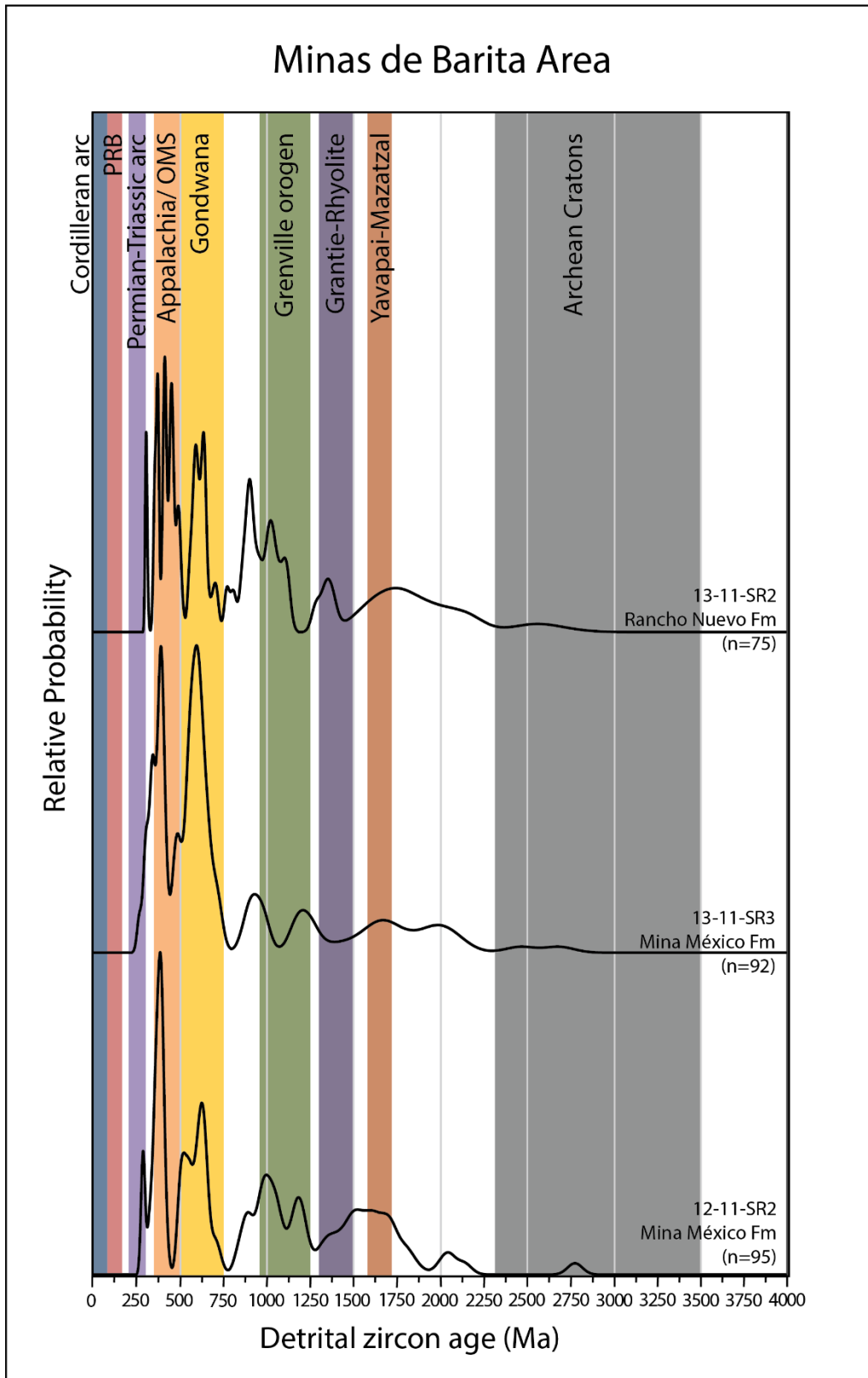
Provenance analysis of the Minas de Barita area includes a youngest population of Carboniferous grains and similar major age peaks throughout the three samples collected (Figure 55). Detrital zircon geochronology indicates that detritus in all the samples is recycled from Gondwana and Laurentian source regions.



**Figure 55.** Simplified geologic map of the Minas de Barita area with location of geochronological samples. Pie charts indicate provenance percentages of each sample.

Samples from the Rancho Nuevo Formation and Mina México Formation of the Minas de Barita area include rare, early Permian grains but the largest population of youngest grains for the samples range from Late Pennsylvanian to Early Mississippian with no clear maximum depositional age (Figures 40-42). Previous studies show an earliest Late Pennsylvanian age for

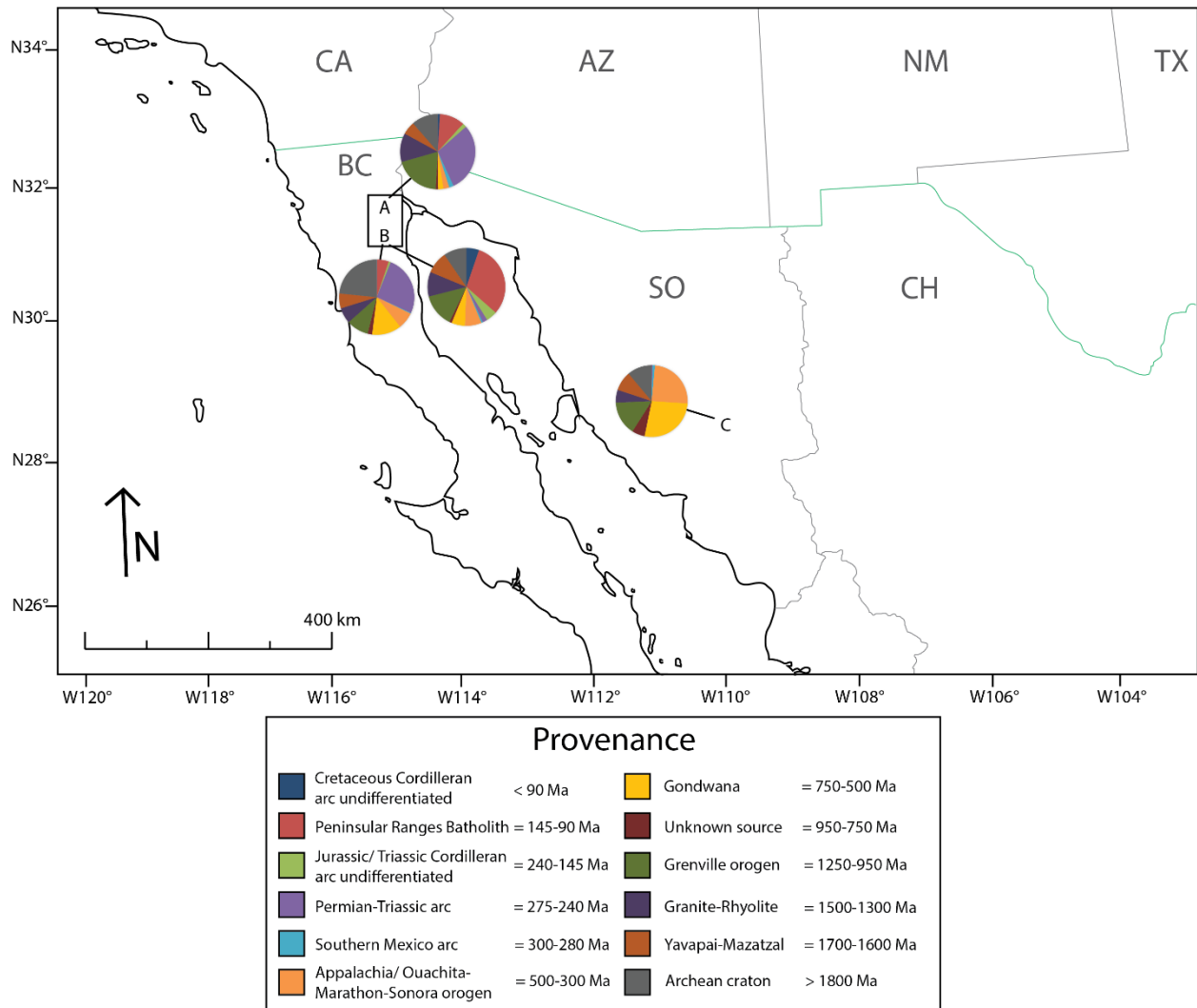
the strata of the Rancho Nuevo Formation and middle Permian age for the Mina México Formation (Poole et al., 2005; 2008). Samples from this study do not provide a more precise emplacement age for the Sonora allochthon strata of the Rancho Nuevo Formation or the Mina México foredeep. The samples include major age peaks at ca. 500-300 Ma and ca. 750-500 Ma, indicating the main source regions are coming from the Appalachian / OMS orogen and Gondwana (Figure 56). The large suite of Gondwanan zircon is very significant for this study as Gondwanan source regions are rare in previous geochronologic analysis of Sonora allochthon strata. Gondwanan-age zircon could have been derived from the reworking of sediments with a cratonic source, such as the Avalon, Carolina, or Suwannee terranes that were accreted during the Appalachian orogeny. Peri-Gondwanan terranes such as the Yucatan, Coahuila, and Oaxaquia terranes accreted during the OMS orogeny contain cratonic sources. Other age populations for the samples include ca. 1250-950 Ma suggesting sediment derived from the Grenville orogen and ca. 1700-1600 Ma zircon likely sourced from the Yavapai-Mazatzal province. Cretaceous and Permo-Triassic zircon populations are absent in the Minas de Barita samples.



**Figure 56.** Normalized probability density plots of samples collected from the Minas de Barita area.

#### 4.1.4 Comparison of Field Areas

Provenance analyses are compared for the Sierra Las Pintas Group, Arroyo Grande Group and Minas de Barita area to determine how strata of the Sierra Las Pintas in Baja California, Mexico, compare to Sonora allochthon strata of the Minas de Barita area in Sonora, Mexico. Previous work by Gastil (1993), Poole et al. (2005), and Navas-Parejo et al., (2018) has generally correlated Paleozoic rocks of the Sonora allochthon of central Sonora and Baja California based on biostratigraphic and lithological correlations. This study provides the first geochronologic analysis for the Sierra Las Pintas. All geochronological analyses are combined for each field area (the Arroyo Grande Group is divided into samples showing dominant Cretaceous or Permo-Triassic source areas) and plotted on the map as pie charts to show relative percentages (Figure 57). All samples were combined in the same fashion and plotted against each other as KDE plots for each field area (Figure 58) and compared to data from previous studies (Figure 59).



**Figure 57.** Index map including all field areas (A: Sierra Las Pintas Group, B: Arroyo Grande Group, and C: Minas de Barita) that show overall provenance percentages. The Arroyo Grande Group is divided into two pie charts to represent samples with a dominant Cretaceous source area vs a dominant Permo-Triassic source area.

Pie charts and provenance plots for samples from the Arroyo Grande Group and Sierra Las Pintas Group indicate two distinct source regions (Figure 57-58). Provenance analysis of the Arroyo Grande Group suggests that samples are primarily derived from either the Permo-Triassic arc to the northeast or the Peninsular Ranges batholith to the west (Figure 1). Samples that contain a dominant Permo-Triassic source area also contain minor source areas suggesting derivation from Gondwana and the Laurentian craton or secondary recycling from clastic

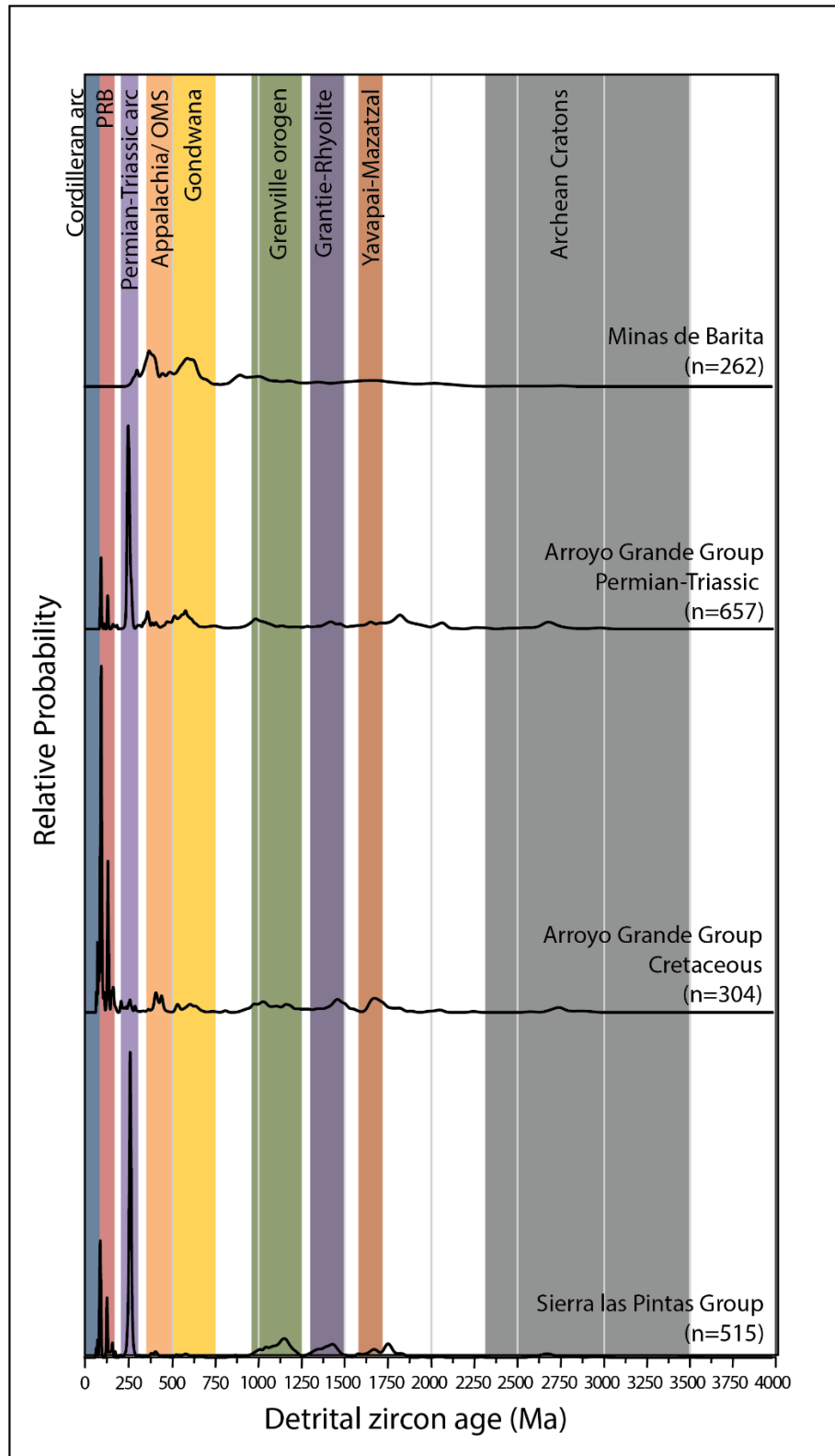
successions that previously formed from these cratons. Source areas for these samples are synonymous with the expected provenance of the Sonora allochthon and suggest possible derivation from Sonora allochthon strata. Samples that contain a dominant Cretaceous source area contain very rare Permo-Triassic zircon and Gondwanan-age zircon, suggesting detritus is primarily derived from the western Peninsular Ranges batholith with rare sediment input from the east or the south. Samples from the Sierra Las Pintas Group contain major source areas from the Permo-Triassic arc and the Peninsular Ranges batholith, indicating a mixing of source regions. The Sierra Las Pintas Group also contains minor source areas from crustal provinces and granitoids of the Laurentian continent, suggesting derivation from the north.

Provenance analyses of the Minas de Barita area samples indicate different source areas from those identified in the Sierra Las Pintas samples. The Rancho Nuevo Formation and Mina México Formation contain major age peaks that indicate detritus dominantly being sourced from the Appalachian/OMS orogen and Gondwana. Other minor source areas include the Grenville orogen and Yavapai-Mazatzal orogen. Provenance analysis indicates primary derivation from Gondwana to the south and Laurentian source areas to the north. Major source areas identified in the Minas de Barita samples support the expected provenance for Sonora allochthon strata and potentially record the Gondwanan- Laurentian suture zone of final Pangea formation.

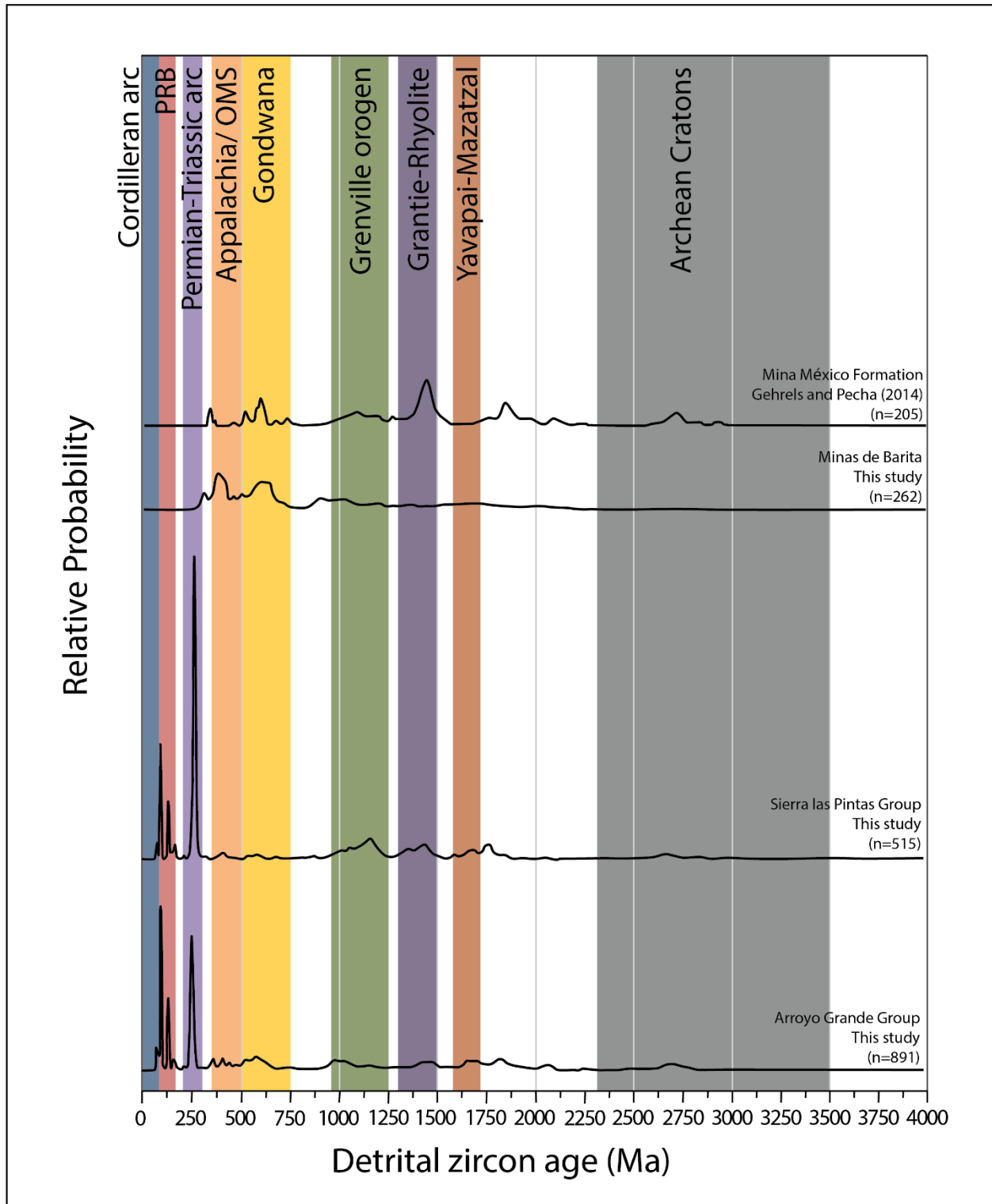
Detrital zircon data from the Mina México Formation of Gehrels and Pecha (2014) are compared to detrital zircon data from this study (Figure 59). All samples from the Arroyo Grande Group are combined into one probability density plot to compare overall source areas interpreted for each field area. Overall, the Sierra Las Pintas Group and Arroyo Grande Group indicate very similar source regions. Both field areas contain similar major age peaks indicating zircon grains likely being sourced from the Peninsular Ranges batholith and Permo-Triassic arc

with minor age peaks indicating derivation from the Grenville orogen, Granite-Rhyolite province, and the Yavapai-Mazatzal orogen. Source areas interpreted for the Sierra Las Pintas vary from major source areas identified in the Minas de Barita area. The Minas de Barita samples contain major source areas from the Appalachian / OMS orogen and Gondwana. Gehrels and Pecha (2014) reanalyzed a sample from the Mina Mexico foredeep, originally reported by Poole et al. (2008). Detrital zircon data from this study align well with Mina México analyses from Gehrels and Pecha (2014) and further support provenance interpretations for the Sonora allochthon of Sonora, Mexico.





**Figure 58.** Normalized probability density plots for all samples from this study, separated by field area.



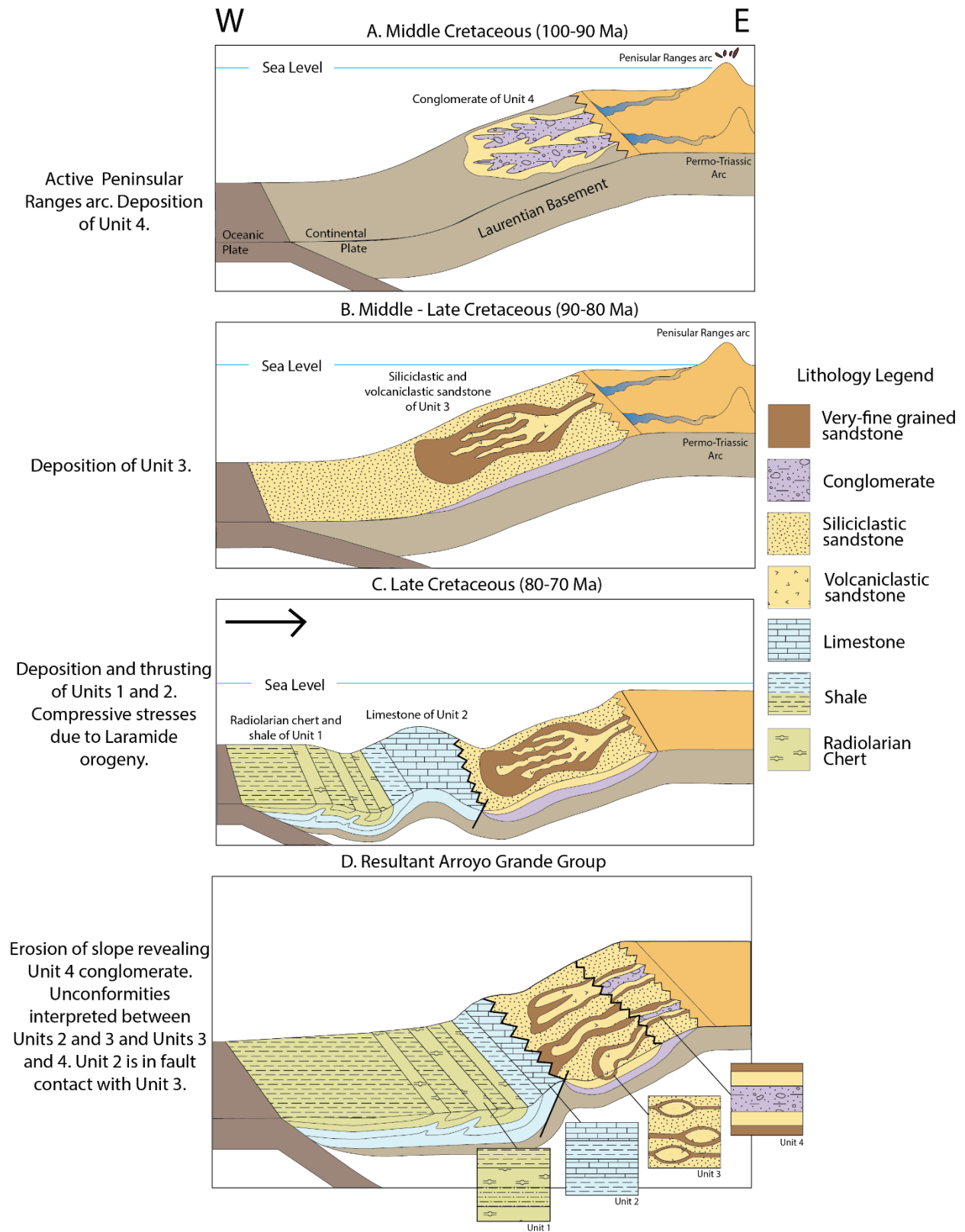
**Figure 59.** Normalized probability density plots for all samples from this study, separated by field area and plotted against previous geochronologic analysis of the Mina México Formation by Gehrels and Pecha (2014).

## **4.2 LITHOLOGIES AND DEPOSITIONAL HISTORY**

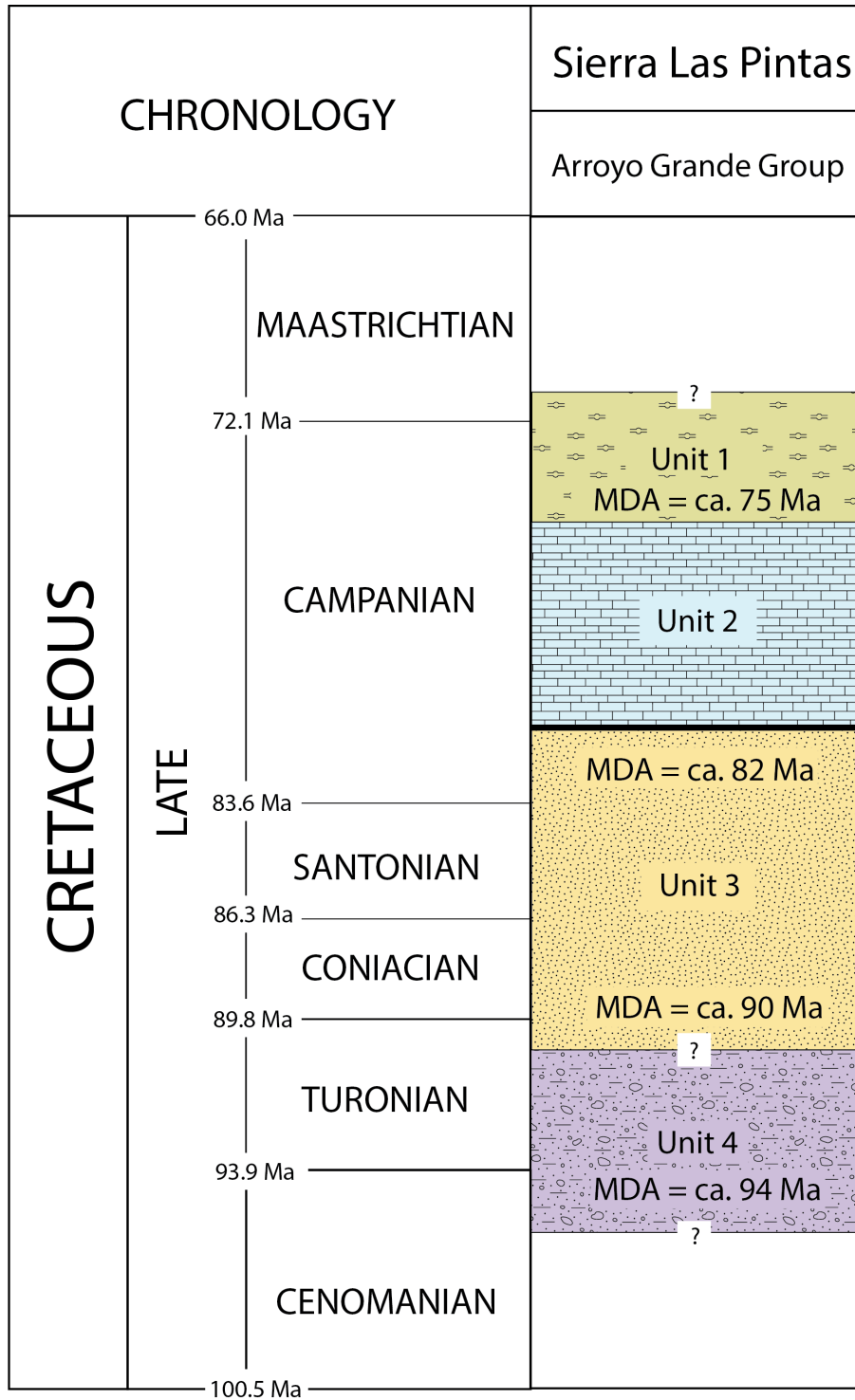
Sonora allochthon strata of Sonora, Mexico, are interpreted as continental-rise and ocean basin rocks that were thrust onto the shallow, continental Laurentian carbonate shelf and foredeep basin rocks of Mina México during collision of Gondwana with Laurentia (Stevens, 2014; Poole et al., 2005; 2008). Paleozoic outcrops of the Sierra Las Pintas have been interpreted as the westernmost exposure of the Sonora allochthon, composed of deep-water succession deposited on the continental slope (Gastil et al., 1993; Leier-Engelhardt, 1993; Poole et al., 2005; Navas-Parejo et al., 2018). Provenance analysis from this study indicates primary derivation from Laurentia and Gondwana source areas. The Arroyo Grande Group and Sierra Las Pintas Group also contain dominant source areas from the Peninsular Ranges batholith and the Permo-Triassic arc. Detritus from the Permo-Triassic arc was likely derived from the northeast and detritus from the Peninsular Ranges batholith was likely derived from the west (Figure 1).

### **4.2.1. Depositional History of the Arroyo Grande Group**

The geochronological and lithological analyses of the Arroyo Grande Group indicate a complex emplacement history. The main lithologies and sedimentary features for the Arroyo Grande Group are summarized in Table 3, but they are reviewed here in order to interpret the depositional environment of the succession. Geologic interpretations and provenance analysis of the Arroyo Grande Group suggest overall deposition along the continental slope and ocean basin within the forearc of the Peninsular Ranges batholith (Figure 60). A chronostratigraphic column of the Arroyo Grande Group was created based on maximum depositional ages for each unit (Figure 61).



**Figure 60.** Cretaceous depositional history of the Arroyo Grande Group along the continental slope. Insets show a cross-sectional view of each unit.



**Figure 61.** Chronostratigraphic column of the Arroyo Grande Group based on maximum depositional ages for each unit. Heavy line between Units 2 and 3 indicates a fault contact.

Unit 1 is composed of radiolarian chert that is interbedded with metashale and metasandstone packages (Figure 10). Syn-sedimentary liquefaction, pinching-out of layers, and soft-sediment-deformation structures such as slumping and convolute laminations suggest deposition on or at the base of a slope, likely emplaced by turbidity currents. Bedded metashale and radiolarian chert indicate deposition in the ocean basin, as a quiet, deep-marine environment would be expected where shale and radiolaria could settle. Unit 1 contains rare Late Cretaceous grains and large suites of zircon ranging from 105-90 and 140-130 Ma, likely indicating a Peninsular Ranges Batholith provenance and maximum depositional age of  $75 \pm 1$  Ma (Figures 29 and 61). Unit 1 contains pervasive isoclinal folds throughout the unit and a gradational contact with Unit 2 (Figure 60).

Unit 2 is cherty metashale interbedded with metalimestone and thin beds of metasandstone (Figure 12). The metalimestone is increasingly replaced by diagenetic chert upsection. The unit includes parallel laminations and soft-sediment-deformation structures such as convolute laminations, slumping, and flame structures that are common characteristics of turbidity currents deposited on a slope. Unit 2 was likely deposited by turbidity currents higher on the continental slope than Unit 1 as indicated by an increase in grain size and the presence of limestone. Unit 2 contains rare, Lower Cretaceous grains and a major age peak at ca. 275-240 Ma, indicating primarily Permo-Triassic arc provenance (Figure 30). The sample contains three Cretaceous grains between 137 and 91 Ma that do not fall within two-sigma uncertainty of each other and no viable youngest population of zircon that could reasonably be interpreted as the maximum depositional age for the unit. Similar to Unit 1, pervasive isoclinal folds are present throughout Unit 2, suggesting post-deposition tectonism. Unit 2 is in fault contact with Unit 3, which may represent an unconformity. It is likely that the units 1 and 2 are part of a separate

succession from the other units of the Arroyo Grande Group. Because the maximum depositional age of Unit 2 could not be established, the unit is interpreted to have been deposited along with Unit 1 based on field evidence, and the stratigraphy of Units 1 and 2 appears to be inverted (Figures 60-61).

Unit 3 is composed of two distinct lithologies, siliciclastic metasandstone and volcanoclastic metasandstone, that each contain unique geochronologic provenance and suggest a complex depositional history. The base of Unit 3 is primarily siliciclastic metashale containing boudinaged very fine- to fine-grained volcanoclastic metasandstone lenses (Figure 14). The volcanoclastic metasandstone lenses coarsen upsection and become thicker and more abundant (Figure 15). The volcanoclastic metasandstone lenses are interpreted as channeled deposits emplaced on the continental slope. The increase in frequency and coarsening upsection of volcanic metasandstone lenses indicates a more proximal portion of the channel.

The siliciclastic metasandstones coarsen upsection as well. Within the siliciclastic metasandstone, the frequency of sedimentary features, such as cross-bedding and parallel laminations, increases upsection. Complete to incomplete Bouma sequences are identified within the siliciclastic metasandstone including layers Ta (massive sandstone), Tb (parallel laminations), and Tc (cross-bedding). The presence of Bouma sequences within the siliciclastic metasandstone supports the hypothesis that the sediment was deposited by turbidity currents, likely on the continental slope, and indicates a higher-energy environment than the volcanoclastic metasandstone lenses. It is important to note that Unit 3 does not contain any folding, as opposed to the severely folded nature of Units 1 and 2, further supporting the hypothesis that Units 1 and 2 are part of a separate succession from Unit 3 (Figure 60).

Petrographic analysis of siliciclastic metasediments indicates primarily sub-rounded, quartz-rich samples with rare, well-rounded feldspars and lithic fragments, suggesting sediment recycled from a continental provenance (Figure 17). The volcanoclastic metasediments are predominantly feldspathic, suggesting a volcanic-arc provenance (Figure 17). The feldspars are pervasively replaced by amphibole and contain extensive sericitization, indicating greenschist metamorphism.

The siliciclastic metasediment sample contains a major age peak at ca. 275-240 Ma, indicating a Permo-Triassic arc source area and maximum depositional age of  $248 \text{ Ma} \pm 2 \text{ Ma}$  (Figure 32). The volcanoclastic metasediments contain major age peaks at 105-90 and 140-130 Ma indicating a Peninsular Ranges batholith origin (Figures 31 and 33). Two samples collected from the volcanoclastic metasediments suggest maximum depositional ages of  $90 \pm 1 \text{ Ma}$  and  $82 \pm 2 \text{ Ma}$ , which are interpreted as the maximum depositional ages for the unit (Figures 31, 33, and 61). The age, compositional, and sedimentological differences between the siliciclastic and volcanoclastic metasediments suggest that each was derived from a distinct source. The siliciclastic metasediments were eroded primarily from a Permo-Triassic arc source and likely deposited by turbidity currents on the continental slope. The volcanoclastic metasediments were primarily sourced from the Peninsular Ranges batholith and were likely formed as channeled deposits within the siliciclastic metasediment (Figure 60). The volcanoclastic metasediments deposits were likely boudinaged in subsequent tectonic events.

Unit 4 contains interbedded metaconglomerate, metashale, and very fine-grained metasediment layers that coarsen upsection into medium-grained metasediment layers (Figure 18). The metaconglomerate packages thicken upward and clast size increases as well. The



metasandstone contains parallel laminations and the metaconglomerate contains flattened and sheared clasts, as well as evidence of slumping.

Petrographic analysis reveals a quartz-rich composition similar to the metasandstone of Unit 3 (Figure 20). The analysis suggests that the metasandstone contains detritus that was recycled from a continental source as the sample is primarily composed of stable minerals such as quartz that are sub- to well-rounded and well sorted (Dickinson et al., 1983). The metaconglomerate is composed of poorly sorted, sub-rounded to angular clasts of chert, shale, and very-fine-grained sandstone. It also contains rare volcanoclastic and sedimentary lithic fragments.

The metasandstone and metaconglomerate of Unit 4 both indicate very similar source regions with major age peaks at ca. 105-90 Ma, ca. 140-130 Ma, and ca. 275-240 Ma (Figures 34-35). The unit includes significant geochronologic signatures indicating major source regions from the Peninsular Ranges Batholith and the Permo-Triassic arc. The maximum depositional age of unit is interpreted as  $94 \pm 2$  Ma (Figures 34-35) suggesting that Unit 4 is the oldest unit of the Arroyo Grande Group (Figure 61). Although the chert, shale, and sandstone clasts identified within Unit 4 appear similar to the rocks that compose Units 1-3, it is possible the clasts do not originate from these units. The clasts may have been derived from higher on the continental shelf or further inland.

Unit 4 was likely deposited by debris flows on the continental slope that incorporate mixed source regions (Figure 60). Unit 4 was likely deposited near the top of the continental slope, potentially near the feeder channel as it is very coarse grained, contains cobble-sized clasts and is poorly sorted. Unfortunately, the stratigraphic relation of Unit 4 to Units 1-3 could not be

determined so it is difficult to establish with confidence how this unit is incorporated in the overall succession of the Arroyo Grande Group. The disconnected outcrops of the metasandstone could be due to Unit 4 representing channeled deposits from an anastomosing channel system, explaining why it is so difficult to identify the relation with other units of the Arroyo Grande Group.

Unit 5 is composed of overlying Cenozoic volcanic rocks and felsic dikes. This unit is not discussed as it does not appear to affect the Arroyo Grande Group depositional history interpretation

#### **4.2.2. Depositional History of the Sierra Las Pintas Group**

The strata of the Sierra Las Pintas Group have previously been interpreted as a flysch-like succession that was deposited on a continental slope (Poole et al., 2005). Navas-Parejo et al. (2018) suggest that the Sierra Las Pintas Group succession was emplaced on the continental slope in a deep-marine environment and locally received calcareous bioclastic debris from a shallow-water platform dominated by crinoid meadows. Field observations made during this study agree with these previous interpretations.

Unit SP1 contains metasandstone interbedded with finely laminated, calcareous metashale layers. The metasandstone coarsens upsection from very fine-grained to medium-grained metasandstone. The unit is heavily altered by greenschist metamorphism and most sedimentary features have not been preserved, except for rare parallel laminations. Petrographic analysis indicates the unit is quartz-rich with rare feldspar. Geochronological analysis indicates a maximum depositional age of  $96 \pm 1$  Ma for the unit and includes major age peaks of ca. 105-90 Ma, ca. 140-130 Ma, and 280-240 Ma, suggesting derivation from the Peninsular Ranges

batholith and the Permo-Triassic arc (Figure 36). Units SP1 and SP2 contain a gradational contact, suggesting that the units are part of the same succession.

SP2 is composed of fine-grained metasandstone interbedded with metashale layers. The unit shows an overall coarsening upsection, from fine- to coarse-grained metasandstone. The metasandstone is interbedded with metaconglomerate containing crinoids, quartz, and feldspar. Sedimentary structures, which include parallel and ripple-cross laminations, are not obvious due to pervasive metamorphism. Petrographic analysis of Unit SP2 indicates that the unit is quartz-rich and includes a higher percentage of calcareous minerals than Unit SP1. Geochronologic analysis of Unit SP2 includes two samples, one with a major age peak at ca. 280-250 Ma and the other with major age peaks at ca. 140-90 Ma and 280-240 Ma, suggesting derivation from the Peninsular Ranges batholith and Permo-Triassic arc (Figures 37-38). The crinoid fauna identified in Unit SP2 by Navas-Parejo et al. (2018) suggest a Middle Pennsylvanian-early Permian age for the unit, however geochronologic analysis of Unit SP2 indicates a maximum depositional age of  $94 \pm 1$  Ma (Figure 37). The much younger MDA than was previously interpreted for the unit suggests that the crinoids could have been reworked and later deposited within the strata of the Sierra las Pintas Group.

Geologic and petrographic analysis of Units SP1 and SP2 support previous interpretations of deposition in a deep-marine environment on the continental slope. The metaconglomerate packages, decrease in metashale beds, and presence of parallel laminations observed in upper SP2 suggest a higher-energy depositional environment than SP1. Geochronological analysis suggests that the units record an interfingering of source regions from the Peninsular Ranges batholith and Permo-Triassic arc.

Unit SP4 is composed of basaltic metalava and metaconglomerate. Geochemical analysis of the basalts by Leier-Engelhardt (1986, 1993) indicated a transitional tectonic setting characterized by an attenuated continental crust. Geochronologic analysis of the basalt yielded 19 concordant zircon grains that contained major age peaks at ca. 105-90 and 140-130 Ma, ages consistent with Peninsular Ranges batholith magmatism. Previous interpretations and geochronologic analysis suggest that the basalt was formed from fissures on the continental slope. Leier-Engelhardt (1993) and Navas-Parejo et al. (2018) identified pillow lava flows in Unit SP5. It is likely that the metabasalt and metaconglomerate of Unit SP4 were eroded from basalt lava flows higher on the continental slope.

#### **4.2.3. Depositional History of the Minas de Barita area**

Samples from the Minas de Barita area were collected from the Mina México Formation and Rancho Nuevo Formation. Poole et al. (2005; 2008) described the Rancho Nuevo Formation as syn-orogenic deep-water black shale, turbidite, and chert and the Mina México Formation as syn-orogenic turbidites and deep-water flysch sequence deposited in a foredeep in front of the evolving Sonora allochthon. While field data for the samples collected for this study were limited, the lithology and sedimentary structures support depositional environment interpretations from previous studies (Poole et al., 2005).

M. Martini described the sampled outcrop from the Rancho Nuevo Formation as primarily composed of calcareous sandstone, shale, and chert that are massive to inversely graded and poorly sorted. The calcareous debris-flow deposits are overlain by granule to cobble debris-flow conglomeratic deposits. Field observations suggest deposition by a debris-flow on the continental slope. The Mina México Formation was interpreted as an interfingering of

siliciclastic sandstone and shale that display typical turbidite characteristics with calcareous sandy-debris-flow deposits. The turbidite sequence contains parallel laminations, ripple marks, fluidification structures, and syn-sedimentary faults. Field observations suggest deposition by turbidity currents and debris flows on a continental slope, which agrees with previous interpretations for the depositional environment of the Mina México Formation.

Provenance analysis from this study indicates major source regions from the Appalachian / OMS orogen and Gondwana, with minor source regions from the Grenville orogen and Yavapai-Mazatzal province. While the youngest population of zircon from the samples range from Early Mississippian to Late Pennsylvanian age, the samples do not contain a coherent youngest population of zircon and maximum depositional age could not be determined. The results of this study agree with previous provenance interpretations for the Minas de Barita area and provide evidence of Gondwana source.

#### **4.3 TECTONIC EVOLUTION**

The results of this study provide an interesting addition to the provenance analysis of the Sierra Las Pintas. While the observations and geochronologic analyses of the Minas de Barita area agree with previous studies, the analyses of the Sierra Las Pintas strata do not support the presence of the Sonora allochthon as was previously interpreted. The most unexpected result from this study is the presence of Cretaceous zircon grains identified within many of the Sierra Las Pintas samples. Multiple theories for the presence of Cretaceous zircon grains are discussed along with the most likely scenario and associated basin model.

### 4.3.1 Origin of Cretaceous Zircon

#### *Contamination*

The first scenario considered was that the Cretaceous grains were the result of contamination of the samples. Great care was taken during processing of the samples and all 15 geochronologic samples were processed in the same manner at the Northern Arizona University mineral-separation lab. This troubling possibility was quickly dismissed as the number of Cretaceous grains was far greater than could be reasonably expected from residue of a previous sample remaining on any of the mineral-separation machines. The same idea applies when considering that alluvium or younger Cretaceous soil was coating the samples collected in the field as Cretaceous zircon present in geochronologic analysis due to soil contamination would be diminutive. Finally, Cretaceous zircon grains were not present in samples such as LP080120-8 (Figure 32). Because samples were processed in the exact same manner, the Cretaceous zircon present in some samples and not others had to be considered as part of the provenance of the rocks and not due to contamination of the samples.

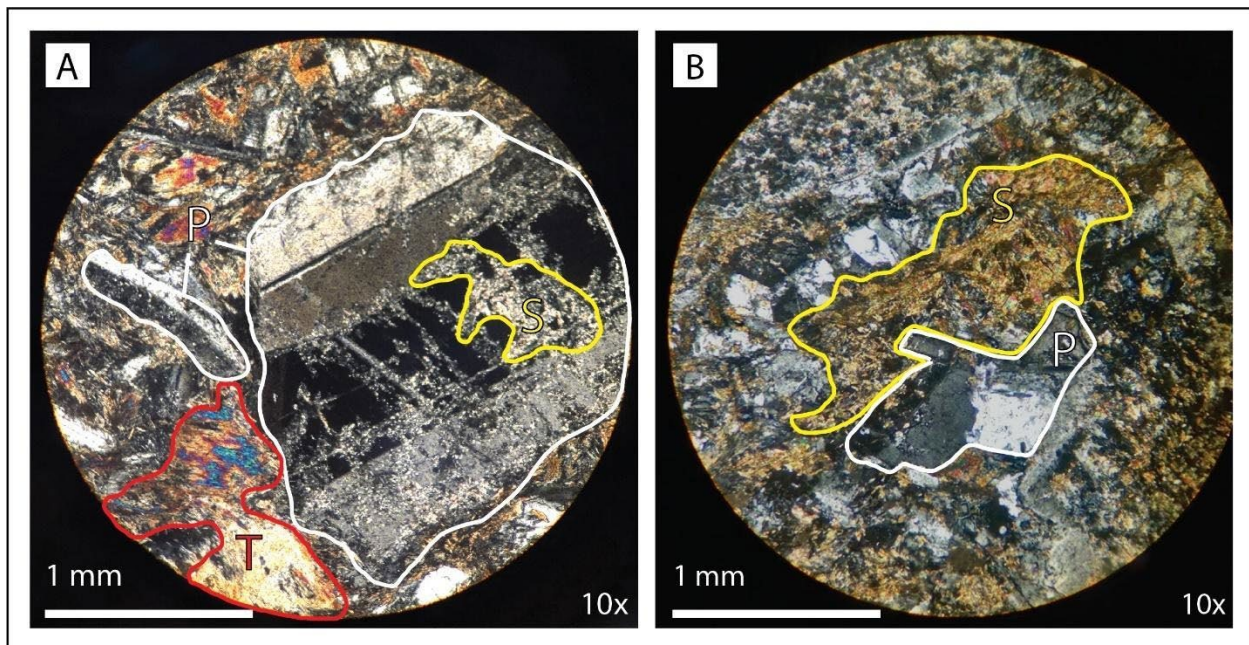
#### *Altered U/Pb Ages*

The next scenario explored was that Cretaceous ages are due to a high-pressure / temperature metamorphic event that resulted in Pb-loss or hydrothermal alteration. A random selection of Cretaceous grains was reanalyzed to determine if the grains contained altered metamorphic rims from five of the samples that contain strong Cretaceous signatures. The geochronologic analysis was repeated, taking care to analyze the core of the grains as opposed to the rims. As was discussed at the beginning of this chapter, only one grain indicated an older core and cathodoluminescence images of the re-analyzed grains indicated normal, oscillatory

patterns of growth on the majority of the Cretaceous-age zircon (Table 4; Figure 49). Trace element geochemistry also indicates primary petrogenic origin for the Cretaceous zircon was magmatic as all Th/U ratios are  $>0.07$  (Figures 46-48).

### ***Intrusive Bodies***

A third possibility considered was that the Cretaceous volcanoclastic metasedimentary lenses of Unit 3 from the Arroyo Grande Group are not boudins, but younger, intrusive volcanic bodies. Petrographic analysis of the volcanoclastic boudins from Unit 3 indicates that the lenses are composed of well-rounded plagioclase feldspar grains, extensively replaced by tremolite and seritization, indicative of eroded and weathered volcanoclastic sediment (Figure 62A). This is different from the petrographic analysis of Unit 5, which indicates the felsic dike is composed primarily of interlocking plagioclase feldspar with pervasive seritization (Figure 62B). This scenario also does not explain the presence of Cretaceous grains within Units 1 and 4, as well as within the samples collected from the Sierra Las Pintas Group.



**Figure 62.** Comparison of volcanoclastic metasandstone boudin of Unit 3 (A) and felsic dike of Unit 5 (B) of the Arroyo Grande Group. Plagioclase feldspar (P) are outlined in white, tremolite (T) in red and sericite (S) in yellow.

#### 4.3.2 Cretaceous Sierra Las Pintas Area

The final, and most likely, scenario is that the Arroyo Grande Group and the Sierra Las Pintas Group of the Sierra Las Pintas are Cretaceous in age. This scenario does not support the hypothesis that the Sonora allochthon is present within the Sierra Las Pintas area. Provenance analysis suggests an earliest Late Cretaceous emplacement age for the strata of the Sierra Las Pintas area with two primary source regions from the Peninsular Ranges batholith and the Permo-Triassic arc.

The units of the Arroyo Grande Group contain a range of MDAs that suggests a complex depositional history. Geochronological data from Unit 4 indicates the oldest MDAs for the area at  $94 \pm 1$  Ma and  $95 \pm 1$  Ma, suggesting that Unit 4 was most likely deposited while the eastern Peninsular Ranges arc was still active. Unit 4 deposits of bedded metasandstone and poorly sorted metaconglomerates suggest deposition by debris flows (Figure 60A). Provenance analysis from Unit 4 suggests sediment derivation from the Peninsular Ranges batholith and Permo-Triassic arc. The unit likely records input of deltaic systems on the continental shelf that transported eroded Peninsular Ranges batholith sediment, as well as sediment derived from the Permo-Triassic arc, which were deposited in the active channel near the shelf edge.

Geochronological analyses of Unit 3 indicate two distinct MDAs at  $248 \pm 1$  Ma for the siliciclastic metasandstone and  $82 \pm 2$  Ma for the larger volcanoclastic metasandstone sample. Unit 3 was likely deposited on the continental slope during middle Cretaceous time (Figure 60B). The siliciclastic and volcanoclastic metasandstone deposits suggest sediment derivation



from two distinct source areas. Sedimentary structures and provenance analysis of the siliciclastic metasandstone suggest primary erosion from the Permo-Triassic arc and deposition by turbidity currents on the continental slope. Gondwana and Laurentian craton sources identified in samples containing a strong Permo-Triassic signature could indicate derivation from Sonora allochthon strata. Cretaceous volcanoclastic metasandstones are interpreted as interbedded lobes of distributary channels that are fed by sediment derived from the Peninsular Ranges batholith (4; Figure 60). The volcanoclastic metasandstone lenses are often found surrounded by metashale to very-fine grained metasandstone beds, which are commonly observed as levees surrounding distributary channels.

Units 1 and 2 contain a gradational contact, which suggests that the units are part of the same succession. Although the MDA for Unit 2 could not be established with confidence, the MDA of Unit 1 is interpreted as  $75 \pm 2$  Ma. Units 1 and 2 at the base of the continental slope and the ocean basin during Late Cretaceous time (Figure 60C). Unit 1 deposits consist of bedded radiolarian chert and metashale containing parallel laminations and soft-sediment-deformation structures, suggesting emplacement by low-density turbidity currents in the ocean basin. The gradual increase in grain size from Unit 1 to Unit 2, presence of limestone, soft-sediment deformation and parallel laminations suggest Unit 2 was deposited by turbidity currents higher on the continental slope. Units 1 and 2 contain pervasive isoclinal folds, while the other units of the Arroyo Grande Group do not contain any folds. Units 1 and 2 likely represent a laterally removed succession that was later faulted against Unit 3, possibly due to compressive stresses of the Laramide orogeny.

The range in MDAs identified in each unit of the Arroyo Grande Group suggest that the units were likely emplaced at different times and are separated by unconformities (Figure 60D).

The stratigraphic relation between Unit 4 and the other units could not be identified. Unit 4 contains the oldest MDA and was likely later revealed due to erosion of the continental slope. The difference in MDAs and absence of folding in Units 3 and 4, as opposed to the severely folded nature of Units 1 and 2, support the hypothesis that an unconformity is present between Units 2 and 3 as well.

#### **4.3.3 Outstanding Research Problems and Recommended Future Work**

Geochronological analyses of the Sierra Las Pintas area provide important detrital zircon ages that establish a Cretaceous maximum depositional age for the strata. The results from this research do not support the presence of the Sonora allochthon in the Sierra Las Pintas and introduce many unknowns for the area.

The proposed tectonic evolution of the Arroyo Grande Group includes many inferences about the modes of emplacement and relative stratigraphy of the units based on geochronologic and field data. Unit 4 is interpreted as the oldest unit but contains clasts of chert, shale, and sandstone that are the same rock types as the strata of Units 1-3. It is possible that the clasts were derived from elsewhere on the continent as they could not be eroded from younger units. Another possibility is that Unit 4 does not record the emplacement age of the unit and is much younger than the MDA suggests. Unit 4 also contains rare volcanoclastic lithics that would be expected from the active Peninsular Ranges arc. It is possible that sea level was higher during the time of deposition and erosion of the arc was much lower than during the emplacement of Unit 3, which contains a large amount of volcanoclastic sediment. Detailed facies analysis and extensive fault mapping can be utilized to further test the proposed depositional history of the area.

While sedimentological analysis of the Sierra Las Pintas Group supports previous interpretations for deposition on the continental slope, the timing of emplacement is controversial. Navas-Parejo et al. (2018) identified crinoid fauna in Unit SP2 that suggest a Middle Pennsylvanian-early Permian age for the unit, however, geochronologic analysis indicates two unique MDAs for Unit SP2. One sample contains an MDA of  $266 \pm 3$  Ma while another sample for the unit contains an MDA of  $94 \pm 1$  Ma. Although the Permian MDA agrees with previous interpretations for a late Permian Sonora allochthon emplacement, other samples from Units SP1 and SP4 also contain Cretaceous MDAs that suggest the Sierra Las Pintas Group is, in fact, Cretaceous. More detailed geochronologic sampling within the units could potentially reveal where the Cretaceous source was cut off and provide a more in-depth understanding for the timing of basin fill.

Provenance analysis is a powerful tool that can determine the tectonic and paleogeographic history for an area. This study presents detrital zircon ages for each sample and the associated source area interpretation, primarily based on established provenance determinations and zircon population size. A multitude of potential sources exist for zircon populations, including primary derivation from cratonic sources and sediment that has experienced multiple recycling events. Whether the sediment is locally derived from nearby sources or far travelled cannot be constrained by the available data and future work in the Sierra Las Pintas area should focus on retracing the sediment-routing pathways for potential source areas.

## **5.0 CONCLUSIONS**

The Sonora allochthon, the westernmost segment of the Ouachita-Marathon-Sonora orogenic belt, has been well documented in Sonora, Mexico, and studies have proposed the presence of the Sonora allochthon in the Sierra Las Pintas of Baja California, Mexico (Leier-Engelhardt,

1993; Poole et al., 2005; Poole et al., 2008; Navas-Parejo et al., 2018). Proposed Sonora allochthon strata of the Sierra Las Pintas have been correlated to known Sonora allochthon strata of central Sonora primarily by biostratigraphic and stratigraphic similarities (Leier-Engelhardt, 1993; Poole et al., 2008; Navas-Parejo et al., 2018). The main purpose of this study was to test the hypothesis that correlations can be made between the Sonora allochthon strata identified in the Minas de Barita area of central Sonora and proposed Sonora allochthon strata of the Arroyo Grande Group and Sierra Las Pintas Group of Baja California, Mexico (Figure 1).

Detrital zircon geochronology indicates significant differences between the Arroyo Grande Group and Sierra Las Pintas Group of the Sierra Las Pintas and the Minas de Barita area, suggesting that the strata of each field area cannot be correlated. Provenance analysis of the Arroyo Grande Group indicates a Late Cretaceous maximum depositional age and identifies two major source areas, the Peninsular Ranges batholith and the Permo-Triassic arc. Other major sources of zircon indicated by the study include Gondwanan source, as well as the Grenville, Granite-Rhyolite, Yavapai-Mazatzal provinces and the Archean craton (Figure 58). Provenance analysis of the Sierra Las Pintas Group indicates the same major source regions as the Arroyo Grande Group as well as a Late Cretaceous maximum depositional age. Stratigraphic analysis indicates that the Arroyo Grande Group was deposited on the continental slope and ocean basin within the forearc of the Peninsular Ranges batholith (Figure 60). Cretaceous maximum depositional ages identified in most units of Sierra Las Pintas strata contradict the proposed late Permian emplacement age of the Sonora allochthon strata. However, provenance analyses of Sierra Las Pintas strata suggest derivation from Gondwana and the Laurentian continent with prominent peaks indicating major sources from the Peninsular Ranges batholith and the Permo-

Triassic arc, as well as from Grenville, Granite-Rhyolite, Yavapai-Mazatzal provinces and the Archean craton.

Provenance analysis of the Rancho Nuevo Formation and Mina México Formation of the Minas de Barita area agrees with previous literature and also provides strong detrital zircon evidence of Gondwanan source in the Sonora allochthon (Figure 59). Gondwanan source has rarely been identified in previous literature and this study provides a major contribution to the Sonora allochthon provenance discussion. Other major source areas suggest derivation from the Appalachian / OMS orogen, the Grenville orogen and the Yavapai-Mazatzal province. Sedimentary features identified in the Rancho Nuevo Formation and Mina México Formation indicate deposition by turbidity currents and debris-flows on the continental slope. Overall, the Minas de Barita area results from this study agree with previous interpretations of provenance and depositional history of the Sonora allochthon strata.

Provenance analysis from this study does not support the hypothesis that Sonora allochthon strata are present in the Sierra Las Pintas and therefore cannot be correlated to the Sonora allochthon strata identified within the Minas de Barita area. Geochronologic and stratigraphic analysis of the Sierra Las Pintas strata indicates a mixed provenance of Laurentian and Gondwanan source regions, as well as Cretaceous Cordilleran arc activity.

## REFERENCES

- Barth, A., Wooden, J., Jacobson, C., and Economos, R., 2013, Detrital zircon as a proxy for tracking the magmatic arc system: The California arc example: *Geology*, v. 41, no. 2, p. 223-226.
- Becker, T.P., Thomas, W.A. and Gehrels, G.E., 2006, Linking late Paleozoic sedimentary provenance in the Appalachian basin to the history of Alleghanian deformation: *American Journal of Science*, v. 306, no. 10, p. 777-798.
- Bell, E.A. and Kirkpatrick, H.M., 2021, Effects of crustal assimilation and magma mixing on zircon trace element relationships across the Peninsular Ranges Batholith: *Chemical Geology*, v. 586, p. 1-16.
- Blakey, R.C., 2007, Carboniferous-Permian paleogeography of the assembly of Pangaea *in* Wong, T.E., eds., Fifteenth International congress on Carboniferous and Permian Stratigraphy, Royal Netherlands Academy of Arts and Sciences: Amsterdam, p. 443-465.
- Bottjer, D.J., 1984, A Synthesis of late Cretaceous Southern California and Northern Baja California Paleogeography *in* Crouch, J.K., and Bachman, S.B., eds., Tectonics and Sedimentation along the California Margin: Pacific Section S.E.P.M., v. 38, p. 171-188.
- Busby, C., 2004, Continental growth at convergent margins facing large ocean basins: a case study from Mesozoic convergent-margin basins of Baja California, Mexico: *Tectonophysics*, v. 392, p. 241-277.
- Busby-Spera, C.J. and Boles, J.R., 1986, Sedimentation and subsidence styles in a Cretaceous forearc basin, southern Vizcaino Peninsula, Baja California, Mexico *in* Abbott, P.L. (Ed.), Cretaceous Stratigraphy, Western North America Pacific Section, Society of Economic Paleontologists and Mineralogists, Los Angeles, p. 79-90.
- Cawood, P.A. and Buchan, C., 2007, Linking accretionary orogenesis with supercontinent assembly: *Earth-Science Reviews*, v. 82, p. 217-256.
- Cawood, P.A., Hawkesworth, C.J., and Dhuime, B., 2012, Detrital zircon record and tectonic setting: *Geology*, v. 40, no. 10, p. 875-878.
- Cecil, M.R., Ferrer, M.A., Riggs, N.R., Marsaglia, K., Kylander-Clark, A., Ducea, M.N., and Stone, P., 2018, Early arc development recorded in Permian-Triassic plutons of the northern Mojave Desert region, California, USA: *Geological Society of America Bulletin*, v. 131, n. 5-6, p. 749-765.
- Cordani, U.G., Teixeira, W., D'Agrella-Filho, M., and Trindade, R., 2009, The position of the Amazonian Craton in supercontinents: *Gondwana Research*, v. 15, no. 3-4, p. 396-407.
- Davis, D., Williams, I.S., and Krogh, T.E., 2003, Historical development of zircon geochronology: *Reviews in Mineralogy and Geochemistry*, v. 53, p. 145-181.

- Dickinson, W.R., Beard, L.S., Brakenridge, G.R., Erjavec, J., Ferguson, R., Inman, K., Knepp, R., Lindberg, F., and Ryberg, P., 1983, Provenance of North American Phanerozoic sandstones in relation to tectonic setting: *Geological Society of America Bulletin*, v. 94, no. 2, p. 222-235.
- Dickinson, W.R., and Gehrels, G.E., 2003, U-Pb ages of detrital zircons from Permian and Jurassic eolian sandstones of the Colorado Plateau, USA: paleogeographic implications: *Sedimentary Geology*, v. 163, no. 1-2, p. 29-66.
- Dickinson, W.R., and Lawton, T.F., 2001, Carboniferous to cretaceous assembly and fragmentation of Mexico: *GSA Bulletin*, v. 113, n. 9, p. 1142-1160.
- Dickinson, W.R., 2004, Evolution of the North American cordillera: *Annual Review of Earth and Planetary Science*, v. 32, p. 13-45.
- Dickinson, W.R., and Gehrels, G.E., 2009, Use of U–Pb ages of detrital zircons to infer maximum depositional ages of strata: a test against a Colorado Plateau Mesozoic database: *Earth and Planetary Science Letters*, v. 288, no. 1, p. 115-125.
- Dobbs, S., 2017, The middle Permian Monos Formation: Stratigraphic and detrital zircon evidence for Permian Cordilleran arc development along the southwest margin of Laurentia (northwest Sonora, Mexico), M.S. thesis, Northern Arizona University, Department of Geological Sciences, Flagstaff, Arizona.
- Folk, Robert, L., 1951, A comparison chart for visual percentage estimation: *Journal of Sedimentary Research*, v. 21, n. 1, p. 32-33.
- Gastil, R.G., 1993, Prebatholithic history of peninsular California, *in* Gastil, R.G., and Miller, R.H., eds., *The prebatholithic stratigraphy of peninsular California*: Geological Society of America Special Paper 279, p. 145–156.
- Gastil, G., Miller, R., Anderson, P., Crocker, J., Campbell, M., Buch, P., Lothringer, C., Leier-Engelhardt, P., DeLattre, M., Hoobs, J., and Roldan-Quitana, J., 1991, The relation between the Paleozoic strata on opposite sides of the Gulf of California *in* Perez-Segura, E., Jacques-Ayala, C., eds., *Studies of Sonoran Geology*: Boulder, Colorado, Geological Society of America Special Paper 254, p. 7-17.
- Gehrels, G. E., Dickinson, W. R., Ross, G. M., Stewart, J. H., & Howell, D. G., 1995, Detrital zircon reference for Cambrian to Triassic miogeoclinal strata of western North America: *Geology*, v. 23, no. 9, p. 831-834.
- Gehrels, G.E., and Stewart, J.H., 1998, Detrital zircon geochronology of Cambrian to Triassic miogeoclinal and eugeoclinal strata of Sonora, Mexico: *Journal of Geophysical Research*, v. 103, p. 2471-2487.
- Gehrels, G.E., 2000, Introduction to detrital zircon studies of Paleozoic and Triassic strata in western Nevada and northern California *in* Gehrels, G.E., and Soreghan, M.J., eds., *Paleozoic*

and Triassic Paleogeography and Tectonics of Western Nevada and Northern California: Boulder, Colorado, Geological Society of America Special Paper 347, p. 1-17.

Gehrels, G.E., 2012, Detrital zircon U-Pb geochronology: current methods and new opportunities in Busby, C. and Azor, A., eds., *Tectonics of Sedimentary Basins: Recent Advances*, p. 47-62.

Gehrels, G., and Pecha, M., 2014, Detrital zircon U-Pb geochronology and Hf isotope geochemistry of Paleozoic and Triassic passive margin strata of western North America: *Geosphere*, v. 10, n. 1, p. 49-65.

Grimes, C.B., John, B.E., Kelemen, P.B., Mazdab, F.K., Wooden, J.L., Cheadle, M.J., Hanghoj, K., and Schwartz, J.J., 2007, Trace element chemistry of zircons from oceanic crust: A method for distinguishing detrital zircon provenance: *Geology*, v. 35, no. 7, p. 643-646.

Grimes, C. B., Wooden, J. L., Cheadle, M. J., and John, B. E., 2015, “Fingerprinting” tectono-magmatic provenance using trace elements in igneous zircon: *Contributions to Mineral and Petrology*, v. 170, no. 5–6, p. 46.

Hatcher, R.D., 2002, Alleghanian (Appalachian) orogeny, a product of zipper tectonics: rotational transpressive continent–continent collision and closing of ancient oceans along irregular margins *in* Martinez Catalan, J.R., Hatcher, R.D., Arenas, R. & Diaz Garcia, F. (eds): *Variscan–Appalachian dynamics: the building of the late Paleozoic basement: Geological Society of America Special Paper 364*, p. 199–208.

Hatcher, R.D., Jr., Thomas, W.A., and Viele, G.W., eds., 1989, *The Appalachian-Ouachita orogen in the United States: Boulder, Colorado, Geological Society of America, The Geology of North America*, v. F-2, 30 chapters, 12 plates, 767 p.

Hatcher, R.D., 2002, Alleghanian (Appalachian) orogeny, a product of zipper tectonics: rotational transpressive continent-continent collision and closing of ancient oceans along irregular margins *in* Martinez Catalan, J.R., Hatcher, R.D., Arenas, R. and Diaz Garcia, F., eds., *Variscan–Appalachian dynamics: the building of the late Paleozoic basement: Geological Society of America Special Paper 364*, p. 199-208.

Handschy, J.W., Keller, G.R., and Smith, K.J., 1987, The Ouachita system in northern Mexico: *Tectonics*, v. 6, n. 3, p. 323-330.

Heatherington, A., Mueller, P., and Nutman, A., 1996, Neoproterozoic magmatism in the Suwannee terrane: Implications for terrane correlation, in Nance, R.D., and Thompson, M.D., eds., *Avalonian and Related Peri-Gondwanan Terranes of the Circum–North Atlantic: Geological Society of America Special Paper 304*, p. 257–268.

Hoffman, P.F., 1989, Precambrian geology and tectonic history of North America *in* Bally, A.W., and Palmer, A.R., eds., *The Geology of North America: An Overview: Boulder, Colorado, Geological Society of America, The Geology of North America*, v. A, p. 447–512.



- Horstwood, M.S., Košler, J., Gehrels, G., Jackson, S.E., McLean, N.M., Paton, C., Pearson, N.J., Sircombe, K., Sylvester, P., Vermeesch, P., and Bowring, J.F., 2016, Community-derived standards for LA-ICP-MS U-(Th-) Pb geochronology—Uncertainty propagation, age interpretation and data reporting: *Geostandards and Geoanalytical Research*, v. 40, no. 3, p. 311-332.
- Hoskin, P.W.O., and Schaltegger, U., 2003, The composition of zircon and igneous and metamorphic petrogenesis: *Mineralogical Society of America Reviews in Mineralogy*, v. 53, p. 27-62.
- James, A.H., 1973, Structure and stratigraphy of the southern Sierra de Pintas, Baja California, Mexico, M.Sc. thesis, San Diego State University, Department of Geological Sciences, San Diego, California, p. 56.
- Kirkland, C.L., Smithies, R.H., Taylor, R.J.M., Evans, N., and McDonald, B. 2015, Zircon Th/U ratios in magmatic environs: *Lithosphere*, v. 212, p. 397-414.
- Kimbrough, D.L., Smith, D.P., Mahoney, J.B., Moore, T.E., Grove, M., Gastil, R.G., Ortega-Rivera, A., and Fanning, C.M., 2001, Forearc-basin sedimentary response to rapid Late Cretaceous batholith emplacement in the Peninsular Ranges of southern and Baja California: *Geology*, v. 29, no. 6, p. 491-494.
- Kroner, U., Roscher, M., and Romer, R.L., 2016, Ancient plate kinematics derived from the deformation pattern of continental crust: Paleo- and Neo- Tethys opening coeval with prolonged Gondwana-Laurussia convergence: *Tectonophysics*, v. 681, p. 220-233.
- Kylander-Clark, A.R., Hacker, B.R., and Cottle, J.M., 2013, Laser-ablation split-stream ICP petrochronology: *Chemical Geology*, v. 345, p. 99-112.
- La Borde, R.T., 1967, Reconnaissance geology of the northern Sierra de Pintas, Baja California, Senior report, vol. 11, San Diego State University, Department of Geological Sciences, San Diego, California, 22.
- Lara-Peña, R.A., Navas-Parejo, P., and Amaya-Martinez, R., 2020, New conodont data related to the western Ouachita-Marathon-Sonora orogen: Age of the autochthonous Laurentian deformation: *Journal of South American Earth Sciences*, v. 103, p. 1-8.
- Leier-Engelhardt, P., 1986, Middle Paleozoic Strata of the Sierra Las Pinta, Northeastern Baja California Norte, Mexico, M.Sc. thesis, San Diego State University, Department of Geological Sciences, San Diego, California.
- Leier-Engelhardt, P., 1993, Middle Paleozoic strata of the Sierra Las Pintas, northeastern Baja California Norte, Mexico, *in* Gastil, R.G., and Miller, R.H., eds., *The Prebatholithic Stratigraphy of Peninsular California*: Boulder, Colorado, Geological Society of America Special Paper 279, p. 23-41.

- Lodes, E., 2019, Geochronologic and stratigraphic evidence of Laurentian subduction initiation (Inyo Mountains, Eastern California), M.Sc. thesis, Northern Arizona University, Department of Geological Sciences, Flagstaff, Arizona, p. 1-133.
- Meert, Joseph G., and Van Der Voo, R., 1997, The assembly of Gondwana 800-550 Ma: *Journal of Geodynamics*, v. 23, no. 3-4, p. 223-235.
- McEldowney, R.C., 1970, Geology of Northern Sierra Pinta, Baja California, Mexico, M.Sc. thesis, San Diego State University, Department of Geological Sciences, San Diego, California, p. 78.
- Morales, H., in prep., Cartografía y Estratigrafía de la Sierra Las Pintas, B.Sc. thesis, Universidad Nacional Autónoma de México, Departamento de Geología, Hermosillo, Mexico.
- Murphy, J.B., and Nance, R.D., 1991, Supercontinent model for the contrasting character of Late Proterozoic orogenic belts: *Geology*, v. 19, no. 5, p. 469-472.
- Navas-Parejo, P., Lara-Pena, R., Torres-Martinez, M.A., and Martini, M., 2018, Biostratigraphy and petrography of upper Paleozoic rocks of Sierra Las Pintas, northern Baja California: *Journal of South American Earth Sciences*, p. 160-171.
- Ortega-River, A., 2003, Geochronological constraints on the tectonic history of the Peninsular Ranges batholith of Alta and Baja California: Tectonic implications for western Mexico, *in* Johnson, S.E., Paterson, S.R., Fletcher, J.M., Girty, G.H., Kimbrough, D.L., Martin-Barajas, A., eds., *Tectonic Evolution of Northwestern Mexico and the Southwestern USA: Geological Society of America Special Paper 374*.
- Poole, F.G. and Amaya-Martínez, R., 2000, Silurian and Devonian carbonate-shelf rocks and Lower Jurassic sequence near Rancho Placeritos, west-central Sonora: Field guide for Field Trip 2 (March 4, 2000), Fourth symposium on the geology of northwest Mexico and adjacent areas (March 6–8, 2000), Center for the Arts, University of Sonora, Hermosillo, Mexico, p. 24.
- Poole, F.G., and Perry, W.J., Jr., 1997, The late Paleozoic Ouachita-Marathon-Sonora orogenic system along the southern margin of North America: *Geologic Society of America Abstracts with Programs*, v. 29, no. 2, p. 43.
- Poole, F.G., Perry, W.J., Jr., Madrid, R.J., and Amaya-Martínez, R., 2005, Tectonic synthesis of the Ouachita-Marathon-Sonora orogenic margin of southern Laurentia: Stratigraphic and structural implications for timing of deformational events and plate-tectonic model, *in* Anderson, T.H., Nourse, J.A., McKee, J.W., and Steiner, M.B., eds., *The Mojave-Sonora megashear hypothesis: Development, assessment, and alternatives: Geological Society of America Special Paper 393*, p. 543-596.

- Poole, F.G., Gehrels, G.E., and Stewart, J.H., 2008, Significance of detrital zircons in Upper Devonian ocean-basin strata of the Sonora allochthon and Lower Permian synorogenic strata of the Mina Mexico foredeep, central Sonora, Mexico, *in* Blodgett, R.B., and Stanley, G.D., Jr., eds., *The terrane puzzle: New perspectives on paleontology and stratigraphy from the North American Cordillera: Geological Society of America Special Paper 442*, p. 121-131.
- Riggs, N.R., Barth, A.P., Wooden, J., and Walker, J.D., 2010, Use of zircon geochemistry to tie volcanic detritus to source plutonic rocks: an example from Permian northwestern Sonora, Mexico: *Geological Society of America Abstracts with Programs*, v. 42, no. 5, p. 267.
- Ross, C.A., 1986, Paleozoic evolution of southern margin of Permian basin: *Geological Society of America Bulletin*, v. 97, no. 5, p. 536-554.
- Rubatto, D., 2002, Zircon trace element geochemistry: Partitioning with garnet and the link between U-Pb ages and metamorphism: *Chemical Geology*, v. 184, p. 123–138.
- Saleeby, J.B., Busby-Spera, C., Oldow, J.S., Dunne, G.C., Wright, J.E., Cowan, D.S., Walker, N.W., Allmendinger, R.W., 1992, Early Mesozoic tectonic evolution of the western U.S. Cordillera: The Cordilleran Orogen: Conterminous U.S. *The Geology of North America*, no. G-3, Geological Society of America, Boulder, CO, p. 107-168
- Saleeby, J., and Dunn, G., 2015, Temporal and tectonic relations of early Mesozoic arc magmatism, southern Sierra Nevada, California: *Geological Society of America Special Papers*, v. 513, SPE513-05.
- Sedlock, R.L., 2003, Geology and tectonics of the Baja California peninsula and adjacent areas, *in* Johnson, S.E., Paterson, S.R., Fletcher, J.M., Girty, G.H., Kimbrough, D.L., Martin-Barajas, A., eds., *Tectonic Evolution of Northwestern Mexico and the Southwestern USA: Geological Society of America Special Paper 374*, p. 1-292.
- Silver, L.T., and Chappell, B.W., 2011, The Peninsular Ranges Batholith: an insight into the evolution of the Cordilleran batholiths of southwestern North America: *Earth and Environmental Science Transactions of the Royal Society Edinburgh*, v. 79, no. 2-3, pg. 105-121.
- Soto-Kerans, G.M., Stockli, D.F., Janson, X., Lawton, T.F., and Covault, J.A., 2020, Orogen proximal sedimentation in the Permian foreland basin: *Geosphere*, v. 16, no. 2, p. 567-593.
- Sláma, J., Košler, J., Condon, D.J., Crowley, J.L., Gerdes, A., Hanchar, J.M., Horstwood, M.S., Morris, G.A., Nasdala, L., Norberg, N., and Schaltegger, U., 2008, Plešovice zircon—a new natural reference material for U–Pb and Hf isotopic microanalysis: *Chemical Geology*, v. 249, no. 1-2, p. 1-35.
- Stampfli, G.M., von Raumer, J.F. and Borel, G.D., 2002a. Paleozoic evolution of pre-Variscan terranes: from Gondwana to the Variscan collision, *in* Martinez Catalan, J.R., Hatcher, R.D.,

- Arenas, R. and Diaz Garcia, F., eds., Variscan-Appalachian dynamics: the building of the late Paleozoic basement: Geological Society of America Special Paper 364, p. 263-280.
- Stevens, C.H., Poole, F.G., and Amaya-Martínez, R., 2014, Late Paleozoic fusulinds from Sonora, México: Importance for interpretation of depositional settings, biogeography, and paleotectonics: *Revista Mexicana de Ciencias Geológicas*, v. 31, no. 1, p. 14-27.
- Stewart, J.H., and Poole, F.G., 2002 Inventory of Neoproterozoic and Paleozoic strata in Sonora, Mexico: USGS Open-File Report, 02-97, p. 1-50.
- Van Lankvelt, A., Schneider, D.A., Biczok, J., McFarlane, C.R.M., Hattori, K., 2016, Decoding zircon geochronology of igneous and alteration events based on chemical and microstructural features: a study from the Western Superior Province, Canada: *Journal of Petrology*, v. 57, no. 7, pg. 1309-1334.
- Vermeesch, P., 2018, IsoplotR: a free and open toolbox for geochronology: *Geoscience Frontiers*, v.9, p.1479-1493, doi:10.1016/j.gsf.2018.04.001.
- Vermeesch, P., 2012, On the visualisation of detrital age distributions: *Chemical Geology*, v. 312, p. 190-194.
- Whitmeyer, S.J., and Karlstrom, K.E., 2007, Tectonic model for the Proterozoic growth of North America: *Geosphere*, v. 3, p. 220–259.
- Wiedenbeck, M.A.P.C., Alle, P., Corfu, F., Griffin, W.L., Meier, M., Oberli, F.V., Quadt, A.V., Roddick, J.C., and Spiegel, W., 1995, Three natural zircon standards for U-Th-Pb, Lu-Hf, trace element and REE analyses: *Geostandards newsletter*, v. 19, no. 1, p.1-23.
- Ziegler, P.A., 1992, Plate tectonics, plate moving mechanisms and rifting *in* Ziegler, P.A., eds., *Geodynamics of Rifting: Tectonophysics*, v. 3, no. 215, p. 9-34.

**APPENDIX Ia:** Uranium, lead, and thorium isotope data for samples collected from the Arroyo Grande Group. Best age:  $^{207}\text{Pb}/^{206}\text{Pb}$  ages used for grains older than 1.0 Ga and  $^{206}\text{Pb}/^{238}\text{U}$  ages for grains younger than 1.0 Ga with 2 sigma uncertainty.











Sample	Grain	Unit	U (ppm)	Th (ppm)	Measured isotopic ratios														Isotopic ages and errors (Ma)									
					$^{206}\text{Pb}/^{238}\text{U}$	$2\sigma$	$^{207}\text{Pb}/^{235}\text{U}$	$2\sigma$	0.00	Correlation	$^{236}\text{Pb}/^{238}\text{U}$	$2\sigma$	$^{206}\text{Pb}/^{238}\text{U}$	$2\sigma$	$^{207}\text{Pb}/^{235}\text{U}$	$2\sigma$	0.00	Correlation	$^{207}\text{Pb}/^{235}\text{U}$	$2\sigma$	$^{206}\text{Pb}/^{238}\text{U}$	$2\sigma$	disc	best age (Ma)	$2\sigma$	internal error		
LPO8012-8s-1	AGG 3	926	204	3.590	0.230	0.238	0.012	0.994	4.202	0.210	0.110	0.002	-0.935	1551	49	1374	61	1792	30	0.77	1792	30	2%					
LPO8012-8L-52	AGG 3	160.7	633.7	3.607	0.280	0.240	0.005	0.876	4.168	0.280	0.110	0.002	-0.936	1550	18	1386	24	1795	25	0.77	1795	25	1%					

Table with columns for sample ID, unit, U (ppm), Th (ppm), and various isotopic ratios (e.g., 206Pb/238U, 207Pb/235U) and errors. Includes a section for 'Rejected Grains'.

Sample LP13010-1

Table for Sample LP13010-1 showing measured isotopic ratios and isotopic ages with error bars. Columns include Grain, Unit, U (ppm), Th (ppm), and various isotopic ratios.

Sample LP09010-2

Table for Sample LP09010-2 showing measured isotopic ratios and isotopic ages with error bars. Columns include Grain, Unit, U (ppm), Th (ppm), and various isotopic ratios.







**APPENDIX Ib:** Uranium, lead, and thorium isotope data for samples collected from the Sierra Las Pintas Group. Best age:  $^{207}\text{Pb}/^{206}\text{Pb}$  ages used for grains older than 1.0 Ga and  $^{206}\text{Pb}/^{238}\text{U}$  ages for grains younger than 1.0 Ga with 2 sigma uncertainty.









Table with columns for sample ID, age, and concentration. Rows include LP110120-1L-14, LP110120-1S-25, and LP110120-1L-116.

Sample 184-P-10

Main table with columns for Unit, U (ppm), Th (ppm), Error (Correlation, 235Pb/238U, 238U, 235Pb/235U, 238U, 235Pb/235U, 238U, 235Pb/235U, 238U), Isotopic ages and errors (Ma) (235Pb/235U, 238U, 235Pb/238U, 238U), discordance, best age (Ma), and internal error. The table contains a large number of rows representing individual measurements and calculations for various samples.



**APPENDIX Ic:** Uranium, lead, and thorium isotope data for samples collected from the Minas de Barita Area. Best age:  $^{207}\text{Pb}/^{206}\text{Pb}$  ages used for grains older than 1.0 Ga and  $^{206}\text{Pb}/^{238}\text{U}$  ages for grains younger than 1.0 Ga with 2 sigma uncertainty. RN: Rancho Nuevo Formation, MM: Mina México Formation.









**APPENDIX IIa:** Detrital zircon trace element data for samples of the Arroyo Grande Group.  
Trace elements: Si, P, Ti, Y, Zr, Nb, La, Ce, Pr, Nd, Sm.









Table with columns: Grain ID, Agg 3, 1.2E+07, 47000, 106.8, 7.5, 19.2, 2.2, 467, 27, 453000, 20000, 4.12, 0.47, 0.018, 0.024, 21.7, 5.4, 0.118, 0.055, 1.79, 0.4, 2.61, 0.56. Includes sections for Rejected Grains and Sample 080120-9.











LP090120-3s-53	AGG 4	12390000	410000	8270	440	396	31	288000	18000	85500000	2900000	844	96	6.8	7.5	18380	750	170	36	433	77	491	63
LP090120-3s-83	AGG 4	14030000	370000	20400	2500	1040	220	750000	100000	92400000	2600000	1020	170	145	46	2550	170	173	41	298	54	585	75
LP090120-3s-113	AGG 4	13660000	360000	9320	470	2960	690	280000	24000	94500000	2500000	1780	330	990	260	5800	400	850	150	1270	200	1650	200
LP090120-3L-57	AGG 4	12730000	380000	3700	220	100	11	72900	3100	88100000	3100000	204	42	0	1	222	33	6.5	7.2	0	1	10.9	8.8
LP090120-3s-96	AGG 4	12760000	530000	49000	29000	179	19	325000	34000	85100000	2100000	489	64	5200	3300	22000	11000	2900	1800	2000	1300	850	360
LP090120-3s-31	AGG 4	12610000	230000	22200	1000	239	24	575000	20000	86100000	1800000	663	93	0	1	7460	350	30	15	102	32	425	68
LP090120-3s-46	AGG 4	12400000	340000	10450	400	528	39	476000	21000	87000000	2800000	510	81	33	16	2580	130	300	63	680	100	1000	110
LP090120-3s-34	AGG 4	13020000	400000	25500	1300	338	52	598000	18000	86100000	2700000	1560	180	20	14	4400	480	250	96	430	110	610	110
LP090120-3s-24	AGG 4	14470000	310000	9000	1200	300	110	341000	54000	96100000	2200000	1890	210	113	81	16600	1500	500	330	670	390	660	280
LP090120-3s-75	AGG 4	12830000	350000	11900	1500	355	30	960000	180000	86300000	2800000	2520	220	10.4	8.5	8000	1200	233	66	700	160	1150	240
LP090120-3L-77	AGG 4	12850000	390000	14210	820	402	26	585000	26000	87600000	1900000	4880	300	260	310	24200	1900	130	120	200	100	398	79
LP090120-3s-67	AGG 4	12900000	280000	8000	640	224	27	176400	9300	87500000	2400000	1120	130	39	19	8840	680	76	33	220	55	213	50
LP090120-3s-20	AGG 4	13190000	410000	7640	490	240	24	207000	8000	85400000	3000000	2160	370	30	17	3370	430	27	19	45	21	105	41
LP090120-3s-11	AGG 4	12620000	340000	10600	1000	209	24	312000	19000	84400000	2400000	830	140	86	52	11930	430	241	67	450	100	570	91

**APPENDIX IIb:** Detrital zircon trace element data for samples of the Arroyo Grande Group.  
Trace elements: Eu, Gd, Tb, Dy, Ho, Er, Tm, Yb, Lu, Hf.























LP090120-3s-34	AGG 4	350	130	2730	220	7670	360	22950	780	34300	1400	56900	3200	44600	2500	118000	13000	71500	7100	2780000	100000
LP090120-3s-24	AGG 4	880	470	2390	590	4330	940	12800	1700	17900	1800	28000	2600	20400	2100	50800	5100	30500	2300	2540000	66000
LP090120-3s-75	AGG 4	256	52	6000	1000	14300	2700	42100	6700	57700	9000	88000	13000	56500	9000	124000	19000	70000	11000	2595000	76000
LP090120-3L-77	AGG 4	556	59	2570	150	6460	430	22700	1000	33600	1300	52700	2000	39400	1500	92700	4000	55600	2000	2505000	90000
LP090120-3s-67	AGG 4	212	73	893	99	2060	170	6310	420	9680	560	14730	980	13000	1100	34100	2900	22600	2300	2596000	64000
LP090120-3s-20	AGG 4	198	76	580	130	1570	270	6420	500	10820	560	20800	1300	17160	990	51800	3800	34900	3000	2930000	120000
LP090120-3s-11	AGG 4	1400	420	1940	170	4160	330	12380	740	17200	1100	25700	1600	19100	1300	48700	4600	31700	2300	2236000	61000

**APPENDIX IIIa:** Detrital zircon trace element data for samples of the Sierra Las Pintas Group.  
Trace elements: Si, P, Ti, Y, Zr, Nb, La, Ce, Pr, Nd, Sm.



		Sample 100120-1																					
Grain	Unit	Si (ppm)	error	P (ppm)	error	Ti (ppm)	error	Y (ppm)	error	Zr (ppm)	error	Nb (ppm)	error	La (ppm)	error	Ce (ppm)	error	Pr (ppm)	error	Nd (ppm)	error	Sm (ppm)	error
LP100120-11-40	SP1	207800	9400	216	18	13.1	2.1	1232	40	603000	24000	4.07	0.57	0.128	0.055	42	2	0.82	0.14	14.8	1.9	24.7	1.8
LP100120-11-44	SP1	201800	9140	91.4	8.6	4.9	1.8	583	50	571000	25000	3.66	0.56	0.006	0.012	16.87	0.88	0.082	0.045	1.41	0.49	3.6	1
LP100120-11-10	SP1	206800	9600	261	23	15.1	2.1	3050	370	596000	22000	8	1	0.04	0.035	144	14	0.504	0.08	9	1.1	22	2.6
LP100120-11-40	SP1	219300	8900	188	34	7.1	1.4	1296	86	587000	28000	11.5	1.2	1.6	0.85	51.1	5.5	0.61	0.28	4.7	1.4	7.1	1.4
LP100120-11-91	SP1	229200	9100	401	26	15.6	4.2	3250	160	607000	25000	24.6	1.5	1.7	1.1	67	14	1.9	1.2	16.1	6.4	26.9	4.3
LP100120-11-54	SP1	219700	8300	172	21	13.6	1.7	1081	85	603000	21000	4.65	0.47	0.16	0.07	62.1	91	24.2	4	107	16	25.5	3.4
LP100120-11-56	SP1	202000	10000	2020	890	13.4	1.8	1372	95	570000	25000	1.9	0.25	15.4	8.8	43	19	3.8	1.8	24	14	10.8	2.1
LP100120-11-70	SP1	219000	13000	760	270	4.4	2.2	770	64	540000	28000	2.04	0.31	4.1	1.6	18.4	2.7	0.83	0.35	4.5	1.4	4.55	0.99
LP100120-11-32	SP1	220000	11000	155	16	4.4	2	920	120	609000	23000	4.88	0.77	0	1	6.92	0.88	0.015	0.018	0.63	0.31	2.78	0.65
LP100120-11-49	SP1	217300	9400	110.6	8.9	6	1.5	600	28	586000	20000	2.38	0.21	0	1	7.12	0.47	0.034	0.021	0.84	0.28	2.11	0.55
LP100120-11-12	SP1	217000	9300	160	11	19.1	2.1	857	24	596000	25000	2.72	0.37	0	1	7.06	0.49	0.134	0.047	1.55	0.52	4.8	1.1
LP100120-11-59	SP1	219300	7800	319	18	7.3	1.9	7040	310	604000	31000	8.14	0.56	0.041	0.036	21.4	1.4	0.979	0.094	21.1	2.3	48	2.8
LP100120-11-79	SP1	208500	8400	146	15	6.1	1.2	728	30	596000	30000	2.18	0.29	0	1	5.7	0.56	0.038	0.022	0.98	0.37	3.38	0.69
LP100120-11-83	SP1	215000	11000	107.3	9.6	5.5	1.3	714	83	597000	26000	1.65	0.25	0	1	1.54	0.23	0.027	0.021	1.16	0.54	3.72	0.93
LP100120-11-37	SP1	216600	8300	90.2	8.9	5.7	1.6	468	42	574000	19000	1.3	0.27	0.006	0.012	5.09	0.47	0.104	0.061	1.1	0.49	2.61	0.61
LP100120-11-66	SP1	215100	9700	99	10	48	24	583	27	592000	23000	2.38	0.3	0.012	0.016	6.01	0.43	0.06	0.027	0.93	0.35	2.39	0.62
LP100120-11-74	SP1	249300	9000	133.7	8.2	27	2.5	1500	42	675000	25000	3.9	0.44	0.023	0.022	5.8	0.45	0.187	0.063	3.9	0.68	9.5	1.5
LP100120-11-46	SP1	206000	11000	510	190	5.3	2.1	2410	160	597000	29000	3.89	0.49	2.6	1.8	16.6	5.6	2	1.4	16.3	5.8	18.4	1.9
LP100120-11-77	SP1	229000	10000	168	10	10.2	1.7	1306	57	612000	18000	4.72	0.47	0.011	0.015	11.98	0.71	0.094	0.051	2.95	0.55	4.19	0.65
LP100120-11-73	SP1	210600	8900	301	51	10.6	2.1	1211	56	607000	17000	2.73	0.41	1.42	0.56	7.5	1.6	0.76	0.19	6.1	1.4	6.51	0.91
LP100120-11-13	SP1	213200	8500	146.4	8.7	9.6	1.8	933	40	599000	19000	2.47	0.31	0.006	0.012	3.55	0.37	0.143	0.052	2.53	0.5	4.98	0.92
LP100120-11-69	SP1	233000	10000	490	150	6.2	1.9	437	22	627000	24000	1.6	0.26	5.8	2.3	17.8	5	1.47	0.63	6.7	2.7	2.48	0.73
LP100120-11-13	SP1	213000	11000	119	11	4.3	1.9	893	66	585000	25000	12.67	0.93	0.006	0.012	25	1.6	0.067	0.045	1.03	0.43	2.84	0.65
LP100120-11-45	SP1	219000	12000	151	12	4.6	2	1245	42	612000	24000	12.14	0.85	0.012	0.023	42.3	2.4	0.045	0.029	0.97	0.35	2.53	0.61
LP100120-11-5	SP1	215800	8200	666	42	6.6	2.1	5230	250	592000	25000	2.5	2	0.076	0.057	41.3	3.5	0.36	0.12	9.7	1.7	29.4	2.8
LP100120-11-3	SP1	217600	7300	146	10	7.9	1.5	1114	61	597000	22000	3.82	0.41	0.011	0.016	7.57	0.7	0.06	0.038	1.77	0.49	4.87	0.72
LP100120-11-56	SP1	215000	10000	110.2	8.4	11.2	2	767	66	590000	24000	1.25	0.25	0.006	0.012	1.63	0.22	0.091	0.043	2.1	0.78	5.17	0.91
LP100120-11-66	SP1	248000	11000	450	31	4.8	5.6	1507	54	674000	29000	3.04	0.39	1.61	0.27	10.28	0.72	0.85	0.12	7.4	1.2	8.81	0.88
LP100120-11-21	SP1	204200	9900	172	14	12.1	1.9	904	35	589000	26000	2.41	0.34	0.012	0.023	11.77	0.53	0.049	0.031	0.79	0.32	3.09	0.6
LP100120-11-38	SP1	207900	10000	192	14	8.7	2	1700	140	593000	20000	1.84	0.26	0.012	0.023	16.5	1.3	0.098	0.051	1.96	0.67	6.4	1.3
LP100120-11-14	SP1	207600	9200	253	21	18.7	3.5	566000	21000	1.96	0.34	0	1	5.58	0.51	0.022	0.016	0.91	0.32	1.55	0.76		
LP100120-11-64	SP1	221500	9500	206	16	18.2	2.2	886	43	605000	30000	1.95	0.3	0	1	9.06	0.72	0.019	0.019	1.06	0.48	2.79	0.75
LP100120-11-34	SP1	201800	8800	232	14	14.9	2.1	1132	50	625000	20000	2.03	0.33	0.006	0.012	12.29	0.83	0.034	0.029	1.24	0.4	4.01	0.81
LP100120-11-28	SP1	215000	11000	213	12	12.2	2.1	1644	88	592000	23000	2.65	0.43	0.012	0.016	18.8	1.5	0.108	0.043	2.17	0.39	7.08	0.82
LP100120-11-89	SP1	209000	6900	219	13	3.7	1.2	2100	170	618000	24000	3.1	0.51	0.011	0.016	15.3	1.4	0.278	0.084	5.41	0.93	11.8	2
LP100120-11-23	SP1	213400	8600	390	57	13.6	2.2	1457	55	573000	22000	2.03	0.36	0.8	0.33	14.74	0.89	0.38	0.11	4.19	0.99	6.54	0.99
LP100120-11-59	SP1	213000	12000	263	15	9.6	2.3	1160	55	613000	21000	1.96	0.34	0	1	12.87	0.6	0.042	0.029	0.99	0.38	3.46	0.66
LP100120-11-54	SP1	208000	13000	164	12	11.1	2.6	1881	68	591000	25000	4.05	0.49	0.041	0.032	10.51	0.69	0.213	0.086	4.06	0.77	9.4	1.4
LP100120-11-18	SP1	222900	9000	317	14	15.5	2.6	2780	100	617000	23000	14.46	0.93	0.017	0.019	104.1	3	0.271	0.082	5	1	11	1.3
LP100120-11-27	SP1	210800	6700	658	59	8.6	2.3	2630	530	583000	25000	31.7	7	8.5	3.2	129	15	1.37	0.41	6.3	1.2	8.7	2.3
LP100120-11-106	SP1	220300	8300	234	21	8.1	1.8	2090	200	607000	27000	6.4	0.57	0.011	0.023	56.4	3.1	0.191	0.068	3.5	0.84	8.9	1.5
LP100120-11-29	SP1	207700	8500	291	20	17.2	2.8	1570	56	616000	26000	2.1	0.31	0.023	0.036	23.8	1.2	0.279	0.085	5.5	0.82	9.1	1.2
LP100120-11-55	SP1	210900	9300	343	13	4.4	1.9	546	29	580000	18000	6.02	0.32	0	1	5.58	0.51	0.022	0.016	0.91	0.32	1.55	0.53
LP100120-11-45	SP1	216100	8500	296	29	17	1.7	2100	130	577000	25000	5.42	0.8	0.71	0.27	19.3	1.3	0.325	0.085	3.7	0.84	8.3	1.2
LP100120-11-51	SP1	211500	9600	118.5	9.1	6.9	1.4	555	26	569000	21000	3.27	0.4	0.006	0.012	14.8	1.2	0.03	0.028	0.68	0.29	1.37	0.43
LP100120-11-15	SP1	220700	8900	162	16	7.1	1.6	2170	140	587000	21000	5.71	0.69	0.018	0.019	15.1	1.5	0.301	0.077	5.5	0.85	10	1.7
LP100120-11-33	SP1	220500	9300	187	12	13.3	1.8	1196	40	567000	22000	5.01	0.51	0.012	0.016	21.3	1	0.119	0.051	1.87	0.49	4.39	0.71
LP100120-11-58	SP1	210500	9000	131.6	8.9	7.9	2	676	29	595000	28000	3.56	0.55	0.012	0.016	14.39	0.96	0.056	0.025	0.64	0.22	1.63	0.51
LP100120-11-67	SP1	212500	9600	192	43	9.2	1.8																

LP100120-15-99	SP1	212500	9900	269	41	25.1	5.8	1380	180	603000	27000	6.87	0.96	0.127	0.052	48	11	1.43	0.69	17.5	7.3	23	10
LP100120-11-30	SP1	210000	8100	189	12	380	907	30	606000	27000	4.2	1.6	0.041	0.036	6.27	0.36	0.17	0.07	2.61	0.5	6.7	1.3	
LP100120-15-110	SP1	213000	13000	286	12	24.8	2.7	1179	41	613000	20000	3.69	0.38	0.011	0.016	7.37	0.39	0.09	0.045	2.39	0.62	6.8	1.2
LP100120-15-16	SP1	219500	9300	127.1	8.4	12.4	1.5	969	44	607000	22000	9.73	0.71	0	1	13.64	0.76	0.071	0.035	1.31	0.34	4.54	0.7
LP100120-15-2	SP1	217000	12000	237	16	8.1	1.6	1301	56	571000	20000	4.59	0.49	0.018	0.026	45.3	3.5	0.089	0.039	2.71	0.54	5.92	0.75
LP100120-11-25	SP1	221100	7200	313	64	23.5	2.7	977	39	612000	21000	5.81	0.48	6	4	28.3	8.6	2.2	1.5	10.3	6	5.8	1.2
LP100120-15-55	SP1	212000	11000	191	15	26	3.2	677	33	616000	20000	3.97	0.37	0.006	0.012	9.95	0.64	0.072	0.035	0.7	0.3	1.12	0.63
LP100120-11-86	SP1	214600	8800	125.4	7.7	13.2	2.5	476	21	639000	24000	2.74	0.26	0.012	0.016	18.14	0.83	0.053	0.033	1.11	0.34	2.46	0.85
LP100120-11-70	SP1	220800	6900	250	18	16.4	2.3	1758	53	634000	24000	4.21	0.46	0.047	0.033	30.2	1.9	0.72	0.12	11.2	1.2	20	1.8
LP100120-15-6	SP1	219700	7900	312	19	26.4	2.7	1753	64	572000	22000	5.98	0.41	0.035	0.035	39.1	1.8	0.249	0.07	4.11	0.72	9.9	1.1
LP100120-11-26	SP1	214500	7300	264	13	22.4	2.1	1443	77	610000	24000	3.28	0.4	0.023	0.022	9.18	0.63	0.181	0.068	3.59	0.72	7.2	1.3
LP100120-11-16	SP1	206800	6500	478	83	17.5	2.2	1142	52	607000	17000	6.81	0.48	9.1	3.5	95.9	6.8	2.31	0.77	12.9	3.1	9.5	1.4
LP100120-15-64	SP1	211600	8700	261	20	6.7	1.8	971	33	600000	22000	5.13	0.43	0.017	0.035	38.4	1.8	0.108	0.06	1.79	0.5	4.14	0.63
LP100120-15-98	SP1	213000	12000	208	14	25.4	2.5	1287	62	571000	25000	2.49	0.4	0.006	0.011	15.46	0.58	0.083	0.047	1.92	0.53	5.68	0.84
LP100120-15-25	SP1	215000	12000	273	21	11	2	1405	69	580000	24000	3.62	0.45	0.064	0.063	27.6	1.5	0.1	0.061	1.73	0.52	4.92	0.67
LP100120-15-63	SP1	211000	13000	495	38	12.7	2.1	2560	110	574000	22000	9.84	0.65	0	1	89	4.6	0.115	0.051	2.92	0.47	10.7	1.2
LP100120-15-88	SP1	219000	13000	110.3	8.5	10.1	2	471	20	574000	22000	2.21	0.3	0	1	10.48	0.58	0.026	0.02	0.6	0.34	1.65	0.5
LP100120-15-94	SP1	218000	11000	246	15	9.4	1.6	2029	70	585000	21000	19.2	1.3	0.04	0.046	30.2	1.7	0.232	0.046	4.25	0.82	10.6	1.2
LP100120-15-18	SP1	214100	8900	301	21	59.6	2.8	1217	50	593000	21000	4.09	0.4	0.047	0.041	18.26	0.79	0.253	0.076	4.4	0.87	8.8	1.8
LP100120-11-8	SP1	215500	8700	191	9.6	12.7	2	714	21	599000	26000	4.12	0.45	0.04	0.035	12.17	0.57	0.248	0.078	3.65	0.73	5.9	1.1
LP100120-11-9	SP1	207900	9900	283	17	55.9	3.7	1930	190	602000	24000	2.91	0.33	0.21	0.11	20.5	1.3	0.94	0.21	13.6	2.6	18.2	3
LP100120-11-68	SP1	224000	11000	122.5	9	4.9	2.1	1634	79	622000	26000	3.1	0.35	0.118	0.077	11.49	0.73	0.82	1.18	12.8	1.4	16.7	1.6
LP100120-15-38	SP1	212600	8100	132.3	9.1	7.1	2.3	1149	89	571000	19000	5.79	0.56	0.011	0.022	8.61	0.74	0.043	0.026	1.63	0.46	4.62	0.91
LP100120-11-67	SP1	229400	6100	261	15	15.6	2.1	1618	59	624000	23000	4.58	0.49	0.006	0.011	7.75	0.53	0.171	0.063	2.81	0.59	7.7	1.2
LP100120-15-53	SP1	213600	8200	920	390	20.3	2.2	2004	89	582000	23000	5.7	0.47	17	11	123	24	6.4	4	34	17	18.2	2.5
LP100120-15-68	SP1	216900	9300	143	12	11	1.9	864	30	583000	18000	7.77	0.62	0	1	116.1	0.75	0.052	0.029	1.57	0.45	3.79	0.69
LP100120-15-71	SP1	223000	10000	343	27	42.8	3	1461	89	586000	23000	5.69	0.5	0.035	0.035	48.1	3.6	0.224	0.054	3.66	0.58	7.9	1.5
LP100120-15-109	SP1	217300	7300	136	10	5.5	1.9	894	34	617000	28000	12.6	1	0.006	0.011	10.72	0.5	0.023	0.022	0.51	0.27	1.84	0.67
LP100120-11-61	SP1	208600	7900	201	14	7.8	1.9	831	49	596000	25000	5.25	0.46	0	1	39.8	2.2	0.026	0.023	0.77	0.3	2.3	0.62
LP100120-15-107	SP1	218000	10000	225	30	15.5	3.9	1740	370	586000	28000	3.64	0.45	0.029	0.029	11.3	2.2	0.27	0.13	5.3	2	9	2.6
LP100120-11-78	SP1	224000	12000	207	14	21.2	2.5	793	35	618000	30000	2.85	0.36	0	1	7.9	0.68	0.061	0.035	0.7	0.19	3.23	0.68
LP100120-15-96	SP1	213000	10000	580	110	10.6	4.0	3440	320	574000	25000	7.4	0.94	0.38	0.26	119	11	1.16	0.21	18.2	3.7	29.9	3.6
LP100120-11-37	SP1	212000	10000	222	15	5.1	1.5	959	57	580000	19000	4.33	0.53	0.046	0.04	50.6	3.2	0.151	0.06	2.47	0.63	4.98	0.98
LP100120-11-7	SP1	221400	7700	158	11	6.8	1.6	823	38	635000	19000	6.77	0.67	0.78	0.83	19.8	1.2	0.27	0.17	1.77	0.79	2.35	0.52
LP100120-15-60	SP1	223000	11000	307	26	3.2	2.3	2203	88	598000	26000	4.68	0.52	0.07	0.058	43.3	2.2	0.71	0.12	10.2	1.3	18.2	2.1
LP100120-15-82	SP1	224000	10000	289	19	4.2	1.7	2710	130	599000	26000	3.77	0.34	0.069	0.067	40.3	2	0.73	0.11	11.9	1.3	18.4	1.1
LP100120-15-50	SP1	210500	8500	180	13	15.4	2.2	753	34	598000	19000	3.4	0.42	0.028	0.032	10.45	0.8	0.115	0.058	1.89	0.51	3.96	0.81
LP100120-15-8	SP1	220000	10000	650	140	7.1	1.7	1650	110	599000	23000	12.15	0.69	2	0.73	58	4.4	1.56	0.54	10.6	3.5	7.4	1.8
LP100120-15-17	SP1	218000	11000	432	16	9.2	2.1	2700	110	587000	22000	18.79	0.9	0.053	0.038	105.4	3.5	0.208	0.073	2.69	0.62	7.9	1
LP100120-15-39	SP1	214500	9500	42.2	6.9	3.8	1.8	119	11	595000	20000	1.38	0.3	0.023	0.028	4.9	1.1	0.019	0.022	0.29	0.24	0.18	0.16
LP100120-11-65	SP1	222000	10000	796	55	19.8	2.3	2520	120	654000	24000	3.82	0.35	0	1	3.97	0.46	0.053	0.04	1.92	0.49	5.58	0.97
LP100120-11-14	SP1	216000	7900	267	54	23.7	2.9	1230	180	621000	27000	4.48	0.55	0	1	9.5	1.1	0.087	0.049	1.99	0.45	5.3	1.1
LP100120-11-41	SP1	210500	7500	264	17	29.7	3.2	985	40	598000	27000	8.14	0.65	1.24	0.51	40.4	1.7	0.38	0.16	3.7	1.1	4.7	0.7
LP100120-15-100	SP1	214000	11000	290	17	39	3.3	1180	40	574000	24000	4.38	0.42	0.034	0.034	61.3	2.9	0.341	0.096	5.68	0.97	11.3	1.6
LP100120-15-43	SP1	220000	10000	578	46	15.9	2	1990	150	573000	24000	1.77	0.27	0.006	0.012	7.56	0.65	0.317	0.086	5.75	0.9	13.8	1.7
LP100120-11-75	SP1	215400	9700	183	12	19.8	2.8	1003	39	628000	20000	3.23	0.36	0.012	0.024	18.02	0.8	0.182	0.052	3.08	0.58	6.51	0.92
LP100120-15-3	SP1	205300	9200	136.9	8.9	27.2	2	561	26	580000	21000	3.04	0.34	0.006	0.012	11.28	0.78	0.186	0.055	3.19	0.79	5.34	0.92
LP100120-11-81	SP1	209800	7400	237	17	25.3	2.9	1016	39	633000	26000	2.89	0.38	0.024	0.022	26.4	1.2	0.163	0.06	4.16	0.74	7.25	0.98
LP100120-15-65	SP1	228000	10000	54	6	4	1.3	343	20	627000	31000	2.13	0.34	0	1	18.2	1.2	0.011	0.106	0.69	0.21	1.37	0.37
LP100120-15-4	SP1	206200	8000	168	16	14.5	2.6	1284	50	594000	22000	2.12	0.36	0.059	0.042	15.23	0.89	0.516	0.099	10.6	1.6	14.2	1.4
LP100120-15-78	SP1	228000	9700	124	14	8.2	2.1	1190	150	617000	18000	5.56	0.51	0.012	0.016	33	2.6	0.109	0.049	1.6	0.41	6.1	1.3
LP100120-15-48	SP1	212000	11000	367	39	5.9	1.6	1890	100	586000	23000	8.7	1.1	0.56	0.4	68.6	3.7	0.39	0.16	5.6	1.3	10.6	1
LP100120-11-72	SP1	215000	12000	137	11	23.2	2.7	411	15	626000	19000	2.57	0.34	0.018	0.026	25.5	1.5	0.132	0.044	2.11	0.5	4.05	0.87
LP100120-15-79	SP1	227000	10000	127	9.6	11.8	2.3	873	31	603000	20000	3.71	0.44	0.012	0.016	55.1	3.3	0.374	0.089	5.64	0.71	8.5	1.1
LP100120-11-17	SP1	214700	8500	105	10	9.4	1.5	576	36	637000	17000	2.42	0.37	0.035	0.03	46.1	3.3	0.294	0.078	6.2			

LP110120-11-27	SP2	219300	7200	251	11	3.8	2.1	1053	27	636000	15000	9.31	0.56	0	1	43.6	1.7	0.045	0.027	1.22	0.43	2.77	0.61
LP110120-11-86	SP2	223300	5200	212	14	10.9	1.7	1316	54	651000	18000	6.72	0.66	0.011	0.015	30.9	1.1	0.141	0.041	2.53	0.63	5.22	0.74
LP110120-11-95	SP2	225500	5800	281	14	3.5	1.2	3990	130	648000	17000	10.32	0.85	0	1	34.7	1.4	0.531	0.067	10.14	0.81	18.8	1.4
LP110120-15-17	SP2	224800	7900	430	120	20.2	2.5	1675	53	613000	17000	5.14	0.45	4.1	2.4	31.9	5	1.49	0.7	11.4	4	9.4	1.8
LP110120-15-35	SP2	218300	5900	172	12	15.1	1.9	1011	38	629000	22000	4.64	0.43	0	1	23.5	1.1	0.126	0.039	1.71	0.44	3.01	0.54
LP110120-11-32	SP2	220800	7600	164.4	9.3	6.4	1.9	1307	37	641000	16000	6.54	0.58	0	1	20.9	1.1	0.121	0.039	1.83	0.44	5.53	0.7
LP110120-11-76	SP2	225000	5800	410	24	7.8	1.3	3110	100	653000	19000	22.44	0.96	0.127	0.045	48.6	1.7	0.314	0.063	3.95	0.55	9.5	1.3
LP110120-11-16	SP2	244100	8100	126	11	3.1	1.5	886	25	668000	22000	5.79	0.33	0.2	0.15	20.3	1	0.114	0.036	1.12	0.31	2.47	0.4
LP110120-11-128	SP2	233000	7300	312	15	9.7	1.9	3860	130	632000	21000	15.9	1.1	0.017	0.019	91.2	3.3	0.428	0.081	8.1	1.1	18.9	1.5
LP110120-11-69	SP2	206400	7200	129.5	9	10.3	1.9	743	34	586000	21000	2.87	0.3	0	1	14	0.5	0.045	0.027	1.07	0.29	3.25	0.87
LP110120-11-90	SP2	220100	7300	107.9	7	10.7	1.8	850	26	650000	17000	2.64	0.33	0	1	14.59	0.76	0.048	0.019	2.12	0.53	4.06	0.73
LP110120-11-102	SP2	221900	5800	174	11	14.2	3.8	1121	30	652000	19000	6.44	0.53	0.029	0.023	15.48	0.54	0.06	0.027	0.54	0.25	2.75	0.41
LP110120-15-14	SP2	236100	8700	174	10	15.6	2	1227	63	599000	18000	3.09	0.31	0.006	0.012	21.1	1.6	0.181	0.07	2.69	0.53	5.82	0.99
LP110120-15-59	SP2	221900	7200	205	12	8.9	1.4	2106	77	607000	18000	6.04	0.51	0.018	0.02	16.6	0.76	0.217	0.064	4.28	0.66	10.15	0.91
LP110120-11-10	SP2	235100	8100	123	10	3.3	6.8	1021	28	656000	22000	5.13	0.33	0.023	0.027	14.71	0.7	0.061	0.029	1.3	0.37	3.34	0.69
LP110120-11-130	SP2	220300	5500	174.9	9.3	1.6	1.9	706	24	644000	15000	3.56	0.35	0	1	18.23	0.78	0.041	0.026	0.88	0.24	2.03	0.53
LP110120-11-23	SP2	223000	5900	153	12	4.9	1.6	842	25	638000	20000	5.37	0.34	0.011	0.015	18.08	0.92	0.023	0.016	1.04	0.36	2.88	0.65
LP110120-11-6	SP2	232700	5300	123	13	6.6	1.2	842	16	636000	17000	4.64	0.55	0	1	17.36	0.63	0.043	0.022	1.22	0.48	2.18	0.38
LP110120-11-56	SP2	221000	5500	170	10	8.8	2.2	1077	41	643000	18000	5.33	0.58	0	1	18.29	0.96	0.052	0.031	1.3	0.45	2.84	0.62
LP110120-11-101	SP2	217100	6400	138.3	7.8	5.7	1.2	844	28	661000	18000	4.19	0.38	0	1	13.24	0.74	0.073	0.028	1.1	0.3	2.37	0.53
LP110120-11-67	SP2	238000	7800	101.1	8	8.8	2.1	546	19	648000	22000	2.08	0.27	0	1	12.08	0.49	0.082	0.038	1.07	0.37	2.24	0.63
LP110120-11-42	SP2	224900	7800	133	11	8.6	1.7	1002	47	616000	15000	4.47	0.39	0.067	0.04	25.3	1.2	0.138	0.042	1.6	0.37	3.62	0.75
LP110120-11-32	SP2	225300	6800	254	13	25.9	1.9	1840	55	618000	25000	4.71	0.45	0.011	0.015	19.34	0.93	0.282	0.089	4.92	0.55	10.1	1
LP110120-11-12	SP2	224100	5500	1680	450	12.1	4.1	1378	45	615000	19000	7.77	0.29	27	10	67	2.7	6.7	2.6	38	14	9.5	2.9
LP110120-11-115	SP2	221400	6100	103	5.8	5.8	1.1	688	21	665000	15000	3.98	0.38	0.012	0.016	10.61	0.57	0.038	0.029	0.68	0.28	1.81	0.46
LP110120-11-74	SP2	225700	6400	106.5	5.9	5.2	1.4	624	14	654800	8200	3.65	0.27	0.017	0.018	11.69	0.73	0.047	0.026	1.05	0.39	1.84	0.54
LP110120-11-72	SP2	220900	7000	181	10	15.9	1.5	825	23	612000	13000	4.32	0.51	0	1	18.39	0.74	0.011	0.013	0.69	0.24	2.02	0.54
LP110120-11-30	SP2	215000	5600	215	15	10.4	1.7	3570	160	634000	12000	8.41	0.52	0.017	0.019	19.9	1.3	0.512	0.066	11.4	1.1	23.2	2.5
LP110120-11-24	SP2	230300	8600	2070	120	13	1.9	4860	210	609000	21000	10.21	0.59	17	1.4	80.1	4.5	6.05	0.52	45.6	3.5	35.2	2
LP110120-11-43	SP2	225000	7700	246	18	10.6	2	2234	74	608000	19000	9.83	0.59	0.011	0.015	22.95	0.69	0.221	0.088	4.18	0.69	10.4	1.1
LP110120-11-69	SP2	219400	5600	833	87	7.6	1.3	730	20	655000	16000	4.58	0.45	8.6	5.3	30.3	6.6	2.48	0.7	12.7	3.6	5.1	1
LP110120-11-89	SP2	223000	8200	122	11	5.4	2.2	1422	74	650000	15000	4.72	0.42	0	1	15.73	0.8	0.183	0.045	3.39	0.84	7.58	1.1
LP110120-11-58	SP2	218900	8200	122.2	9.9	8.2	1.5	688	26	622000	16000	3.68	0.32	0	1	15.75	0.86	0.043	0.027	1	0.31	3.02	0.66
LP110120-11-88	SP2	215600	5100	138	11	6.7	1.8	1133	61	639000	16000	3.99	0.44	0.024	0.022	15.8	1.1	0.065	0.032	1.32	0.41	4.45	0.42
LP110120-11-1	SP2	228500	7100	145.3	8.1	6.9	1.6	1360	38	669000	18000	6.49	0.43	0.023	0.021	15.69	0.8	0.187	0.067	2.26	0.45	5.06	0.79
LP110120-11-11	SP2	217700	6500	110.4	8	11	2.4	481	15	628000	15000	3.29	0.39	0.017	0.024	13.47	0.45	0.048	0.026	0.55	0.23	1.21	0.41
LP110120-11-16	SP2	216300	7500	221	12	26.6	2.3	875	22	594000	15000	3.06	0.27	0	1	14.93	0.81	0.111	0.045	2.33	0.56	4.72	0.7
LP110120-11-55	SP2	225500	7100	150	10	4.1	1.2	1376	38	607000	20000	4.33	0.49	0	1	9.44	0.53	0.129	0.04	2.16	0.46	5.04	0.79
LP110120-11-121	SP2	226400	5200	332	16	17.4	3.6	2082	83	659000	16000	5.21	0.39	2.3	1.3	22	2.1	0.9	0.24	9	1	12.4	1.4
LP110120-11-29	SP2	244300	6500	483	22	13.9	2.5	3660	180	721000	19000	14.06	0.81	2.76	0.97	45.1	3.6	1.2	0.34	10.6	1.7	16.1	1.6
LP110120-11-68	SP2	219300	6300	133	12	6.3	1.1	1155	31	630000	12000	4.01	0.47	0	1	14.79	0.85	0.069	0.037	2.09	0.48	3.98	0.7
LP110120-11-68	SP2	215600	6100	115	11	5.2	1.2	653	26	591000	18000	3.77	0.48	0	1	11.12	0.72	0.041	0.024	0.81	0.31	2.1	0.48
LP110120-11-70	SP2	216400	5600	193	14	4.0	1.5	1489	47	595000	15000	8.09	0.51	0.25	0.11	9.93	0.63	0.11	0.04	2.52	0.55	3.64	0.81
LP110120-11-65	SP2	236400	7800	246	20	78.8	9.1	3020	230	600000	17000	9.72	0.88	1.05	0.15	26.4	11	2.24	0.24	32	1.6	49.2	4.6
LP110120-11-22	SP2	220600	4700	895	54	42.6	8.1	3990	130	661000	15000	5.06	0.6	0.61	0.18	11.9	2	1.73	0.57	19.1	5.6	31.8	7.9
LP110120-11-127	SP2	232000	6800	152.4	67	35.1	2.4	6740	400	669000	13000	3.11	0.31	0.037	0.024	3.44	0.27	0.69	0.13	14	2	33.4	4.1
LP110120-11-33	SP2	226300	9900	229	17	19	3.4	653	29	624000	14000	4.44	0.44	0.172	0.079	18.96	0.97	0.11	0.068	1.54	0.65	2.94	0.85
LP110120-11-39	SP2	240300	9000	451	28	5.6	1.8	3690	160	652000	16000	8.69	0.7	0.3	0.12	31.6	2.7	0.63	0.16	8.8	1.3	21.9	2.5
LP110120-11-83	SP2	214700	6400	755	33	31.4	3.3	3020	130	632000	16000	2.45	0.4	0.127	0.048	2.25	0.28	0.446	0.099	9	1.3	17.5	1.4
LP110120-11-63	SP2	213300	7900	177	12	7.2	1.6	598	15	577000	19000	8.4	1	0.017	0.019	22.3	0.79	0.041	0.031	0.51	0.22	1.42	0.38
LP110120-11-109	SP2	221700	5800	118.9	8.3	24.3	2.2	686	23	645000	11000	4.07	2.5	0.171	0.066	14.47	0.96	1.12	0.19	16.1	1.4	16.7	1.4
LP110120-11-30	SP2	227200	7100	108.4	8.7	8.3	1.5	395	23	622000	17000	2.55	0.19	0	1	8.98	0.78	0.023	0.016	0.45	0.18	1.89	0.46
LP110120-11-31	SP2	216400	9200	136	10	6	1.6	1704	57	589000	18000	6.88	0.58	0.039	0.03	17.55	0.71	0.217	0.067	4.24	0.64	9.47	0.98
LP110120-11-49	SP2	219600	6900	226	13	18.6	2.3	1665	61	627000	13000	5.35	0.4	0.32	0.088	10.03	0.42	0.293	0.074	4.89	0.62	10.2	1
LP110120-11-67	SP2	223000	5600	65	4.8	8.2	1.6	715	21	639000	15000	2.26	0.27	0	1	12.08	0.19	0	1	0.14	0.1	0.11	0.1

LP110120-1s-38	SP2	208200	7100	243	21	17.8	1.6	1026	40	601000	14000	5.22	0.48	6.4	1.6	23.1	2.3	2.12	0.37	12.8	1.7	7.8	1	
LP110120-11-119	SP2	219900	7600	247	13	11.3	1.5	1696	39	659000	14000	4.47	0.46	0.029	0.023	98.1	2.9	0.28	0.057	5.86	0.85	10.9	1.2	
LP110120-1s-34	SP2	225900	7300	314	26	12.2	2.2	1578	52	612000	17000	5.86	0.46	0.251	0.084	7.36	0.52	0.58	0.13	5.44	0.93	7.47	0.92	
LP110120-11-112	SP2	219700	6200	198	14	24.8	2.5	1120	55	664000	23000	3.32	0.3	0	1	12.72	0.49	0.247	0.061	3.59	0.64	8.7	1.1	
LP110120-11-124	SP2	234000	5400	201	12	19.8	4.2	865	37	676000	16000	5.87	0.44	0.38	0.2	33.7	1.4	0.353	0.085	3.5	0.8	5.86	0.72	
LP110120-1s-64	SP2	225500	5400	256	13	6.4	1.6	1748	57	618000	16000	5.01	0.46	0.018	0.02	54.8	1.8	0.506	0.094	8.3	1	17	1.6	
LP110120-11-50	SP2	228900	8000	341	23	10.4	1.8	2036	99	635000	19000	7.87	0.45	0	1	11.61	0.58	0.138	0.048	2.25	0.47	6.3	1.1	
LP110120-11-63	SP2	224000	6100	713	28	16.3	2.2	2183	50	633000	13000	2.8	0.33	0	1	1.21	0.17	0.062	0.031	1.59	0.43	5.97	0.76	
LP110120-11-53	SP2	223300	6100	286	14	43.6	2.4	1283	32	641000	15000	4.27	0.4	0.036	0.026	15.92	0.61	0.48	0.1	6.53	0.74	8.7	1.1	
LP110120-11-9	SP2	219000	6900	555	27	25.5	2.7	1847	39	621000	17000	3.24	0.42	0	1	5.18	0.37	0.022	0.016	1.64	0.44	4.58	0.59	
LP110120-1s-45	SP2	226800	7600	237	11	10.7	1.6	901	37	612000	19000	3.75	0.32	0	1	14.58	0.75	0.063	0.028	1.37	0.42	3.89	0.61	
LP110120-1s-48	SP2	222600	5000	159	12	8.7	1.6	515	17	605000	17000	2.11	0.29	0.017	0.019	29.4	1.1	0.138	0.042	2.62	0.44	4.72	0.81	
LP110120-11-120	SP2	228300	5600	166.2	8.1	10.1	1.7	907	23	681000	20000	3.29	0.34	0	1	17.38	0.78	0.131	0.048	2.01	0.5	4.87	0.6	
LP110120-1s-53	SP2	219300	7600	200	21	6.1	1.7	1460	170	601000	28000	4.8	0.39	0	1	70.6	4	0.307	0.083	5.7	1.1	12.5	2.2	
LP110120-1s-60	SP2	225300	5800	138	10	5.1	1.1	393	11	621000	17000	2.6	0.36	0.035	0.025	13.23	0.61	0.101	0.037	1.23	0.39	1.83	0.46	
LP110120-11-78	SP2	226200	8800	225	9.8	16.5	2.5	534	21	637000	15000	2.26	0.3	0	1	9.72	0.43	0.129	0.038	2.06	0.55	4.84	0.75	
LP110120-11-8	SP2	226600	6600	158	11	1.2	1.8	726	20	629000	20000	3.39	0.28	0	1	10.18	0.52	0.047	0.03	1.51	0.36	3.21	0.68	
LP110120-1s-8	SP2	219500	6800	268	14	7	1.7	1200	42	602000	18000	4.48	0.49	0.017	0.018	33.3	1.1	0.048	0.03	1.88	0.33	4.82	0.74	
<i>Rejected Grains</i>																								
LP110120-11-39	SP2	207900	6300	1687	89	6.8	2	1230	39	601000	13000	9.7	0.77	31.7	2.4	114.7	5.5	8.8	0.76	41.3	4.2	10.9	1.3	
LP110120-11-57	SP2	220300	5600	331	64	10.4	1.5	1536	50	604000	17000	5.47	0.31	1.02	0.8	33.4	1.5	0.46	0.23	5.5	1.5	7.61	0.78	
LP110120-11-21	SP2	239300	7200	170	14	10.5	1.8	982	40	634000	14000	3.92	0.36	0.35	0.31	18.4	1	0.18	0.11	2.27	0.65	4.92	0.83	
LP110120-11-105	SP2	223200	4600	203	15	29.2	2.7	1269	45	635000	17000	2.8	0.27	0.03	0.024	24.6	1.1	0.389	0.082	6.81	0.84	10.2	1	
LP110120-11-118	SP2	184900	5200	199	15	25.7000	4200	1886	64	1796	51	5770	190	5510	160	15650	370	1913	48	7400	170	1168	44	
LP110120-1s-52	SP2	227400	5500	154	16	11.2	2.5	1170	210	629000	17000	2.75	0.43	2.06	0.71	38.1	6	0.88	0.2	6.7	1.2	7.4	1.4	
LP110120-1s-12	SP2	210900	9100	3150	490	7.3	2	1115	54	580000	19000	2.49	0.36	6.2	10	148	28	16.6	3.7	76	14	19.2	2.6	
LP110120-11-13	SP2	229300	8000	123.1	9.1	23.7	8.8	728	37	600000	21000	2.5	0.36	0.115	0.072	3.32	0.3	0.108	0.044	1.78	0.51	4.43	0.67	
LP110120-11-91	SP2	191800	5800	204	10	281500	6000	2079	68	311.8	9.6	559	20	674	24	2430	100	401	16	2214	70	651	18	
LP110120-11-42	SP2	226800	6500	845	46	99.7	4.1	3091	84	614000	18000	12.98	0.61	10.89	0.71	99	3.4	12.08	0.77	86.9	4.6	63.2	3.3	
LP110120-1s-20	SP2	207500	6500	180	20	14	1.7	804	47	609000	20000	3.95	0.31	0.105	0.068	22.6	1.1	0.077	0.034	0.75	0.26	1.93	0.62	
LP110120-11-123	SP2	230800	5100	377	33	72.7	6.6	3990	230	683000	13000	10.43	0.84	11.9	1.8	1116	94	45.3	5.6	330	37	239	26	
LP110120-1s-1	SP2	222400	6800	320	30	5.2	7.3	1218	48	629000	14000	3.29	0.28	1.23	0.24	19.1	1.4	1.87	0.29	15.3	2.3	25.4	2.8	
LP110120-11-75	SP2	242300	8600	257	15	38.4	3.7	1355	84	663000	20000	6.32	0.43	0.196	0.096	33.3	1.8	0.71	0.17	6.7	1.1	8.2	1.6	
LP110120-11-14	SP2	254700	6100	824	48	93.7	5.2	5650	280	672000	17000	46.3	1.5	1.08	0.14	184	11	7.16	0.52	69.1	5	104.6	6.7	
LP110120-1s-25	SP2	217000	5700	179.2	5.8	30.9	4	1767	52	669000	13000	4.79	0.39	0.188	0.073	33	1.1	0.367	0.09	9.2	1.2	17.9	1.8	
LP110120-11-116	SP2	218400	7100	165	12	18.7	1.6	1024	36	651000	15000	4.41	0.37	0.04	0.026	12.89	0.59	0.287	0.064	6.45	0.76	10.99	0.95	
LP110120-1s-51	SP2	227000	8000	101.5	7.2	6.4	1.7	353	13	586000	19000	2.23	0.2	0.066	0.011	12.05	0.66	0.007	0.01	0.19	0.11	1.57	0.4	
LP110120-11-31	SP2	212500	6600	185	15	1.6	2151	49	629000	15000	5.99	0.34	0.04	0.026	8.6	0.44	0.98	0.11	16.2	1.5	24.1	1.9		
<b>Sample X181218</b>																								
Grain	Unit	Si (ppm)	error	P (ppm)	error	Ti (ppm)	error	Y (ppm)	error	Zr (ppm)	error	Nb (ppm)	error	La (ppm)	error	Ce (ppm)	error	Pr (ppm)	error	Nd (ppm)	error	Sm (ppm)	error	
181218-1b-8	SP4	15800000	1300000	13320	460	217	42	179000	17000	70100000	6300000	1100	140	19	12	5070	530	14	11	34	16	102	32	
181218-1b-13	SP4	15800000	1300000	16550	990	460	120	222000	21000	69500000	5800000	710	110	130	69	8060	810	52	24	109	34	183	49	
181218-1b-7	SP4	15600000	1300000	19700	1600	550	170	230000	20000	72100000	9300000	810	120	570	180	4680	610	231	81	180	45	155	40	
181218-1b-5	SP4	16000000	1700000	28600	2200	670	190	891000	97000	64800000	7700000	3230	360	850	140	12700	1300	980	120	1120	170	1120	180	
181218-1b-24	SP4	15000000	1400000	16230	740	260	58	278000	27000	65800000	5900000	1650	190	3.1	4.3	8980	930	13.8	8.5	60	21	177	46	
181218-1b-9	SP4	14800000	1200000	16910	730	238	41	236000	22000	68800000	5800000	695	99	6.2	9.8	2630	310	32	15	151	34	297	62	
181218-1b-15	SP4	16800000	1600000	14400	530	345	54	147000	13000	64600000	6000000	542	92	28	18	1840	200	36	15	64	22	111	31	
181218-1b-11	SP4	15300000	1400000	19300	1000	303	59	327000	30000	69000000	6600000	563	91	1.6	3.1	5260	510	38	16	78	29	213	55	
181218-1b-12	SP4	14700000	1200000	16570	770	266	51	244000	21000	67900000	5900000	483	87	4.7	6.9	4100	410	28	17	48	17	114	38	
181218-1b-17	SP4	15600000	1500000	14970	660	180	36	191000	18000	69000000	6800000	770	110	1.6	3.1	1270	170	12.5	9.1	70	21	120	30	
181218-1b-2	SP4	16000000	1400000	13550	600	1200	1400	155000	15000	68000000	6000000	860	130	62	33	7510	710	56	31	96	46	108	51	
181218-1b-26	SP4	15000000	1300000	19600	1000	730	210	290000	27000	67500000	6400000	1510	190	19	12	9900	1000	139	30	293	55	441	81	
181218-1b-25	SP4	15200000	1400000	24700	2500	559	82	537000	73000	73200000	6800000	590	100	1900	1200	10600	3100	980	360	1610	460	1400	210	
181218-1b-1	SP4	14400000	1400000	14320	440	343	56	81300	9100	67700000	7200000	462	71	80000	15000	4830	600	35	16	69	27	144	41	
181218-1b-16	SP4	15500000	1300000	24200	1500	426	53	266000	28000	68100000	6200000	1510	170	25	16	1900	240	59	28	89	34	241	59	
181218-1b-21	SP4	15500000	1300000	18350	920	381	57	546000	49000	68600000	6200000	1270	150	111	26	24500	2300	550	62	1190	150	1380	170	
181218-1b-6	SP4	15700000	1400000	17600	730	345	52	503000	45000	71600000	6700000	1210	140	12	12	5840	640	174	39	615	83	930	130	

**APPENDIX IIIb:** Detrital zircon trace element data for samples of the Sierra Las Pintas Group.  
Trace elements: Eu, Gd, Tb, Dy, Ho, Er, Tm, Yb, Lu, Hf.

Sample 100120-1																					
Grain	Unit	Eu (ppm)	error	Gd (ppm)	error	Tb (ppm)	error	Dy (ppm)	error	Ho (ppm)	error	Er (ppm)	error	Tm (ppm)	error	Yb (ppm)	error	Lu (ppm)	error	Hf (ppm)	error
LP100120-1L-40	SP1	8.26	0.68	63	3.3	16.85	0.98	159.2	8.4	45.5	1.8	172.1	7.6	39.9	1.9	388	24	48.2	2.4	11360	510
LP100120-1S-44	SP1	1.45	0.23	15.3	2.8	4.82	0.66	57.5	5.1	20.3	2	86	7.3	23.3	2.4	266	21	34	3.3	11610	450
LP100120-1L-10	SP1	8.45	0.9	87	10	26.5	2.9	317	37	113	14	482	62	111	12	1060	110	154	16	9470	350
LP100120-1S-40	SP1	2.07	0.36	31.2	3.7	9.67	0.87	114.8	7.1	43.9	3.6	196	14	50	2.9	573	34	82.4	3.8	12870	480
LP100120-1S-91	SP1	4.7	1	106	8.3	32.2	2.2	386	25	125.3	6.6	500	34	117.7	7.5	1130	110	144	10	13170	440
LP100120-1L-54	SP1	5.18	0.54	32.3	2.7	8.38	0.77	103.2	8.5	37.3	3.1	170	14	45.2	2.7	542	38	77.4	6.1	12130	640
LP100120-1S-56	SP1	1.95	0.52	40	4	12.7	1	152	13	49.7	3.4	209	12	52.5	4.4	478	42	60.9	3.8	11890	550
LP100120-1S-70	SP1	0.86	0.21	18.8	2.3	5.77	0.65	79.2	8.7	26.8	2	127	12	32.2	3.1	351	32	46.4	3.9	11510	600
LP100120-1L-32	SP1	0.26	0.12	17.6	3.1	6.72	0.81	93	13	30.4	3.9	143	20	35.8	4.5	364	45	48.4	5.5	16530	590
LP100120-1S-49	SP1	0.55	0.11	11.9	1.3	3.9	0.32	53.8	4.2	21.09	0.99	104.8	6.7	28	1.9	326	15	50.2	2.7	11580	470
LP100120-1S-12	SP1	0.58	0.12	23	2.4	7.96	0.7	92.6	5.9	32.3	1.6	134.4	6.4	32.6	1.4	336	17	42.4	2.3	11070	520
LP100120-1S-59	SP1	3.64	0.39	241	10	71.1	3.5	840	34	269	17	1037	32	214.1	8.6	2060	130	256	8.6	10190	430
LP100120-1L-79	SP1	0.55	0.14	15.4	1.8	4.9	0.46	65.8	5.1	24.9	1.4	114.5	5.3	28.1	2.1	337	22	46.3	2.4	11720	540
LP100120-1L-83	SP1	0.38	0.15	17.8	2.6	6.09	0.73	78	10	26.6	3.7	118	15	27.4	2.5	285	26	37.1	3.5	12480	550
LP100120-1S-37	SP1	0.56	0.17	11.2	2	3.39	0.53	46.7	4.9	17.8	1.5	80.5	6.8	23.3	1.9	273	20	37.8	2.5	12610	550
LP100120-1S-66	SP1	0.5	0.13	12	1.3	3.99	0.36	49.6	3.6	20	1.2	92.9	4.6	25.1	1.6	292	13	43.7	2.6	12240	400
LP100120-1S-74	SP1	0.86	0.19	45.3	2.7	12.94	0.78	162.9	7.4	56	3.2	254	12	59.1	2.6	580	27	82.5	4.1	12300	440
LP100120-1S-46	SP1	1.57	0.27	80.4	6.1	23.3	1.4	303	14	102	5.6	409	25	92.4	4.9	904	48	118.2	8.3	10760	400
LP100120-1S-77	SP1	1.04	0.23	25	2.5	8.46	0.76	113.3	6.3	44.7	2.7	209	11	56.5	2.9	609	32	91.7	5.5	11490	460
LP100120-1L-73	SP1	0.9	0.17	32.5	2.6	9.8	0.55	125.6	5.5	43.9	1.8	190.6	8.7	45.9	2.5	481	25	63.9	3.6	9140	490
LP100120-1L-13	SP1	0.72	0.13	25.9	2.7	7.99	0.58	95	5.7	34.2	1.4	156	7.1	38.7	1.9	365	20	52.9	2.3	9700	450
LP100120-1L-69	SP1	0.45	0.12	8.9	1.4	3.24	0.32	38.3	2.9	13.55	0.72	69.4	4.3	18.4	1.2	219.4	9.4	31.1	2.3	12310	520
LP100120-1S-13	SP1	0.53	0.11	15.5	2.5	5.56	0.7	81.7	7.9	32.3	1.9	151.1	9.4	46.7	2.7	518	32	71.1	4.4	12110	540
LP100120-1L-45	SP1	0.85	0.23	15	2.3	6.26	0.35	93.9	6.2	38.9	1.7	212	11	63.5	2.8	828	33	135.3	3.9	12230	530
LP100120-1S-5	SP1	0.79	0.18	177	12	54.3	3.8	634	36	211	12	799	32	182.8	9.4	1743	95	217	13	10690	570
LP100120-1L-33	SP1	0.42	0.12	26.8	2.4	8.93	0.66	120.5	6.5	42	2.5	194	12	44.5	2.2	440	17	65.3	4	11030	540
LP100120-1S-56	SP1	0.79	0.21	23.8	3.3	7.39	0.73	93	10	28.9	2.9	124	10	28.8	2.1	300	27	39.9	3.2	9390	490
LP100120-1L-66	SP1	1.23	0.23	37.7	2.8	11.63	0.71	154.3	8.5	55.3	2.8	233	14	55.8	2.7	619	31	77.9	3.6	12520	670
LP100120-1L-21	SP1	0.281	0.082	16.4	1.5	5.97	0.37	81.7	5.1	29.8	1.3	140.5	6	36.4	1.6	374	17	52.6	2.9	12750	550
LP100120-1L-38	SP1	0.69	0.21	37.2	5.1	12.6	1.6	161	15	57.2	4.9	266	24	62.6	5.5	661	64	93.3	9.8	13270	600
LP100120-1S-14	SP1	0.503	0.099	17.6	1.4	6.37	0.5	89.2	5.9	31.6	1.2	148.2	7.3	37.9	1.6	403	21	51.7	2.7	10890	470
LP100120-1L-64	SP1	0.36	0.15	16.6	2	6.47	0.35	81.7	4.6	29	1.6	136.1	6.4	32.6	1.5	349	18	43.7	2.4	11520	560
LP100120-1L-34	SP1	0.38	0.12	22.4	3	7.59	0.42	102.4	6.2	38.6	1.8	177.4	9.7	41.1	2.5	419	19	56	2.4	12980	640
LP100120-1S-28	SP1	0.78	0.13	33.1	2.2	12.96	0.78	160.4	8.9	59.2	2.4	253.4	9.5	62.9	3.7	681	38	84.5	3.6	12140	450
LP100120-1L-89	SP1	2.22	0.48	46.5	5.2	17.3	1.7	214	19	70.5	6	352	32	83.8	7	917	73	121	11	11600	480
LP100120-1S-23	SP1	0.92	0.17	31.9	3.6	11.16	0.76	141.3	6.5	52.2	2.2	225.2	8.8	55	2.7	576	23	71.3	2.5	11860	510
LP100120-1S-59	SP1	0.53	0.16	20.5	1.7	7.55	0.58	111.7	6.9	39.4	2	188	10	43.3	2.6	494	21	62.6	3.1	12310	600
LP100120-1S-54	SP1	1.45	0.23	51.1	2.7	14.91	0.88	202.4	9.6	69	2.9	311	14	76.4	2.7	790	44	96	4	10650	410
LP100120-1L-18	SP1	2.74	0.42	51	3	18.7	1.3	247	10	97.5	3.5	454	21	118.7	5.5	1249	62	183.4	9.1	11390	480
LP100120-1S-27	SP1	1.2	0.26	39.1	9.5	14.6	3.4	214	48	87	19	428	84	126	22	1380	200	191	27	13020	510
LP100120-1S-106	SP1	1.95	0.33	44.4	5.4	14.5	1.4	193	18	71.2	6	345	28	89.5	7.8	949	71	140	13	12040	400
LP100120-1L-29	SP1	4	0.35	42.3	3.2	12.75	0.64	168.8	9.2	56.3	2.1	255.6	8.6	64.4	2.3	707	30	101.6	5.4	9030	340
LP100120-1S-55	SP1	0.56	0.12	8.2	1.5	2.87	0.32	46.9	2.6	19.2	1.1	95.5	5.3	28.8	1.7	326	16	53.3	2.4	9700	310
LP100120-1S-45	SP1	0.9	0.15	44.2	4.4	14.69	0.97	211	13	77.2	3.8	336	19	91.7	4.9	982	57	135.7	5	11090	470
LP100120-1S-51	SP1	0.44	0.11	9.1	1.3	3.12	0.3	44.4	4.1	18.1	0.81	97.9	5.2	29.9	2.1	378	25	56.7	3.4	11200	550
LP100120-1S-15	SP1	1.52	0.28	48.5	5.1	14.7	1.2	187	16	73.2	5.9	335	26	93.4	7.4	1021	87	142	9	11130	440
LP100120-1S-33	SP1	1.43	0.31	21	2.5	7.52	0.57	100.8	7.1	40.9	2	202	11	59.3	3.2	698	51	105.5	4.1	10630	550
LP100120-1S-58	SP1	0.63	0.2	10.4	1.7	3.8	0.33	52.1	3.3	22.03	0.99	111.1	7.1	34.2	2	419	25	67	3.1	12010	570
LP100120-1S-67	SP1	1.09	0.22	23.8	2.5	7.52	0.91	93.1	9.3	33.5	2.4	155.1	9.4	40.6	3.3	404	29	60.7	4.6	10940	470
LP100120-1L-77	SP1	6.64	0.77	87	6.5	28.2	2.6	359	34	122.6	9.4	568	41	141	11	1422	97	202	13	10610	400
LP100120-1L-84	SP1	0.33	0.11	18.4	1.7	6.93	0.57	102.2	5.3	37.2	1.9	187.9	8.9	49.1	2.8	560	34	74.1	3.2	11950	420
LP100120-1S-92	SP1	2.59	0.32	42.9	2.8	13.46	0.67	165	10	58.3	2.2	251.2	9.4	61.5	2.5	607	42	83.1	5.7	10220	420
LP100120-1S-21	SP1	1.98	0.28	48.8	3.6	16.7	1	223.4	9.9	87.2	3.9	388	18	98.2	3	1075	49	142.4	5.5	8710	320
LP100120-1S-90	SP1	1.25	0.23	24.4	3	7.71	0.63	113	9.5	43.1	2.3	217	14	58.5	5.2	589	45	93.6	4.7	10570	410
LP100120-1S-75	SP1	7.14	0.71	105.7	6	30.3	2.4	364	25	128.8	9.1	567	36	142.4	8.7	1371	89	196	13	8590	250
LP100120-1S-69	SP1	0.5	0.12	16.6	2.3	6.23	0.5	96.1	6.6	38.2	2.2	196	11	55.3	3.3	591	27	88.9	4.5	11360	430
LP100120-1L-19	SP1	1.11	0.17	27	2.8	9.22	0.81	117.6	7.2	48.1	2.6	240	15	65	3.7	727	41	113.1	5.6	11470	500
LP100120-1S-24	SP1	0.59	0.14	11.6	1.7	3.94	0.44	47.7	4.2	17.9	1.3	82.3	4.9	23.6	1.3	283	20	37.1	2.2	11780	520
LP100120-1S-104	SP1	0.67	0.21	11.8	2.2	3.77	0.64	55.2	7.2	22.8	2.8	111	12	32.8	3	381	42	57.1	4.1	11770	680
LP100120-1S-108	SP1	1.73	0.28	34.4	3.4	11.9	1	148	9.2	58.5	3.1	264	13	70.7	4.9	755	48	120.1	7.1	10500	580
LP100120-1L-63	SP1	2.62	0.31	34.9	2.5	11.6	1.1	152.2	8	58.8	3.7	279	13	73.5	4.5	890	62	118.8	6.6	10790	330
LP100120-1L-5	SP1	0.83	0.16	24.2	2.1	8.95	0														

LP100120-1L-28	SP1	0.45	0.14	26.5	3.3	7.16	0.55	73.4	4.1	19.3	1.5	63.9	2.9	12.7	1.4	106.2	3.9	12.35	0.66	12990	520
LP100120-1L-88	SP1	2.24	0.3	72.1	3.8	19.2	1.2	209	11	64.6	4.1	265	12	56	2.7	545	25	64.7	2.4	11720	370
LP100120-1S-52	SP1	0.47	0.098	25.6	3.2	8.16	0.74	111.3	9.5	36.7	3.8	157	11	41.1	2.5	421	23	53.2	3.1	11960	360
LP100120-1L-82	SP1	0.64	0.15	17.9	2.8	6.76	0.65	93.9	4.4	37	2.4	183	12	47.4	3	564	25	75.2	4.9	9790	560
LP100120-1L-53	SP1	1.69	0.32	54.9	8.1	16.2	1.7	193	19	59.2	4.3	251	20	57.6	3.7	581	28	72.6	4.1	12310	390
LP100120-1L-4	SP1	1.83	0.26	30.3	2.4	9.8	0.72	122.7	5.4	40.8	1.6	172.4	9.3	38.6	2	348	17	46	1.6	7900	300
LP100120-1S-89	SP1	5.18	0.83	91	13	23.7	3.1	262	33	82.5	9.6	299	35	71	11	618	78	72.5	6.2	10200	520
LP100120-1S-73	SP1	2.4	0.3	59	4	17.4	1.1	194	11	63.1	3.5	244.2	9.4	56.2	2.2	523	21	69.1	2.1	10640	350
LP100120-1L-80	SP1	0.111	0.068	28	2.3	11.57	0.56	154.9	7.9	52.7	2.2	255	12	57.9	2.5	625	33	78.6	3.5	14950	530
LP100120-1L-24	SP1	2.3	0.29	56.1	3.8	16.2	1.1	224.5	9.7	81.6	4.6	350	15	85.8	5.1	871	47	115.7	5.7	9650	290
LP100120-1S-101	SP1	0.62	0.19	30.9	5.5	11.9	2	162	23	59.5	7.5	257	31	58.4	7.3	580	59	74.9	9.6	12560	610
LP100120-1S-99	SP1	8.6	3.8	47	16	12.1	3	139	24	46.9	6	198	15	54.8	4.9	557	64	82.7	6.7	13300	460
LP100120-1L-30	SP1	0.95	0.24	25.4	2	8.14	0.54	100.3	4.9	33.9	1.6	142	7.2	34.4	1.6	341	17	42.9	2	9790	320
LP100120-1S-110	SP1	0.37	0.12	30.9	2.9	10.17	0.61	118.4	6.1	43.1	1.9	186.3	8.6	44.1	2.4	414	18	57.8	2.5	11220	500
LP100120-1S-16	SP1	0.131	0.069	20.9	2	7.78	0.59	99.4	5.3	38.8	2.2	167.5	6.6	42.8	1.9	461	27	54.6	2	13330	600
LP100120-1S-2	SP1	1.36	0.18	29.2	2.1	9.36	0.68	126.6	7.8	48.3	3.6	207.6	9.7	56.9	3.2	624	37	80.8	3.5	10690	560
LP100120-1L-25	SP1	0.31	0.11	25.9	2.5	7.58	0.6	102.6	5.2	34.8	1.6	168.9	7.1	38.3	1.5	397	15	52.9	2	13130	450
LP100120-1L-55	SP1	0.42	0.13	13.1	1.5	4.5	0.31	64	4.8	24.3	1.4	111.6	5.7	29.8	1.7	325	13	42.8	2.5	12270	550
LP100120-1L-86	SP1	0.33	0.1	10.9	1.4	3.35	0.32	43.6	2.7	15.99	0.85	72.2	3.6	18	1.1	193	11	27.4	1.5	13400	580
LP100120-1L-70	SP1	1.32	0.23	62.6	3.4	18.9	1	203	11	59.6	2.9	265	11	58.6	3.2	595	20	75.2	4.2	12810	460
LP100120-1S-6	SP1	1.71	0.26	47.8	3.8	15.04	0.87	191.1	8.1	71.5	3	299	13	76.5	3.2	774	30	101.5	5.7	11040	590
LP100120-1L-26	SP1	1.43	0.25	33.6	3	11.23	0.91	141.6	9	51.3	2.9	236	17	58.2	2.8	614	39	82.4	4.8	9570	390
LP100120-1L-16	SP1	2.2	0.32	33.7	2.7	9.84	0.51	120.2	7.1	42.1	1.6	180	8.2	44.5	2.2	442	21	62.3	3.8	11070	420
LP100120-1S-64	SP1	1.27	0.3	18.8	1.6	6.5	0.45	82.7	4.5	32.6	1.9	160.1	9.3	43.8	2.7	491	30	71.5	2.9	12730	520
LP100120-1S-98	SP1	1.39	0.24	32	2.1	10.12	0.79	135	6.8	48.8	2.4	212	12	50.4	2.4	490	21	64.3	3.3	10440	450
LP100120-1S-25	SP1	0.84	0.15	26.1	2.9	9.52	0.51	133.2	6	52.9	2.4	237	12	62.2	3	691	25	87.7	3.9	12290	430
LP100120-1S-63	SP1	1.74	0.24	53.2	2.6	18.6	1.2	267	15	100.5	3.2	434	22	109.6	5.5	1080	52	142.4	6.2	8600	420
LP100120-1S-88	SP1	0.36	0.14	8.1	1.4	2.81	0.29	40	2.1	15.72	0.98	81.3	5	23.19	0.99	261	18	42.8	1.6	12010	350
LP100120-1S-94	SP1	0.64	0.12	51.4	3.7	17	1.1	219	10	82.6	4.3	342	14	79.7	3.8	787	41	95.4	4.5	11350	510
LP100120-1S-18	SP1	2.1	0.27	38.6	3.9	11.89	0.89	141.6	7.4	48.7	2.2	195.8	8.4	47	1.6	494	35	60.3	2.2	9560	430
LP100120-1L-8	SP1	2.54	0.55	21.9	2.4	6.98	0.49	75.9	3.2	23.5	1.1	102	4.7	23.1	1.3	247.3	8.1	36	2	9940	480
LP100120-1L-9	SP1	4.11	0.66	69.6	8.9	19.5	2.1	223	23	71	7.5	296	30	64.5	6.7	607	48	84.9	7.1	10040	380
LP100120-1L-68	SP1	0.6	0.18	60.2	4.4	17.2	1	208.2	9.1	63.3	3	261	13	57	2.6	596	34	78.3	4	9520	360
LP100120-1S-38	SP1	0.48	0.14	25.6	2.5	8.58	0.62	120.6	9.8	43.5	2.9	194	13	45	3	492	25	62.1	2.8	11590	470
LP100120-1L-67	SP1	0.233	0.087	38.1	3.3	12.88	0.94	174.9	9.2	56.7	2.2	252	11	59.6	1.8	601	26	74.7	3.1	12400	500
LP100120-1S-53	SP1	4.36	0.43	64.9	4.5	17.6	1	213	10	73.9	3.2	325	12	80.7	3.7	792	35	100.9	4.3	9490	350
LP100120-1S-68	SP1	0.144	0.059	20.4	1.5	6.38	0.47	85.4	6.1	31.4	1.7	144.8	8.5	36.2	2	344	19	48	2.5	11390	420
LP100120-1S-71	SP1	1.86	0.28	36.8	3.7	12.4	1	149	12	57.7	4.4	248	18	62.9	4.6	620	49	85.9	4.4	11560	580
LP100120-1S-109	SP1	0.059	0.05	10.9	1.3	5.21	0.48	75.9	4.5	32.5	1.8	160.9	9.4	44.8	2.2	497	26	72.5	3.3	15790	740
LP100120-1L-61	SP1	0.34	0.1	12.5	1.8	4.91	0.69	72.7	7.1	27.9	2	138	11	37.5	2.7	428	28	60.2	3.5	11920	560
LP100120-1L-107	SP1	0.45	0.19	42	11	14.8	3.2	184	42	68	16	293	59	67	13	620	110	90	15	11470	540
LP100120-1L-78	SP1	0.39	0.13	15.5	1.5	5.8	0.47	80.1	3.9	28.6	1.5	138.6	6.5	31.9	1.5	345	12	44.6	2.3	12190	510
LP100120-1S-96	SP1	3.97	0.56	103	11	32	3.4	374	41	134	13	558	51	135	11	1207	99	164	14	9290	390
LP100120-1L-37	SP1	1.92	0.4	22.9	2.4	7.7	0.68	97.3	8	36	2.4	165	11	39.1	2.6	426	25	66.2	3.6	9190	380
LP100120-1L-7	SP1	0.61	0.12	13.3	1.8	5.62	0.5	73.6	4.4	29.7	1.8	138.8	6.1	36.3	1.8	406	13	61.2	2.7	14080	590
LP100120-1S-60	SP1	5.91	0.44	75.3	4.2	22.1	1.4	278	12	91	4.7	382	18	87.8	4.4	870	56	111.5	5.1	9580	430
LP100120-1S-82	SP1	5.16	0.4	76.6	5.3	23	1.4	302	14	102.3	5.4	454	18	107.6	6.6	1058	43	138.8	7.9	8640	300
LP100120-1S-50	SP1	0.245	0.075	19.5	1.7	6.13	0.56	81.2	4.8	29.1	1.5	129.3	7	33.4	2.5	328	24	43.5	2.8	13040	490
LP100120-1S-8	SP1	0.79	0.2	28	3.8	11.1	1.1	151.4	9.1	60.6	4.3	289	17	79.2	4.3	845	36	111.7	6.2	12170	410
LP100120-1S-17	SP1	0.77	0.16	47.9	3.1	17.56	0.9	262	11	102.7	3.7	460	18	120.8	5.8	1299	48	163.6	6.6	11150	420
LP100120-1S-39	SP1	0.2	0.1	14.1	0.54	0.56	0.2	7.6	1	3.77	0.48	21.6	2.1	7.33	0.7	99	6.7	19.5	1.1	10870	470
LP100120-1L-65	SP1	0.334	0.089	34	2	14.85	0.76	214	12	84.7	5.2	421	25	106.1	5.1	1187	73	152.2	8.5	13850	430
LP100120-1L-14	SP1	0.44	0.14	29	4.2	9.4	1.3	124	17	44.7	6.8	196	28	48.8	8.7	461	81	60	9.2	12450	490
LP100120-1L-41	SP1	0.94	0.17	20.5	1.7	7.24	0.65	94.5	6	34.1	1.6	159.4	7.7	40.1	1.9	436	22	60.3	3.1	11090	400
LP100120-1S-100	SP1	5.41	0.57	42.1	3.7	11.67	0.93	130.9	7	47.2	3	179.2	8.2	46	1.9	432	26	61.8	2.3	9270	360
LP100120-1S-43	SP1	1.89	0.22	55.4	4.9	18.5	1.5	222	17	77.8	5.1	337	26	80.6	5.3	843	52	104.4	9.4	12150	380
LP100120-1L-75	SP1	0.48	0.14	30.7	2.4	9.95	0.85	116.2	6.5	37	1.8	159	8.5	34.2	1.5	346	15	40.7	1.9	12780	540
LP100120-1S-3	SP1	0.98	0.23	21.2	2	5.66	0.4	65	3.6	21.6	1.4	91.4	4.6	22.7	1.7	216	13	28.1	1.9	9450	410
LP100120-1L-81	SP1	1.3	0.23	26.4	2.2	7.44	0.57	95	4.9	35.1	1.9	160.4	5.9	41.2	1.5	469	22	62.8	2.9	10370	430
LP100120-1S-65	SP1	0.79	0.14	7.5	1	2.22	0.31	28.5	2.2	11.2	0.86	53	2.9	15.6	1.2	187.8	9.9	30.5	1.6	13570	640
LP100120-1S-4	SP1	2.38	0.42	44	3.3	13.83	0.99	147.6	6.9	49	1.8	201.9	7.8	50.7	2.6	514	23	61.5	2	8690	440
LP100120-1S-78	SP1	1.27	0.36	35.2	6.6	9.7	1.4	130	18	44.6	5.7	202	23	46.3	4.5	431	28	59.8	4.7	12110	390
LP100120-1S-48	SP1	4.16	0.43	53.8	3.4	17.1	1.2	200	11	69.2	3.5	291	14	71.7</							

LP110120-15-27	SP2	0.95	0.14	40.1	3	15.4	0.92	206	14	79.7	3.4	374	14	92	3.2	1021	35	136.2	7.3	12820	470
LP110120-1L-64	SP2	0.173	0.065	14.2	1.7	4.78	0.37	73.2	3.5	29.1	1.4	139.1	6.4	35.8	1.5	405	12	54.6	2	15290	360
LP110120-15-13	SP2	1.01	0.17	92.5	7.3	31.3	2.6	411	24	146.3	8.3	669	41	155.7	7.8	1509	86	192.4	8.3	12080	330
LP110120-1L-44	SP2	0.48	0.16	43.5	2.7	13.41	0.76	179	6.1	65.6	2.1	307	11	69.2	2.9	672	24	85.5	2.8	14620	450
LP110120-15-57	SP2	0.47	0.12	42.3	3.1	13.78	0.75	166.4	7.4	63.9	2.8	283	10	66	2	677	29	87.6	2.7	14350	400
LP110120-1L-61	SP2	0.097	0.053	9.2	1	3.38	0.31	45.2	2.7	18.19	0.84	92.3	3.3	23.04	0.81	258	11	34.5	1.3	15380	560
LP110120-15-18	SP2	1.45	0.2	23.8	1.7	8.39	0.71	109.3	5.6	41.5	2.9	199	13	51.8	2.2	596	26	79.8	4.1	12000	400
LP110120-15-40	SP2	4.66	0.55	131.1	6	39.9	1.9	450	16	162.5	6.6	717	20	161.9	6.2	1517	58	194.5	7.2	10830	350
LP110120-1L-93	SP2	1.98	0.27	28.4	3.5	8.81	0.58	112.6	5	4.5	1.9	226.8	6.8	60.7	2.2	699	26	107.7	2.7	11280	340
LP110120-1L-98	SP2	1.51	0.24	16.9	1.6	6.2	0.48	80	3.1	31.5	1.2	155.1	4.4	44.2	1.2	512	22	77.7	2.5	11940	400
LP110120-15-54	SP2	2.4	0.28	19.9	2.3	7.29	0.69	92.6	4.8	36.4	1.7	186.2	6.5	52.3	2	607	16	100.6	2.8	13800	460
LP110120-15-66	SP2	5.72	0.84	94	13	30	3.7	348	39	136	1.6	612	83	165	23	1810	230	247	25	9710	240
LP110120-1L-15	SP2	0.469	0.093	8.17	0.94	2.79	0.25	38.9	2.1	16.21	0.79	87.1	4	26.3	1.2	325	14	52.8	2.2	12670	320
LP110120-1L-77	SP2	2.31	0.43	29.8	2.5	8.99	0.53	117.8	6.2	44.4	2.7	240	18	66.7	6.3	791	75	114.8	8.5	11990	320
LP110120-1L-43	SP2	1.26	0.17	24.6	1.3	7.85	0.51	106.7	5.3	41.8	1.6	211.7	6.2	51.4	1.5	615	33	86.1	3.1	11460	390
LP110120-1L-17	SP2	7.08	0.51	110.3	5.1	34	1.3	448	16	158.4	7.2	795	19	197.1	8.5	2093	71	277.6	8.1	11610	320
LP110120-1L-34	SP2	1.07	0.16	22.1	2.2	6.98	0.38	100.6	3.4	40.8	2.2	218.5	5.5	60.5	2.4	751	23	113.6	4.1	13080	290
LP110120-1L-40	SP2	1.36	0.3	27.4	2.5	9.14	0.68	139	6.3	54.3	1.6	272	7.8	71.6	1.7	887	34	127	5.9	11730	380
LP110120-1L-85	SP2	3.08	0.36	47.7	3.2	12.75	0.32	160.8	6.4	57.4	2.1	269.5	9.9	67.2	3	686	22	97.4	3.9	10770	170
LP110120-1L-3	SP2	0.72	0.12	18.4	1.4	6.05	0.32	86.9	4.2	33.1	1.7	172.7	6.4	47.8	1.9	570	23	84	2.8	13810	350
LP110120-1L-28	SP2	0.54	0.13	10.8	1.2	3.43	0.25	50.9	2.3	19.95	0.83	110.9	3.8	30.4	1.1	357	13	53.6	1.9	12230	240
LP110120-1L-82	SP2	1.37	0.17	19.1	1.6	6.95	0.41	100.5	5.5	41.6	1.9	218.2	8.6	63.1	2.7	762	35	128.9	3.4	10570	250
LP110120-1L-27	SP2	0.86	0.16	14.6	1.6	5.55	0.44	76.2	3.8	31.2	1.3	179.6	5.5	53	2.2	706	22	111.7	2.3	12930	330
LP110120-1L-86	SP2	1.04	0.17	25.5	2.6	7.99	0.44	105.1	5.2	44.5	2.3	223.4	9	60.5	2.3	720	35	105.9	4.9	12240	240
LP110120-1L-95	SP2	2.92	0.29	94.3	4.8	28.9	1.2	380	10	142.5	4.2	673	28	165.2	6.6	1793	61	264	7.3	13670	390
LP110120-15-17	SP2	2.31	0.25	42.4	2.8	13.29	0.73	161.5	8.2	60.7	2.5	279	11	68.4	2.6	753	30	100.8	3.8	10320	320
LP110120-15-35	SP2	1.03	0.18	17.5	1.1	5.63	0.38	76.9	4.1	32.4	1.3	182.1	7.6	51.7	2.6	630	29	99.8	3.8	11040	220
LP110120-1L-32	SP2	0.88	0.2	23.4	1.7	7.79	0.41	108.9	4.2	44.1	1.4	213.6	7	57	2	694	18	103.9	4.3	11660	280
LP110120-1L-76	SP2	1.54	0.2	55.9	2.9	19.59	0.6	267.4	7.7	101.2	2.9	496	18	132.1	4.9	1522	38	210.4	8.4	14200	410
LP110120-1L-16	SP2	0.62	0.12	15.9	1.3	5.51	0.32	72.3	3.8	27.26	0.99	147.9	5.1	41.3	1.7	484	16	70.2	2.6	13110	460
LP110120-1L-128	SP2	5.61	0.43	96.3	4.3	29.5	1.4	375	15	140.8	5.8	647	26	160.2	6.8	1712	64	238	10	11350	250
LP110120-15-69	SP2	0.87	0.21	14.1	2	4.75	0.5	63	4.6	24.6	1.3	128.1	8	35	1.9	436	29	66.1	3.1	12130	360
LP110120-1L-90	SP2	1.32	0.19	18.2	2	5.44	0.28	77	4.1	29	1.5	137.3	4.1	40.1	1.5	471	17	70	2.1	11850	310
LP110120-1L-102	SP2	0.267	0.078	19.6	1.8	7.1	0.46	97.9	4.5	38.5	1.5	192	4.2	48.1	1.8	541	23	81.2	2.9	11640	360
LP110120-15-14	SP2	1.28	0.23	27.6	2.7	9.78	0.59	116.1	6.8	43.7	2	205	10	52.6	3.2	572	32	80.5	4.1	10660	210
LP110120-15-59	SP2	2.27	0.29	42	2.4	14.78	0.95	182	14	70.6	3.3	336	14	91	5	1023	62	151.9	5	9550	240
LP110120-1L-10	SP2	0.82	0.17	17.3	1.4	6.28	0.44	81.7	3.2	32.5	1.3	175.1	7	46.6	2	577	25	85.7	2.1	12150	420
LP110120-1L-130	SP2	0.76	0.14	13	1.3	4.42	0.35	60	2.9	23.7	1.1	118.5	6.4	30.2	1.5	338	16	47	1.8	11330	380
LP110120-1L-23	SP2	0.65	0.12	16	1.2	5.38	0.37	70.5	2.6	25.9	1.1	140	6	36.3	1.4	440	16	66.7	2.7	11760	410
LP110120-1L-6	SP2	0.57	0.13	15.3	1.7	5.3	0.38	69.2	3.9	26.48	0.93	143.8	4.8	37.5	1.5	452	16	65.8	2	12220	270
LP110120-1L-56	SP2	0.99	0.16	17.9	2.1	5.96	0.46	83.4	5.4	34.9	1.8	194.5	7.1	51.1	1.7	615	26	95.3	4.1	11420	250
LP110120-1L-101	SP2	0.83	0.17	14.4	1.6	4.74	0.31	70.5	3.1	27.3	1.2	143.9	6.3	38.9	2.2	467	22	67.7	2.9	10790	340
LP110120-15-67	SP2	0.82	0.19	9.1	1.3	3.59	0.3	44.4	3.2	18.42	0.76	93.2	4	27.2	1.4	345	13	52.7	2.5	12690	400
LP110120-15-42	SP2	1.29	0.21	19.1	2.1	6.12	0.65	84.3	4.6	32.5	2.3	166.6	9.2	50.2	2.6	608	33	93.6	4.7	12350	430
LP110120-15-32	SP2	1.78	0.25	45.1	2.8	14.54	0.68	172.2	6.1	66.3	2.5	298	12	73.8	1.7	813	30	108.7	4.6	9740	360
LP110120-1L-12	SP2	1.17	0.24	25.3	3	8.06	0.5	105.6	4.3	43.8	1.2	235.9	9.1	60.5	2.4	719	24	107	3.3	12980	390
LP110120-1L-115	SP2	0.49	0.12	11.2	1.3	3.55	0.34	51.1	2.6	21.63	0.85	113.4	3.8	32.5	1.2	407	14	62	1.9	11670	300
LP110120-1L-74	SP2	0.65	0.13	10.5	1	3.41	0.37	50.9	2.7	20.18	0.65	107.2	5.7	29.1	1	359	13	53.8	2.6	11620	250
LP110120-1L-72	SP2	0.51	0.14	14.5	1.6	4.74	0.42	69.1	2.9	27.4	1.1	138.5	5.6	35.8	1.4	402	16	62.6	2.4	11980	250
LP110120-15-30	SP2	3.34	0.32	114.9	6	34.3	2	401	15	138.2	7.2	564	24	128.2	7.2	1318	96	164.5	6.5	8890	340
LP110120-15-24	SP2	8.76	0.57	147.6	8.9	44.2	1.8	509	20	181.7	5.7	790	30	191.3	6.6	2095	81	289	13	10270	360
LP110120-15-43	SP2	1.61	0.25	61.4	3.1	19.9	1.2	229.2	8.4	85.4	3.4	357	14	83.6	3.2	845	26	109.9	3.9	10120	340
LP110120-1L-69	SP2	0.59	0.12	15.2	1.6	4.64	0.35	58.1	3.3	23.7	1.1	124.8	4.6	34.2	1.6	412	15	66.2	3.1	12860	350
LP110120-1L-89	SP2	1.52	0.27	30.6	2.7	9.29	0.73	122.2	6.2	43.9	2	227.8	8.6	59.9	2.8	708	30	106.8	4	11710	330
LP110120-15-58	SP2	0.487	0.098	13.6	1.5	4	0.33	57.5	2.6	23.7	1.4	111.7	4.6	31	1.4	373	13	58.6	2.3	11740	360
LP110120-1L-88	SP2	1.17	0.16	21	1.6	7.02	0.61	98.6	6	37	2.5	185.9	9.6	49	2.9	586	31	87.8	3.7	11700	280
LP110120-1L-1	SP2	1.41	0.24	24.9	1.8	8.19	0.41	106.2	3.5	43.9	1.5	228.1	8.9	57.4	2.2	706	25	104.4	3.6	10990	350
LP110120-15-11	SP2	0.53	0.12	7.8	1	2.59	0.23	35.6	1.5	15.14	0.79	78	2.5	23.9	1.3	323	15	52.9	2.2	11190	410
LP110120-15-16	SP2	1.17	0.18	18.7	1.6	6.57	0.51	80.7	4.2	29.83	0.94	142.2	6.1	36.8	1.5	399	18	60.3	2.5	9630	260
LP110120-15-55	SP2	0.89	0.21	25.7	1.8	8.79	0.58	110.9	6.5	48.5	1.8	235	12	61.3	3	686	30	101.7	3.1	11360	370
LP110120-1L-121	SP2	3.84	0.34	54.5	3	15.8	1.1	190	12	69.5	3.8	330	20	85.8	4.4	974	47	137.1	5.8	9850	280
LP110120-15-29	SP2	3.47	0.45	79.2	5.5	27.1	1.7	347	20	135.3	6.7	652	42	161.1	8.8	1776	75	247	1		



LP110120-1L-110	SP2	0.86	0.16	58	2.4	17.56	0.9	213.7	6.4	78.9	3.1	339	14	75.3	2.7	760	27	96.5	3.3	11780	310
LP110120-1L-117	SP2	0.31	0.12	12.5	1.5	5.56	0.33	81.2	3.7	31.8	1.8	136.9	5.3	35	1.3	327	12	44.5	1.5	14610	430
LP110120-1L-62	SP2	0.206	0.072	17	1.6	5.01	0.35	64.5	3.4	24.8	1.1	113.9	5.6	28.03	0.89	289	9.4	36.7	1.1	11820	330
LP110120-1L-94	SP2	1.07	0.19	15.3	1.6	5.24	0.39	76.7	3.2	30.6	1.4	151.6	4.6	40	1.5	457	15	69.6	3.1	12230	230
LP110120-1L-92	SP2	0.42	0.12	19.2	1.7	7.24	0.53	101.8	4	42.3	1.3	210.2	7.7	52.1	2.1	577	17	77.8	2.7	12480	330
LP110120-1L-81	SP2	0.522	0.085	24.2	2.3	6.77	0.33	83.6	3.8	29.87	0.99	132.3	6.1	30.4	1.1	304	11	41.9	1.4	10990	340
LP110120-1L-41	SP2	0.86	0.18	49	3.3	14.76	0.74	194.2	7	67.9	2.5	314	16	69.8	2.2	727	25	88.6	3.1	8960	270
LP110120-1S-70	SP2	1.24	0.28	15.3	1.8	6.34	0.44	80.9	4.4	31.4	1.4	157.1	7.7	43	1.8	476	17	65.7	2.4	13030	500
LP110120-1S-7	SP2	0.46	0.12	20	2	6.65	0.26	86.9	4	32.3	1.4	150.5	4.6	38	1.6	406	18	53	2.3	12520	270
LP110120-1S-61	SP2	1.74	0.19	121	4.5	34	1.3	353	14	114.6	4.4	461	16	101.6	3.7	1023	44	127.8	4.6	11950	340
LP110120-1L-111	SP2	1.79	0.26	64.2	3.4	17.7	0.71	210.4	7.8	74.2	3.1	324	12	79.4	3.3	743	28	97.6	4.3	11940	300
LP110120-1L-71	SP2	8.47	0.8	67	5.5	20.8	1.3	238	12	80.8	3	371	16	92.3	4.4	1072	37	153.1	4.4	9850	240
LP110120-1L-29	SP2	0.223	0.095	31	2	9.41	0.47	131.8	4.5	49.9	1.9	228.7	7	58.7	2.4	605	15	79.7	2.9	14710	460
LP110120-1S-49	SP2	0.599	0.096	63.1	3.8	22.76	0.83	270.6	8.2	106.8	4.4	496	16	119.5	5.3	1210	46	146.3	5.3	15170	530
LP110120-1S-5	SP2	0.53	0.14	22.7	1.7	6.36	0.48	77	3.5	26.05	0.87	116.7	6.1	26.6	1.3	275.4	9	36.4	1.8	10680	370
LP110120-1L-58	SP2	1.01	0.22	26.7	2.5	8.06	0.54	105.9	5.8	36.6	1.8	171.2	8.5	38.3	2.1	409	18	53.7	2.2	12530	300
LP110120-1S-2	SP2	0.135	0.074	23.6	2.1	8.33	0.46	104.9	5.3	38.7	1.8	183.8	5.8	47	1.4	475	10	60.1	2.3	12900	390
LP110120-1L-71	SP2	0.79	0.13	37.1	3.4	13.11	0.85	153.1	8.7	58.1	2.6	264	11	60.3	3.3	600	23	77.3	3.5	10620	320
LP110120-1L-113	SP2	0.267	0.086	16.2	1.7	6.13	0.38	73.8	2.7	28.3	1.3	125.5	5.5	29.9	1.3	324	16	42	1.4	11830	300
LP110120-1L-129	SP2	1.66	0.29	25.6	2.5	8.81	0.49	104.9	4.1	39.1	1.6	191.8	7	47.5	1.7	527	15	76.9	2.8	13810	430
LP110120-1L-84	SP2	5.7	1.1	85	12	14.7	1.6	111.5	5.6	33.4	1.5	125	5.6	26.9	1.1	251.8	8.9	32.26	0.96	12930	360
LP110120-1L-22	SP2	2.36	0.25	70	4.4	20	1.2	239.4	9.1	77.1	3.2	333	11	71.6	3.1	676	24	87	2.6	9940	310
LP110120-1L-26	SP2	0.47	0.13	85.6	4.7	27.1	1.1	325	14	119.3	3.9	550	19	124.3	4.2	1334	35	164.2	4.3	13610	310
LP110120-1L-97	SP2	1.04	0.26	56.4	5.2	17.5	1.2	223	11	84.1	2.2	368	16	92.5	3	966	32	131.5	4.2	12830	400
LP110120-1S-6	SP2	0.061	0.033	23.2	1.6	7.12	0.41	100.4	5.1	38.1	1.8	170.1	7.6	42	2	454	15	58.7	1.6	12430	440
LP110120-1S-37	SP2	1.7	0.65	53	14	10.5	1.8	109	11	38	2.6	190	7.8	49	2	535	19	76.8	3	14510	550
LP110120-1S-4	SP2	1.19	0.2	24.7	2.6	8.01	0.54	100.3	3.3	39.1	1.4	182.7	9	42.5	1.7	487	16	65.3	1.9	11670	370
LP110120-1S-33	SP2	0.39	0.1	32.9	2.8	10.22	0.58	136.6	7.9	51.2	1.9	244.3	9	57.3	2	567	26	79.1	3.7	12500	380
LP110120-1L-2	SP2	0.13	0.053	8.63	0.92	3.21	0.24	47	2.4	16.93	0.85	93.7	3.4	22.93	0.94	254	10	34.5	1.5	12740	450
LP110120-1L-106	SP2	1.46	0.22	31.4	1.9	9.73	0.52	133.5	5.7	48.8	1.6	226.5	4.3	59.7	2.9	644	26	91.6	2.6	11530	270
LP110120-1S-26	SP2	4.52	0.51	49.8	4.1	14.3	1	158.5	6.6	57.5	2.5	274	13	69.9	2.1	730	31	105.4	3.6	9790	400
LP110120-1L-125	SP2	1.23	0.24	32.9	2.6	9.84	0.57	131.8	6	50.5	2	233.9	8.9	61.9	3.3	663	28	91.3	3.2	11750	270
LP110120-1L-87	SP2	3	0.38	47.1	3.8	13.54	0.67	158	6.4	56.5	2.5	259	10	61.3	2.4	635	28	85.7	3.4	12380	240
LP110120-1S-38	SP2	1.19	0.21	30.2	2.3	8.98	0.79	109.2	5	37.8	1.5	161.9	8.2	39.5	1.2	390	15	50.7	2.1	10680	380
LP110120-1L-119	SP2	3.78	0.34	48.2	2.9	13.39	0.78	169.9	6.9	61.8	1.9	278.5	8.3	67.1	2	709	24	96.1	2.5	8960	270
LP110120-1S-34	SP2	2.07	0.38	36	2.7	13.44	0.68	152.8	6.3	58.6	2.2	273	11	65.4	2.6	725	31	90.9	3	12370	390
LP110120-1L-112	SP2	0.93	0.19	31.2	2.5	9.33	0.65	115.3	6.7	40.6	2.3	176.8	8	43	2.6	458	26	62.7	2.1	10070	250
LP110120-1L-124	SP2	1.66	0.21	20.8	2	6.63	0.57	88.1	4.2	32.7	1.3	150.1	6.6	36	2	369	20	51.1	2.1	15000	400
LP110120-1S-64	SP2	2.93	0.27	61.3	5.3	16.7	1.1	189.8	9.9	66.8	2.5	269	10	70.4	3.2	657	25	86.2	2.9	11480	400
LP110120-1L-50	SP2	0.41	0.13	43.4	3.6	15.15	0.91	205.2	9.8	76	3.4	343	15	80.2	4.3	809	29	103.9	3.5	13160	370
LP110120-1L-63	SP2	0.173	0.073	38.9	3.1	14.18	0.76	202.5	8.6	78.7	3	382	12	88.5	2.6	910	30	118.5	3.4	14730	620
LP110120-1L-53	SP2	1.4	0.2	38.9	2.8	11.28	0.65	137.7	5.6	48	1.7	208.9	6.7	47.5	2	463	18	60.8	2	11270	360
LP110120-1L-9	SP2	0.156	0.074	31.8	2.5	11.43	0.62	170.9	9.2	62.4	2.5	313.8	9.2	74.3	2.8	794	26	106	2.7	14360	480
LP110120-1S-45	SP2	0.035	0.028	24.4	1.4	7.64	0.57	95.4	4.5	33.1	1.3	150.5	6.1	34.6	1.5	364	16	47.8	1.5	13480	420
LP110120-1S-48	SP2	1.94	0.24	19.3	1.2	5.35	0.43	55.3	2.6	18.09	0.62	76.6	2.8	17.87	0.62	207.2	9.3	27.6	1.1	10580	370
LP110120-1L-120	SP2	2.44	0.21	27.4	2.4	7.49	0.47	89.9	5	31.9	1.6	136	5.7	31.5	1.6	334	16	45	1.4	12480	280
LP110120-1S-53	SP2	2.86	0.45	44.6	5.8	13	1.7	141	19	48.8	6	215	28	51.4	6	537	57	67.8	6.6	11680	410
LP110120-1S-60	SP2	0.41	0.13	9.2	1.1	3.05	0.21	38.6	2.4	14.6	0.63	61.8	3.4	16.11	0.76	168.9	4.7	23.4	1.2	14200	450
LP110120-1L-78	SP2	0.27	0.089	19.6	2	5.37	0.49	60	3.5	19.6	0.95	84.9	3.1	20.72	0.98	215.7	9.5	29.4	1.1	13050	280
LP110120-1L-8	SP2	0.94	0.15	16.9	1.6	5.14	0.28	69.5	3.3	23.51	0.94	117.1	4.2	29.9	1.2	317	12	45.7	1.5	10470	300
LP110120-1S-8	SP2	0.83	0.13	23.7	1.8	8.81	0.55	113.5	4.5	41.6	2	205.6	9.3	50.5	1.8	542	28	75.1	3.6	11310	360
Rejected Grains																					
LP110120-1L-39	SP2	0.63	0.16	24.5	1.6	7.82	0.36	109.5	4.3	39.7	1.8	213.4	5.3	54.7	2.3	583	23	83	2.8	14230	430
LP110120-1L-57	SP2	3.85	0.39	38.8	2.1	11.48	0.71	144.6	4.9	51.7	1.3	249.8	8.6	64	2.2	708	26	111.3	4.2	11720	400
LP110120-1S-21	SP2	1.57	0.23	25.8	2.4	7.22	0.39	89.8	4.1	34.1	1.5	155.3	5.1	40.9	1.7	475	17	66.2	3	12650	310
LP110120-1L-105	SP2	3.96	0.33	43.9	2.4	12.27	0.74	138.2	4.8	46.4	1.4	205.2	7.1	47.2	1.6	474	12	66.5	1.9	9350	290
LP110120-1L-118	SP2	250	9.3	707	33	79.7	2.7	402	14	72.1	3.3	190.2	4.6	27	1.3	179.4	6.7	18.74	0.81	72.1	2.6
LP110120-1S-52	SP2	3.44	0.71	38.7	8.4	9.8	2.1	117	24	43.5	8.2	194	34	45.3	7.3	496	67	72.5	8.8	12090	300
LP110120-1S-12	SP2	1.07	0.26	37.6	4.1	9.28	0.74	113.2	4.9	39.4	2.5	172.2	7.7	44	1.9	433	29	61.7	2.9	11960	330
LP110120-1L-13	SP2	0.66	0.13	22.1	1.8	5.77	0.57	77.2	4.1	26.2	1.4	124	6.5	29.3	1.6	293	18	40.5	2.6	10660	330
LP110120-1L-91	SP2	102.4	3.4	625	19	86.6	2.8	512	17	88.8	2.7	209.1	9.4	27.38	0.87	163.6	6.2	18.9	1	30	1.9
LP110120-1L-42	SP2	24.11	0.98	119	6	34.8	1.7	382	18	104.8	3.5	455	12	107.4	3.7	1068	43	133.9	4.7	15630	390
LP110120-1S-20	SP2	0.65	0.11	13.6	1.7	5.16	0.36	64.9	3.1	28.4	1.6	135.4	5.4	3							

**APPENDIX IV:** Detrital zircon trace element data for samples from the Minas de Barita Area.  
Trace elements: P, Sc, Ti, Y, Nb, La, Ce, Pr, Nd, Sm, Eu, Gd, Tb, Dy, Ho, Er, Yb, Lu, Hf, Pb,  
Th, U.

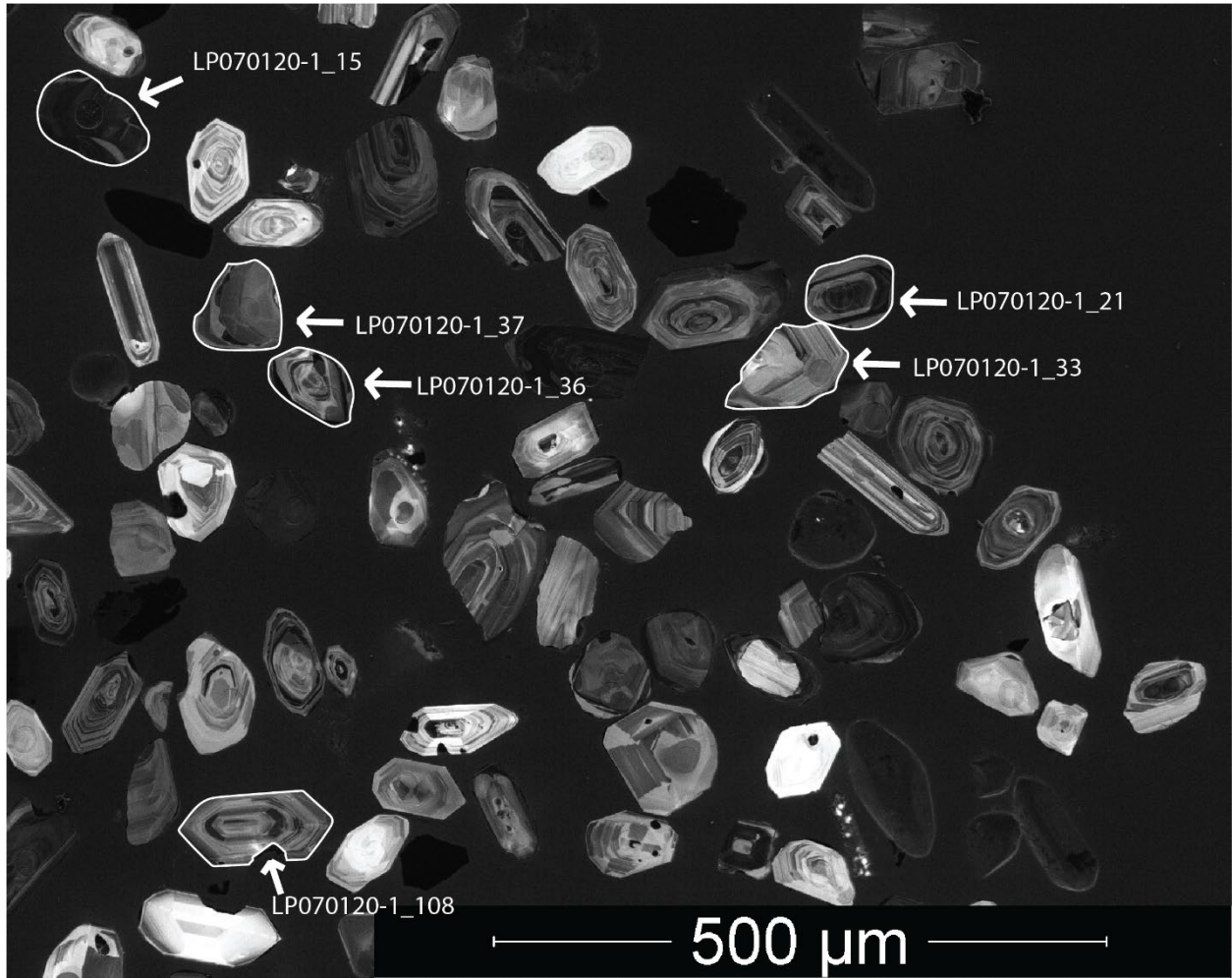
Sample 13-11-SR2																							
Grain	Unit	P (ppm)	Sc (ppm)	Ti (ppm)	Y (ppm)	Nb (ppm)	La (ppm)	Ce (ppm)	Pr (ppm)	Nd (ppm)	Sm (ppm)	Eu (ppm)	Gd (ppm)	Tb (ppm)	Dy (ppm)	Ho (ppm)	Er (ppm)	Yb (ppm)	Lu (ppm)	Hf (ppm)	Pb (ppm)	Th (ppm)	U (ppm)
1311-SR2_zrn-09	RN	240	106.3	10.5	4130	5.69	0.11	27.3	0.93	9.3	23.5	7.1	108.2	36.9	415	148	609	1035	199	8720	19.6	327.7	302.2
1311-SR2_zrn-89	RN	500	455	20.7	1310	2.15	0.087	2.28	0.157	18.5	3.18	0.81	17.6	8.0	106	38.4	177	449	109	12430	46.8	34.7	480
1311-SR2_zrn-64	RN	290	109.6	7.4	578	0.86	0.017	6.9	0.087	1.09	2.76	0.83	13.1	4.27	49.6	18.8	84.7	182	402	9470	17.0	134.8	316
1311-SR2_zrn-03	RN	784	196	5.6	2960	1.35	0	1.15	0.033	11.1	4.35	0.113	38	17.54	237	105.2	490	952	185.4	11720	15.1	55.8	251
1311-SR2_zrn-17	RN	1050	105.5	2.8	1970	4.72	1.54	34.1	1.3	10.4	12.3	2.42	50.7	16.3	175	64.4	283	534	108	8600	43.4	449	774
1311-SR2_zrn-45	RN	450	168	7.7	1990	1.85	0.05	3.72	0.222	5.5	10.9	1.32	54.7	17	193	69.9	299	321	102.2	9430	28.9	119.3	387.5
1311-SR2_zrn-81	RN	0	213	7.9	1729	4.58	0.0034	50.7	2.92	44.7	7.68	2.73	42.3	13.71	160.6	61.8	274	557	115.7	11770	43.8	446	618
1311-SR2_zrn-50	RN	710	132.5	3.5	1990	2.15	0	5.01	0.034	1.18	5.31	0.119	33.7	13.7	176	68.4	314	576	113.3	11310	34.1	148.2	644
1311-SR2_zrn-83	RN	520	267	11.1	1410	1.54	0	3.68	0.083	1.67	4.87	0.388	29.4	9.97	120.3	47.2	217.5	408	84.2	9970	27.1	133	402
1311-SR2_zrn-22	RN	410	129.8	6.9	1527	1.49	0.012	26.9	0.33	6.66	9.4	3.57	44.4	14.18	152.3	54.5	234	402	81.8	8090	13.1	192.9	218
1311-SR2_zrn-26	RN	362	140.4	12.4	1188	1.3	0.0037	6.37	0.217	3.46	6.63	1.38	33.2	10.25	116.8	42.6	183.6	314	62	8490	10.1	81.9	150.5
1311-SR2_zrn-59	RN	460	340	7.5	2410	4.62	0	52.2	0.106	2.92	8.2	3.06	53.2	18	221	88.1	395	705	144	9150	18.9	320	265
1311-SR2_zrn-58	RN	280	96	9.9	1190	0.94	0.18	10.5	0.4	3.77	4.58	0.91	30.7	9.3	112	38.4	161	276	53.6	9210	35.8	198	312
1311-SR2_zrn-76	RN	1650	517	5.4	2950	0.65	0.08	0.83	0.18	0.33	4.7	0.3	32.9	15.8	234	97	472	940	192	13200	35.0	23.92	398.2
1311-SR2_zrn-90	RN	520	290	4	3120	6	0	2.45	1.93	25.4	25.5	1.12	82.5	27	294	112.5	452	775	154	10230	40.0	273.8	493
1311-SR2_zrn-04	RN	-80	85.8	27.7	361	0.95	0.3	12.2	0.108	1.14	1.36	0.43	6.33	2.02	28	11	55.3	132	30.7	10130	13.9	82.5	185
1311-SR2_zrn-10	RN	70	216	2.2	1707	2.07	0	31.7	0.097	1.28	3.43	2.37	35	11.6	140	53.7	249	593	128	10640	22.3	150	256
1311-SR2_zrn-61	RN	200	101	7	980	1.5	0	7.1	0.08	1.24	2.32	0.52	18.5	7.41	97	35	147	261	50.2	10100	12.4	37	81.1
1311-SR2_zrn-48	RN	840	326	4.6	1830	1.09	0.01	0.74	0.085	1.12	5.56	0.166	34.6	15.1	181	60.2	234	389	67.5	12370	80.3	174	1290
1311-SR2_zrn-41	RN	440	221	-0.00103	720	1.29	0.048	0.25	0.16	0.23	0	0.14	6.8	4.87	63.3	23.8	102.6	214	44.4	10700	31.5	10.2	244
1311-SR2_zrn-49	RN	-50	87.8	7.2	305	0.78	0	4.59	0.073	1.92	3.29	0.38	12.4	3.38	34.7	10.5	39.1	57.2	10.2	8440	17.7	47.4	162.8
1311-SR2_zrn-12	RN	-80	119.3	7.1	1136	1.33	0	12.15	0.056	1.28	3.49	1.15	18	6.42	81.6	35.9	184.7	463	108.9	10830	14.8	98.3	142.7
1311-SR2_zrn-54	RN	160	106.5	380	546	0.88	1	14.8	0.37	2.9	2.33	0.76	12.38	4.06	46.7	17.77	80.5	176.5	39.1	9390	6.0	46.39	64.4
1311-SR2_zrn-05	RN	20	134	6	1290	1.71	0.2	122	1.45	2.7	31.7	10.8	88	20.2	170	48.3	169	246	44.8	9480	27.8	484	299
1311-SR2_zrn-32	RN	580	105.2	7.4	1370	1.81	0.41	45.7	0.521	5.95	10.1	3.79	41.3	12.7	135	46.7	202	378	75.1	8580	23.1	288	246.8
1311-SR2_zrn-26	RN	298	274	11.6	1980	5.93	0	22.9	0.132	22.9	5.94	2.16	38	13.62	169.6	68.5	315	611	124.9	8560	26.8	157	252
1311-SR2_zrn-62	RN	210	142.7	1.7	1452	6.27	0	53.9	0.069	1.38	3.93	1.16	26	9.49	119.4	48.2	230.2	489	104.1	10490	40.4	320	395
1311-SR2_zrn-25	RN	620	110.1	18.5	756	1.24	0.031	15.8	0.198	2.58	5	0.81	21.9	6.44	68.3	26.3	108.6	206	42.3	8990	13.4	112.1	124.8
1311-SR2_zrn-11	RN	-74	94.2	9.5	697	1.49	0.087	17.19	0.167	2.23	4.18	0.761	18.6	5.86	64.1	23.4	106	203	41.8	11660	36.8	177.7	319
1311-SR2_zrn-30	RN	378	70	6.4	1247	4.81	0.076	18.13	0.223	4.04	6.74	0.315	32.2	10.73	123.2	45	191.7	322	61.6	8060	30.8	162.1	312
1311-SR2_zrn-23	RN	730	164	6.6	1001	1.35	0	31.7	0.088	1.64	3.04	0.47	21.8	7.27	87.1	34	157	261.2	89.0	112	45.5	115.1	52.1
1311-SR2_zrn-77	RN	-60	111.5	3.7	806	1.74	0.039	22.1	0.086	11.7	2.15	0.54	11.3	4.27	55.9	24.5	122.7	314	74.8	12070	51.3	1083	407
1311-SR2_zrn-13	RN	30	158	31	1220	3.92	0.17	41.4	0.149	1.81	4	1.4	22.4	8.6	116	43	201	407	82.3	12200	15.9	108.6	121.4
1311-SR2_zrn-55	RN	440	81.8	6.5	551	4.01	0.065	24.8	0.054	1	1.71	0.61	10.1	3.49	40.8	16.6	89.9	211	46.1	8440	53.3	20.1	424
1311-SR2_zrn-71	RN	1210	85	9.9	800	2.1	0.255	17.8	0.301	3.14	3.33	0.5	16.9	5.98	71	27.4	126.6	244	51.7	11200	31.8	105.4	212.8
1311-SR2_zrn-53	RN	100	89.9	5.4	954	2.3	0.085	34.3	0.34	6.7	8.3	1.59	26.4	8	83.5	30.6	132	266	51.5	8280	17.2	75	84.5
1311-SR2_zrn-65	RN	560	287	20.3	1570	5.9	1.58	19.1	3.19	20	15.6	5.1	27.1	9.1	112	42.4	223	720	167	12500	172.3	53	832
1311-SR2_zrn-18	RN	-120	87.3	13.8	890	4.82	0	58.3	0.062	1.45	3.9	0.81	17.9	6.18	76.9	29.7	144	332	65.5	10430	33.6	113.2	204.3
1311-SR2_zrn-33	RN	380	70.8	12.6	1300	2.44	0.044	9.87	0.216	4.55	8.6	0.42	41.4	11.9	132	45.2	181	285	50.8	8540	24.3	62.9	141.6
1311-SR2_zrn-78	RN	880	91	10.9	1350	9.5	0.038	73.6	0.154	2.73	7.1	1.38	34.7	11.9	130	48.3	196	327	63.2	10880	51.4	56.01	89.51
1311-SR2_zrn-87	RN	640	235	15.6	1450	1.38	0.41	5.7	0.29	3.9	5.8	0.42	37.2	13.5	154	49.8	194	304	67.2	11730	42.8	123.2	267.3
1311-SR2_zrn-57	RN	50	54.4	85	113	3.84	0	5	0.012	0.11	0.23	0.058	1.18	0.559	6.36	3.38	18.3	61.7	17.8	7540	28.2	4.79	188
1311-SR2_zrn-02	RN	30	107.6	14.1	996	1.13	0.62	6.88	0.81	10.6	13.1	1.33	48.2	12.83	117.1	37.4	136.7	198	38.4	8510	9.4	31.6	50.4
1311-SR2_zrn-43	RN	220	105	25.3	674	1.56	0.083	13.9	0.136	2.3	5.3	1.6	22.6	6.76	70.3	24.3	94.2	165	33.8	8180	4.6	24.69	34.8
1311-SR2_zrn-01	RN	380	93.6	21.7	791	3.25	0	26	0.151	2.49	4.82	0.78	23.2	7.4	78.6	27.6	117.3	213	42.9	9640	8.5	59.3	48.1
1311-SR2_zrn-34	RN	420	85.6	14.1	755	6.6	0	34.5	0.071	1.12	3.27	0.41	16.9	6.19	74.7	26.8	118.9	222	43.3	10050	23.2	67.1	129
1311-SR2_zrn-08	RN	0	93.8	19.1	646	2.13	0.93	12.3	0.44	3.86	4.91	0.7	19.8	6.37	66.4	22.7	95.2	167.2	32.7	9250	20.9	45.4	113.4
1311-SR2_zrn-69	RN	280	112.3	11.7	896	3.26	0	17.42	0.161	2.58	5.64	1.37	28.1	8.75	92.6	31.9	132	233	43.7	10140	18.2	63.3	97
1311-SR2_zrn-72	RN	180	87	15	850	1.91	2.3	11.1	1.02	7.1	4.14	0.53	21.7	5.55	65.3	27.6	140	324	79.1	9220	68.8	87.3	346.6
1311-SR2_zrn-42	RN	210	79.5	18.8	1132	1.66	0.026	9.35	0.148	5.64	8.28	0.61	35.9	11.09	115.6	40.4	170.3	302	58.1	8160	17.6	52.2	85.3
1311-SR2_zrn-14	RN	40	83.7	4.2	808	1.41	0.045	22	0.11	1.9	3.74	0.9	16.2	5.49	68.4	26.9	126	283	59.9	11550	64.8	112.6	285
1311-SR2_zrn-07	RN	420	79.5	10.6	618	3.16	0.008	12.4	0.033	0.69	2.25	0.165	12.4	4.43	54.5	22.2	99.7	197.9	42.7	9860	14.0	31.7	58
1311-SR2_zrn-31	RN	340	82	4	219	2.41	0	9.6	0	0	0.3	0.134	2.82	10.3	14.6	6.28	36.1	99	20.6	9890	51.8	34.7	205.8
1311-SR2_zrn-38	RN	170	73.6	5	1670	4.19	0.021	11.4	0.11	2.5	6.2	0.88	37.2	13.4	157	64	267	467	96	8630	73.3	111.3	275.6
1311-SR2_zrn-75	RN	210	72	14.4	633	2.76	0	5.8	0.02	0.88	1.82	0.069	1.2	4.64	56.6	21.21	95.4	182	36.3				

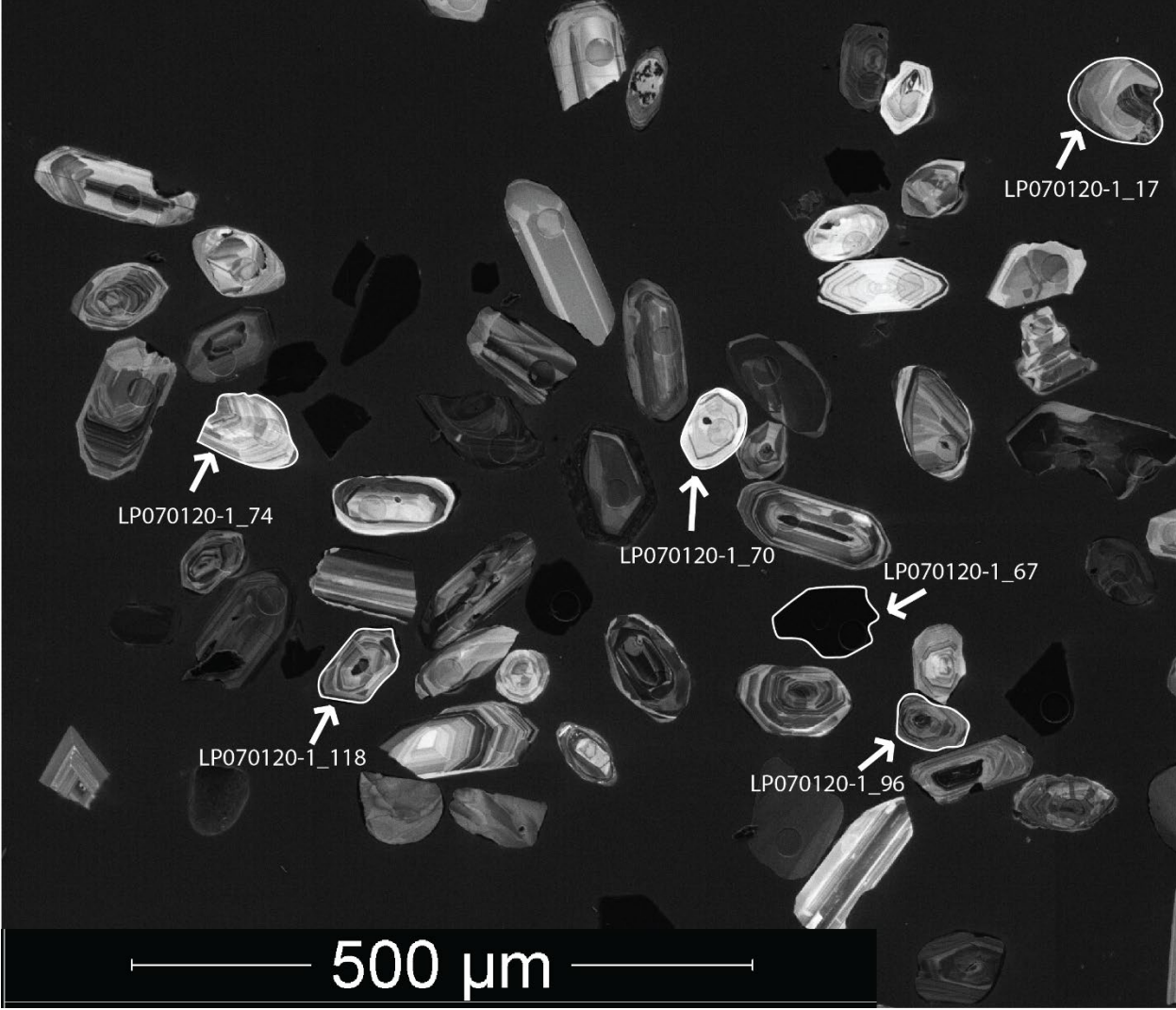
1211-SR2a_Zrn-25	MM	310	153.6	8.7	1527	1.81	0.007	7.7	0.279	3.26	8.6	11.6	37.8	12.85	149.5	52.9	224	387	81.1	9270	116.8	396	395
1211-SR2a_Zrn-26	MM	160	219	3.9	1470	8.7	0.121	51.6	0.111	1.82	4.95	1.36	23.4	8.8	107	44.8	221	548	132.1	12340	57.8	333.2	515
1211-SR2a_Zrn-27	MM	80	80.6	3.1	387	1.62	0	20.7	0.044	0.95	1.7	0.462	8.23	2.77	32	12.32	56.3	135.3	31.4	10870	34.2	135.6	298
1211-SR2a_Zrn-28	MM	20	168	28	1200	2.08	0.09	11.1	0.35	58.1	7.3	1.86	35	11.1	118	41.3	170	295	59.8	10750	17.1	266	438
1211-SR2a_Zrn-29	MM	100	93.6	4.3	2130	3.58	0	72	0.277	5.45	10.9	1.03	47.9	16.7	198	74.9	317	538	108.5	9060	39.0	106.8	118.3
1211-SR2a_Zrn-30	MM	250	160	7.5	1530	1.82	0.067	29.5	0.58	10.5	14.8	5.2	53.7	16	155	52.3	209	377	80.3	9350	46.8	509	708
1211-SR2a_Zrn-31	MM	270	82	6.8	931	5.11	0	9.25	0.055	1.22	3.45	0.221	19.3	7.49	86.8	32.2	141.4	254	51.4	9210	71.8	64.3	116.6
1211-SR2a_Zrn-32	MM	320	218	20.4	1604	1.53	0.048	15.3	0.56	8.8	16.4	2.97	63.2	17	179	57.1	224	348	67.7	8920	46.3	204	199.8
1211-SR2a_Zrn-33	MM	1630	60.3	16.3	1060	1.76	56	130	15.7	7.2	17.5	0.92	34.2	9.09	96.7	34.8	155	277	53	1190	28.2	72.4	135.2
1211-SR2a_Zrn-34	MM	-160	183	4.2	1173	2.2	0.018	54.5	0.17	2.22	5.6	1.71	26.4	7.77	101.1	40.7	191	371	77.6	10090	38.3	168	149.1
1211-SR2a_Zrn-35	MM	180	116.8	11.2	634	1.06	0	15.5	0.02	0.52	1.37	0.3	10.7	4.01	49.2	20.2	97.2	208	44.4	10940	12.0	104.9	196.9
1211-SR2a_Zrn-36	MM	10	81.7	5.1	325	0.26	0	2.82	0.012	0.54	0.85	0.44	5.48	2	23.3	10.33	50.3	136	32.9	8310	4.9	44.3	49.8
1211-SR2a_Zrn-37	MM	130	101.4	13.1	1191	2.68	0.42	10.67	0.235	3.18	4.83	0.63	25.6	9.09	106.9	41.7	177.7	332	67.2	10720	50.5	79.4	228
1211-SR2a_Zrn-38	MM	-40	123.4	5.3	992	3.61	0	9.2	0.054	0.92	2.41	0.394	17	5.6	77.1	31.7	161	374	95.2	10650	61.3	72.4	723
1211-SR2a_Zrn-39	MM	420	201	4.5	861	0.91	0	3.31	0	0.26	1.05	0.032	10.6	4.57	64.1	28.2	149.5	356	76.9	12430	35.0	29.7	241.4
1211-SR2a_Zrn-40	MM	1140	117	8.3	923	1.58	6.6	27.8	1.63	7.6	2.91	0.58	12.3	5.02	65.9	29.3	152.5	363	84	11450	17.0	68.3	119.3
1211-SR2a_Zrn-41	MM	260	161	8.2	1520	4.09	0.29	40	0.67	6.7	11.4	6.5	57	15.8	168	48.2	183	374	89.3	12600	50.0	43.3	695
1211-SR2a_Zrn-42	MM	-50	88.2	4.3	366	0.48	0	3.14	0.018	0.163	0.6	0.262	5.02	1.87	26	11.59	56.6	128.7	29.3	12710	27.1	41.6	140.9
1211-SR2a_Zrn-43	MM	470	106	27	690	1.2	0.055	11.9	0.13	2.31	3.6	0.44	14.9	4.8	57.2	21.2	90	162	32.2	10800	18.8	54.7	130
1211-SR2a_Zrn-44	MM	280	96.4	9.5	561	3.1	0.024	16.2	0.022	0.96	1.72	0.61	8.4	3.35	43.8	18.2	85	184	41.8	11390	28.8	69.3	132.3
1211-SR2a_Zrn-45	MM	400	155.2	23	807	2.33	0	29.7	0.101	1.33	2.99	1.02	16.8	5.56	68.8	28	126.4	245	53.6	10030	53.0	124.5	156.5
1211-SR2a_Zrn-46	MM	210	104.2	3.5	1184	3.12	0.014	27.9	0.099	1.72	3.4	0.51	20.5	7.39	93.4	37.8	178	350	69.9	10380	123.8	30.4	467
1211-SR2a_Zrn-47	MM	20	94.6	3.5	432	2.32	0	13.7	0.014	0.68	0.94	0.132	6.38	2.26	29	12.5	63.6	149.3	33.6	12610	25.5	47.4	160.8
1211-SR2a_Zrn-48	MM	-100	100.7	14.6	488	0.58	0	25	0.069	1.38	2.67	0.98	13.3	4.12	46.7	16.4	71.8	132.8	27.9	9230	9.5	63.6	81.3
1211-SR2a_Zrn-49	MM	10	133	12.4	672	2.42	0	15.5	0.025	0.57	1.69	0.23	10.7	4.22	51.3	21.3	107.6	235	53.2	11350	72.5	44.4	167.3
1211-SR2a_Zrn-50	MM	230	106.8	14.4	1800	2.87	0.006	4.65	0.235	4.01	7.28	0.88	42.2	15.1	167	61.3	260	460	93.5	9520	39.3	56.4	116
1211-SR2a_Zrn-51	MM	480	167	10.6	1030	1.68	0.16	30.1	0.58	10	11.2	4.33	42.9	11.01	111.3	35.9	141	229	47.3	9180	27.8	117.1	162.5
1211-SR2a_Zrn-52	MM	90	70.9	13	2570	9.6	0.061	17	0.34	6.2	11.7	0.42	68.2	21.8	247	91.5	396	584	112.2	12170	8.8	80.7	155
1211-SR2a_Zrn-53	MM	6000	72.2	9.7	532	3.03	480	900	82	288	43	5.2	40	7.14	59.8	164.2	65.8	109.9	21.6	8780	71.8	224	161
1211-SR2a_Zrn-54	MM	160	125	21.6	2070	2.12	0.051	22.3	0.101	2.88	6.2	3.05	39.1	13.6	172	65.3	305	620	136.2	7190	10.9	169	208.8
1211-SR2a_Zrn-55	MM	120	93.7	9.5	638	3.32	0.031	20.9	0.075	1.27	2.61	0.199	13.2	4.72	57.1	22.1	98.9	189.6	39.6	10760	38.3	74.6	139.5
1211-SR2a_Zrn-56	MM	120	106.6	10.4	146	0	0	63.3	0.083	2.27	5.29	1.2	30.1	12.14	159	63.7	314	671	141.1	8850	41.5	524	194.7
1211-SR2a_Zrn-57	MM	1180	200.2	7.4	2610	0.75	0	2.28	0.099	2.56	7.2	0.162	49.7	18.4	233	87.2	375	630	123.5	12330	24.8	115	224.8
1211-SR2a_Zrn-58	MM	320	148.7	6.6	886	1.21	0.011	28.7	0.086	2.33	3.71	1.25	19.9	6.58	78	30.3	140.9	271	59.5	9030	15.0	48.35	49.8
1211-SR2a_Zrn-59	MM	350	173.5	4.9	1081	1.53	0	18.18	0.072	1.12	2.73	1.08	16.9	5.81	75.8	31.8	165.7	427	109.2	9700	32.0	147.5	367
1211-SR2a_Zrn-60	MM	710	356	4.8	1504	1.79	0	1.73	0.023	0.78	2.49	0.242	19.8	9.32	129.6	51.1	225	441	88.8	11530	27.1	40.5	380
1211-SR2a_Zrn-61	MM	3010	1280	4.8	3750	2.39	0	3.12	0.033	0.57	3.12	1.29	27.7	16.5	269	121.5	660	1650	353	12500	32.0	17.1	324
1211-SR2a_Zrn-62	MM	-50	136.3	4.5	152	0.25	0	0.227	0	0	0.09	3.07	3.97	1.63	15	4.97	19.6	35.5	6.86	13440	32.8	7.59	482.8
1211-SR2a_Zrn-63	MM	-50	97	8.2	665	1.86	0.16	22.4	0.115	0.98	3.4	0.78	12.2	4.63	56.5	22.1	102	212	45.4	10900	15.4	72.5	103.7
1211-SR2a_Zrn-64	MM	40	79.5	10.4	394	2.7	0	31	0.055	0.63	1.67	0.386	8.41	27.9	33.3	12.76	58.9	127.2	28.3	10420	12.2	56.4	66.5
1211-SR2a_Zrn-65	MM	350	95.8	10.5	479	0.9	0	1.95	0.033	1.6	3.73	0.074	22.5	5.73	52.3	16.1	56.8	75.3	14.8	11790	76.5	115.8	177.9
1211-SR2a_Zrn-66	MM	440	148	16.2	986	1.86	0	30.6	0.037	1.57	4.44	1.4	24.4	7.45	86.4	34.2	152	280	57.6	9420	5.0	52.3	46.9
1211-SR2a_Zrn-67	MM	700	160	6.2	1360	1.46	0	2.44	0.092	1.9	3.17	0.15	27.1	10	111.6	44.8	203	382	78.9	11880	68.3	99	278
1211-SR2a_Zrn-68	MM	300	105.6	7.4	436	1.47	0	8.15	0	0.43	0.61	1.8	0.045	6.46	2.57	146.2	71.3	153.3	33.4	11930	87.8	51	233
1211-SR2a_Zrn-69	MM	1010	233	8.4	1690	0.43	0	0.75	0.063	1.36	4.02	0.32	28.6	10.27	133.6	60.4	306	604	125.5	11110	8.6	44.8	139.1
1211-SR2a_Zrn-70	MM	-10	113.2	5.6	531	0.88	0	1.6	0.021	1.06	1.43	0.7	10.6	3.41	41.5	16.5	80.1	184	43.4	10920	23.7	126.1	245
1211-SR2a_Zrn-71	MM	620	68.5	25.8	3260	4.64	0.022	7.94	0.233	4.28	9.58	1.54	69	24.1	286	110.3	484	806	157.2	9370	53.3	287.2	312
1211-SR2a_Zrn-72	MM	250	118	5.6	1082	3.69	0.055	95.6	0.269	4.17	7.6	2.02	29.5	8.52	97	36.3	157	308	63.9	9200	88.5	325	404
1211-SR2a_Zrn-73	MM	210	167	10.1	1731	1.72	0.176	5.69	0.47	6.15	14.5	5.37	67.1	19.4	186.6	54.8	205	340	68.6	10650	122.3	68.5	440
1211-SR2a_Zrn-74	MM	570	95.5	5.7	1940	6.63	0.51	42.2	0.335	6.6	8.5	1.81	44.8	14.9	167	62.5	296	566	111.6	9030	70.8	755	428
1211-SR2a_Zrn-75	MM	110	70	5.5	225	0.525	0.213	7.01	0.045	0.44	0.49	0.218	4.06	1.49	18.6	7.36	35.4	85.3	18.3	10910	60.0	99.9	299
1211-SR2a_Zrn-76	MM	1170	173	9	2570	1.8	0	2.33	0.082	1.27	6.1	1.36	36.3	15.6	219	83.7	395	751	151	13080	153.8	102.2	511
1211-SR2a_Zrn-77	MM	930	245	13.9	2490	0.59	0.095	2.05	0.51	7.9	15.4	0.48	77.9	23.6	241	84.9	353	680	331	11170	15.0	61.3	195.3
1211-SR2a_Zrn-78	MM	470	84.6	12.7	890	3.46	0.222	12.6	0.184	1.99	2.46	1.04	16	5.72	72.3	27.1	122	260	56.5	10780	40.8	346	260.8
1211-SR2a_Zrn-79	MM	830	111	19	3200	4.91	0.55	68.6	0.6	8	26.6	13.6	150	43	400	107	372	532	100.4	9880	44.0	658	643
1211-SR2a_Zrn-80	MM	650	138	17	1470	4.7	0.4	31.8	1.82	3.28	13.3	6.2	25.5	8.7	116	44.8	235	690					

1311-SR3a_b_Zm-40	MM	240	263	4.2	1490	9.4	0.083	68	0.231	3.39	6.1	1.82	28.5	8.69	120	48.5	230	569	124	11210	81.0	799	958
1311-SR3a_b_Zm-41	MM	360	250	5.6	852	3.95	0	7.76	0	0.33	1.31	0.26	11.6	5.33	64	26.7	137	314	67.9	12260	69.8	116.7	568
1311-SR3a_b_Zm-42	MM	120	139	10.5	458	1.12	1.72	14.7	0.86	6.1	6.9	0.92	21.2	5.7	49	15.6	58.8	104.5	18.9	12300	34.8	126	434
1311-SR3a_b_Zm-43	MM	350	89.4	7.9	1190	5.15	0.022	39.4	0.142	2.16	4.8	0.3	25.2	8.68	106.8	39.4	184	332	67.4	9620	34.0	669	465.5
1311-SR3a_b_Zm-44	MM	0	114.5	4.2	636	2.32	0	16.2	0.016	0.45	1.05	0.3	8.1	3.13	41.9	19	103.3	304	73.2	10820	33.1	242.8	420
1311-SR3a_b_Zm-45	MM	380	279	12.6	1740	3.21	0.321	11.5	0.206	3.7	7.1	2	37	13.3	157	60.1	270	579	121.2	10810	182.8	185.8	647
1311-SR3a_b_Zm-46	MM	590	461	11.6	2360	2.22	0.085	19.4	0.84	10.7	22	10.9	93	28.5	276	83.2	341	625	125.1	12050	109.3	163.7	346
1311-SR3a_b_Zm-47	MM	180	173	17.6	2110	1.7	0.64	44.1	0.64	9.4	13.8	6.76	62.7	19	208	75.6	320	574	118.3	6920	7.4	116.9	96.7
1311-SR3a_b_Zm-48	MM	810	338	8.2	2270	0.82	0.057	0.86	0.114	2.67	7.2	0.4	54.1	20.3	232	75.8	288	434	76.6	11430	24.0	79.3	387
1311-SR3a_b_Zm-49	MM	170	235	6.3	1160	1.1	0.065	8.57	0.109	2.9	3.9	2.65	17.2	6.62	88	34.2	173	461	117	10750	29.3	48.5	378
1311-SR3a_b_Zm-50	MM	1070	488	18.5	3450	1.14	0.0045	1.1	0.236	3.98	10.61	0.207	62.8	24	301	118	536	1009	205.8	10410	37.4	80.7	490
1311-SR3a_b_Zm-51	MM	250	287	4.1	1165	3.53	5.4	9.2	0.97	8.2	2.6	0.36	12.4	6.82	98.5	36.4	149.9	287	60.3	12650	74.0	33.4	910
1311-SR3a_b_Zm-52	MM	380	120.4	14.3	2020	7.17	0.2	98.9	0.51	7.46	12.1	2.49	51.3	15.6	173	63.1	290	572	118	10020	162.0	864	631
1311-SR3a_b_Zm-53	MM	190	63.8	4.8	1577	14.1	0.022	21.7	0.193	2.22	5.43	0.66	33.2	11.96	146.2	56.4	244	420	79.3	9830	67.5	168	408
1311-SR3a_b_Zm-54	MM	990	526	5.3	2820	2.84	0.231	5.39	0.51	7.9	24.2	11.1	92	26.1	265	93	426	1080	225	12140	137.0	70.9	789
1311-SR3a_b_Zm-55	MM	80	109	1.4	771	0.79	0.082	6.49	0.27	2.8	3.99	0.99	20.5	5.65	61.6	23.9	113	253	54.9	10600	99.0	107.8	250.3
1311-SR3a_b_Zm-56	MM	550	175	7.9	2020	2.14	0.01	3.95	0.161	2.36	7.6	0.33	41	15.2	172	66.9	300	564	111.4	11090	29.5	143.8	464
1311-SR3a_b_Zm-57	MM	220	132	36	670	4.6	0.21	11.8	0.174	1.41	2.57	1.06	18.6	5.9	67.7	23.5	100.6	184	35.5	9840	11.7	26.4	63.8
1311-SR3a_b_Zm-58	MM	430	242	40	2590	4.37	2.8	22.5	2.54	19.3	28.2	10.1	90	28	275	88.8	367	677	131.8	10690	79.5	306.4	685
1311-SR3a_b_Zm-59	MM	700	167.8	7.4	4130	5.41	0.136	7.3	0.49	7.5	16.3	2	89	32.2	391	143.2	613	1063	192	10090	31.1	229	337
1311-SR3a_b_Zm-61	MM	-210	131	21	2450	4.7	0.59	14.7	1.72	24.1	29.7	9.1	106	31.7	297	88	298	429	76	8900	24.3	80.6	97.4
1311-SR3a_b_Zm-62	MM	310	877	46	3500	34.6	0.31	35.7	0.7	14.2	19.1	3.9	90	33.5	369	130	472	698	117	8490	14.9	161.3	183
1311-SR3a_b_Zm-63	MM	442	270	10	2332	6.65	0	88.8	0.134	1.99	7.12	2.84	43.5	15.24	186.6	73	339	733	155	9700	81.5	1260	889
1311-SR3a_b_Zm-64	MM	810	331	12.2	3380	1.36	0.165	1.47	0.275	3.54	9.2	1.12	57.1	22.7	290	115.7	508	913	172	12140	28.4	85	473.8
1311-SR3a_b_Zm-65	MM	170	99	15.5	1310	2.62	0.158	32.7	0.52	5.31	6.65	2.08	30.6	9.9	114	40.9	195	394	85.2	10380	27.8	116.6	208
1311-SR3a_b_Zm-66	MM	165	163.8	6.1	2520	3.63	0.249	14.5	0.94	14.7	24.2	2.44	95.5	26.9	267	88.6	339	543	99.9	7290	101.8	368	851
1311-SR3a_b_Zm-67	MM	30	57	1.8	300	1.01	0	3.78	0	0.24	0.52	0.062	2.9	1.22	17.2	9.1	50.7	136	33.1	12300	19.3	34.5	154.3
1311-SR3a_b_Zm-68	MM	940	256	4.4	3880	0.72	0	0.86	0.079	2.1	7.7	0.207	55.9	24	333	133.5	600	1011	184	11560	14.8	54.1	224
1311-SR3a_b_Zm-69	MM	540	97.5	12.2	1321	1.1	2.47	10.2	1.36	10.2	1.76	0.38	39.1	11.8	130.2	47.9	191	325	63.1	7950	11.9	33.5	65.4
1311-SR3a_b_Zm-70	MM	290	102.5	7.1	672	3.76	0	10.9	0.032	0.8	1.46	0.38	8.9	4.1	52.5	22.5	112.8	281	61.6	11250	109.0	84.7	506
1311-SR3a_b_Zm-71	MM	860	454	4.7	2230	2.67	0.186	1.82	0.43	5	8.1	2.8	33.1	13.3	179	70.1	330	771	164	12940	92.8	43.9	1512
1311-SR3a_b_Zm-72	MM	560	186.2	11.9	1743	0.72	0	1.28	0.124	3.02	8.45	0.188	53.7	18.3	190	58.8	201	245	42.1	10100	13.4	54.8	142
1311-SR3a_b_Zm-73	MM	670	329	12.7	1907	1.17	0	9.54	0.126	2.74	5.65	1.25	37.2	13.91	170.5	66.3	301	569	114.8	10310	43.4	70.4	136.8
1311-SR3a_b_Zm-74	MM	490	105.7	6.6	2920	9.08	0.135	23.9	0.445	7.73	13.63	1.05	73.9	24.9	282	104.7	428	692	135	8570	42.8	311	376
1311-SR3a_b_Zm-75	MM	290	148	14.3	991	1.64	0	21.9	0.102	1.86	4.36	0.92	21.3	7.07	84.2	32.9	152.7	308	68	8780	41.0	83.1	123
1311-SR3a_b_Zm-76	MM	120	154	12.2	1545	4.82	0.239	43.8	0.351	2.78	6.5	1.77	30	9.64	124.8	49.4	237	503	110.9	9500	12.9	143	133.9
1311-SR3a_b_Zm-77	MM	340	448	6.7	511	0.78	0.088	0.52	0.063	0.71	0.99	0.67	3.5	2.2	35.4	16.9	85	319	73.5	12600	103.3	14	642
1311-SR3a_b_Zm-78	MM	420	99.2	3.9	792	1.69	3	16.4	1.68	10	6.2	2.99	20.1	5.05	56.4	22.3	109.4	260	65.4	11720	24.1	105.6	282
1311-SR3a_b_Zm-79	MM	30	119.3	2.9	650	2.65	0	31.7	0.032	0.64	1.42	0.338	8.9	2.79	40.2	17.6	97	293	76.6	11360	51.8	373	505
1311-SR3a_b_Zm-80	MM	170	133.1	5.7	498	1.93	0.112	10.08	0.208	2.83	7.8	1.51	27.8	6.54	63.4	16	57.2	92	17.3	12030	88.8	63.2	457.4
1311-SR3a_b_Zm-81	MM	220	171	6.4	1430	3.62	0.291	45.4	0.99	13	20.4	6.52	72.2	17.3	153	45.2	170	289	55.9	11310	39.5	459	620
1311-SR3a_b_Zm-82	MM	310	78.8	9.5	1314	2.11	0.039	14.2	0.356	4.25	7.27	0.75	35.7	10.42	126.1	45.1	196	348	68.1	9930	48.8	181	343
1311-SR3a_b_Zm-83	MM	300	106.8	11.6	1379	4.56	0.035	21	0.165	2.29	5.19	0.41	28.1	9.71	114.8	44.8	212	408	88.4	10090	85.5	141.6	264
1311-SR3a_b_Zm-84	MM	120	105.8	2.8	788	2.02	0	8.74	0.173	1.85	3.28	2	20.4	6.39	71.7	25.4	111.6	233	53.5	10610	44.8	23.7	129.7
1311-SR3a_b_Zm-85	MM	220	124	14.4	773	1.24	0.064	12	0.119	2.07	3.7	1.12	15.8	5.52	58.1	23.8	107	226	46.6	9410	10.9	53.5	102.8
1311-SR3a_b_Zm-86	MM	500	161	11.2	2050	1.4	1.23	34.3	1.59	14.5	19.9	8.19	67.7	20.1	199	57.7	222	407	79.9	9620	14.2	171	155
1311-SR3a_b_Zm-87	MM	140	137	6.5	169	0.8	0	0.34	0.024	0.86	0.14	0.08	1.6	0.76	11.4	4.64	24.6	38.2	9.4	11370	8.8	3.89	65.2
1311-SR3a_b_Zm-88	MM	290	134	8.7	1290	2.84	0.032	34.6	0.116	2.77	6	1.24	27.6	9.32	114.9	42.3	200	392	81.3	9620	71.3	176.7	222.6
1311-SR3a_b_Zm-89	MM	580	391	14.1	1271	0.95	0.022	2.32	0.114	4.17	7.5	0.68	34.8	11.43	124	41.8	178	319	64.8	9810	21.3	119.6	370
1311-SR3a_b_Zm-90	MM	240	138	8.7	588	0.8	0.049	12.14	0.168	2.43	2.9	1.46	14	5.06	55.4	18.6	80.2	173	40.3	10610	25.0	42.7	197.7
1311-SR3a_b_Zm-91	MM	117	115.4	5.4	442	2.29	0.007	2.54	0	0.135	1.09	0.047	7.73	3.3	42	14.48	58.1	86.1	18	11660	55.7	73.2	736
1311-SR3a_b_Zm-92	MM	390	156	70	2700	5.28	1.82	68.2	1.71	16.7	20.7	8.7	96	28.9	281	88.6	357	616	120	9020	54.5	404	470
1311-SR3a_b_Zm-93	MM	230	108	8.8	668	1.06	0	14.7	0.05	1	3.1	1.03	18.5	5.47	59.5	22.3	95.7	178	35.8	9600	12.9	103.8	146.9
1311-SR3a_b_Zm-94	MM	770	198	6	2020	1.26	0	2.1	0.141	2.82	7.38	0.366	43.7	16.74	189	67.9	280	489	94.1	9990	31.0	107	361
1311-SR3a_b_Zm-95	MM	110	69	1.2	332	1.08	0.005	2.42	0.029	0.84	1.16	0.292	6.04	2.29	28.7	11.19	53.8	128	28	8710	6.0	8.88	69
1311-SR3a_b_Zm-96	MM	250	92.7	3.4	578	1.45	0.105	34.8	0.104	1.4	2.5	0.92	10.2	3.52	41.5	17.9	82.4	197.9					

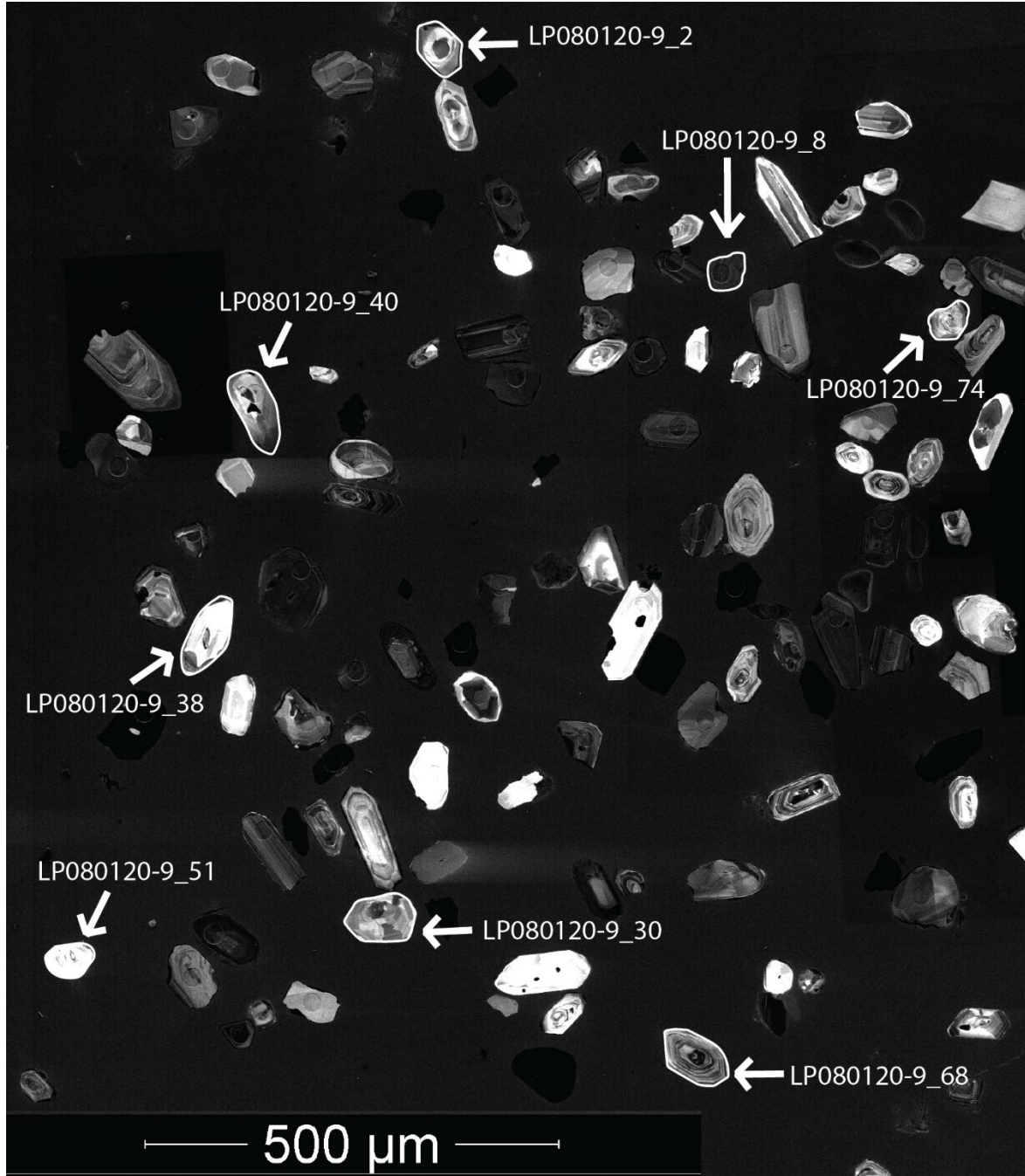
**APPENDIX V:** Cathodoluminescence images of reanalyzed Cretaceous zircon grains from samples LP070120-1, LP080120-9, LP100120-1, and LP110120-1. Cretaceous zircon grains from each sample are outlined in white and labelled.

Sample LP070120-1

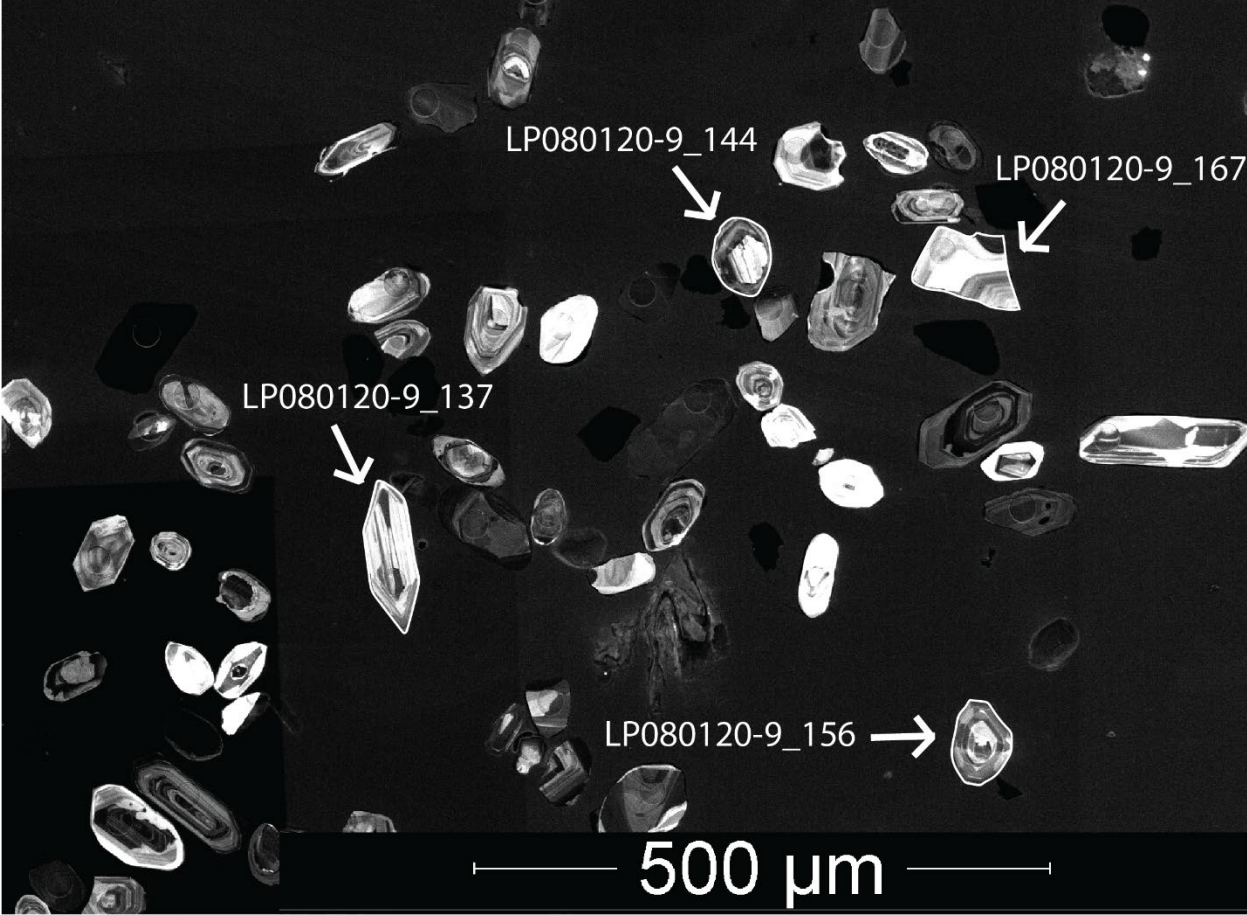




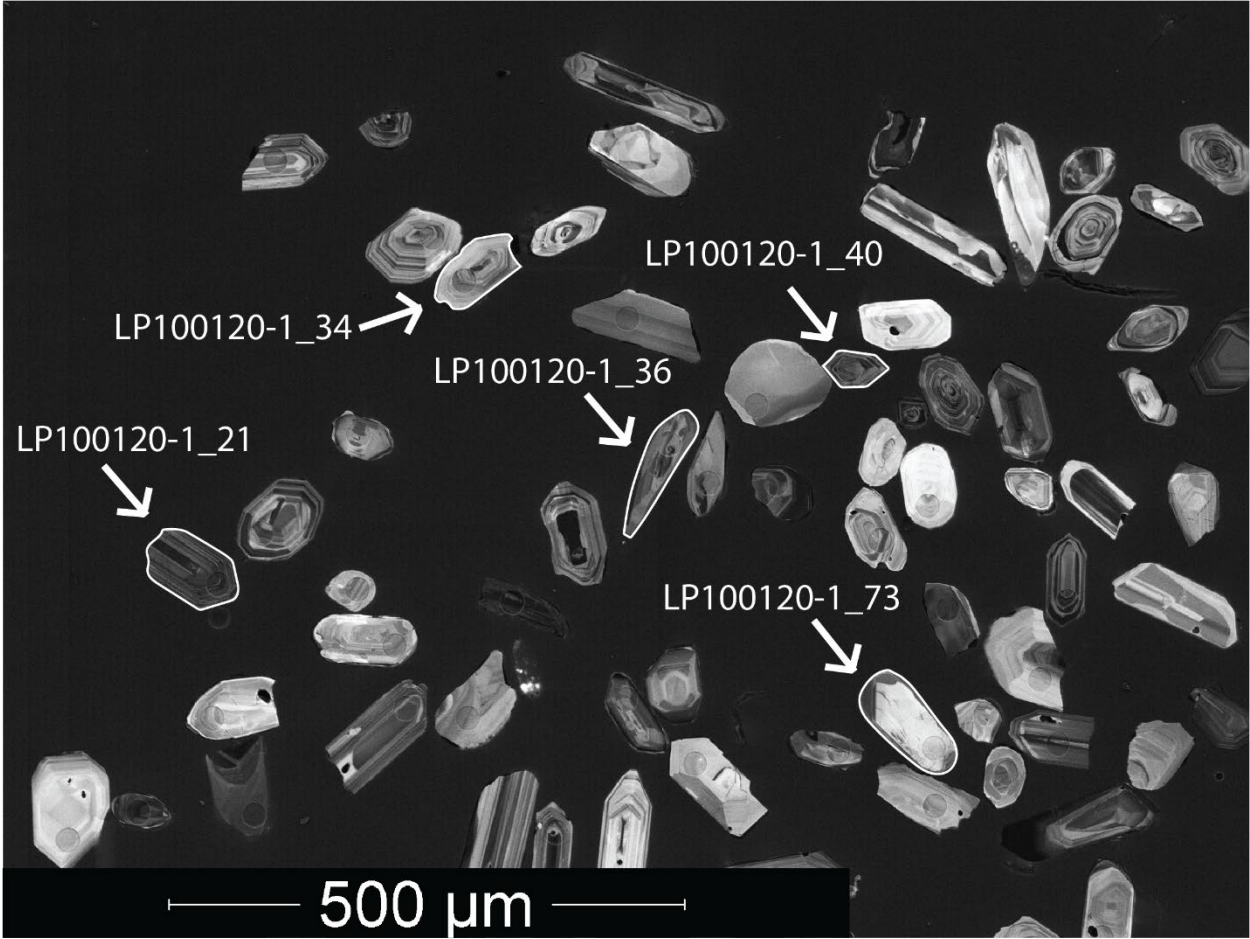
Sample LP080120-9

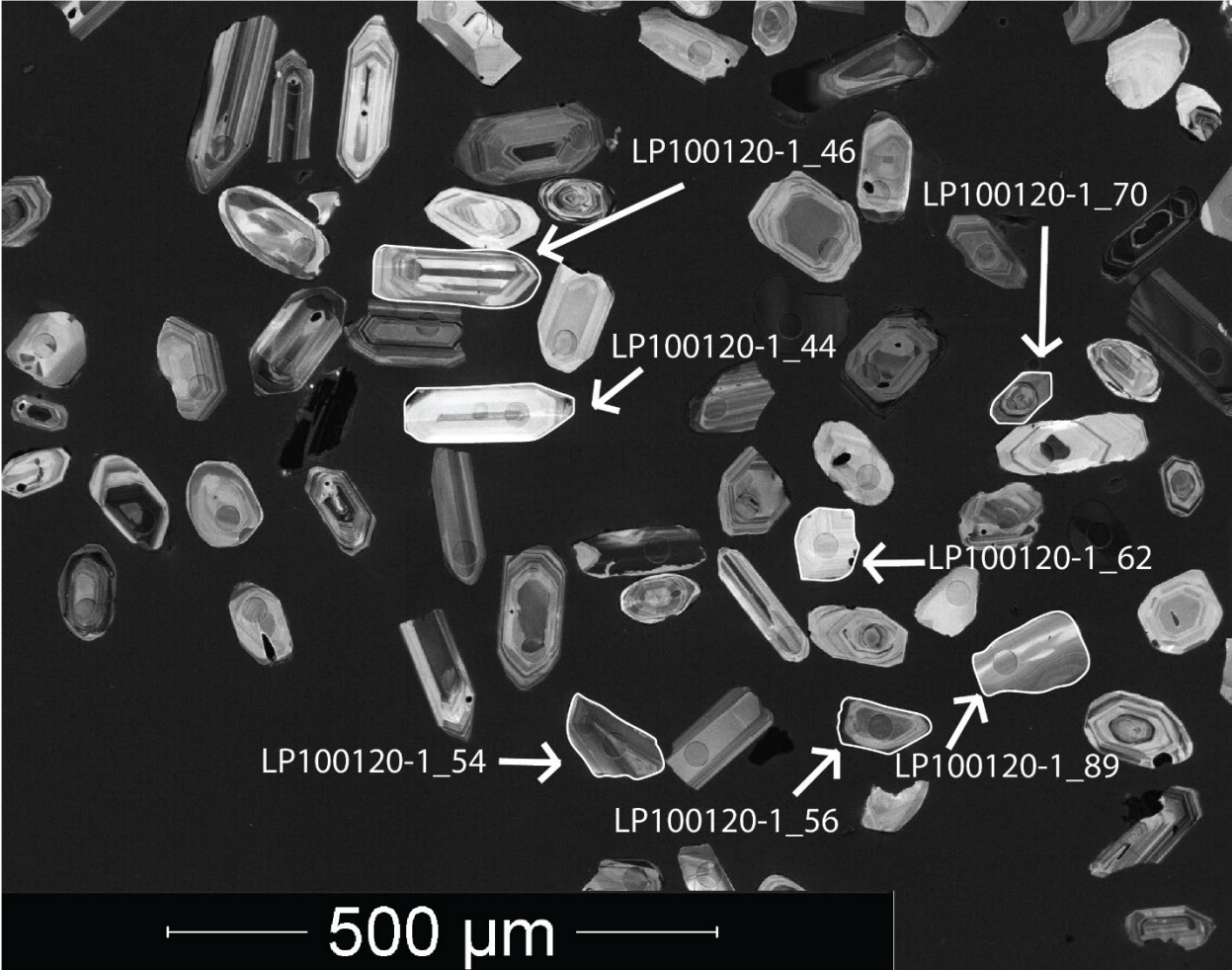






Sample LP100120-1





Sample LP110120-1

